AWARD NUMBER: W81XWH-15-1-0282

TITLE: HGF/c-MET Pathway in AIDS-Related Lymphoma

PRINCIPAL INVESTIGATOR: Zhiqiang Qin

CONTRACTING ORGANIZATION: Louisiana State University System
New Orleans, LA 70112-7021

REPORT DATE: September 2016

TYPE OF REPORT: Annual Report

PREPARED FOR: U.S. Army Medical Research and Materiel Command
Fort Detrick, Maryland 21702-5012

REPORT DOCUMENTATION PAGE

Form Approved
OMB No. 0704-0188

1. REPORT DATE	2. REPORT TYPE	3. DATES COVERED
September 2016	Annual Report	15 Aug 2015 - 14 Aug 2016

4. TITLE AND SUBTITLE

HGF/c-MET Pathway in AIDS-Related Lymphoma

5a. CONTRACT NUMBER

5b. GRANT NUMBER
W81XWH-15-1-0282

5c. PROGRAM ELEMENT NUMBER

6. AUTHOR(S)
Lu Dai, Chris Parsons, Zhiqiang Qin*

E-Mail: zqin@lsuhsc.edu

5d. PROJECT NUMBER

5e. TASK NUMBER

5f. WORK UNIT NUMBER

7. PERFORMING ORGANIZATION NAME(S) AND ADDRESS(ES)

Louisiana State University System
Health Sciences Center, New
Orleans, LA 70112-7021

8. PERFORMING ORGANIZATION REPORT NUMBER

9. SPONSORING / MONITORING AGENCY NAME(S) AND ADDRESS(ES)

U.S. Army Medical Research and Materiel Command
Fort Detrick, Maryland 21702-5012

10. SPONSOR/MONITOR'S ACRONYM(S)

11. SPONSOR/MONITOR'S REPORT NUMBER(S)

12. DISTRIBUTION / AVAILABILITY STATEMENT

Approved for Public Release; Distribution Unlimited

13. SUPPLEMENTARY NOTES

14. ABSTRACT

In the first year of funding period, we have almost completed Specific Aim1 subtasks listed in the SOW forms. We also have obtained some promising data for Specific Aim3 subtasks. In summary, we found targeting HGF/c-MET pathway induced KSHV+ PEL cell apoptosis through cell cycle arrest and DNA damage. The Illumina microarray data indicated that there are much more host factors potentially controlled by the HGF/c-MET pathway within PEL cells than we previously expected. We also found that selective c-MET inhibitor can effectively prevent PEL expansion in the xenograft model, although the underlying mechanisms still being further investigated. During this funding period, we have totally published 8 peer-reviewed articles about the molecular mechanisms of KSHV viral oncogenesis, and developing novel therapeutic strategy against these malignancies, including one in *BLOOD* journal. In all these publications, I serve as the corresponding or co-corresponding author. We also had oral presentation and/or poster display on several national or international meetings. With the support by this DOD award, I recently got a Leukemia Research Foundation pilot funding about the sphingolipid metabolism in AIDS-related lymphomas.

15. SUBJECT TERMS
HGF, c-MET, KSHV, primary effusion lymphoma, apoptosis, cell cycle, DNA damage

16. SECURITY CLASSIFICATION OF:			17. LIMITATION OF ABSTRACT	18. NUMBER OF PAGES	19a. NAME OF RESPONSIBLE PERSON
a. REPORT	b. ABSTRACT	c. THIS PAGE			USAMRMC
Unclassified	Unclassified	Unclassified	Unclassified	97	19b. TELEPHONE NUMBER *(include area code)*

Table of Contents

Page

1. INTRODUCTION

Viruses are the most common cause of lymphoma in patients with immune dysfunction, and virus-associated lymphomas incur high mortality for these patients due to a lack of effective therapeutic strategies. Studies in this proposal are designed to elucidate mechanisms for regulation of AIDS/KSHV-associated lymphoma pathogenesis by the oncogenic protein HGF/c-MET, and whether targeting HGF/c-MET reduce virus-associated lymphoma progression *in vivo*.

2. KEYWORDS

HGF, c-MET, KSHV, primary effusion lymphoma, apoptosis, cell cycle, DNA damage

3. ACCOMPLISHMENTS

3.1. What were the major goals of the project?

There are 3 specific aims in this project, Aim 1: To identify the complex mechanisms of the HGF/c-MET pathway controlling cell survival/growth for PEL tumor cells. Aim 2: To understand the mechanisms viral oncogenic proteins used to activate the HGF/c-MET pathway. Aim 3: To determine whether a selective small-molecule inhibitor of c-MET, PF-2341066, can repress PEL progression and/or reduce established tumor in an immune-deficient xenograft mice model.

The following are the condition of subtask completion as indicated in SOW:

Specific Aim 1(specified in proposal)	**Timeline**	**Site 1**
Major Task 1	Months	
Subtask 1: *HGF/c-MET affects viral gene expression (ongoing)*	2-3	Dr. Qin
Subtask 2: *HGF/c-MET affects downstream signaling pathways (ongoing)*	3-4	Dr. Qin
Subtask 3: *HGF/c-MET affects cell cycle checkpoints (completed)*	2-3	Dr. Qin
Subtask 4: *HGF/c-MET affects HGF secretion from PEL cells (completed)*	1-2	Dr. Qin
Specific Aim 2 (specified in proposal)	**Timeline**	**Site 1**
Major Task 2	Months	
Subtask 1: *viral proteins are essential for activation of HGF/c-MET (not started)*	2-3	Dr. Qin
Subtask 2: *key domain or amino acid residues essential for activation of HGF/c-MET (not started)*	4-6	Dr. Qin

Subtask 3: *the role of c-MET phosphorylation in signaling activation (not started)*	2-3	Dr. Qin
Specific Aim 3 (specified in proposal)	**Timeline**	**Site 1**
Major Task 3	Months	
Subtask 1: *c-MET inhibitor prevents PEL development in NOD/SCID mice model (ongoing)*	4-5	Dr. Qin
Subtask 2: *c-MET inhibitor reduces established PEL progression in NOD/SCID mice model (ongoing)*	5-7	Dr. Qin

3.2. What was accomplished under these goals?

In the first year of funding period, we have almost completed Specific Aim1 subtasks, and have obtained some promising data for Specific Aim3 subtasks as listed in the SOW forms above. During this funding period, we have totally published 8 peer-reviewed articles about the molecular mechanisms of KSHV viral oncogenesis, and developing novel therapeutic strategies against these malignancies, including one in *BLOOD* journal. In all these publications, I serve as the corresponding or co-corresponding author. We also had oral presentation and/or poster display on several national or international meetings (please see below details in **PRODUCTS**).

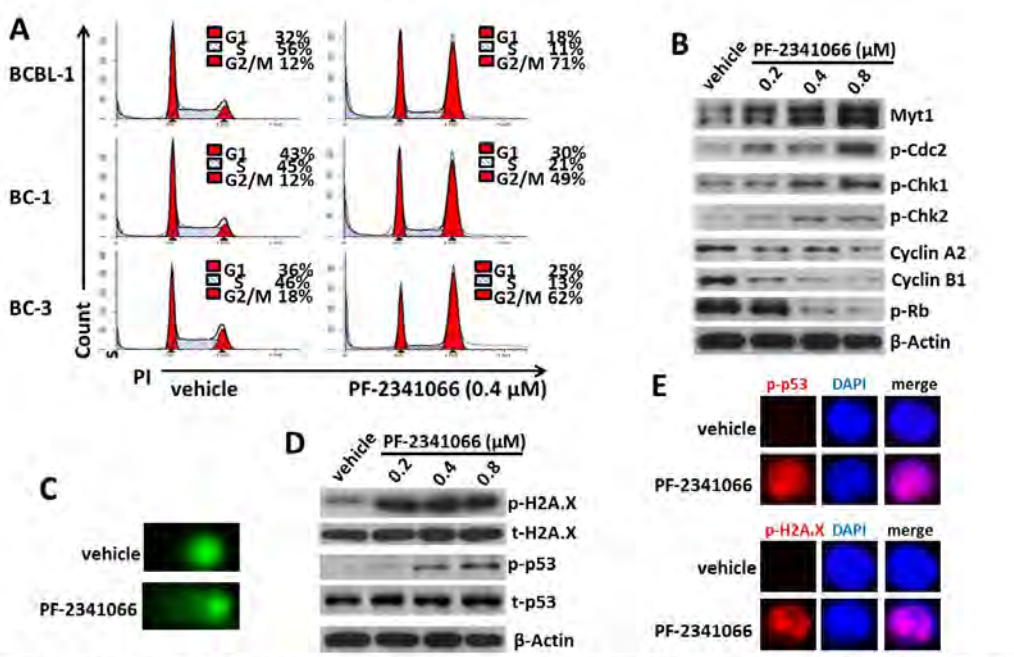

Figure 1. Targeting HGF/c-MET causes G2/M cell cycle arrest and DNA damage in KSHV1 PEL cells. (A) PEL cells were incubated with 0.4 mM PF-2341066 or vehicle control for 24 hours, then stained by PI and analyzed by flow cytometry. (B-D) The protein expression and DNA damage in BCBL-1 were measured by immunoblots and CometAssay, respectively. (E) The cellular expression of DNA damage markers phosphor-p53 and phosphor-H2A.X was detected by immunofluorescence, and the nuclear was shown by DAPI staining.

In summary of significant results: **1) Targeting HGF/c-MET pathway induced KSHV+ PEL cell apoptosis through cell cycle arrest and DNA damage.** To seek the potential mechanisms involved in c-MET inhibitor induced PEL apoptosis, we found that PF-2341066 treatment obviously caused cell cycle G2/M arrest when compared to vehicle control by flow cytometry analysis (**Fig.1A**). Further analysis indicated that PF-2341066 affected the expression of several check point regulatory proteins (positive/negative): increasing Myt1, phosphor-Cdc2/Chk1/Chk2, while reducing Cyclin A2, Cyclin B1 and phosphor-Rb from BCBL-1 cells (**Fig.1B**). Interestingly, we found that PF-2341066 treatment

also caused obvious DNA damage of PEL cells, as indicated by the CometAssay and the upregulation of DNA damage marker, phosphor-p53 and phosphor-H2A.X but not the total protein levels, respectively (**Fig.1C-E**).

2) Identifying downstream genes controlled by HGF/c-MET pathway in KSHV+ PEL cell-lines. We used the HumanHT-12 v4 Expression BeadChip (Illumina) to study the gene profile altered between vehicle- or PF-2341066-treated 3 KSHV+ PEL cell-lines (BCBL-1, BC-1 and BCP-1). Intersection analysis indicated that there were totally 51 common genes significantly altered within all the 3 PF-2341066-treated cell-lines (up/down≥2 folds and p<0.05); 20 similar genes altered between BCBL-1 and BC-1, 188 similar between BCBL-1 and BCP-1, and 13 similar between BC-1 and BCP-1; 282 genes altered were unique to BCBL-1, 148 unique to BCP-1 and 52 unique to BC-1 (**Fig.2A**). We also performed enrichment analysis of these common, similar and unique set of genes using the Pathway map, Gene Ontology (GO) Processes and Process Networks modules from Metacore Software. Our analysis showed that several major cellular functions were affected within PF-2341066-treated PEL cells, including apoptosis/ER stress response pathway, epigenetic regulation of gene expression, cell cycle/checkpoint and DNA damage related proteins (**Fig.2B-D**).

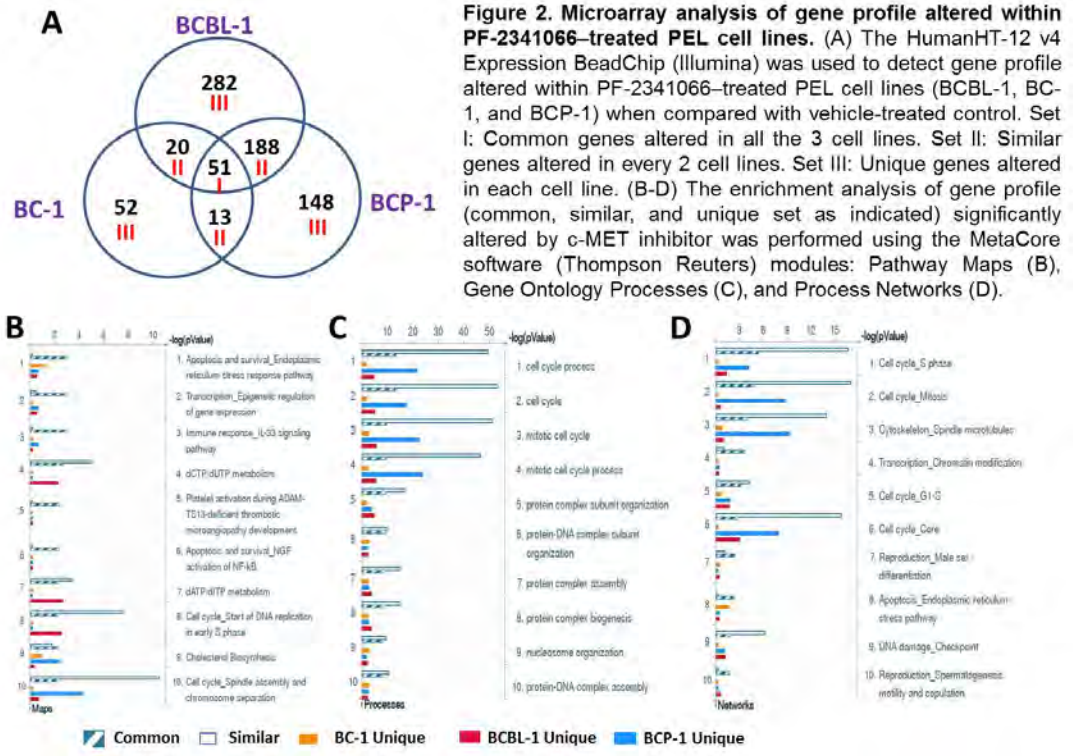

Figure 2. Microarray analysis of gene profile altered within PF-2341066–treated PEL cell lines. (A) The HumanHT-12 v4 Expression BeadChip (Illumina) was used to detect gene profile altered within PF-2341066–treated PEL cell lines (BCBL-1, BC-1, and BCP-1) when compared with vehicle-treated control. Set I: Common genes altered in all the 3 cell lines. Set II: Similar genes altered in every 2 cell lines. Set III: Unique genes altered in each cell line. (B-D) The enrichment analysis of gene profile (common, similar, and unique set as indicated) significantly altered by c-MET inhibitor was performed using the MetaCore software (Thompson Reuters) modules: Pathway Maps (B), Gene Ontology Processes (C), and Process Networks (D).

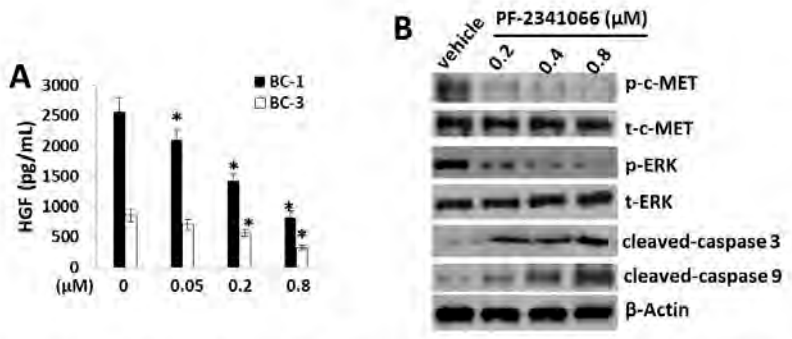

Figure 3. The c-MET selective inhibitor PF-2341066 reduces HGF production from KSHV+ PEL cells. (A) PEL cells were incubated with the indicated concentrations of PF-2341066 for 24 hours, then the HGF concentrations in supernatant were determined by ELISA. Error bars represent the S.E.M. for 3 independent experiments. *=P < .01. (B) The protein expression in BCBL-1 was measured by immunoblots.

3) c-MET inhibitor treatment reducing HGF production from PEL cells. We found that c-MET inhibitor, PF-2341066 treatment greatly reduced HGF production from KSHV+ PEL cell-lines, although the underlying mechanisms remain unclear (**Fig.3A**). By using immunoblots, we confirmed that PF-2341066 treatment increased the expression of cleaved-caspase 3 and 9, while reducing phosphor-c-MET and downstream phosphor-ERK activities (**Fig.3B**).

4) Selective c-MET inhibitor treatment effectively preventing PEL expansion in

the xenograft model. We administered PF-2341066 (or vehicle) intraperitoneally (i.p.) within 24 hours of BCBL-1 cell injection and for a 5-week treatment. We found that PF-2341066 treatment dramatically suppressed PEL tumor progression including reducing ascites formation and spleen enlargement over this timeframe (**Fig.4A-C**). By using the H&E staining, we observed huge tumor infiltration into the spleen of vehicle-treated mice, while only small tumor nodules were dispersed in the spleen of PF-2341066-treated mice (**Fig.4D**).

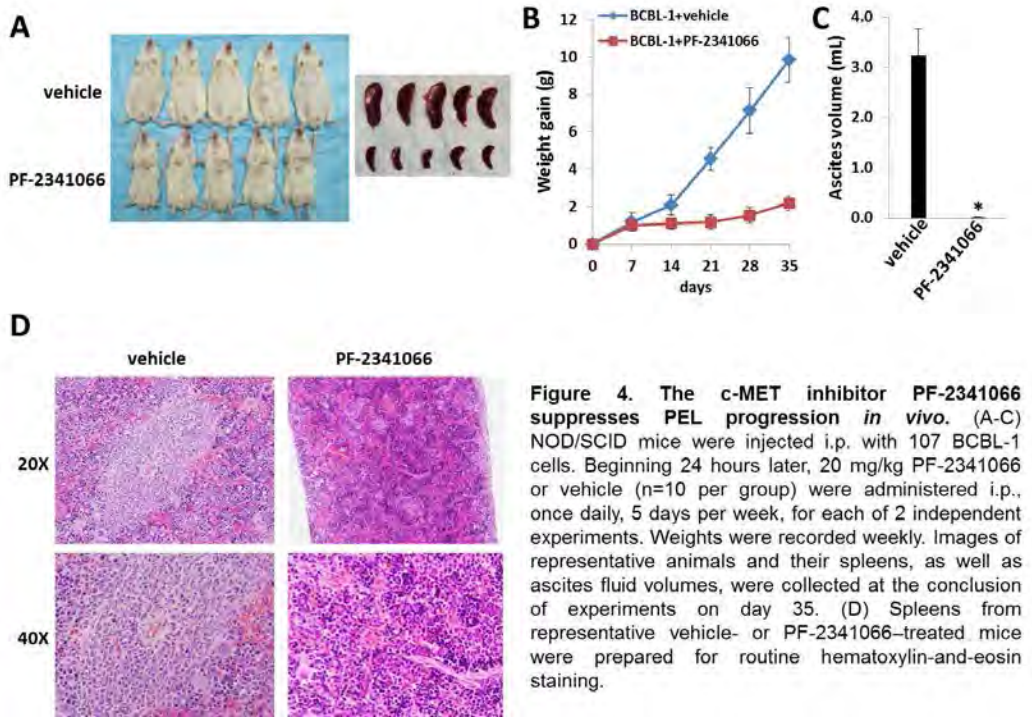

Figure 4. The c-MET inhibitor PF-2341066 suppresses PEL progression *in vivo*. (A-C) NOD/SCID mice were injected i.p. with 107 BCBL-1 cells. Beginning 24 hours later, 20 mg/kg PF-2341066 or vehicle (n=10 per group) were administered i.p., once daily, 5 days per week, for each of 2 independent experiments. Weights were recorded weekly. Images of representative animals and their spleens, as well as ascites fluid volumes, were collected at the conclusion of experiments on day 35. (D) Spleens from representative vehicle- or PF-2341066–treated mice were prepared for routine hematoxylin-and-eosin staining.

3.3. What opportunities for training and professional development has the project provided?

I have trained one postdoctor in my lab, Dr. Lu Dai, and she has published 8 papers during this funding period (as the first author in most publications). We also have displayed our data in several national or international meetings such as International Workshop on Kaposi's Sarcoma Associated Herpesvirus (KSHV) and Related Agents. With the support by this DOD award, I recently got a Leukemia Research Foundation pilot funding about the sphingolipid metabolism in AIDS-related lymphomas, although which is NOT overlapped with the current project.

3.4. How were the results disseminated to communities of interest?

Nothing to Report.

3.5. What do you plan to do during the next reporting period to accomplish the goals?

We will continue to study: **1)** whether HGF/c-MET pathway affects viral gene expression in PEL cells; **2)** functional validation of HGF/c-MET controlled downstream genes identified by microarray analysis and their contribution to PEL pathogenesis; **3)** how viral proteins activate HGF/c-MET pathway from PEL cells; **4)** the underlying mechanisms through which c-MET inhibitor suppression of PEL expansion *in vivo*.

4. IMPACT

4.1. What was the impact on the development of the principal discipline(s) of the project?

Our results have illuminated the molecular mechanisms through which the HGF/c-MET pathway regulates KSHV+ PEL cell survival. Our promising *in vivo* data have provided the framework for development and implementation of clinical trials for evaluating strategies targeting HGF/c-MET for the treatment of lymphoma in HIV-infected patients including military personnel.

4.2. What was the impact on other disciplines?

Nothing to Report.

4.3. What was the impact on technology transfer?

Nothing to Report.

4.4. What was the impact on society beyond science and technology?

Nothing to Report.

5. **CHANGES/PROBLEMS**

Nothing to Report.

6. PRODUCTS

6.1. Journal publications (totally 8, # as the corresponding author, all have acknowledgement of DoD federal support):

1. Dai L, Bai L, Lin Z, Yang L, Flemington EK, Zabaleta J, **Qin Z #**. Transcriptomic analysis of KSHV-infected primary oral fibroblasts: the role of interferon-induced genes in the latency of oncogenic virus. *Oncotarget,* 2016 May 30. doi: 10.18632/oncotarget.9720. [Epub ahead of print]. PMID: 27363016.
2. Dai L, Qiao J, Struckhoff AP, Nguyen D, Del Valle L, Parsons C, Ochoa AC, Toole BP, Renne R, **Qin Z #**. Role of heme oxygenase-1 in the pathogenesis and tumorigenicity of Kaposi's sarcoma-associated herpesvirus. *Oncotarget*. 2016;7(9):10459-71. PMCID: PMC4891132.
3. **Qin Z #,** Cao Y, Dai L **#**. Genomic analysis of xCT-regulatory network in KSHV+ primary effusion lymphomas. *Genomics Data*. 2016; 8: 16–7. PMCID: PMC4818344.
4. Dai L., Trillo-Tinoco J., Chen Y., Bonstaff K., Valle LD., Parsons C., Ochoa AC., Zabaleta J., Toole BP., **Qin, Z #**. CD147 and downstream ADAMTSs promote the tumorigenicity of Kaposi sarcoma-associated herpesvirus. *Oncotarget*, 2016;7(4):3806-18. PMCID: PMC4826171.
5. Dai L., Trillo-Tinoco J., Cao Y., Bonstaff K., Doyle L., Valle LD., Whitby D., Parsons C., Reiss K., Zabaleta J., **Qin, Z #**. Targeting HGF/c-MET induces cell cycle arrest, DNA damage and apoptosis for primary effusion lymphoma. *Blood,* 2015;126(26):2821-31. PMCID: PMC4692142.
6. Dai L., Trillo-Tinoco J., Bai A., Chen Y., Bielawski J., Valle LD., Smith CD., Ochoa AC., **Qin, Z #**., Parsons C **#.** Ceramides promote apoptosis for virus-infected lymphoma cells through induction of ceramide synthases and viral lytic gene expression. *Oncotarget*. 2015;6(27):24246-60. PMCID: PMC4695183.
7. Dai, L., Chen Y., Toole BP., Parsons, C., **Qin, Z #**. Induction of Hyaluronan Production by oncogenic KSHV and the Contribution to Viral Pathogenesis in AIDS Patients. *Cancer Lett*. 2015;362(2):158-66. PMCID: PMC4410079.
8. Dai, L., Cao Y., Chen Y., Kaleeba, J.A.R., Zabaleta**,** J., **Qin, Z #**. Genomic analysis of xCT-mediated regulatory network: identification of novel targets against AIDS-associated lymphoma. *Oncotarget*. 2015;6(14):12710-22. PMCID: PMC4494968.

6.2. Other publications, conference papers, and presentations:

1. Dai L, Trillo-Tinoco J, Lin Z, Del Valle L, Flemington EK and **Qin Z #**. "Role of HERV-K Transactivation in KSHV-related Malignancies". (Oral presentation) 19th International Workshop on Kaposi's Sarcoma Associated Herpesvirus (KSHV) and Related Agents, Los Angeles, CA, US, 2016.

2. Bonsignore L, Passelli K, Pelzer C, Konrad A, Thurau M, Stürzl M, Dai L, Trillo-Tinoco J, Del Valle L, **Qin Z #** and Thome M **#**. "A Role for MALT1 Activity in Kaposi's Sarcoma-Associated Herpesvirus Latency and Growth of Primary Effusion Lymphoma". The 2016 ASH Meeting on Lymphoma Biology in Colorado Springs, CO, US, 2016.

3. **Qin Z #,** Dai L and Toole BP. "The Role of Hyaluronan and Signaling in Virus-associated Lymphoma Chemoresistance". The 2016 ASH Meeting on Lymphoma Biology in Colorado Springs, CO, US, 2016.

4. Dai L, Trillo-Tinoco J, Del Vella L, Zabaleta J and **Qin Z #.** "Targeting HGF/c-MET pathway in KSHV+ Primary Effusion Lymphoma". (Oral presentation) 18th International Workshop on Kaposi's Sarcoma Associated Herpesvirus (KSHV) and Related Agents, Miami, FL, US, 2015.

5. **Qin Z,** Dai L, Trillo-Tinoco J, Del Vella L, Smith CD and Parsons C **#**. "Targeting Sphingolipid Metabolism in Virus-associated Lymphoma". (Oral presentation) 18th International Workshop on Kaposi's Sarcoma Associated Herpesvirus (KSHV) and Related Agents, Miami, FL, US, 2015.

6.3. Other Products:

We have deposited our microarray data about the regulatory network of HGF/c-MET pathway in KSHV+ PEL cell-lines to Gene Expression Omnibus (GEO) database (Accession number: GSE70594).

7. PARTICIPANTS & OTHER COLLABORATING ORGANIZATIONS

7.1. What individuals have worked on the project?

Name:	*Zhiqiang Qin*
Project Role:	*PI*
Researcher Identifier (e.g. ORCID ID):	*N/A*
Nearest person month worked:	*6*
Contribution to Project:	*Dr. Qin is responsible for experimental design, data analysis, animal work and manuscript preparation*
Funding Support:	*Leukemia Research Foundation (NO-overlapping with the current project)*

Name:	*Chris Parsons*
Project Role:	*Mentor*
Researcher Identifier (e.g. ORCID ID):	*N/A*
Nearest person month worked:	*1.5*

Contribution to Project:	*Dr. Parsons is responsible for mentoring Dr. Qin's research work and participated in experimental design, manuscript preparation*
Funding Support:	*NIH/NCI (NO-overlapping with the current project)*

Name:	*Lu Dai*
Project Role:	*Postdoctor*
Researcher Identifier (e.g. ORCID ID):	*N/A*
Nearest person month worked:	*6*
Contribution to Project:	*Dr. Dai is responsible for cell culture, qRT-PCR, immunoblots, animal work etc*
Funding Support:	*N/A*

7.2. Has there been a change in the active other support of the PD/PI(s) or senior/key personnel since the last reporting period?

For Dr. Zhiqiang Qin:

Completed:

P20GM103501 (PI: Augusto Ochoa) 01/01/2012-06/30/2015 2.5 CM
NIH-NIGMS $120,000
Mentoring Translational Researchers in Louisiana
Project 12: KSHV regulation of emmprin, drug resistance, and tumor progression
Role: Pilot Project Leader

Active:

Leukemia Research Foundation 07/01/2016-06/30/2017 1.0CM
$100,000
Targeting sphingolipid metabolism in AIDS-related lymphomas
Role: Principal Investigator
NO-overlapping with the current project

For Dr. Chris Parsons:

Completed:

R01CA142362 02/01/2010-12/31/2014 4.2 CM
NIH-NCI $181,148

Regulation of the Tumor Microenvironment by KSH
Role: Principal Investigator

Active:

R42-CA183708 09/01/2014-08/31/2017 2.4 CM
NIH/NCI $900,092
An Early-Phase Clinical Trial Evaluating ABC294640 in Patients with Refractory/Relapsed Diffuse Large B-cell lymphoma
Role: Principal Investigator
NO-overlapping with the current project

UG1CA189854 (PI: Augusto Ochoa) 09/01/2014-08/31/2019 2.4 CM
NIH/ NCI $954,750
Gulf South Minority-based NCI Community Oncology Research Program (GS-MB-NCORP)
Role: Director – HIV Malignancies Program
NO-overlapping with the current project

7.3. What other organizations were involved as partners?

Nothing to Report.

8. SPECIAL REPORTING REQUIREMENTS

N/A

9. APPENDICES

The original copies of total 8 journal articles published during this funding period.

Transcriptomic analysis of KSHV-infected primary oral fibroblasts: The role of interferon-induced genes in the latency of oncogenic virus

Lu Dai[1,2,4,*], Lihua Bai[2,*], Zhen Lin[6], Jing Qiao[5], Liang Yang[7], Erik K. Flemington[6], Jovanny Zabaleta[8], Zhiqiang Qin[1,2,3]

[1]Department of Oncology, East Hospital, Tongji University School of Medicine, Shanghai, 200120, China

[2]Research Center for Translational Medicine and Key Laboratory of Arrhythmias, East Hospital, Tongji University School of Medicine, Shanghai, 200120, China

[3]Departments of Microbiology/Immunology/Parasitology, Louisiana State University Health Sciences Center, Louisiana Cancer Research Center, New Orleans, LA, 70112, USA

[4]Department of Medicine, Louisiana State University Health Sciences Center, Louisiana Cancer Research Center, New Orleans, LA, 70112, USA

[5]Department of Pediatrics, East Hospital, Tongji University School of Medicine, Shanghai, 200120, China

[6]Department of Pathology, Tulane University Health Sciences Center, Tulane Cancer Center, New Orleans, LA, 70112, USA

[7]Singapore Centre for Environmental Life Sciences Engineering (SCELSE), Nanyang Technological University, Singapore, 637551, Singapore

[8]Department of Pediatrics, Louisiana State University Health Sciences Center, Louisiana Cancer Research Center, New Orleans, LA, 70112, USA

[*]These authors contributed equally to this work

Correspondence to: Zhiqiang Qin, **email:** zqin@lsuhsc.edu

Keywords: *KSHV, interferon, oral fibroblast, viral oncogenesis*

Received: *March 27, 2016* ***Accepted:*** *May 20, 2016* ***Published:*** *May 30, 2016*

ABSTRACT

The Kaposi sarcoma-associated herpesvirus (KSHV) is the causative agent of Kaposi sarcoma (KS), the most common HIV/AIDS-associated tumor worldwide. Involvement of the oral cavity portends a poor prognosis for patients with KS, but the mechanisms for KSHV regulation of the oral tumor microenvironment are largely unknown. Infiltrating fibroblasts are found within KS lesions, and KSHV can establish latent infection within human primary fibroblasts *in vitro* and *in vivo*, but contributions for KSHV-infected fibroblasts to the KS microenvironment have not been previously characterized. In the present study, we used Illumina microarray to determine global gene expression changes in KSHV-infected primary human oral fibroblasts (PDLF and HGF). Among significantly altered candidates, we found that a series of interferon-induced genes were strongly up-regulated in these KSHV-infected oral cells. Interestingly, some of these genes in particular *ISG15* and *ISG20* are required for maintenance of virus latency through regulation of specific KSHV microRNAs. Our data indicate that oral fibroblasts may represent one important host cellular defense component against viral infection, as well as acting as a reservoir for herpesvirus lifelong infection in the oral cavity.

INTRODUCTION

Kaposi sarcoma-associated herpesvirus (KSHV) is one of the most common etiologic agents for cancers arising in the setting of immune suppression, including Kaposi sarcoma (KS)—the most common HIV/AIDS-associated tumor worldwide and a leading cause of morbidity and mortality in this population [1]. Oral involvement occurs in a substantial proportion of patients with KS [2]. Published literatures suggest that KSHV dissemination within and from the oral cavity are critical factors for KSHV infection and oral KS progression in HIV-infected patients [3–7]. Person-to-person transmission of KSHV is thought to occur primarily through exchange of oropharyngeal secretions [3, 4], and epidemiologic data indicate that sexual practices

involving contact with the oral cavity may promote KSHV transmission [5]. Furthermore, people have found that combination antiretroviral therapy (cART) cannot reduce KSHV replication within the oropharynx [3, 5] or KSHV transmission [7].

Oral KS lesions usually display higher KSHV viral loads and may portend more ominous prognoses relative to KS in other anatomic locations [8, 9]. We recently reported that KSHV successfully established latent infection in primary human gingival fibroblasts (HGF) or periodontal ligament fibroblasts (PDLF) *in vitro*, and virus *de novo* infection induced a tumor-associated fibroblast (TAF)-like phenotype within these cells [10]. Others also demonstrated that fibroblasts represented an imporant component within KS lesions and supported *de novo* KSHV infection [11, 12]. In addition, we recently reported that some pathogen-associated molecular patterns (PAMPs) molecules from periodontal pathogenic bacteria increased KSHV entry and subsequent viral latent gene expression within oral fibroblasts [13]. Despite this knowledge, the global altered gene expression profile in KSHV-infected oral fibroblasts has never been reported. KSHV needs to manipulate a number of host genes to facilitate the establishment of lifelong latent infection. In the current study, we used Illumina microarray to assess the altered gene profile in KSHV-infected PDLF and HGF relative to unifected mock cells. We found that the expression of various gene sets are significantly changed in virus-infected cells. In particular, KSHV *de novo* infection strongly up-regulates a series of interferon-induced gene in these oral cells, which are closely related to the maintenancy of virus latency.

RESULTS AND DISCUSSION

Microarray analysis of the global gene expression changes in *KSHV*-infected primary oral fibroblasts

We first used the HumanHT-12 v4 Expression BeadChip (Illumina), which contains more than 47,000 probes derived from the NCBI RefSeq Release 38 and other sources, to study global gene expression changes altered within KSHV-infected PDLF or HGF cells. We found that in PDLF cells, 134 genes were significantly up-regulated and 80 were down-regulated (≥ 2 fold and $p < 0.05$); in HGF cells, 166 genes were up-regulated and 268 down-regulated (Figure 1A). Intersection analysis indicated that 39 "common" genes were significantly up-regulated and 3 were down-regulated in both cell lines (listed in Table 1). We also performed enrichment analysis of these "common" genes in both cell lines by using the Pathway map, Gene Ontology (GO) Processes and Process Networks modules from Metacore Software (Thompson Reuters) [14]. Our analysis showed that most genes belong to several major cellular function categories, such as cellular response to type I interferon (IFN), inflammatory cytokine production, and other innate immune responses (Figure 2A–2B). The top 2 scored pathway maps (immune response_IFN α/β signaling pathway and immune response_Thymic stromal lymphopoietin [TSLP] signaling pathway) for these "common" genes are shown in Supplementary Figure S1. Interestingly, aberrant TSLP/TSLPR signaling has been associated with a variety of human diseases including asthma, atopic dermatitis, inflammatory bowel disease, eosinophilic esophagitis and acute lymphoblastic leukemia [15], but it has never been reported in KSHV infection and/or related malignancies.

IFN-induced genes are highly up-regulated in *KSHV*-infected primary oral fibroblasts

Among these "common" genes, we noticed that a series of IFN-induced genes were strongly up-regulated in KSHV-infected primary oral fibroblasts (Table 1). We next selected 8 IFN-induced genes from Table 1 for validation of their transcriptional changes by using qRT-PCR analysis. Our results indicated that all of these genes (*IFI27*, *IFI44*, *IFIT1*, *IFIT2*, *MX1*, *MX2*, *ISG15* and *ISG20*) were significantly up-regulated in a manner comparable to those found in the microarray data (Figure 1B–1C), demonstrating the credibility of our microarray analysis. Interestingly, when compared to the microarray data in KSHV-infected primary endothelial cells (HUVEC) we recently published [16], we found that the up-regulation of IFN-induced genes were much stronger in KSHV-infected PDLF/HGF than those in KSHV-infected HUVEC cells (Figure 2C). Production of IFN, in particular type I IFN is one of the most important host anti-viral immune responses, which can induce an anti-viral transcriptional program, producing proteins that cooperate to inhibit the spread of infection. Therefore, our data indicate that oral fibroblasts may represent an important cellular resource for type I IFN production during KSHV infection stimulus in the microenvironment of oral cavity. However, KSHV has successfully established the escape mechanisms from host immune responses, including the type I IFN response. For example, KSHV encodes 4 viral homologs of cellular interferon regulatory factors (named as vIRF1, −2, −3, and −4) with pleiotropic functions such as evasion of cell death, increased proliferation and evasion of immune responses [17]. For example, previous data have demonstrated that the expression of vIRF1 and vIRF2 can inhibit increases in IFN-β mediated by Toll-like receptor 3 (TLR3) [18]. In addition to their immunoregulatory effects, KSHV-encoded vIRFs were also shown to modulate cell growth by targeting the function of the tumor suppressor p53 and enhancing the activity of the c-Myc proto-oncogene [19]. While the KSHV-encoded vIRFs share an ability to block IFN or p53 signaling, each vIRF demonstrates a unique ability to block specific cellular functions [17].

IFN-induced genes, *ISG15* and *ISG20*, are required for maintenance of *KSHV* latency in oral fibroblasts

Like other herpesviruses, KSHV can establish a lifelong infection in the host, and in more than 90% of infected host cells, the virus exists in a latency stage. Here we found that at least 2 IFN-induced genes, *ISG15* and *ISG20*, are required for maintenance of KSHV latency in oral fibroblasts. Our data indicated that directly targeting *ISG15* or *ISG20* by RNAi significantly caused viral lytic gene (e.g. *Rta*, *vGpcr* and *K8.1*) transcripts from latently-infected PDLF with qRT-PCR analysis (Figure 3A and Supplementary Figure S2). We also confirmed the strong up-regulation of lytic K8.1 protein expression in either *ISG15* or *ISG20* "knock-down" KSHV-infected PDLF by using immunoblots (Figure 3B). Next, we isolated the KSHV virions from conditioned medium of *ISG15* or *ISG20* "knock-down" or control cells, then infected fresh PDLF cells. We found that silencing of either *ISG15* or *ISG20* greatly increased the virion release (there were more *Lana* transcripts in these infected groups compared to controls) (Figure 3C). Interestingly, one very recent study also reported that silencing of *ISG15* in KSHV latently infected iSLK.219 cells resulted in a higher level of virus reactivation and an increase in infectious virus production [20]. They also found that KSHV-encoded vIRF1 protein can inhibit IFN activation in response to viral infection, through interaction with HERC5, an ISG15 E3 ligase, to alter ISG15 modification of cellular proteins [20]. Interestingly, vIRF1 itself was also a target of ISG15 conjugation. KSHV-infected cells exhibited increased ISG15 conjugation upon reactivation from latency in coordination with increased IFN [20].

KSHV microRNAs are involved in viral lytic reactivation caused by silencing of *ISG15* or *ISG20*

KSHV-microRNAs (mostly miR-K12-1, 3, 4, 5, 7, 9 and 11) have been shown to positively or negatively regulate viral latency in a variety of infected host cells, through either directly targeting the viral lytic reactivation activator, Rta [21, 22], or through indirect mechanisms including targeting host factors such as IκBα, nuclear factor I/B (NFIB), Rbl2, BCLAF1 and IKKε [23–27]. By using qRT-PCR screening analysis, we found that silencing of *ISG15* prominently reduced the transcripts of miR-K12-1 and miR-K12-11, while silencing of *ISG20* caused a significant reduction of miR-K12-1 and miR-K12-3 in PDLF cells (Figure 4A–4B). To further confirm the role of specific viral microRNA in *ISG15*- or *ISG20*-mediated virus latency, we used individual recombinant construct encoding miR-K12-1 as described previously [28] to restore its expressional level. We found that this overexpression of miR-K12-1 significantly repressed KSHV lytic gene expression for infected PDLF

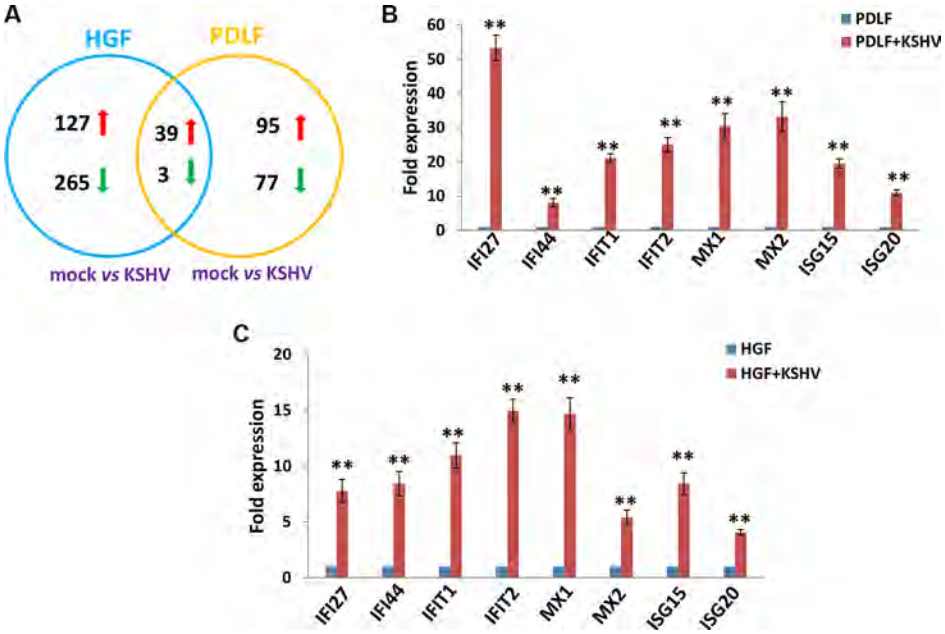

Figure 1: Intersection analysis and experimental validation of gene profile alterations in KSHV-infected primary oral fibroblast cells. (**A**) The HumanHT-12 v4 Expression BeadChip (Illumina) was used to detect alterations in gene profile in PDLF or HGF cells infected by KSHV (MOI~10, *vs* respective mock cells). Intersection analysis of significantly altered genes (up/down ≥ 2 fold and $p < 0.05$) was performed using the Illumina GenomeStudio Software. (**B**–**C**) The transcriptional levels of 8 selected 'common' candidate genes that were up-regulated in both sets of microarray data were validated by using qRT-PCR. Error bars represent the S.E.M. for 3 independent experiments. ** = $p < 0.01$ (*vs* PDLF or HGF).

Table 1: The "common" genes set altered within KSHV-infected HGF and PDLF cells (*vs* mock cells)

Gene Symbol	Gene Description	PDLF (folds)	HGF (folds)
IFI27	Interferon alpha-inducible protein 27, mitochondrial	57.85	6.07
RSAD2	Radical S-adenosyl methionine domain-containing protein 2	43.99	4.48
MX1	Interferon-induced GTP-binding protein Mx1	36.48	15.76
MX2	Interferon-induced GTP-binding protein Mx2	36.48	3.26
IFIT2	Interferon-induced protein with tetratricopeptide repeats 2	28.42	12.6
ISG15	Ubiquitin-like protein ISG15	23.67	7.46
IFIT1	Interferon-induced protein with tetratricopeptide repeats 1	19.65	11.95
IFITM1	Interferon-induced transmembrane protein 1	16.44	3.16
HERC6	Probable E3 ubiquitin-protein ligase HERC6	14.97	4.47
IFIT3	Interferon-induced protein with tetratricopeptide repeats 3	14.77	3.84
ISG20	Interferon-stimulated gene 20 kDa protein	12.03	3.38
IFI6	Interferon alpha-inducible protein 6	9.5	4.89
IFI44	Interferon-induced protein 44	9.13	9.24
SAMD9	Sterile alpha motif domain-containing protein 9	8.07	3.16
EPSTI1	Epithelial-stromal interaction protein 1	7.02	3.53
RARRES3	Retinoic acid receptor responder protein 3	5.71	2.19
IFI35	Interferon-induced 35 kDa protein	5.64	2.35
XAF1	XIAP-associated factor 1	5.32	2.22
DDX58	Probable ATP-dependent RNA helicase DDX58	4.85	2.19
SAMD9L	Sterile alpha motif domain-containing protein 9-like	4.7	3.08
STAT1	Signal transducer and activator of transcription 1-alpha/beta	4.6	2.29
PARP12	Poly [ADP-ribose] polymerase 12	4.38	2.06
DDX60	Probable ATP-dependent RNA helicase DDX60	4.04	2.25
MYPN	Myopalladin	3.26	2.3
IL12A	Interleukin-12 subunit alpha	3.03	5.81
PSG7	Putative pregnancy-specific beta-1-glycoprotein 7	3.02	4.46
COL4A1	Collagen alpha-1(IV) chain	2.72	2.56
PSG1	Pregnancy-specific beta-1-glycoprotein 1	2.67	4.46
PSG2	Pregnancy-specific beta-1-glycoprotein 2	2.67	6.05
ANO3	Anoctamin-3	2.54	6.2
IL7R	Interleukin-7 receptor subunit alpha	2.48	6.46
NR2C1	Nuclear receptor subfamily 2 group C member 1	2.39	6.34
PSG4	Pregnancy-specific beta-1-glycoprotein 4	2.39	6.34
GBP2	Interferon-induced guanylate-binding protein 2	2.38	2.44
KRTAP1-1	Keratin-associated protein 1-1	2.24	2.48
VEGFC	Vascular endothelial growth factor C	2.23	3.04

MT1M	Metallothionein-1M	2.21	2.05
KRT34	Keratin, type I cuticular Ha4	2.1	9.24
PSME2	Proteasome activator complex subunit 2	2.02	2.19
RCAN2	Calcipressin-2	0.47	0.41
CEMIP	Cell migration-inducing and hyaluronan-binding protein	0.4	0.07
ATP8B4	Probable phospholipid-transporting ATPase IM	0.38	0.25

cells during "knock-down" *ISG15* or *ISG20* with RNAi (Figure 4C). Published data have shown that miR-K12-1 can targets IκBα, an inhibitor of NF-κB complexes, thereby promoting NF-κB-dependent viral latency and cell survival [23]. Our recent data also demonstrate that the NF-κB pathway is important to KSHV-positive lymphoma cell survival and viral latency [29]. Therefore, ongoing work will try to understand the involvement of NF-κB pathway in either *ISG15*- or *ISG20*-mediated virus latency for oral cells.

In summary, we provide for the first time global gene expression profile alterations in KSHV-infected oral fibroblasts by microarray analysis. Among the altered candidates, many interferon-induced genes are strongly up-

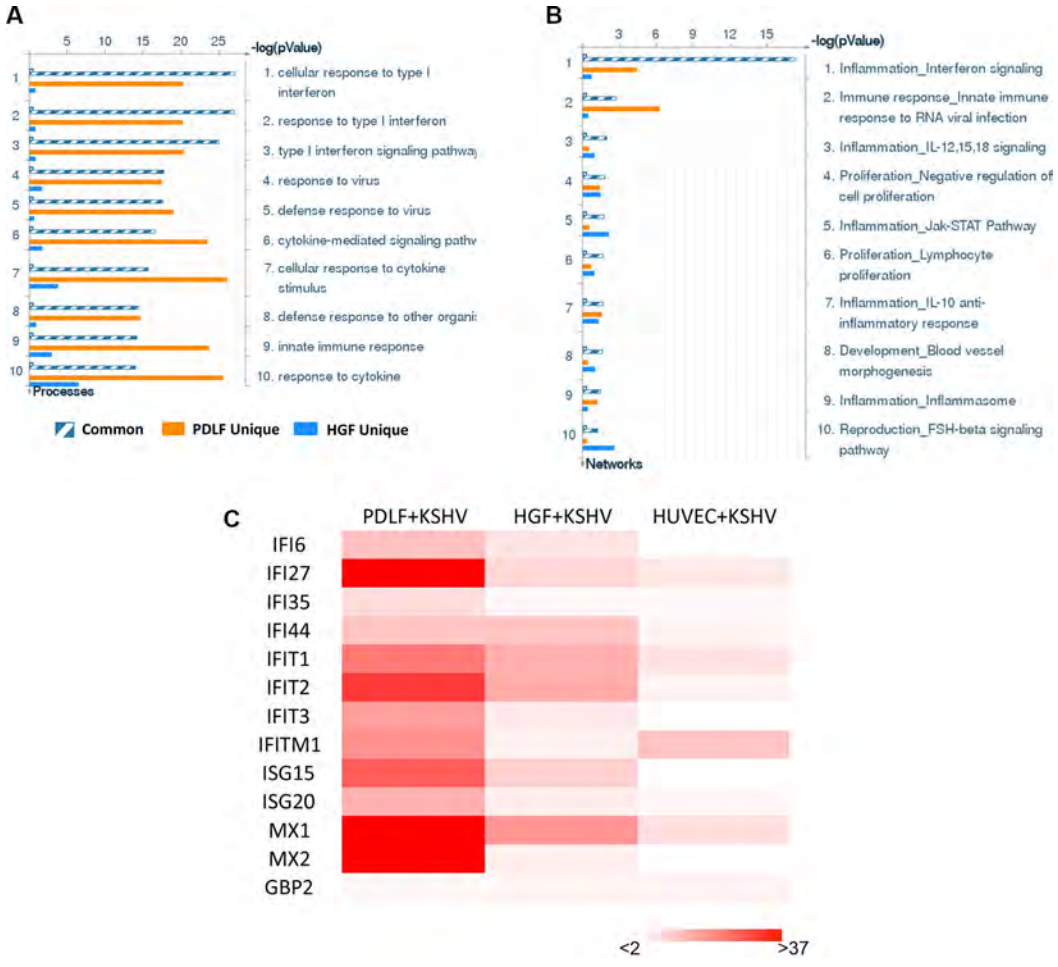

Figure 2: The enrichment analysis of gene profile alterations in KSHV-infected primary oral fibroblast cells. (**A**–**B**) The enrichment analysis of gene profile significantly altered (up/down ≥ 2 fold and $p < 0.05$) in KSHV-infected PDLF or HGF cells (*vs* mock cells) was performed using the Metacore Software (Thompson Reuters) Modules: Gene Ontology Processes (A) and Process Networks (B). (**C**) Heat map of interferon-induced genes signature altered in KSHV-infected PDLF, HGF and HUVEC cells (*vs* respective mock cells) was made by using Microsoft Excel 2010.

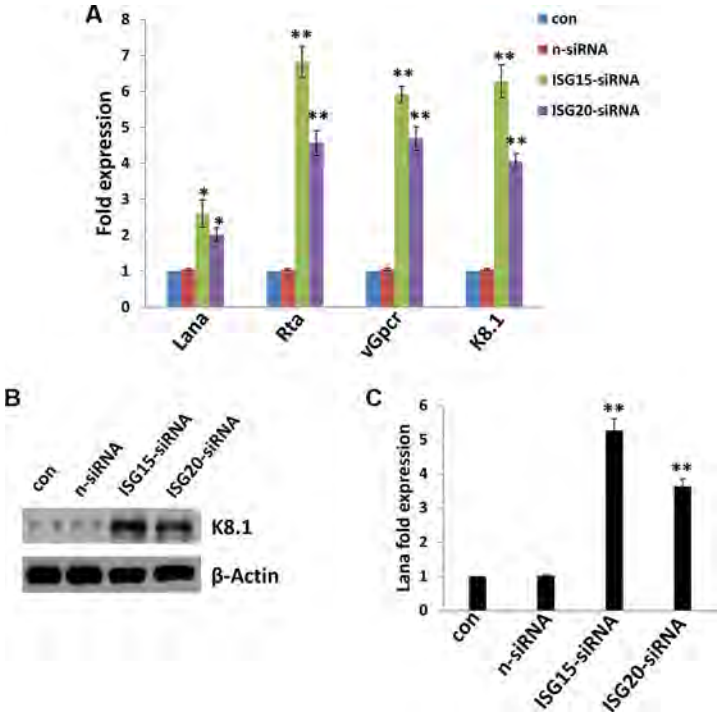

Figure 3: Targeting *ISG15* and/or *ISG20* induces KSHV lytic reactivation from infected primary oral fibroblast cells. (**A**–**B**) PDLF were first incubated with purified KSHV (MOI~10) for 2 h, then after 24 h p.i. transfected with either control non-target (n-siRNA), *ISG15*-siRNA or *ISG20*-siRNA for additional 48 h. Viral representative latent (*Lana*) and lytic gene (*Rta*, *vGpcr*, *K8.1*) transcripts were quantified using qRT-PCR. Protein expression was measured by immunoblots. (**C**) Released virions was isolated and purified from supernatant from groups in (A), then used to infect fresh PDLF cells. After 24 h p.i., *Lana* transcripts were quantified using qRT-PCR. Error bars represent the S.E.M for three independent experiments. * = $p < 0.05$, ** = $p < 0.01$ (*vs* n-siRNA group).

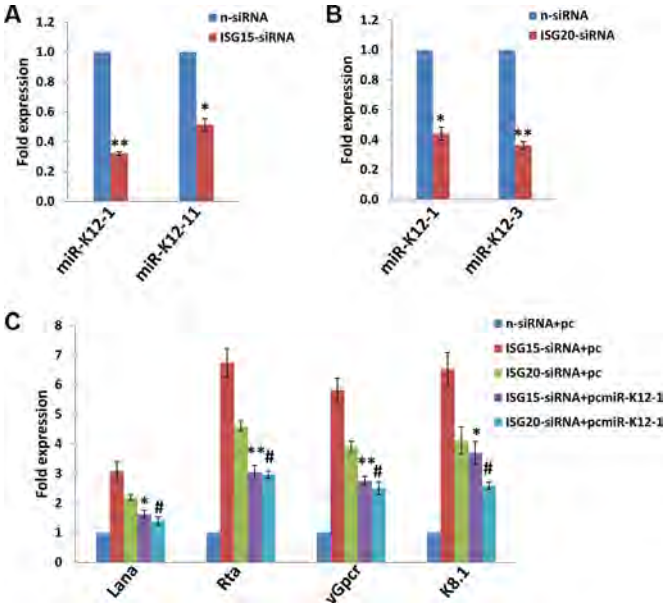

Figure 4: Targeting *ISG15* and/or *ISG20* induces KSHV lytic gene expression through suppression of KSHV microRNAs. (**A**–**B**) PDLF were first incubated with purified KSHV (MOI~10) for 2 h, then after 24 h p.i. transfected with either control non-target (n-siRNA), *ISG15*-siRNA or *ISG20*-siRNA for additional 48 h. KSHV microRNA transcripts were quantified using qRT-PCR as described in Methods. (**C**) PDLF were incubated with purified KSHV for 2 h, then transfected with control vector (pc), or vectors encoding miR-K12-1 (pcmiR-K12-1) for additional 24 h. Thereafter, cells were transfected with either control non-target (n-siRNA), *ISG15*-siRNA or *ISG20*-siRNA for additional 48 h. Viral representative latent (*Lana*) and lytic gene (*Rta*, *vGpcr*, *K8.1*) transcripts were quantified using qRT-PCR. Error bars represent the S.E.M for three independent experiments. */# = $p < 0.05$, ** = $p < 0.01$ (*vs ISG15*-siRNA+pc or *ISG20*-siRNA+pc groups, respectively).

regulated in these oral cells, while some of them such as *ISG15* and *ISG20* are required for the maintenance of virus latency. Our data indicate that oral fibroblasts may represent one of the important host cellular defense components for anti-viral infection, as well as acting as a reservoir for herpesvirus lifelong infection in the oral cavity.

MATERIALS AND METHODS

Cell culture, reagents and infection protocol

Body cavity-based lymphoma cells (BCBL-1, $KSHV^{+}/EBV^{-}$) were maintained in RPMI 1640 medium (Gibco) with supplements as described previously [29]. Primary human gingival fibroblasts (HGF) and periodontal ligament fibroblasts (PDLF) were purchased from ScienCell. These cells were maintained in Dulbecco's modified Eagle's medium (DMEM, Mediatech) supplemented with 10% FBS, 10 mM HEPES (pH 7.5), 100 U/mL of penicillin, 100 µg/mL streptomycin, and 0.25 µg/mL amphotericin B. All cells were incubated at 37°C in 5% CO_2. All experiments were carried out using cells harvested at low (< 20) passages. To obtain KSHV for infection experiments, BCBL-1 cells were incubated with 0.6 mM valproic acid for 6 days, and purified virus was concentrated from culture supernatants and infectious titers were determined as described previously [28].

Microarray

Total RNA was isolated using Qiagen RNeasy kit (Qiagen), and 500 ng of total RNA was used to synthesize dscDNA. Biotin-labeled RNA was generated using the TargetAmp-Nano Labeling Kit for Illumina Expression BeadChip (Epicentre), according to the manufacturers' instructions, and hybridized to the HumanHT-12 v4 Expression BeadChip (Illumina), which contains more than 47,000 probes derived from the NCBI RefSeq Release 38 and other sources, at 58°C for 16 h. The chip was washed, stained with streptavadin-Cy3, and scanned with the Illumina BeadStation 500 and BeadScan. Using the Illumina's GenomeStudio software, we normalized the signals using the "cubic spline algorithm" that assumes that the distribution of transcript abundance is similar in all samples, according to the method proposed by Workman *et al.* [30]. The background signal was removed using the "detection *p*-value algorithm" to remove targets with signal intensities equal or lower than that of irrelevant probes (with no known targets in the human genome but thermodynamically similar to the relevant probes). Common and unique sets of genes and enrichment analysis were performed using the MetaCore Software (Thompson Reuters) as previously reported [14]. The microarray original data have been submitted to Gene Expression Omnibus (GEO) database (Accession number: GSE79548).

RNA interference and plasmid transfection

ISG15 and *ISG20* ON-TARGET plus SMART pool siRNA, or negative control siRNA (n-siRNA) (Dharmacon), were delivered using the DharmaFECT transfection reagent according to the manufacturer's instructions. For plasmid transfection, PDLF were transfected in 12-well plates with miR-K12-1 recombinant construct or control vector as previously described [28] by using Lipofectamine 3000 (Invitrogen) for 48 h. Transfection efficiency was normalized through co-transfection of a lacZ reporter construct and determination of β-galactosidase activity using a commercial β-galactosidase enzyme assay system according to the manufacturer's instructions (Promega).

Immunoblotting

Total cell lysates (20 µg) were resolved by 10% SDS–PAGE, transferred to nitrocellulose membranes, and immunoblotted with antibodies for K8.1 (ABI) and β-Actin (Sigma) for loading controls. Immunoreactive bands were identified using an enhanced chemiluminescence reaction (Perkin-Elmer), visualized by autoradiography and quantitated using Image-J software.

qRT-PCR

Total RNA was isolated using the RNeasy Mini kit (QIAGEN), and cDNA was synthesized from equivalent total RNA using a SuperScript III First-Strand Synthesis SuperMix Kit (Invitrogen) according to the manufacturer's instructions. Primers used for amplification of target genes are displayed in Supplementary Table S1. Amplification was carried out using an iCycler IQ Real-Time PCR Detection System, and cycle threshold (Ct) values were tabulated in duplicate for each gene of interest in each experiment. "No template" (water) controls were used to ensure minimal background contamination. Using mean Ct values tabulated for each gene, and paired Ct values for β-actin as a loading control, fold changes for experimental groups relative to assigned controls were calculated using automated iQ5 2.0 software (Bio-rad). For amplification of viral miRNAs, cDNA was synthesized using the Taqman miRNA RT kit (Applied Biosystems), and qPCR was performed using the Taqman MicroRNA Assays kit (Applied Biosystems) and a 7500 Real Time PCR System. Fold changes for microRNA were calculated using paired Ct values for RNU6B as recommended by the manufacturer (Applied Biosystems).

Statistical analysis

Significance for differences between experimental and control groups was determined using the two-tailed Student's *t*-test (Microsoft Excel 2010), and p values < 0.05 or <0.01 were considered significant or highly significant.

ACKNOWLEDGMENTS AND FUNDING

This work was supported by grants from a DOD Career Development Award (CA140437), the SOM Research Enhancement Funding (2015–2016) to Z.Q., the National Institute of General Medical Sciences (NIGMS P20GM103501 subproject 2, P30GM114732, U54GM104940-01), the National Institute on Minority Health and Health Disparities (NIMHD P20MD004817, U54MD008176-01) and the Louisiana Cancer Research Consortium to J.Z., a Louisiana Clinical and Translational Science Center Pilot grant (U54GM104940 from NIH) to Z.L., R01AI101046 and R01AI106676 from NIH to E.K.F., as well as awards from the National Natural Science Foundation of China (81272191, 81472547 to Z.Q. and 81400164 to L.D.). J.Q. was supported by funding from Shanghai Science and Technology committee (14411971400) and Pudong Science and Technology committee, Shanghai (PK2013-17). Funding sources had no role in study design, data collection and analysis, decision to publish, or preparation of the manuscript.

CONFLICTS OF INTEREST

All the authors declare no conflicts of interest.

REFERENCES

1. Chang Y, Cesarman E, Pessin MS, Lee F, Culpepper J, Knowles DM, Moore PS. Identification of herpesvirus-like DNA sequences in AIDS-associated Kaposi's sarcoma. Science. 1994; 266:1865–1869.
2. Feller L, Lemmer J, Wood NH, Jadwat Y, Raubenheimer EJ. HIV-associated oral Kaposi sarcoma and HHV-8: a review. J Int Acad Periodontol. 2007; 9:129–136.
3. Pauk J, Huang ML, Brodie SJ, Wald A, Koelle DM, Schacker T, Celum C, Selke S, Corey L. Mucosal shedding of human herpesvirus 8 in men. N Engl J Med. 2000; 343:1369–1377.
4. Casper C, Redman M, Huang ML, Pauk J, Lampinen TM, Hawes SE, Critchlow CW, Morrow RA, Corey L, Kiviat N, Wald A. HIV infection and human herpesvirus-8 oral shedding among men who have sex with men. J Acquir Immune Defic Syndr. 2004; 35:233–238.
5. Dukers NH, Renwick N, Prins M, Geskus RB, Schulz TF, Weverling GJ, Coutinho RA, Goudsmit J. Risk factors for human herpesvirus 8 seropositivity and seroconversion in a cohort of homosexual men. Am J Epidemiol. 2000; 151:213–224.
6. Miller CS, Berger JR, Mootoor Y, Avdiushko SA, Zhu H, Kryscio RJ. High prevalence of multiple human herpesviruses in saliva from human immunodeficiency virus-infected persons in the era of highly active antiretroviral therapy. J Clin Microbiol. 2006; 44:2409–2415.
7. Osmond DH, Buchbinder S, Cheng A, Graves A, Vittinghoff E, Cossen CK, Forghani B, Martin JN. Prevalence of Kaposi sarcoma-associated herpesvirus infection in homosexual men at beginning of and during the HIV epidemic. JAMA. 2002; 287:221–225.
8. Rohrmus B, Thoma-Greber EM, Bogner JR, Rocken M. Outlook in oral and cutaneous Kaposi's sarcoma. Lancet. 2000; 356:2160.
9. Gorsky M, Epstein JB. A case series of acquired immunodeficiency syndrome patients with initial neoplastic diagnoses of intraoral Kaposi's sarcoma. Oral Surg Oral Med Oral Pathol Oral Radiol Endod. 2000; 90:612–617.
10. Dai L, Qin Z, Defee M, Toole BP, Kirkwood KL, Parsons C. Kaposi sarcoma-associated herpesvirus (KSHV) induces a functional tumor-associated phenotype for oral fibroblasts. Cancer Lett. 2012; 318:214–220.
11. Akula SM, Naranatt PP, Walia NS, Wang FZ, Fegley B, Chandran B. Kaposi's sarcoma-associated herpesvirus (human herpesvirus 8) infection of human fibroblast cells occurs through endocytosis. J Virol. 2003; 77:7978–7990.
12. Offermann MK. Kaposi's sarcoma and HHV-8. Trends Microbiol. 1996; 4:419.
13. Dai L, DeFee MR, Cao Y, Wen J, Wen X, Noverr MC, Qin Z. Lipoteichoic acid (LTA) and lipopolysaccharides (LPS) from periodontal pathogenic bacteria facilitate oncogenic herpesvirus infection within primary oral cells. PLoS One. 2014; 9:e101326.
14. Kim SH, Sierra RA, McGee DJ, Zabaleta J. Transcriptional profiling of gastric epithelial cells infected with wild type or arginase-deficient Helicobacter pylori. BMC Microbiol. 2012; 12:175.
15. Zhong J, Sharma J, Raju R, Palapetta SM, Prasad TS, Huang TC, Yoda A, Tyner JW, van Bodegom D, Weinstock DM, Ziegler SF, Pandey A. TSLP signaling pathway map: a platform for analysis of TSLP-mediated signaling. Database (Oxford). 2014; 2014:bau007.
16. Dai L, Trillo-Tinoco J, Chen Y, Bonstaff K, Del Valle L, Parsons C, Ochoa AC, Zabaleta J, Toole BP, Qin Z. CD147 and downstream ADAMTSs promote the tumorigenicity of Kaposi's sarcoma-associated herpesvirus infected endothelial cells. Oncotarget. 2016; 7:3806–3818.
17. Jacobs SR, Damania B. The viral interferon regulatory factors of KSHV: immunosuppressors or oncogenes? Frontiers Immunol. 2011; 2:19.
18. Jacobs SR, Gregory SM, West JA, Wollish AC, Bennett CL, Blackbourn DJ, Heise MT, Damania B. The viral interferon regulatory factors of kaposi's sarcoma-associated herpesvirus differ in their inhibition of interferon activation mediated by toll-like receptor 3. J Virol. 2013; 87:798–806.
19. Baresova P, Pitha PM, Lubyova B. Distinct roles of Kaposi's sarcoma-associated herpesvirus-encoded viral interferon regulatory factors in inflammatory response and cancer. J Virol. 2013; 87:9398–9410.

20. Jacobs SR, Stopford CM, West JA, Bennett CL, Giffin L, Damania B. Kaposi's Sarcoma-Associated Herpesvirus Viral Interferon Regulatory Factor 1 Interacts with a Member of the Interferon-Stimulated Gene 15 Pathway. J Virol. 2015; 89:11572–11583.

21. Lin X, Liang D, He Z, Deng Q, Robertson ES, Lan K. miR-K12-7-5p encoded by Kaposi's sarcoma-associated herpesvirus stabilizes the latent state by targeting viral ORF50/RTA. PLoS One. 2011; 6:e16224.

22. Bellare P, Ganem D. Regulation of KSHV lytic switch protein expression by a virus-encoded microRNA: an evolutionary adaptation that fine-tunes lytic reactivation. Cell Host Microbe. 2009; 6:570–575.

23. Lei X, Bai Z, Ye F, Xie J, Kim CG, Huang Y, Gao SJ. Regulation of NF-kappaB inhibitor IkappaBalpha and viral replication by a KSHV microRNA. Nat Cell Biol. 2010; 12:193–199.

24. Lu CC, Li Z, Chu CY, Feng J, Sun R, Rana TM. MicroRNAs encoded by Kaposi's sarcoma-associated herpesvirus regulate viral life cycle. EMBO Rep. 2010; 11:784–790.

25. Liang D, Gao Y, Lin X, He Z, Zhao Q, Deng Q, Lan K. A human herpesvirus miRNA attenuates interferon signaling and contributes to maintenance of viral latency by targeting IKKepsilon. Cell Res. 2011; 21:793–806.

26. Ziegelbauer JM, Sullivan CS, Ganem D. Tandem array-based expression screens identify host mRNA targets of virus-encoded microRNAs. Nat Genet. 2009; 41:130–134.

27. Lu F, Stedman W, Yousef M, Renne R, Lieberman PM. Epigenetic regulation of Kaposi's sarcoma-associated herpesvirus latency by virus-encoded microRNAs that target Rta and the cellular Rbl2-DNMT pathway. J Virol. 2010; 84:2697–2706.

28. Dai L, Plaisance-Bonstaff K, Voelkel-Johnson C, Smith CD, Ogretmen B, Qin Z, Parsons C. Sphingosine kinase-2 maintains viral latency and survival for KSHV-infected endothelial cells. PLoS One. 2014; 9:e102314.

29. Qin Z, Dai L, Trillo-Tinoco J, Senkal C, Wang W, Reske T, Bonstaff K, Del Valle L, Rodriguez P, Flemington E, Voelkel-Johnson C, Smith CD, Ogretmen B, et al. Targeting Sphingosine Kinase Induces Apoptosis and Tumor Regression for KSHV-Associated Primary Effusion Lymphoma. Mol Cancer Ther. 2014; 13:154–164.

30. Workman C, Jensen LJ, Jarmer H, Berka R, Gautier L, Nielser HB, Saxild HH, Nielsen C, Brunak S, Knudsen S. A new non-linear normalization method for reducing variability in DNA microarray experiments. Genome Biol. 2002; 3:research0048.

Role of heme oxygenase-1 in the pathogenesis and tumorigenicity of Kaposi's sarcoma-associated herpesvirus

Lu Dai[1,3,*], Jing Qiao[4,*], David Nguyen[5], Amanda P. Struckhoff[6], Lisa Doyle[3], Karlie Bonstaff[3], Luis Del Valle[6], Chris Parsons[3], Bryan P. Toole[7], Rolf Renne[8] and Zhiqiang Qin[1,2]

[1] Research Center for Translational Medicine and Key Laboratory of Arrhythmias, East Hospital, Tongji University School of Medicine, Shanghai, China

[2] Departments of Microbiology/Immunology/Parasitology, Louisiana State University Health Sciences Center, Louisiana Cancer Research Center, New Orleans, LA, USA

[3] Department of Medicine, Louisiana State University Health Sciences Center, Louisiana Cancer Research Center, New Orleans, LA, USA

[4] Department of Pediatrics, East Hospital, Tongji University School of Medicine, Shanghai, China

[5] William Carey University College of Osteopathic Medicine, Hattiesburg, MS, USA

[6] Department of Pathology, Louisiana State University Health Sciences Center, Louisiana Cancer Research Center, New Orleans, LA, USA

[7] Department of Regenerative Medicine & Cell Biology, Medical University of South Carolina and Hollings Cancer Center, Charleston, SC, USA

[8] Department of Molecular Genetics Microbiology, University of Florida, Gainesville, FL, USA

[*] These authors have contributed equally to this work

Correspondence to: *Zhiqiang Qin,* ***email***: *zqin@lsuhsc.edu*

Keywords: KSHV, Kaposi's sarcoma, HO-1, SnPP

Received: *December 20, 2015* ***Accepted***: *January 27, 2016* ***Published***: *February 07, 2016*

ABSTRACT

Kaposi's Sarcoma-associated Herpesvirus (KSHV) is the etiologic agent of several malignancies, including Kaposi's Sarcoma (KS), which preferentially arise in immunocompromised patients such as HIV+ subpopulation and lack effective therapeutic options. Heme oxygenase-1 (HO-1) has been reported as an important regulator of endothelial cell cycle control, proliferation and angiogenesis. HO-1 has also been found to be highly expressed in KSHV-infected endothelial cells and oral AIDS-KS lesions. We previously demonstrate that the multifunctional glycoprotein CD147 is required for KSHV/LANA-induced endothelial cell invasiveness. During the identification of CD147 controlled downstream genes by microarray analysis, we found that the expression of HO-1 is significantly elevated in both CD147-overexpressing and KSHV-infected HUVEC cells when compared to control cells. In the current study, we further identify the regulation of HO-1 expression and mediated cellular functions by both CD147 and KSHV-encoded LANA proteins. Targeting HO-1 by either RNAi or the chemical inhibitor, SnPP, effectively induces cell death of KSHV-infected endothelial cells (the major cellular components of KS) through DNA damage and necrosis process. By using a KS-like nude mouse model, we found that SnPP treatment significantly suppressed KSHV-induced tumorigenesis *in vivo*. Taken together, our data demonstrate the important role of HO-1 in the pathogenesis and tumorigenesis of KSHV-infected endothelial cells, the underlying regulatory mechanisms for HO-1 expression and targeting HO-1 may represent a promising therapeutic strategy against KSHV-related malignancies.

INTRODUCTION

Kaposi sarcoma-associated herpesvirus (KSHV) represents a principal causative agent of cancers arising in immunocompromised patients, such as Kaposi's Sarcoma (KS) [1]. In some Acquired Immunodeficiency Syndrome (AIDS) pandemic counties of Africa, KS has become one of the commonest cancers affecting men and children with significant morbidity and mortality [2-5]. Although the incidence of AIDS-associated KS (AIDS-KS) in the Western world has declined since the widespread implementation of combined antiretroviral treatment (cART), up to 50% of patients with AIDS-KS never achieve total remission [6]. In addition, the issues of KS in the context of immune reconstitution inflammatory syndrome (IRIS) and its impact on cART rollout initiatives have become increasingly apparent recently [7-9]. Furthermore, although treatments for KS exist, none is curative, which requires better understanding the mechanisms for viral pathogenesis and tumorigenesis and developing more effective therapeutic strategies.

Heme oxygenases (HOs) are responsible for the oxidative cleavage of the heme ring, the rate-limiting step in heme catabolism [10]. Enzymatic degradation of heme releases carbon monoxide (CO), free iron, and biliverdin, which is subsequently converted to bilirubin by biliverdin reductase [10]. So far, 3 mammalian isoforms of HO have been identified: the stress-inducible HO-1 and the constitutive HO-2 and HO-3. Among them, HO-1 is strongly and rapidly up-regulated by noxious stimuli leading to oxidative stress such as transitional metals, glutathione-depleting agents and heat shock [11]. HO-1 has been recently defined as an important regulator of endothelial cell cycle control, proliferation, vascular endothelial growth factor (VEGF) secretion, and angiogenesis [12]. Interestingly, a recent study has shown the elevated HO-1 expression and activity in KSHV-infected endothelial cells as well as oral AIDS-KS lesions [13]. Another study has shown that targeting HO-1 by shRNA and chemical inhibitor, tin protoporphyrin IX (SnPP), can impair KSHV-encoded G protein-coupled receptor (vGPCR)-induced survival, proliferation, transformation and tumor growth [14]. However, the vGPCR ectopic expressed cells cannot completely represent whole virus infection situation either *in vitro* or *in vivo*. During KSHV *de novo* infection, only a small proportion of infected cells expressing vGPCR, since it is a lytic protein while most cells are in latency. Another remaining question is that the mechanisms for KSHV activation of HO-1 through either viral proteins or host factors still remain largely unknown.

The multifunctional transmembrane protein, CD147, also known as Emmprin or Basigin, induces the expression and secretion of multiple matrix metalloproteinases (MMPs), thereby promoting tumor cell invasion and other malignant behaviors [15, 16]. We recently reported that enhancement of invasiveness in primary endothelial cells (the major cellular components of KS), following *de novo* KSHV infection, results from upregulation of CD147 by the KSHV-encoded latency-associated nuclear antigen (LANA) protein [17]. Our recent microarray data indicate that as one of CD147 potentially controlled downstream candidates, the transcription of *HO-1* gene is significantly elevated in both CD147-overexpressing and KSHV-infected human umbilical vein endothelial cells (HUVEC) (25.8 and 2.31 folds, respectively) [18]. Therefore, in the current study we will continue to experimentally validate the regulation of HO-1 by CD147 and viral latent protein, investigate the role of HO-1 in KSHV-infected endothelial cell pathogenesis and tumorigenesis, and determine the anti-cancer effects of a HO-1 selective inhibitor by using an established KS-like xenograft model.

RESULTS

KSHV infection upregulates HO-1 expression through CD147 *in vitro* and *in vivo*

We first used qRT-PCR to validate the microarray data as mentioned above. Our results indicated that the transcriptional level of *HO-1* was increased ~25 and ~4.5 folds in CD147-overexpressing and KSHV-infected HUVEC, respectively (Figure 1A). Moreover, the expression of HO-1 protein was also significantly upregulated in CD147-overexpressing and KSHV-infected HUVEC, when compared to the controls (Figure 1B). We next compared the expression of CD147 and HO-1 between KSHV long-term-infected telomerase-immortalized human umbilical vein endothelial (TIVE-LTC) and non-infected parental TIVE cells [19]. We found that the expressional levels of CD147 and HO-1 were much higher in TIVE-LTC than in TIVE cells (Figure 1C). Silencing of CD147 by RNAi greatly reduced HO-1 expression in TIVE-LTC and KSHV-infected HUVEC (Figure 1D and S1). Furthermore, we found significantly elevated expression of CD147 and HO-1 within KS tumor tissues isolated from 3 cohort HIV+ patients when compared to adjacent normal area (Figure 1E). Taken together, our data demonstrate that KSHV upregulates HO-1 expression through CD147 in endothelial cells, and the high co-expression of these 2 proteins in AIDS-KS tissues indicating their importance to tumor development.

Inhibition of HO-1 inducing KSHV-infected endothelial cell death is independent of apoptosis

We next tested the effects of the HO-1 selective inhibitor, SnPP, on KSHV-infected endothelial cell growth/survival. We first confirmed the inhibition of HO-1

enzymatic activities from TIVE-LTC by SnPP treatment (Figure S2), using a biochemical assay [13, 20]. By using the WST-1 assays, we found that SnPP treatment reduced TIVE-LTC proliferation in a dose-dependent manner, whereas it only slightly reduced non-infected TIVE proliferation especially at the highest concentration (50 μM) (Figure 2A). Additionally, flow cytometry data confirmed that SnPP treatment significantly induced TIVE-LTC cell death (PI+) in a dose-dependent manner, whereas it only affected a small percentage of non-infected TIVE cells at the highest concentration (50 μM) (Figure 2B-2C). Interestingly, we did not detect any Annexin V+ cells at the time of collecting samples (Figure 2C). To determine whether this kind of cell death is really independent of apoptosis or is converted from early apoptotic cells, we collected SnPP-treated TIVE-LTC at early time points (10-120 min) and performed a similar flow cytometry analysis. Our time-course results indicated that SnPP gradually induced TIVE-LTC cell death which is indeed independent of apoptosis (no Annexin V+ cells were detected at any time-point during the period) (Figure 2D-2E). To further support the flow cytometry results, we also detected the expression of apoptosis markers including cleaved-caspase 3 and 9 [21] in these samples and found no detectable cleaved-caspases expression in SnPP-treated cells (data not shown). Also, the pan-caspase inhibitor Z-VAD-FMK [22] pretreatment cannot prevent SnPP-induced cell death in TIVE-LTC (Figure 2F). To exclude the off-target effects of SnPP causing cell death, we knocked down HO-1 by RNAi and found that it also induced significant TIVE-LTC cell death while minimally affecting TIVE cell viability (Figure S3).

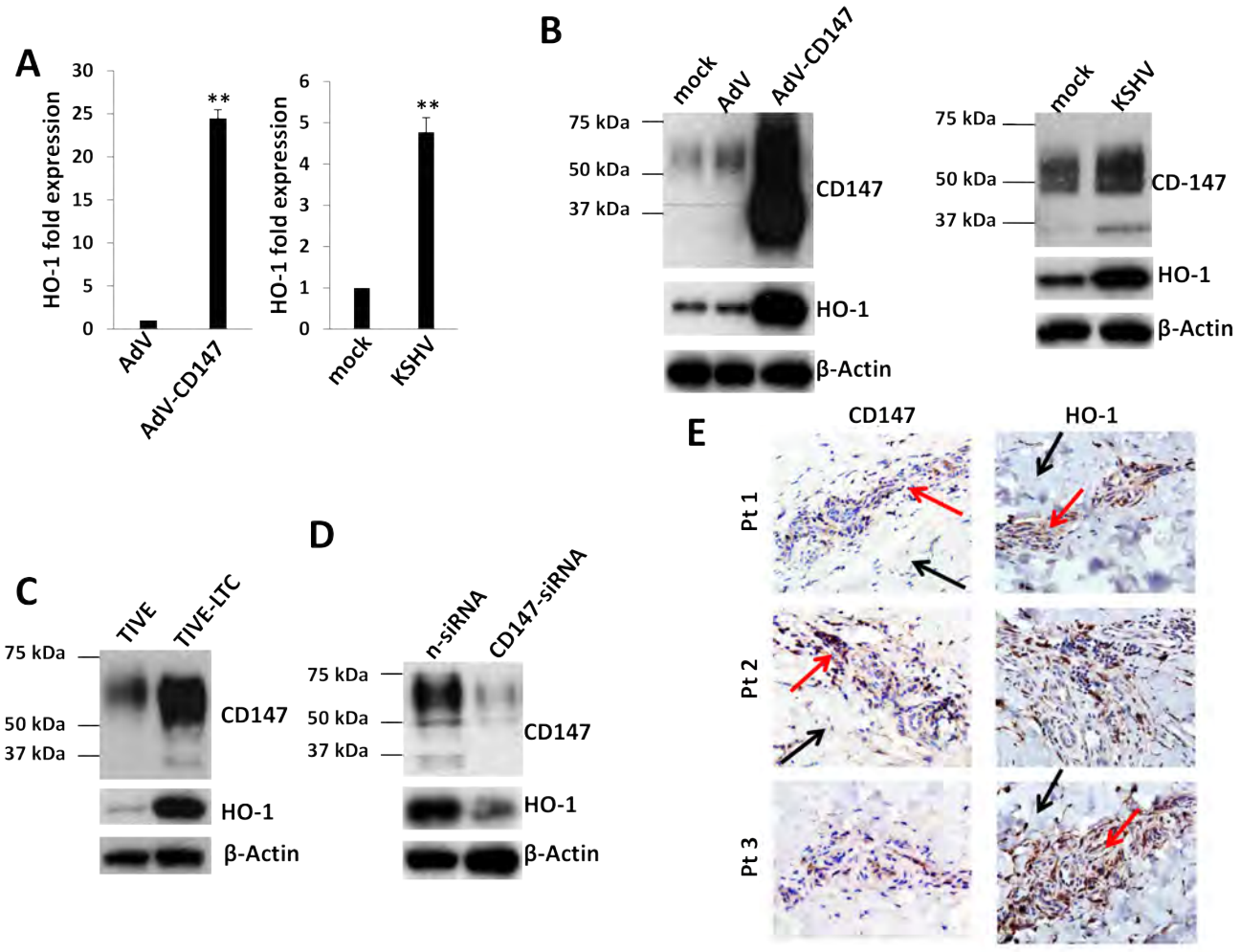

Figure 1: KSHV infection upregulates HO-1 expression through CD147 *in vitro* and *in vivo*. A.-B. HUVEC were transduced using a recombinant human CD147-encoding adenovirus (AdV-CD147), or control adenovirus (AdV) for 48 h, or infected by purified KSHV (MOI ~ 10) for 48 h. Gene transcription and protein expression were measured by qRT-PCR and immunoblots, respectively. Error bars represent the S.E.M. for 3 independent experiments. ** = $p < 0.01$. **C.-D.** Protein expression within KSHV stably infected TIVE-LTC and non-infected parental TIVE was compared by immunoblots. Some TIVE-LTC were transfected with negative control siRNA (n-siRNA) or *CD147*-siRNA for 48 h, prior to immunoblots. **E.** The expression of CD147 and HO-1 within KS tumor tissues from 3 cohort HIV-infected patients was detected by immunohistochemistry (400x magnification). Red arrows indicate the KS tumor area and black arrows indicate the adjacent normal area from the same patient.

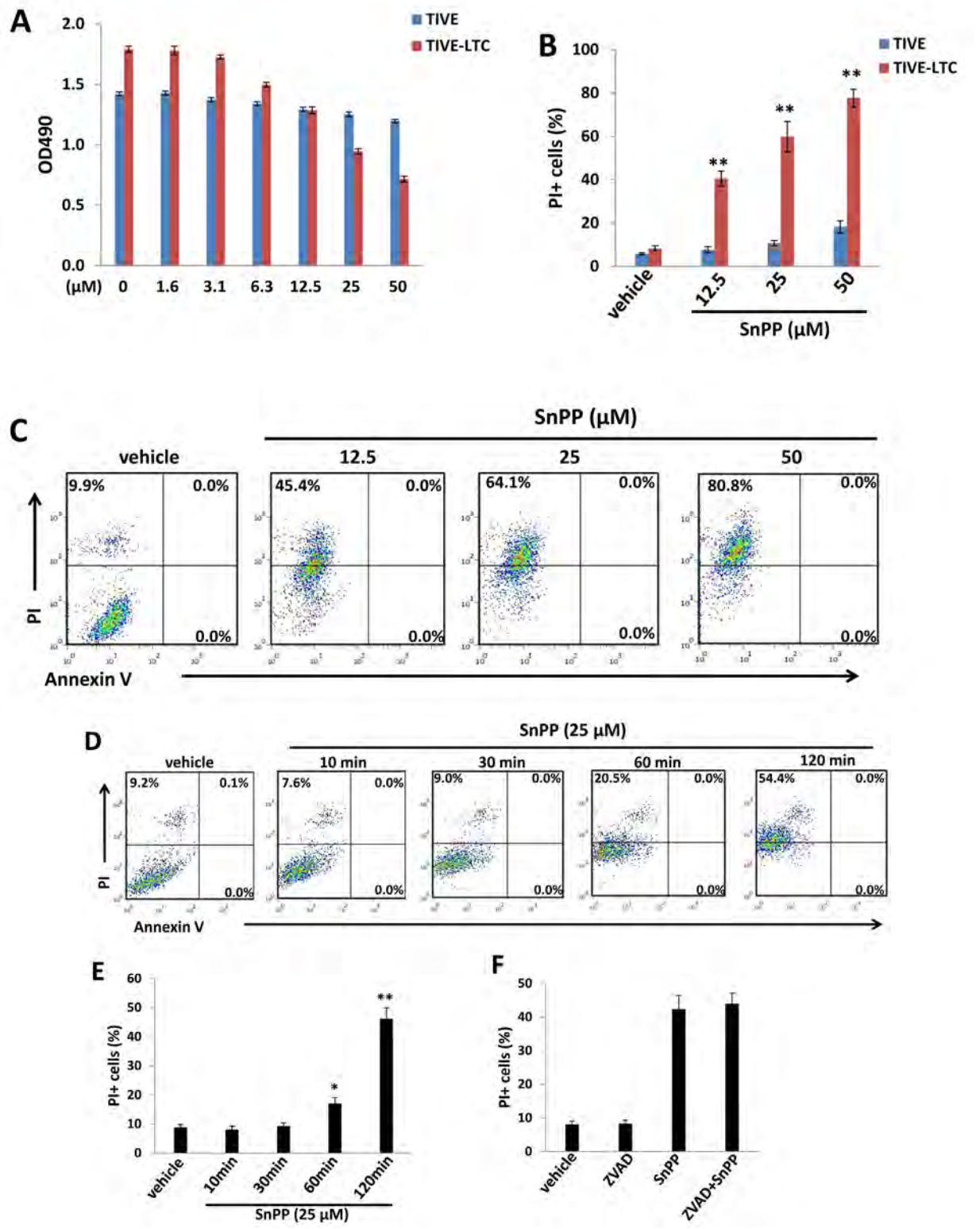

Figure 2: Targeting HO-1 by SnPP inducing KSHV-infected endothelial cell death is independent of apoptosis. A. TIVE-LTC and TIVE were incubated with indicated concentrations of SnPP for 48 h, then cell proliferation was measured by the WST-1 assays as described in the Methods. **B.-C.** TIVE-LTC and TIVE were incubated with vehicle or indicated concentrations of SnPP for 24 h, then cell viability and apoptosis were measured by Annexin V-PI staining and flow cytometry analysis. TIVE-LTC were shown as an example for cell subpopulation diagram in panel C. **D.-E.** TIVE-LTC were incubated with vehicle or 25 μM of SnPP for indicated time, then cell viability and apoptosis were measured as above. **F.** TIVE-LTC were incubated with or without the pan-caspase inhibitor Z-VAD-FMK (ZVAD, 25 μM) for 2 h, followed by vehicle or 25 μM of SnPP treatment for another 2 h. Error bars represent the S.E.M. for 3 independent experiments. * = $p < 0.05$, ** = $p < 0.01$.

Targeting HO-1 by SnPP causes DNA damage and necrosis in KSHV-infected endothelial cells

To further understand how SnPP causes cell death of TIVE-LTC, we analyzed the expression of DNA damage and necrosis markers. SnPP treatment greatly increased the expression of DNA damage marker, phosphor-H2A.X as well as two necrosis makers, Cyclophilin-A and HMGB1 [23] in TIVE-LTC as demonstrated by immunoblots analysis (Figure 3A). In comparison, we found no change of autophagy marker, LC3 [24], in SnPP-treated TIVE-LTC when compared to vehicle-treated controls (data not shown), indicating SnPP-caused cell death is not through autophagy. Immunofluorescence analysis confirmed the apparent upregulation of phosphor-H2A.X, Cyclophilin-A and HMGB1 in SnPP-treated TIVE-LTC (Figure 3B and S4). SnPP caused DNA damage was further demonstrated by CometAssay (the obvious comet tail moment in SnPP-treated TIVE-LTC when compared to vehicle-treated cells as shown in Figure 3C).

Low doses of SnPP impair TIVE-LTC invasiveness and anchorage-independent growth

Pro-angiogenic cytokines such as VEGF, are secreted by KSHV-infected cells, and their presence within KS lesions and the peripheral circulation of KS patients is thought to facilitate KSHV-associated cellular pathogenesis and angiogenesis [25, 26]. Moreover, acquisition of a migratory or invasive phenotype represents one hallmark of KSHV-infected endothelial cells, with implications for both viral dissemination and angiogenesis within KS lesions [27]. Here we found that low doses of SnPP (0.5-1.0 μM) effectively reduced VEGF production as well as VEGF receptor gene transcription in particular VEGFR1 in TIVE-LTC (Figure 4A-4B). Furthermore, we found that low doses of SnPP significantly impaired TIVE-LTC invasiveness and anchorage-independent growth, by using transwell and soft agar assays, respectively (Figure 4C-4D).

KSHV-encoded LANA protein is responsible for upregulation of HO-1 expression

We next aimed to determine which viral proteins are potentially responsible for upregulation of HO-1 in endothelial cells. We previously reported that KSHV-encoded latency-associated nuclear antigen (LANA) alone was sufficient to induce CD147 expression in HUVEC [17, 28]. The LANA protein sequence can be divided into three functional domains: a conserved proline- and serine-rich N-terminal region (domain A), a central region composed of several acidic repeats (domain B), and a conserved C-terminal domain containing a proline-rich region and a region rich in charged and hydrophobic amino acids (domain C) [29]. Both N- and C- terminal domains contain a nuclear localization sequence (NLS, Figure 5A). By using a variety of LANA deletion fragment and full-length constructs, we found that LANA domain A (LANA-A) was sufficient for the upregulation of CD147 and HO-1 expression as full-length LANA did in HUVEC (Figure 5B). We also found that silencing of CD147 by RNAi significantly reduced the expression of HO-1 in LANA-transfected HUVEC (Figure S5). Furthermore, ectopic expression of LANA in HUVEC increased VEGF production and cell invasion, whereas which can be significantly blocked by silencing of HO-1 with specific siRNA (Figure 5C-5E).

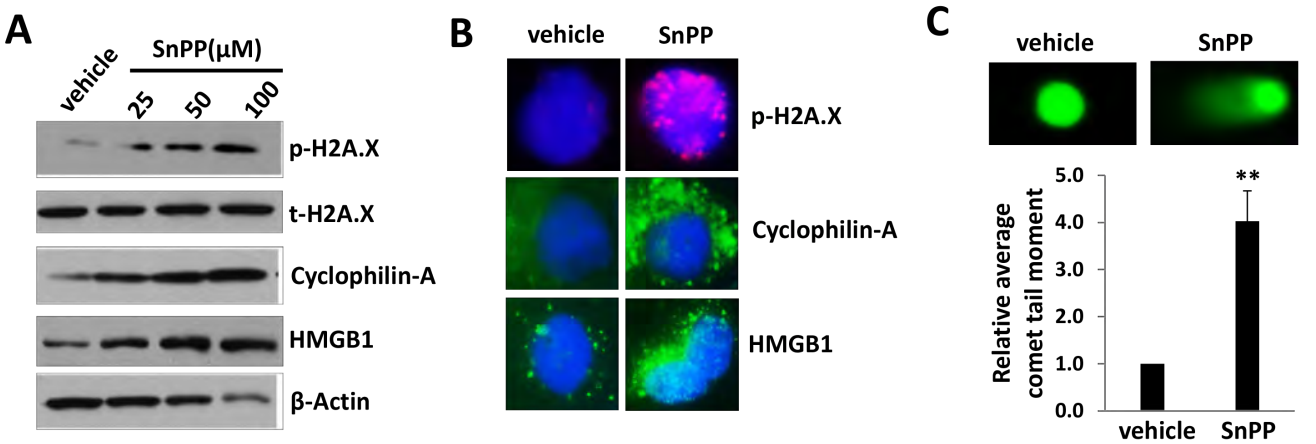

Figure 3: SnPP treatment causes DNA damage and necrosis for KSHV-infected endothelial cells. A. TIVE-LTC were incubated with vehicle or indicated concentrations of SnPP for 24 h, then protein expression were measured by immunoblots. **B.-C.** TIVE-LTC were incubated with vehicle or 50 μM of SnPP for 24 h, then protein expression and DNA damage were measured by immunofluorescence and CometAssay, respectively. Error bars represent the S.E.M. for 2 independent experiments. ** = $p < 0.01$.

SnPP treatment effectively suppresses TIVE-LTC tumorigenesis *in vivo*

By using an established KS-like nude mouse model with TIVE-LTC [18, 19], we tested the effects of SnPP on TIVE-LTC tumorigenesis *in vivo*. We injected TIVE-LTC (5×10^5 cells 1:1 with growth factor-depleted Matrigel) subcutaneously into the right and left flanks of nude mice (3 mice per group), respectively. When tumors reached 10-15 mm in diameter (~1.5weeks), mice received *in situ* subcutaneous injection with either vehicle or SnPP (10

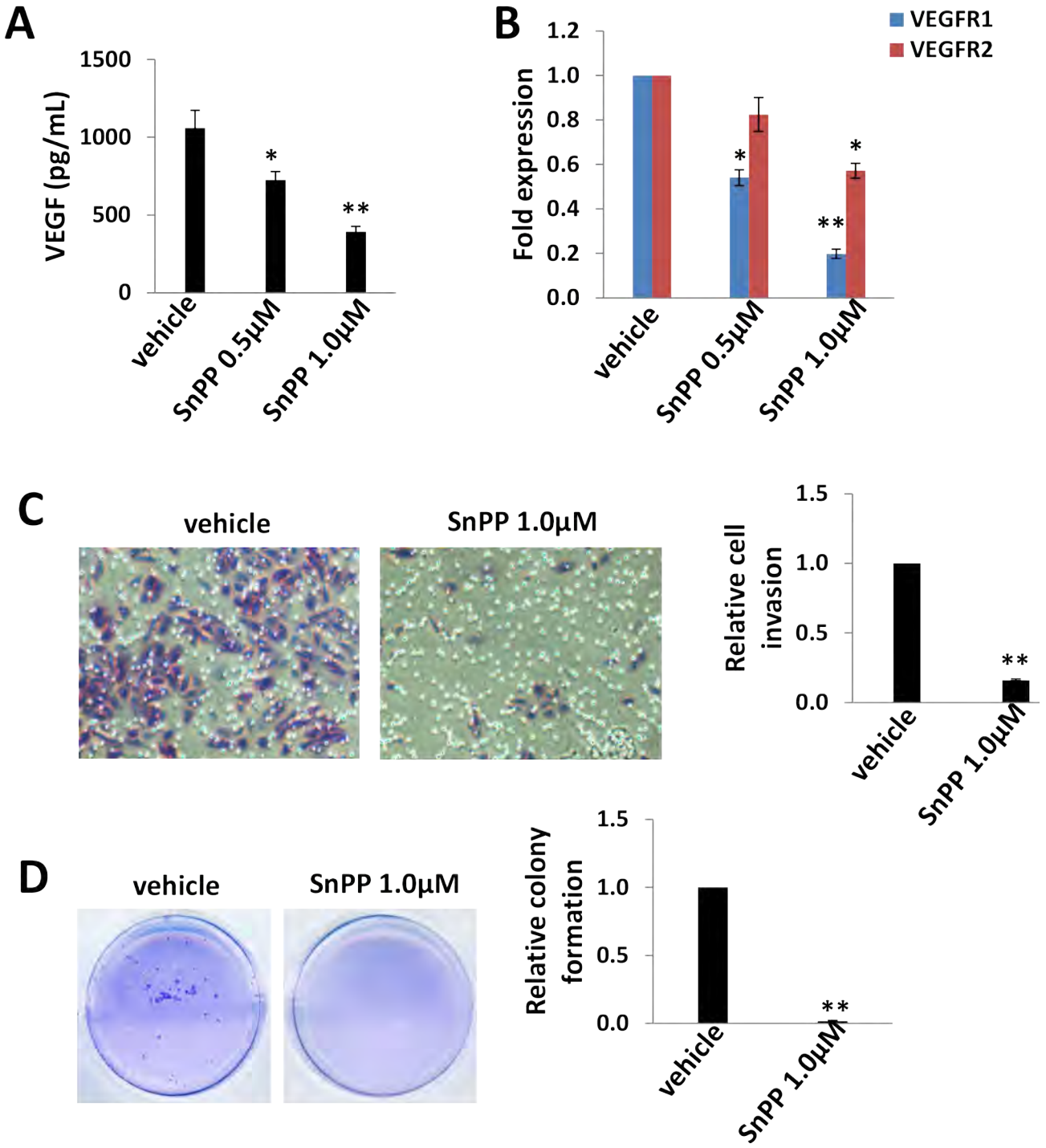

Figure 4: Low doses of SnPP impair TIVE-LTC invasiveness and anchorage-independent growth. A.-B. TIVE-LTC were incubated with low doses of SnPP for 24 h, then the concentrations of VEGF in culture supernatants were determined using ELISA. Gene transcription was measured by qRT-PCR. **C.-D.** Cells were treated as above, then cell invasion and anchorage-independent growth abilities were measured by using the transwell and soft agar assays as described in the Methods. Error bars represent the S.E.M. for 3 independent experiments. * = $p < 0.05$, ** = $p < 0.01$.

μmol/kg of body weight), 5 days/week. The mice were observed every 2~3 d and palpable tumors were measured for additional 2 weeks. Our results indicated that SnPP treatment significantly repressed tumor growth in mice while vehicle had no effect (Figure 6A). SnPP treated mice formed significantly smaller tumors when compared to vehicle treated group after 2-week treatment (Figure 6B). Immunohistochemistry analysis results indicated the increased expression of phosphor-H2A.X and Cyclophilin-A, while the reduced expression of LANA and cellular proliferation indicator Ki67 in tumor tissues isolated from representative SnPP-treated mice when compared to those from vehicle-treated mice (Figure 6C).

DISCUSSION

In the current study, we identify for the first time the upregulation of HO-1 expression by either host CD-147 or viral LANA proteins within endothelial cells. Ongoing work focuses on identifying the mechanisms for upregulation of HO-1 by CD147 either directly (CD147 binding to HO-1 promoter region), or indirectly through other cellular transcriptional factors (e.g. CREB and Nrf2) and/or signaling pathway (e.g. MEK/ERK or PI3K/AKT) [30]. We do not exclude other regulatory mechanisms which may exist, and actually, one very recent study has shown that one of KSHV microRNAs, miR-K12-11, an ortholog of human oncomir miR-155 [31, 32] can induce

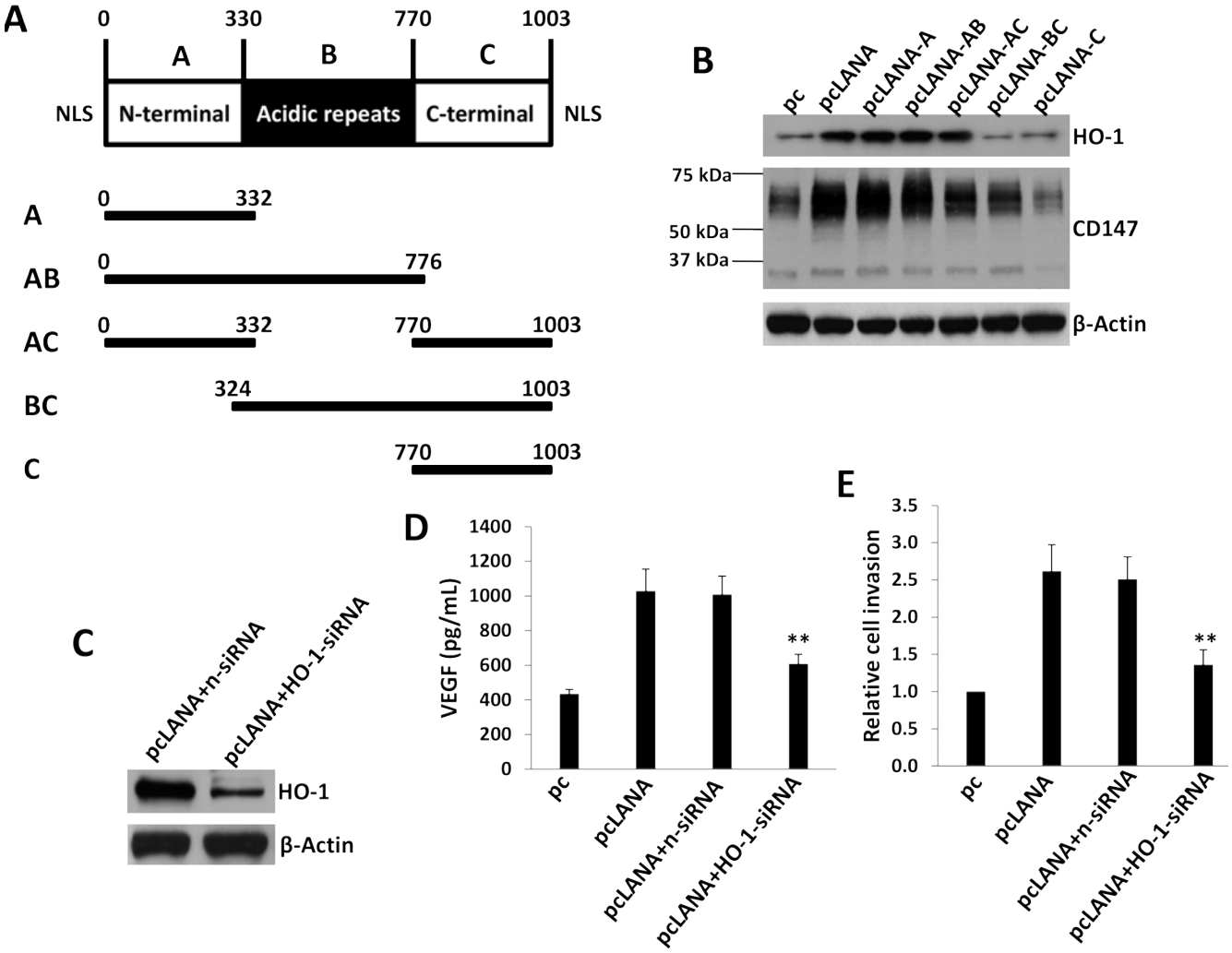

Figure 5: KSHV-encoded LANA protein is responsible for upregulation of HO-1 expression. A. Putative domain structure of LANA based on primary sequence features. The N-terminal region (domain A) is rich in prolines and serines and contains a putative nuclear localization sequences (NLS). The central region of LANA (domain B) is comprised of several repeats and is very acidic. The C-terminal region (domain C) also contains a putative NLS. All fragment variants and their coordinates are depicted below the domain model of LANA. **B.** HUVEC were transfected with control vector pc, full-length LANA construct (pcLANA) and fragment variants, respectively, for 48 h. Immunoblots was used to detect protein expression. **C.-E.** HUVEC were first transfected with negative control siRNA (n-siRNA) or *HO-1*-siRNA for 48 h, then transfected with either control vector pc or pcLANA construct for additional 48 h. Protein expression were measured by immunoblots. The concentrations of VEGF in culture supernatants were determined using ELISA and cell invasion was measured by the transwell assays. Error bars represent the S.E.M. for 3 independent experiments. ** = $p < 0.01$.

HO-1 expression from lymphatic endothelial cells (LEC) through directly targeting BACH1 [33], a cellular HO-1 transcriptional repressor [34]. Interestingly, these authors indicate that there are other viral microRNA-independent mechanisms for induction of HO-1 expression in LEC [33]. These data and our findings in the current study suggest a model in which KSHV infection induces HO-1 expression and its downstream activities through multiple viral and host factors, although it still requires further investigation.

As mentioned above, HO-1 can cleave the porphyrin ring-releasing equimolar quantities of CO, free iron, and biliverdin. Free iron then stimulates the production of the iron-scavenging protein, Ferritin, while biliverdin is rapidly reduced to bilirubin by biliverdin reductase [10]. In fact, these HO-1 metabolites have important roles in endothelial cell physiology. For example, CO produced by HO-1 activity has been shown to protect endothelial cells from both CD95/Fas- and tumor necrosis factor (TNF)-mediated apoptosis [35, 36]. In addition, bilirubin together with upregulated Ferritin has been shown to protect endothelial cells from oxidative damage resultant from myriad noxious stimuli [37, 38]. Since the typical "spindle" KS tumor cells are endothelial derived [39], it will be interested to understand how these HO-1 metabolites contribute to the pathogenesis of KSHV-infected endothelial cells and KS development.

One of our findings is that targeting HO-1 by SnPP induces cell death in KSHV-infected endothelial cells through necrosis but not apoptosis, which is different from some previous studies. For example, Marinissen *et al* have reported that SnPP treatment induces endothelial cell apoptosis [14]. However, in this study the authors used vGPCR- or HO-1-transfected Simian virus 40, large T-antigen-immortalized, murine endothelial cells (SVECs) [14], instead of human endothelial cells such as TIVE-LTC we used in the present study. We assume that different cell-lines with genetic modification may cause varied responses to SnPP treatment, although this still requires experimental validation. Therefore, we will treat more primary or immortalized endothelial cell-lines with SnPP to observe its effect.

By using a KS-like nude mouse model, we found that SnPP treatment can effectively suppress TIVE-

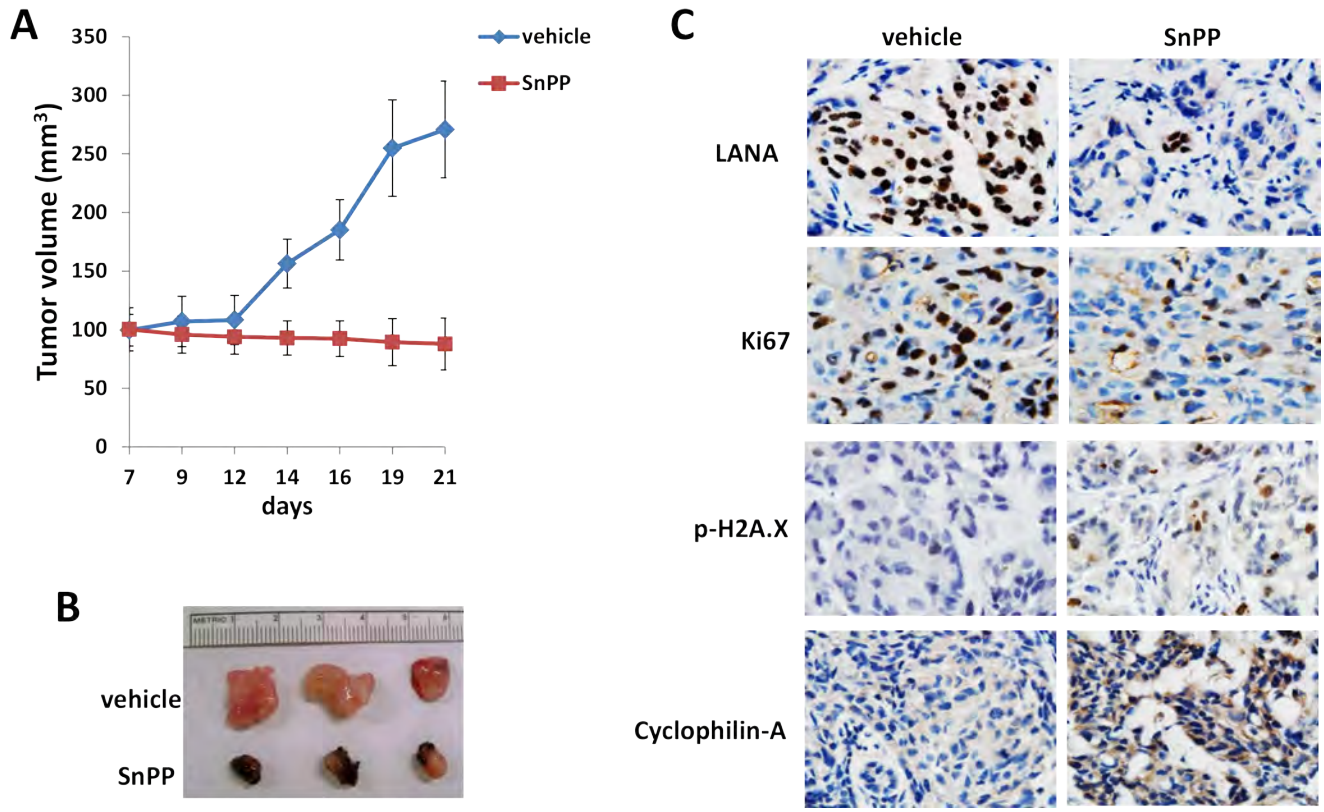

Figure 6: Targeting HO-1 by SnPP effectively suppresses TIVE-LTC tumorigenesis *in vivo*. A.-B. TIVE-LTC (5 x 10^5 cells 1:1 with growth factor-depleted Matrigel) were injected subcutaneously into the right and left flanks of nude mice (3 mice per group), respectively. When tumors reach 10-15 mm in diameter (~1.5weeks), mice were received *in situ* subcutaneous injection with either vehicle or SnPP (10 μmol/kg of body weight), 5 days/week. The mice were observed and measured every 2~3 d for the size of palpable tumors for additional 2 weeks. At the end of experiment, the tumors were excised from the site of injection for subsequent analysis. In SnPP treated mice, some dark substance (SnPP residues) around the tumors were observed when they were excised, which can be easily stripped from tumor tissues. Error bars represent the S.E.M. for one of 2 independent experiments. **C.** Protein expression in tumor tissues from representative mice was measured by immunohistochemistry as described in the Methods.

LTC tumorigenesis *in vivo*. Interestingly, it also greatly reduced LANA expression in the tumor tissues, although the underlying mechanisms remain unknown. However, considering that high dose of SnPP displays some cytotoxicity especially to non-infected endothelial cells such as TIVE (Figure 2A-2B) and HUVEC (data not shown), it might be better to combine SnPP with other chemotherapeutical regimens for clinical treatment or to develop other HO-1 selective inhibitors such as the imidazole-dioxolane compounds [40]. Unlike the metalloporphyrins such as SnPP, these imidazole-dioxolane compounds are selective for the inhibition of HO with minimal effects on other heme-dependent enzymes such as nitric oxide synthase and soluble guanylyl cyclase [40]. Interestingly, some chemotherapeutical agents such as paclitaxel and rapamycin (both of which have been used for KS treatment) [41, 42] have been found to induce HO-1 expression and activities [43, 44]. Therefore, future study will test whether combination of HO-1 inhibitors can reduce tumor burden as well as KS tumor cell resistance to chemotherapy.

MATERIALS AND METHODS

Cell culture, reagents and infection protocol

Body cavity-based lymphoma cells (BCBL-1, $KSHV^{+}/EBV^{neg}$) were kindly provided by Dr. Dean Kedes (University of Virginia) and maintained in RPMI 1640 medium (Gibco) with supplements as described previously [45]. Telomerase-immortalized human umbilical vein endothelial (TIVE) and KSHV long-term-infected TIVE cells (TIVE-LTC) were cultured as previously described [19]. Human umbilical vein endothelial cells (HUVEC) were grown in DMEM/F-12 50/50 medium (Cellgro) supplemented with 5% FBS. All cells were incubated at 37°C in 5% CO_2. All experiments were carried out using cells harvested at low (< 20) passages. SnPP and the pan-caspase inhibitor Z-VAD-FMK were purchased from Sigma. To obtain KSHV for infection experiments, BCBL-1 cells were incubated with 0.6 mM valproic acid for 6 days, and purified virus was concentrated from culture supernatants; infectious titers were determined as described previously [46]. For overexpression of CD147, HUVEC were transduced as previously described with a recombinant adenoviral vector (MOI ~ 10) encoding CD147 (AdV-CD147), or a control vector (AdV), for 48 h prior to subsequent analysis [47].

RNA interference and plasmid transfection

CD147 or *HO-1* ON-TARGET plus SMART pool siRNA, or negative control siRNA (n-siRNA) (Dharmacon), were delivered using the DharmaFECT transfection reagent according to the manufacturer's instructions. For plasmid transfection, HUVEC were transfected with control vector pcDNA3.1, pcDNA3.1-LANA (pcLANA) or LANA deletion fragments (pcLANA-A, pcLANA-AB, pcLANA-AC, pcLANA-BC and pcLANA-C) [28] in 12-well plates for 48 h using Lipofectamine 2000 (Invitrogen) according to the manufacturer's instruction. Transfection efficiency was determined through co-transfection of a lacZ reporter construct and quantified as described previously [46].

Immunoblotting

Total cell lysates (20μg) were resolved by 10% SDS-PAGE, transferred to nitrocellulose membranes, and immunoblotted with antibodies for CD147 (BD), HO-1, p-H2A.X/t-H2A.X, Cyclophilin-A, HMGB1 (Cell Signaling) and β-Actin (Sigma) for loading controls. Immunoreactive bands were identified using an enhanced chemiluminescence reaction (Perkin-Elmer), and visualized by autoradiography.

Immunofluorescence

Cells were incubated in 1:1 methanol-acetone at -20°C for fixation and permeabilization, then with a blocking reagent (10% normal goat serum, 3% bovine serum albumin, and 1% glycine) for an additional 30 min. Cells were then incubated for 1 h at 25°C with 1:400 dilution of a rabbit anti-p-H2A.X, anti- Cyclophilin-A or anti-HMGB1 antibody (Cell Signaling) followed by 1:200 dilution of a goat anti-rabbit secondary antibody conjugated to Texas Red or Alexa 488 (Invitrogen). For identification of nuclei, cells were subsequently counterstained with 0.5 mg/mL 4',6-diamidino-2-phenylindole (DAPI; Sigma) in 180 mM Tris-HCl (pH 7.5). Slides were washed once in 180 mM Tris-HCl for 15 minutes and prepared for visualization using a Leica TCPS SP5 AOBS confocal microscope.

HO enzymatic activity

Crude endothelial cell protein extracts were prepared as previously described [13, 20]. Briefly, following 24-h incubation in complete media alone or with SnPP, monolayers were rinsed with PBS and scraped directly into 300 μL sonication buffer (0.25 M sucrose, 20 mM Tris-HCl, 50 μg/mL Pefabloc SC, 4 μg/mL leupeptin; pH 7.4) sonicated on ice 2 times for 30 s and centrifuged for 20 min at 18,000 g. The protein concentration of the resultant supernatant was determined using BCA as described above. HO activity was measured by the spectrophotometric determination of bilirubin production as described elsewhere [13, 20]. HO activity was reported

as picomoles of bilirubin produced per milligram endothelial cell protein extract per hour.

Cometassay

The DNA damage was evaluated by using the Reagent Kit for Single Cell Gel Electrophoresis Assay/CometAssay (Trevigen), according to the manufacturer's instructions. The slides were viewed by using epifluorescence microscopy. The tail moment was calculated from 100 cells collected per single measurement by utilizing specialized comet software included in the Automated Comet Assay System (Loats Associates Inc).

qRT-PCR

Total RNA was isolated using the RNeasy Mini kit (QIAGEN), and cDNA was synthesized from equivalent total RNA using a SuperScript III First-Strand Synthesis SuperMix Kit (Invitrogen) according to the manufacturer's instructions. Primers used for amplification of target genes are displayed in Supplemental Table 1. Amplification was carried out using an iCycler IQ Real-Time PCR Detection System, and cycle threshold (Ct) values were tabulated in duplicate for each gene of interest in each experiment. "No template" (water) controls were used to ensure minimal background contamination. Using mean Ct values tabulated for each gene, and paired Ct values for *β-actin* as a loading control, fold changes for experimental groups relative to assigned controls were calculated using automated iQ5 2.0 software (Bio-Rad).

Cell proliferation and apoptosis assays

Cell proliferation was measured by using the WST-1 assays (Roche) according to the manufacturers' instructions. For apoptosis assays, the FITC-Annexin V and propidium iodide (PI) Apoptosis Detection Kit I (BD Pharmingen) was used. Samples were analyzed on a FACS Calibur 4-color flow cytometer (BD Bioscience).

ELISA

Concentrations of VEGF in culture supernatants were determined using human VEGF-A (Pierce Biotechnology) ELISA kits according to the manufacturers' instructions.

Transwell invasion assays

Matrigel Invasion Chambers (BD) were hydrated for 4 h at 37°C with culture media. Following hydration, media in the bottom of the well was replaced with fresh media, then 2×10^4 HUVEC or TIVE-LTC were plated in the top of the chamber. After 24 h, cells were fixed with 4% formaldehyde for 15 min at room temperature and chambers rinsed in PBS prior to staining with 0.2% crystal violet for 10 min. After washing the chambers, cells at the top of the membrane were removed and cells at the bottom of the membrane counted using a phase contrast microscope. Relative invasion was determined for cells in experimental groups as follows: relative invasion = # invading cells in experimental group / # invading cells in control groups.

Soft agar assays

A base layer containing 0.5% agarose medium and 5% FCS was poured into six-well plates. Then, 10,000 cells were mixed with 0.4% agarose in Earl's minimal essential medium (EMEM) containing 5% FCS to form a single-cell suspension. After being seeded, the plates were incubated for 2 weeks. Colonies were stained with 0.005% crystal violet and photographed under a phase-contrast microscope (Leica DFC320).

KS-like nude mouse model

Cells were counted and washed once in ice-cold PBS, and 5 x 10^5 TIVE-LTC in 50 μL PBS plus 50 μL growth factor-depleted Matrigel (BD Biosciences) were injected subcutaneously into the two flanks of nude mice (Jackson Laboratory). The mice were observed and measured every 2~3 d for the presence of palpable tumors. When tumors reach 10-15 mm in diameter (~1.5weeks), mice were received *in situ* subcutaneous injection with either vehicle or SnPP (10 μmol/kg of body weight dissolved in 0.1 N NaOH in PBS, pH 7.5), 5 days/week. At the end of experiment, the tumors were excised from the site of injection for subsequent analysis such as immunohistochemistry. All protocols were approved by the LSUHSC Animal Care and Use Committee in accordance with national guidelines.

KS tumor tissues from HIV+ patients and immunohistochemistry

KS tissues from HIV-infected patients were provided by the LSUHSC HIV Outpatient (HOP) Clinic and Biospecimens Bank (LSUHSC IRB approved No. 8079). Formalin-fixed, paraffin-embedded tissues were microtome-sectioned to a thickness of 4 uM, placed on electromagnetically charged slides (Fisher Scientific), and stained with hematoxylin & eosin (H&E) for routine histologic analysis. Immunohistochemistry was performed using the Avidin-Biotin-Peroxidase complex system, according to the manufacturer's instructions (Vectastain

Elite ABC Peroxidase Kit; Vector Laboratories). In our modified protocol, sections were deparaffinized in xylene and re-hydrated through a descending alcohol gradient. For non-enzymatic antigen retrieval, slides were heated in 0.01 M sodium citrate buffer (pH 6.0) to 95ºC under vacuum for 40 min and allowed to cool for 30 min at room temperature, then rinsed with PBS and incubated in MeOH/3% H_2O_2 for 20 min to quench endogenous peroxidase. Slides were then washed with PBS and blocked with 5% normal goat serum in 0.1% PBS/BSA for 2 h at room temperature, then incubated overnight with indicated antibody at 1:200-1:400 dilution in 0.1% PBS/BSA. The following day, slides were incubated with appropriate secondary antibody at room temperature for 1 h, followed by avidin-biotin peroxidase complexes for 1 h at room temperature. Finally, slides were developed using a diaminobenzidine substrate, counterstained with hematoxylin, dehydrated through an ascending alcohol gradient, cleared in xylene, and coverslipped with Permount. Images were collected using an Olympus BX61 microscope equipped with a high resolution DP72 camera and CellSense image capture software.

Statistical analysis

Significance for differences between experimental and control groups was determined using the two-tailed Student's *t*-test (Excel 8.0), and p values < 0.05 and/or < 0.01 were considered significant.

ACKNOWLEDGMENTS AND FUNDINGS

This work was supported by grants from a DOD Career Development Award to Z.Q. (CA140437), the SOM Research Enhancement Funding to ZQ, as well as awards from the National Natural Science Foundation of China (81272191, 81472547 to Z.Q. and 81400164 to L.D.). J.Q. was supported by funding from Shanghai Science and Technology committee (No.14411971400) and Pudong Science and Technology committee, Shanghai (No.PK2013-17). De-identified human KS tumors were provided by the HIV Cancer Care Program Biorepository which is supported by grants from the National Institute of Health to C.P. (UM1-CA181255 and R01-CA142362). D.N. was supported by a Short-term Summer Program of LSUHSC (Z.Q. is the mentor). Funding sources had no role in study design, data collection and analysis, decision to publish, or preparation of the manuscript.

CONFLICTS OF INTEREST

All the authors declare no conflicts of interest.

REFERENCES

1. Chang Y, Cesarman E, Pessin MS, Lee F, Culpepper J, Knowles DM and Moore PS. Identification of herpesvirus-like DNA sequences in AIDS-associated Kaposi's sarcoma. Science. 1994; 266:1865-1869.
2. Wabinga HR, Nambooze S, Amulen PM, Okello C, Mbus L and Parkin DM. Trends in the incidence of cancer in Kampala, Uganda 1991-2010. Int J Cancer. 2014; 135:432-439.
3. Chokunonga E, Borok MZ, Chirenje ZM, Nyakabau AM and Parkin DM. Trends in the incidence of cancer in the black population of Harare, Zimbabwe 1991-2010. Int J Cancer. 2013; 133:721-729.
4. Carrilho C, Ferro J, Lorenzoni C, Sultane T, Silva-Matos C and Lunet N. A contribution for a more accurate estimation of the incidence of Kaposi sarcoma in Mozambique. Int J Cancer. 2013; 132:988-989.
5. Davidson A, Wainwright RD, Stones DK, Kruger M, Hendricks M, Geel J, Poole J, Reynders D, Omar F, Mathew R and Stefan DC. Malignancies in South African children with HIV. J Pediatr Hematol Oncol. 2014; 36:111-117.
6. Robey RC and Bower M. Facing up to the ongoing challenge of Kaposi's sarcoma. Curr Opin Infect Dis. 2015; 28:31-40.
7. Letang E, Lewis JJ, Bower M, Mosam A, Borok M, Campbell TB, Naniche D, Newsom-Davis T, Shaik F, Fiorillo S, Miro JM, Schellenberg D and Easterbrook PJ. Immune reconstitution inflammatory syndrome associated with Kaposi sarcoma: higher incidence and mortality in Africa than in the UK. AIDS. 2013; 27:1603-1613.
8. Mosam A, Shaik F, Uldrick TS, Esterhuizen T, Friedland GH, Scadden DT, Aboobaker J and Coovadia HM. A randomized controlled trial of highly active antiretroviral therapy *versus* highly active antiretroviral therapy and chemotherapy in therapy-naive patients with HIV-associated Kaposi sarcoma in South Africa. J Acquir Immune Defic Syndr. 2012; 60:150-157.
9. Cox CM, El-Mallawany NK, Kabue M, Kovarik C, Schutze GE, Kazembe PN and Mehta PS. Clinical characteristics and outcomes of HIV-infected children diagnosed with Kaposi sarcoma in Malawi and Botswana. Pediatr Blood Cancer. 2013; 60:1274-1280.
10. Choi AM and Alam J. Heme oxygenase-1: function, regulation, and implication of a novel stress-inducible protein in oxidant-induced lung injury. Am J Respir Cell Mol Biol. 1996; 15:9-19.
11. Maines MD. The heme oxygenase system: a regulator of second messenger gases. Annu Rev Pharmacol Toxicol. 1997; 37:517-554.
12. Dulak J, Loboda A, Zagorska A and Jozkowicz A. Complex role of heme oxygenase-1 in angiogenesis. Antioxid Redox Signal. 2004; 6:858-866.

13. McAllister SC, Hansen SG, Ruhl RA, Raggo CM, DeFilippis VR, Greenspan D, Fruh K and Moses AV. Kaposi sarcoma-associated herpesvirus (KSHV) induces heme oxygenase-1 expression and activity in KSHV-infected endothelial cells. Blood. 2004; 103:3465-3473.

14. Marinissen MJ, Tanos T, Bolos M, de Sagarra MR, Coso OA and Cuadrado A. Inhibition of heme oxygenase-1 interferes with the transforming activity of the Kaposi sarcoma herpesvirus-encoded G protein-coupled receptor. J Biol Chem. 2006; 281:11332-11346.

15. Biswas C, Zhang Y, DeCastro R, Guo H, Nakamura T, Kataoka H and Nabeshima K. The human tumor cell-derived collagenase stimulatory factor (renamed EMMPRIN) is a member of the immunoglobulin superfamily. Cancer Res. 1995; 55:434-439.

16. Yan L, Zucker S and Toole BP. Roles of the multifunctional glycoprotein, emmprin (basigin; CD147), in tumour progression. Thromb Haemost. 2005; 93:199-204.

17. Qin Z, Dai L, Slomiany MG, Toole BP and Parsons C. Direct activation of emmprin and associated pathogenesis by an oncogenic herpesvirus. Cancer Res. 2010; 70:3884-3889.

18. Dai L, Trillo-Tinoco J, Chen Y, Bonstaff K, Del Valle L, Parsons C, Ochoa AC, Zabaleta J, Toole BP and Qin Z. CD147 and downstream ADAMTSs promote the tumorigenicity of Kaposi's sarcoma-associated herpesvirus infected endothelial cells. Oncotarget. 2015 Dec 12. doi: 10.18632/oncotarget.6584.

19. An FQ, Folarin HM, Compitello N, Roth J, Gerson SL, McCrae KR, Fakhari FD, Dittmer DP and Renne R. Long-term-infected telomerase-immortalized endothelial cells: a model for Kaposi's sarcoma-associated herpesvirus latency *in vitro* and *in vivo*. J Virol. 2006; 80:4833-4846.

20. Ryter SW, Si M, Lai CC and Su CY. Regulation of endothelial heme oxygenase activity during hypoxia is dependent on chelatable iron. Am J Physiol Heart Circ Physiol. 2000; 279:H2889-2897.

21. Qin Z, Dai L, Trillo-Tinoco J, Senkal C, Wang W, Reske T, Bonstaff K, Del Valle L, Rodriguez P, Flemington E, Voelkel-Johnson C, Smith CD, Ogretmen B and Parsons C. Targeting Sphingosine Kinase Induces Apoptosis and Tumor Regression for KSHV-Associated Primary Effusion Lymphoma. Mol Cancer Ther. 2014; 13:154-164.

22. Davis DA, Naiman NE, Wang V, Shrestha P, Haque M, Hu D, Anagho HA, Carey RF, Davidoff KS and Yarchoan R. Identification of Caspase Cleavage Sites in KSHV Latency-Associated Nuclear Antigen and Their Effects on Caspase-Related Host Defense Responses. PLoS Pathog. 2015; 11:e1005064.

23. Christofferson DE and Yuan J. Cyclophilin A release as a biomarker of necrotic cell death. Cell Death Differ. 2010; 17:1942-1943.

24. Lee JS, Li Q, Lee JY, Lee SH, Jeong JH, Lee HR, Chang H, Zhou FC, Gao SJ, Liang C and Jung JU. FLIP-mediated autophagy regulation in cell death control. Nat Cell Biol. 2009; 11:1355-1362.

25. Ensoli B and Sturzl M. Kaposi's sarcoma: a result of the interplay among inflammatory cytokines, angiogenic factors and viral agents. Cytokine Growth Factor Rev. 1998; 9:63-83.

26. Sivakumar R, Sharma-Walia N, Raghu H, Veettil MV, Sadagopan S, Bottero V, Varga L, Levine R and Chandran B. Kaposi's sarcoma-associated herpesvirus induces sustained levels of vascular endothelial growth factors A and C early during *in vitro* infection of human microvascular dermal endothelial cells: biological implications. J Virol. 2008; 82:1759-1776.

27. Qian LW, Xie J, Ye F and Gao SJ. Kaposi's sarcoma-associated herpesvirus infection promotes invasion of primary human umbilical vein endothelial cells by inducing matrix metalloproteinases. J Virol. 2007; 81:7001-7010.

28. Dai L, Chen Y, Toole B, Parsons C and Qin Z. Induction of hyaluronan production by oncogenic KSHV and the contribution to viral pathogenesis in AIDS patients. Cancer Lett. 2015; 362:158-166.

29. Garber AC, Shu MA, Hu J and Renne R. DNA binding and modulation of gene expression by the latency-associated nuclear antigen of Kaposi's sarcoma-associated herpesvirus. J Virol. 2001; 75:7882-7892.

30. Chuang JI, Huang JY, Tsai SJ, Sun HS, Yang SH, Chuang PC, Huang BM and Ching CH. FGF9-induced changes in cellular redox status and HO-1 upregulation are FGFR-dependent and proceed through both ERK and AKT to induce CREB and Nrf2 activation. Free Radic Biol Med. 2015; 89:274-286.

31. Skalsky RL, Samols MA, Plaisance KB, Boss IW, Riva A, Lopez MC, Baker HV and Renne R. Kaposi's sarcoma-associated herpesvirus encodes an ortholog of miR-155. J Virol. 2007; 81:12836-12845.

32. Gottwein E, Mukherjee N, Sachse C, Frenzel C, Majoros WH, Chi JT, Braich R, Manoharan M, Soutschek J, Ohler U and Cullen BR. A viral microRNA functions as an orthologue of cellular miR-155. Nature. 2007; 450:1096-1099.

33. Botto S, Totonchy JE, Gustin JK and Moses AV. Kaposi Sarcoma Herpesvirus Induces HO-1 during De Novo Infection of Endothelial Cells *via* Viral miRNA-Dependent and -Independent Mechanisms. mBio. 2015; 6:e00668.

34. Sun J, Hoshino H, Takaku K, Nakajima O, Muto A, Suzuki H, Tashiro S, Takahashi S, Shibahara S, Alam J, Taketo MM, Yamamoto M and Igarashi K. Hemoprotein Bach1 regulates enhancer availability of heme oxygenase-1 gene. EMBO J. 2002; 21:5216-5224.

35. Ke B, Buelow R, Shen XD, Melinek J, Amersi F, Gao F, Ritter T, Volk HD, Busuttil RW and Kupiec-Weglinski JW. Heme oxygenase 1 gene transfer prevents CD95/Fas ligand-mediated apoptosis and improves liver allograft survival *via* carbon monoxide signaling pathway. Hum Gene Ther.

2002; 13:1189-1199.

36. Brouard S, Berberat PO, Tobiasch E, Seldon MP, Bach FH and Soares MP. Heme oxygenase-1-derived carbon monoxide requires the activation of transcription factor NF-kappa B to protect endothelial cells from tumor necrosis factor-alpha-mediated apoptosis. J Biol Chem. 2002; 277:17950-17961.
37. Eisenstein RS, Garcia-Mayol D, Pettingell W and Munro HN. Regulation of ferritin and heme oxygenase synthesis in rat fibroblasts by different forms of iron. Proc Natl Acad Sci U S A. 1991; 88:688-692.
38. Stocker R, Glazer AN and Ames BN. Antioxidant activity of albumin-bound bilirubin. Proc Natl Acad Sci U S A. 1987; 84:5918-5922.
39. Mesri EA, Cesarman E and Boshoff C. Kaposi's sarcoma and its associated herpesvirus. Nat Rev Cancer. 2010; 10:707-719.
40. Kinobe RT, Ji Y, Vlahakis JZ, Motterlini R, Brien JF, Szarek WA and Nakatsu K. Effectiveness of novel imidazole-dioxolane heme oxygenase inhibitors in renal proximal tubule epithelial cells. J Pharmacol Exp Ther. 2007; 323:763-770.
41. Reddy-Holdcraft S, Mehta PS and Agrawal AK. Paclitaxel for relapsed or recurrent HIV-associated pediatric Kaposi's sarcoma. AIDS. 2014; 28:800-802.
42. Dittmer DP and Krown SE. Targeted therapy for Kaposi's sarcoma and Kaposi's sarcoma-associated herpesvirus. Curr Opin Oncol. 2007; 19:452-457.
43. Choi BM, Kim YM, Jeong YR, Pae HO, Song CE, Park JE, Ahn YK and Chung HT. Induction of heme oxygenase-1 is involved in anti-proliferative effects of paclitaxel on rat vascular smooth muscle cells. Biochem Biophys Res Commun. 2004; 321:132-137.
44. Visner GA, Lu F, Zhou H, Liu J, Kazemfar K and Agarwal A. Rapamycin induces heme oxygenase-1 in human pulmonary vascular cells: implications in the antiproliferative response to rapamycin. Circulation. 2003; 107:911-916.
45. Dai L, Trillo-Tinoco J, Bai L, Kang B, Xu Z, Wen X, Del Valle L and Qin Z. Systematic analysis of a xenograft mice model for KSHV+ primary effusion lymphoma (PEL). PLoS One. 2014; 9:e90349.
46. Qin Z, Dai L, Defee M, Findlay VJ, Watson DK, Toole BP, Cameron J, Peruzzi F, Kirkwood K and Parsons C. Kaposi's sarcoma-associated herpesvirus suppression of DUSP1 facilitates cellular pathogenesis following de novo infection. J Virol. 2013; 87:621-635.
47. Dai L, Bratoeva M, Toole BP, Qin Z and Parsons C. KSHV activation of VEGF secretion and invasion for endothelial cells is mediated through viral upregulation of emmprin-induced signal transduction. Int J Cancer. 2012; 131:834-843.

Genomics Data 8 (2016) 16–17

Contents lists available at ScienceDirect

Genomics Data

journal homepage: www.elsevier.com/locate/gdata

Data in Brief

Genomic analysis of xCT-regulatory network in KSHV + primary effusion lymphomas

Zhiqiang Qin [a,b,*], Yueyu Cao [a], Lu Dai [a,c,*]

[a] Research Center for Translational Medicine and Key Laboratory of Arrhythmias of the Ministry of Education of China, East Hospital, Tongji University School of Medicine, 150 Jimo Road, Shanghai 200120, China
[b] Department of Microbiology, Immunology & Parasitology, Louisiana State University Health Sciences Center, Louisiana Cancer Research Center, 1700 Tulane Ave., New Orleans, LA 70112, USA
[c] Department of Medicine, Louisiana State University Health Sciences Center, Louisiana Cancer Research Center, 1700 Tulane Ave., New Orleans, LA 70112, USA

ARTICLE INFO

Article history:
Received 15 February 2016
Accepted 16 February 2016
Available online 18 February 2016

ABSTRACT

Kaposi's sarcoma-associated herpesvirus (KSHV) is the etiological agent of primary effusion lymphoma (PEL), a rapidly progressing malignancy mostly arising in HIV-infected patients Chen et al. (2007) [1]. Even under conventional chemotherapy, PEL continues to portend nearly 100% mortality within several months, which urgently requires novel therapeutic strategies. We have previously demonstrated that targeting xCT, an amino acid transporter for cystine/glutamate exchange, induces significant PEL cell apoptosis through regulation of multiple host and viral factors [2]. More importantly, one of xCT selective inhibitors, Sulfasalazine (SASP), effectively prevents PEL tumor progression in an immune-deficient xenograft model [2]. In the current study, we use Illumina microarray to explore the profile of genes altered by SASP treatment within 3 KSHV + PEL cell-lines, and discover that many genes involved in oxidative stress/antioxidant defense system, apoptosis/anti-apoptosis/cell death, and cellular response to unfolded proteins/topologically incorrect proteins are potentially regulated by xCT Dai et al. (2015) [3]. The microarray original data have been submitted to Gene Expression Omnibus (GEO) database (Accession number: GSE65418).

Specifications	
Organism/cell line/tissue	Homo sapiens/KSHV + primary effusion lymphoma cell lines, BC-1, BCP-1 and BCBL-1
Sex	Male
Sequencer or array type	Illumina BeadStation 500 and BeadScan
Data format	Raw data: FASTAQ file
Experimental factors	Cells were treated with vehicle or the xCT selective inhibitor SASP (0.5 mM) for 48 h
Experimental features	Microarray gene expression profiling to identify transcripts that are regulated by SASP
Consent	Data are publicly available
Sample source location	LSUHSC, New Orleans, Louisiana

1. Direct link to deposited data

http://www.ncbi.nlm.nih.gov/geo/query/acc.cgi?acc=GSE65418.

* Corresponding authors at: Research Center for Translational Medicine and Key Laboratory of Arrhythmias of the Ministry of Education of China, East Hospital, Tongji University School of Medicine, 150 Jimo Road, Shanghai 200120, China.
E-mail addresses: zqin@lsuhsc.edu (Z. Qin), ldai@lsuhsc.edu (L. Dai).

2. Experimental design, materials and methods

2.1. Cell culture and reagents

The PEL cell-line BCBL-1 ($KSHV^{+}/EBV^{neg}$) was maintained in RPMI 1640 medium (Gibco) with supplements as described previously [1,2]. The other PEL cell-lines BC-1 ($KSHV^{+}/EBV^{+}$) and BCP-1 ($KSHV^{+}/EBV^{neg}$) were purchased from American Type Culture Collection (ATCC) and maintained in complete RPMI 1640 medium (ATCC) supplemented with 20% FBS. All cells were cultured at 37 °C in 5% CO_2. All experiments were carried out using cells harvested at low (<20) passages. Sulfasalazine (SASP) was purchased from Sigma.

2.2. Microarray and data analysis

Microarray analysis was performed and analyzed at the Stanley S. Scott Cancer Center's Translational Genomics Core at LSUHSC. BC-1, BCP-1 and BCBL-1 cells were treated with vehicle or the xCT selective inhibitor SASP (0.5 mM) for 48 h, respectively. Total RNA was isolated using Qiagen RNeasy kit (Qiagen), and 500 ng of total RNA was used to synthesize dscDNA. Biotin-labeled RNA was generated using the TargetAmp-Nano Labeling Kit for Illumina Expression BeadChip

http://dx.doi.org/10.1016/j.gdata.2016.02.011

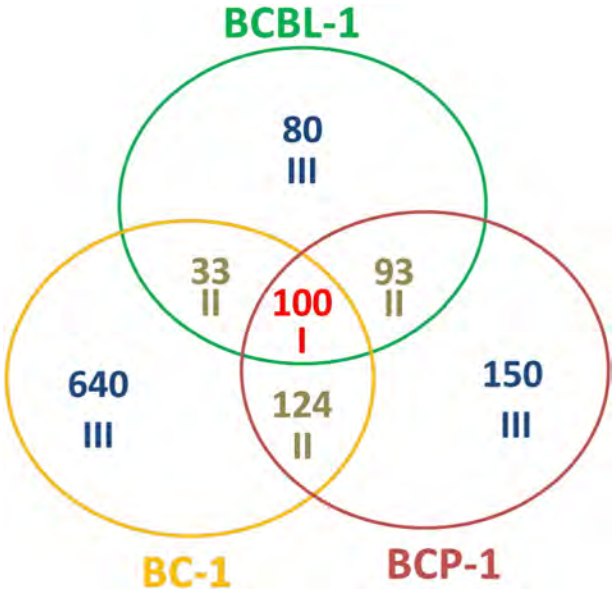

Fig. 1. Intersection analysis of gene profile altered within SASP-treated KSHV+ PEL cell-lines. The HumanHT-12 v4 Expression BeadChip (Illumina) was used to detect genomic gene profile altered within 3 SASP-treated KSHV+ PEL cell-lines (BCBL-1, BC-1 and BCP-1) when compared with vehicle-treated controls. Intersection analysis of significantly altered genes (up/down ≥ 2 folds and $p < 0.05$) was performed using the Illumina GenomeStudio Software. Set I: Common genes altered in all the 3 cell-lines; Set II: Similar genes altered in every 2 cell-lines; Set III: Unique genes altered in each cell-line.

(Epicenter), according to the manufacturers' instructions, and hybridized to the HumanHT-12 v4 Expression BeadChip (Illumina) which contains more than 47,000 probes derived from the NCBI RefSeq Release 38 and other sources, at 58 °C for 16 h. The chip was washed, stained with streptavadin-Cy3, and scanned with the Illumina BeadStation 500 and BeadScan.

Using the Illumina's GenomeStudio software, we normalized the signals using the "cubic spline algorithm" that assumes that the distribution of the transcript abundance is similar in all samples. The background signal was removed using the "detection p-value algorithm" to remove targets with signal intensities equal or lower than that of irrelevant probes (with no known targets in the human genome but thermodynamically similar to the relevant probes). The microarray experiments were performed twice for each group and the average values were used for analysis. Common, similar, and unique sets of genes and enrichment analysis were performed using the MetaCore Software (Thompson Reuters), and the results were summarized in Fig. 1. Enrichment analysis shows that several major cellular functions were affected within SASP-treated PEL cells, including oxidative stress/antioxidant defense system, apoptosis/anti-apoptosis/cell death, and cellular response to unfolded proteins/topologically incorrect proteins, which is consistent with the SASP-induced apoptosis phenotype that we recently observed in KSHV+ PEL cell-lines [2,3]. Therefore, our microarray data indicate that xCT as well as downstream controlled genes may represent new "drug targets" for better PEL treatment.

Conflict of interest

The authors declare no conflict of interests.

Acknowledgments

This work was supported by grants from a DOD Career Development Award to Z.Q. (CA140437), the SOM Research Enhancement Funding (2015-2016) to Z.Q., as well as awards from the National Natural Science Foundation of China (81272191, 81472547 to Z.Q. and 81400164 to L.D.).

References

[1] Y.B. Chen, A. Rahemtullah, E. Hochberg, Primary effusion lymphoma. Oncologist 12 (5) (2007) 569–576.
[2] L. Dai, Y. Cao, Y. Chen, C. Parsons, Z. Qin, Targeting xCT, a cystine-glutamate transporter induces apoptosis and tumor regression for KSHV/HIV-associated lymphoma. J. Hematol. Oncol. 7 (2014) 30.
[3] L. Dai, Y. Cao, Y. Chen, J.A.R. Kaleeba, J. Zabaleta, Z. Qin, Genomic analysis of xCT-mediated regulatory network: identification of novel targets against AIDS-associated lymphoma. Oncotarget 6 (14) (2015) 12710–12722.

CD147 and downstream ADAMTSs promote the tumorigenicity of Kaposi's sarcoma-associated herpesvirus infected endothelial cells

Lu Dai[1,3], Jimena Trillo-Tinoco[4], Yihan Chen[1], Karlie Bonstaff[3], Luis Del Valle[4], Chris Parsons[3], Augusto C. Ochoa[5], Jovanny Zabaleta[5], Bryan P. Toole[6], Zhiqiang Qin[1,2]

[1]Research Center for Translational Medicine and Key Laboratory of Arrhythmias, East Hospital, Tongji University School of Medicine, Shanghai 200120, China

[2]Departments of Microbiology/Immunology/Parasitology, Louisiana State University Health Sciences Center, Louisiana Cancer Research Center, New Orleans, LA 70112, USA

[3]Departments of Medicine, Louisiana State University Health Sciences Center, Louisiana Cancer Research Center, New Orleans, LA 70112, USA

[4]Departments of Pathology, Louisiana State University Health Sciences Center, Louisiana Cancer Research Center, New Orleans, LA 70112, USA

[5]Department of Pediatrics, Louisiana State University Health Sciences Center, Louisiana Cancer Research Center, New Orleans, LA 70112, USA

[6]Department of Regenerative Medicine and Cell Biology, Medical University of South Carolina and Hollings Cancer Center, Charleston, SC 29425, USA

Correspondence to: Zhiqiang Qin, **e-mail:** zqin@lsuhsc.edu

Keywords: *KSHV, Kaposi's sarcoma, CD147, microarray*

Received: *August 26, 2015* ***Accepted:*** *November 25, 2015* ***Published:*** *December 12, 2015*

ABSTRACT

Kaposi's Sarcoma-associated Herpesvirus (KSHV) is the etiologic agent of several human cancers, including Kaposi's Sarcoma (KS), which preferentially arise in immunocompromised patients and lack effective therapeutic options. We have previously shown that KSHV or viral protein LANA up-regulates the glycoprotein CD147, thereby inducing primary endothelial cell invasiveness. In the current study, we identify the global network controlled by CD147 in KSHV-infected endothelial cells using Illumina microarray analysis. Among downstream genes, two specific metalloproteases, ADAMTS1 and 9, are strongly expressed in AIDS-KS tissues and contribute to KSHV-infected endothelial cell invasiveness through up-regulation of IL-6 and VEGF. By using a KS-like nude mouse model, we found that targeting CD147 and downstream ADAMTSs significantly suppressed KSHV-induced tumorigenesis *in vivo*. Taken together, targeting CD147 and associated proteins may represent a promising therapeutic strategy against these KSHV-related malignancies.

INTRODUCTION

Kaposi sarcoma-associated herpesvirus (KSHV) represents one of major causative agent of cancers arising in immunocompromised patients, including Kaposi's Sarcoma (KS) [1]. Furthermore, despite the reduced incidence of KS in the era of combined Antiretroviral Therapy (cART) for Human Immunodeficiency Virus (HIV) infection, KS still remains the most common Acquired Immunodeficiency Syndrome (AIDS)-associated tumor and a leading cause of morbidity and mortality in this setting [2, 3]. In addition, a longitudinal study conducted among solid organ transplant recipients in United States reported a high prevalence (15%) of KSHV seropositivity in this population [4]. Transplant recipients who develop primary KSHV infection after transplantation have a relatively high probability of developing KSHV-related malignancies, especially KS [5], which is likely associated with the intensity of immunosuppressive treatment post-transplantation [6]. Therefore, KSHV-induced malignancies, in particular KS, still represent a serious threat to immunosuppressed patients due to the lack of effective therapies. In fact, KSHV has now become a model pathogen for virus-induced cancer research. However, many key questions regarding its mechanisms of oncogenesis still remain unanswered, thus hindering identification of rational targets and development of novel therapeutic strategies.

The multifunctional transmembrane protein, CD147, also known as Emmprin or Basigin, induces the expression and secretion of multiple matrix metalloproteinases (MMPs), thereby promoting tumor cell invasion and other malignant behaviors [7–9]. We recently reported that enhancement of invasiveness for primary endothelial cells (the major cellular components of KS), following *de novo* KSHV infection, resulted from up-regulation of CD147 by the KSHV-encoded latency-associated nuclear antigen (LANA) protein [10]. Further study indicated that PI3K/Akt and MAPK activation of vascular endothelial growth factor (VEGF) was required for CD147-mediated endothelial cell invasion [11]. In addition, CD147 and related proteins are also involved in multidrug-resistance of primary effusion lymphoma (PEL), another KSHV-caused malignancy [12]. These data demonstrate the important role of CD147 in KSHV-associated malignancies. However, the global gene profile controlled by CD147 within primary endothelial cells, in particular KSHV-infected cells, remains unknown. It will also be interested to understand the cellular functions of CD147-downstream proteins *in vitro* and *in vivo*, as well as their clinical relevance within AIDS-KS tumor tissues. In the current study, we used Illumina microarray to identify the global network controlled by CD147 within either CD147-overexpressed or KSHV-infected endothelial cells. We also tested the contribution of two CD147-controlled proteins, ADAMTS (A Disintegrin and Metalloprotease with ThromboSpondin motifs) 1 and 9 to KSHV pathogenesis and their clinical correlations in AIDS-KS tissues. Finally, using a KS-like nude mouse model with KSHV long-term-infected, telomerase-immortalized human umbilical vein endothelial (TIVE-LT) cells [13], we assessed the role of CD147 and downstream ADAMTSs in KSHV-related tumorigenesis *in vivo*.

RESULTS

Microarray analysis of the CD147 regulatory network in CD147-overexpressed and KSHV-infected endothelial cells

We first used the HumanHT-12 v4 Expression BeadChip (Illumina), which contains more than 47,000 probes derived from the NCBI RefSeq Release 38 and other sources, to study the gene profile altered within CD147-overexpressed HUVEC cells by using a recombinant adenoviral vector AdV-CD147 [11] or within KSHV-infected HUVEC cells. We found that 184 genes were significantly up-regulated and 148 were down-regulated ($\geq$ 2 fold and $p < 0.05$) within CD147-overexpressed endothelial cells; in KSHV-infected cells, 963 genes were up-regulated and 1042 down-regulated. Intersection analysis indicated that 71 "common" genes were significantly up-regulated and 75 were down-regulated in both sets (Figure 1A); the top 10 up-regulated and down-regulated candidate genes were listed in Table 1, respectively. We next selected 5 "common" genes in both sets from Table 1 for validation of their transcriptional change by using qRT-PCR. Our results indicated that all of the 10 selected genes were significantly altered in a manner comparable to those found in the microarray data, demonstrating the credibility of our microarray analysis. Specifically, *ADAMTS1*, *ADAMTS9*, *HMOX1*, *TRIB1* and *IL-6* were significantly up-regulated, while *ZnT3*, *GDF3*, *FBLN5*, *COL1A2*, *SDPR* were significantly down-regulated within either CD147-overexpressed or KSHV-infected endothelial cells (Figure 1B–1C).

Interestingly, some of the top altered candidate genes listed have been reported to be closely associated with KSHV pathogenesis. For example, KSHV infection induces heme oxygenase-1 (HMOX-1 or HO-1), an inducible enzyme responsible for the rate-limiting step in heme catabolism, in infected endothelial cells and/or AIDS-KS tissues [14]. Increased HMOX-1 enzymatic activity *in vitro* has been shown to enhance proliferation of KSHV-infected endothelial cells in the presence of free heme. Fibulin-5 (FBLN5), one of the most down-regulated genes, is greatly decreased in KSHV-infected endothelial cells and/or AIDS-KS tissues, while addition of recombinant Fibulin-5 suppresses VEGF production by KSHV-infected endothelial cells [15]. In contrast, some other candidates have never been reported in KSHV pathogenesis but are thought to be involved in progression of other cancers, such as ADAMTS1 and 9. The ADAMTS family of extracellular metalloproteases, including ADAMTS1 and 9, has been widely implicated in remodeling of the tumor microenvironment during cancer development, growth and progression [16–19]. In particular, elevated ADAMTS1 promotes pro-tumorigenic changes such as increased tumor cell proliferation, decreased apoptosis and altered vascularization [20]. Importantly, it facilitates significant peritumoral remodeling of the extracellular matrix (ECM) microenvironment to promote tumor progression and metastasis. For these reasons we chose ADAMTS1 and 9 for further investigations.

We also performed enrichment analysis of the "common" genes in both sets by using the Pathway map, Gene Ontology (GO) Processes and Process Networks modules from Metacore Software (Thompson Reuters) [21]. Our analysis showed that these genes belong to several major cellular function categories, including cellular immune response to inflammation, blood vessel development, regulation of epithelial-mesenchymal transition (EMT), cell adhesion and cell cycle/proliferation (Supplementary Figure S1A–S1C), some of which have been reported closely related to KSHV pathogenesis or tumorigenesis [22, 23]. In addition, the top 2 scored pathway maps and protein networks for these "common" genes were shown in Supplementary Figure S2 and Figure S3, respectively.

Clinical relevance of CD147 and downstream ADAMTSs within AIDS-KS tissues

Due to the important role of ADAMTS family members in cancer progression, we further examined their regulation by CD147 in endothelial cells and their expression in AIDS-KS tumors. We previously demonstrated up-regulation of CD147 expression in HUVEC by either a recombinant CD147 adenovirus (AdV-CD147) transduction or KSHV *de novo* infection [10, 11]. Here we showed the elevated expression of ADAMTS1 and 9 after both treatments in cultured HUVEC cells (Figure 2A–2B). Furthermore, we measured their expression levels in KS tumor tissues directly isolated from cohort 3 AIDS patients without chemotherapy treatments. Our results showed the strong expression of CD147, as well as ADAMTS1 and 9 within KS tumor tissues from all the patients (CF0002, JG004 and XX007) (Figure 2C). In addition, we found that CD147, ADAMTS1 and 9 were all expressed mostly in "spindle cells", the typical LANA+ KS tumor cells [24] (Figure 2D). Taken together, these data strongly suggest the involvement of CD147 and downstream ADAMTS proteins in KSHV-related malignancies, specifically KS.

Targeting CD147 and downstream ADAMTSs represses pro-inflammatory, pro-angiogenic cytokine production and endothelial cell invasion

Pro-inflammatory and pro-angiogenic cytokines, in particular IL-6 and VEGF, are secreted by KSHV-infected cells. Their presence within KS lesions and the peripheral circulation of KS patients is thought to facilitate KSHV-associated cellular pathogenesis and angiogenesis [25–27]. Moreover, acquisition of a migratory or invasive phenotype represents one hallmark of KSHV-infected endothelial cells, with implications for both viral dissemination and angiogenesis within KS lesions [28]. Here our results indicated that targeting *CD147*, *ADAMTS1* or *9* by RNAi significantly reduced IL-6 and VEGF production from KSHV-infected HUVEC, as well as the transcripts for their receptors (IL-6R, VEGFR1 and VEGFR2) (Figure 3A–3C and Supplementary Figure S4). By using the transwell assays, we found that silencing of *CD147*, *ADAMTS1* or *9* effectively reduced KSHV-infected HUVEC invasion (Figure 3D). Moreover, silencing of *CD147*, *ADAMTS1* or *9* also significantly reduced CD147-overexpressed HUVEC invasion (Figure 3E), demonstrating that these ADAMTSs are indeed required for CD147-mediated endothelial cell invasion.

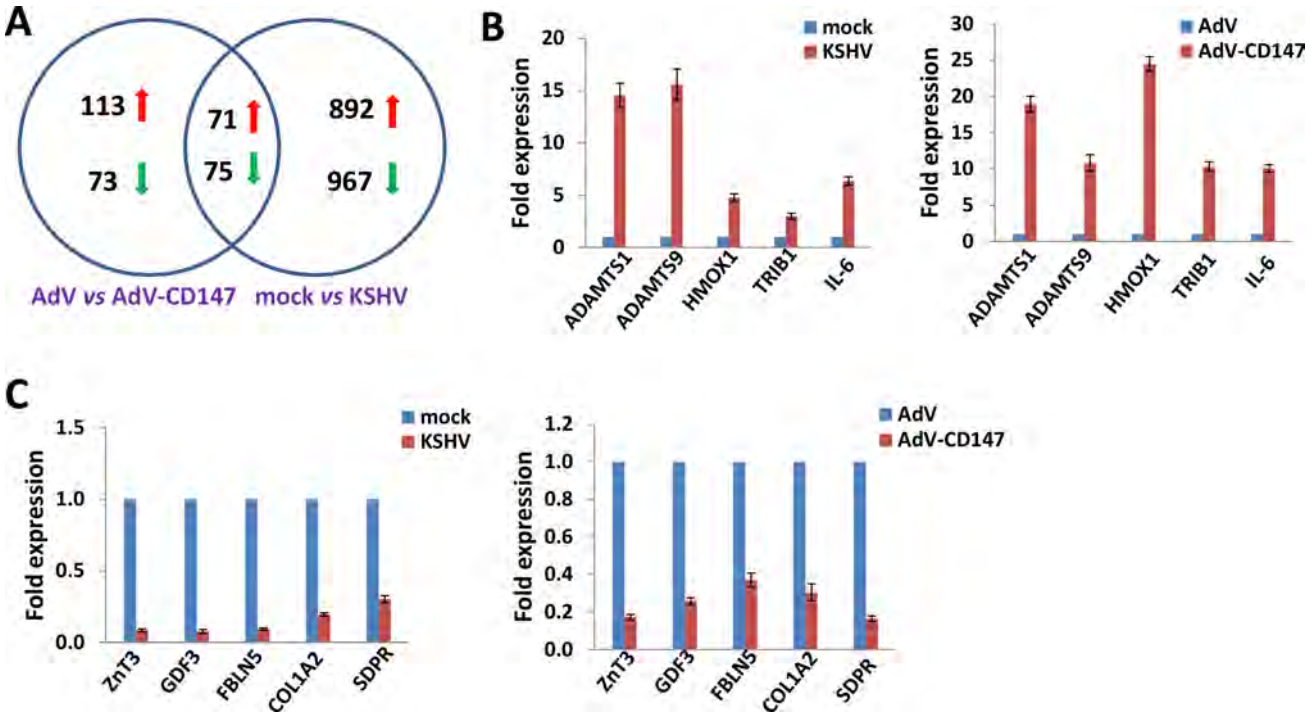

Figure 1: Intersection analysis and experimental validation of gene profile alterations in KSHV-infected and CD147-overexpressed endothelial cells. (**A**) The HumanHT-12 v4 Expression BeadChip (Illumina) was used to detect alterations in gene profile in HUVEC cells infected by KSHV (*vs* mock cells), or cells transduced with AdV-CD147 (*vs* AdV-transduced cells). Intersection analysis of significantly altered genes (up/down ≥ 2 fold and $p < 0.05$) was performed using the Illumina GenomeStudio Software. (**B–C**) The transcriptional levels of 5 selected 'common' candidate genes that were up-regulated (B) or down-regulated (C) in each set of microarray data were validated by using qRT-PCR. Error bars represent the S.E.M. for 3 independent experiments.

Table 1: The top 10 'common' candidate genes upregulated or downregulated within both CD147-overexpressed and KSHV-infected HUVEC cells

Gene symbol	Description	Fold change	
		CD147-overexpressed	KSHV-infected
ADAMTS1	A disintegrin and metalloproteinase with thrombospondin motifs 1	16.72	19.26
HMOX1	Heme oxygenase 1	25.8	2.31
RASD1	Dexamethasone-induced Ras-related protein 1	19.74	2.21
ADAMTS9	A disintegrin and metalloproteinase with thrombospondin motifs 9	6.69	12.89
TMEM158	Transmembrane protein 158	14.15	2.44
TRIB1	Tribbles homolog 1	12.23	3.58
DUSP12	Dual specificity protein phosphatase 12	12.8	2.81
IL6	Interleukin-6	8.13	6.69
RGS2	Regulator of G-protein signaling 2	3.73	10.64
CXCL2	C-X-C motif chemokine 2	11.96	2.35
ZnT3	Zinc transporter 3	0.13	0.13
GDF3	Growth/differentiation factor 3	0.16	0.12
MYH10	Myosin-10	0.03	0.26
LTBP2	Latent-transforming growth factor beta-binding protein 2	0.12	0.25
FBLN5	Fibulin-5	0.24	0.15
COL1A2	Collagen alpha-2(I) chain	0.24	0.18
STAT1	Signal transducer and activator of transcription 1-alpha/beta	0.07	0.36
GPR126	G-protein coupled receptor 126	0.2	0.23
GPR124	G-protein coupled receptor 124	0.23	0.28
SDPR	Serum deprivation-response protein	0.08	0.47

Establishment of a KS-like nude mouse model using TIVE-LT cells

KSHV-infected primary endothelial cells usually cannot form tumors even in immunodeficiency mice [24]. Recently, a stable KSHV latency cell-line, named TIVE-LT cells has been established, which can induce KS-like tumor formation in nude mice [13]. Here we found robust LANA expression in the nuclei of TIVE-LT cells (a molecular marker for KSHV latency) [29], while none was observed in the uninfected parental TIVE cells (Figure 4A). Interestingly, TIVE-LT cells displayed much higher levels of CD147, ADAMTS1 and 9 expression than TIVE cells (Figure 4B). Accordingly, TIVE-LT cells possessed much stronger capacities for cell invasion and anchorage-independent growth than TIVE cells, the latter forming almost no colonies in the soft agar assay (Figure 4C–4D).

We next examined the ability of TIVE and TIVE-LT cells to form tumors after subcutaneous injection into nude mice. We found that all the mice injected with TIVE-LT cells developed visible tumors by 28 day (4/4), while none (0/4) of the mice injected with TIVE cells did (Figure 4E). H & E staining of tumor tissues from TIVE-LT-injected mouse displayed KS-like features, including a mixture of elongated-spindle-cell and undifferentiated morphologies with prominent mitotic Figures. Immunohistochemistry (IHC) staining showed that most tumor cells expressed KS-specific viral/cellular marker molecules [24], such as LANA, CD31 and LYVE-1 (Figure 4F).

Targeting CD147 and downstream ADAMTS1 suppresses KSHV+ TIVE-LT cell tumorigenesis *in vivo*

Since TIVE-LT cells displaying high CD147 expression, we found that silencing of CD147 by RNAi reduced the expression of ADAMTS1 and 9 (Figure 5A), as well as their transcripts (data not shown). Silencing of CD147 by RNAi significantly blocked TIVE-LT cell invasion and anchorage-independent growth, when compared to negative control siRNA (n-siRNA) group (Figure 5B–5C). We also observed long-term "knock-down" of CD147 expression by RNAi for at least 2 weeks *in vitro* culture (Supplementary Figure S5). Next, we injected TIVE-LT cells transfected with n-siRNA or *CD147*-siRNA subcutaneously into the right and left flanks of nude mice, respectively. These mice were observed and measured every 2~3 day for the presence of palpable tumors for 21 days. Our results indicated that silencing of CD147 significantly repressed tumor growth in nude mice. Mice injected with *CD147*-siRNA formed smaller tumors when compared to n-siRNA groups at 21 days (Figure 5D–5E). Immunoblot results confirmed the higher levels of CD147, ADAMTS1 and 9 expression in tumor lysates from mice with n-siRNA than those from mice with *CD147*-siRNA, demonstrating the successful silencing of CD147 and downstream ADAMTSs *in vivo* (Figure 5F). Our additional data indicated that direct silencing of ADAMTS1 by siRNA also significantly repressed tumor growth in nude mice (Supplementary Figure S6). Taken

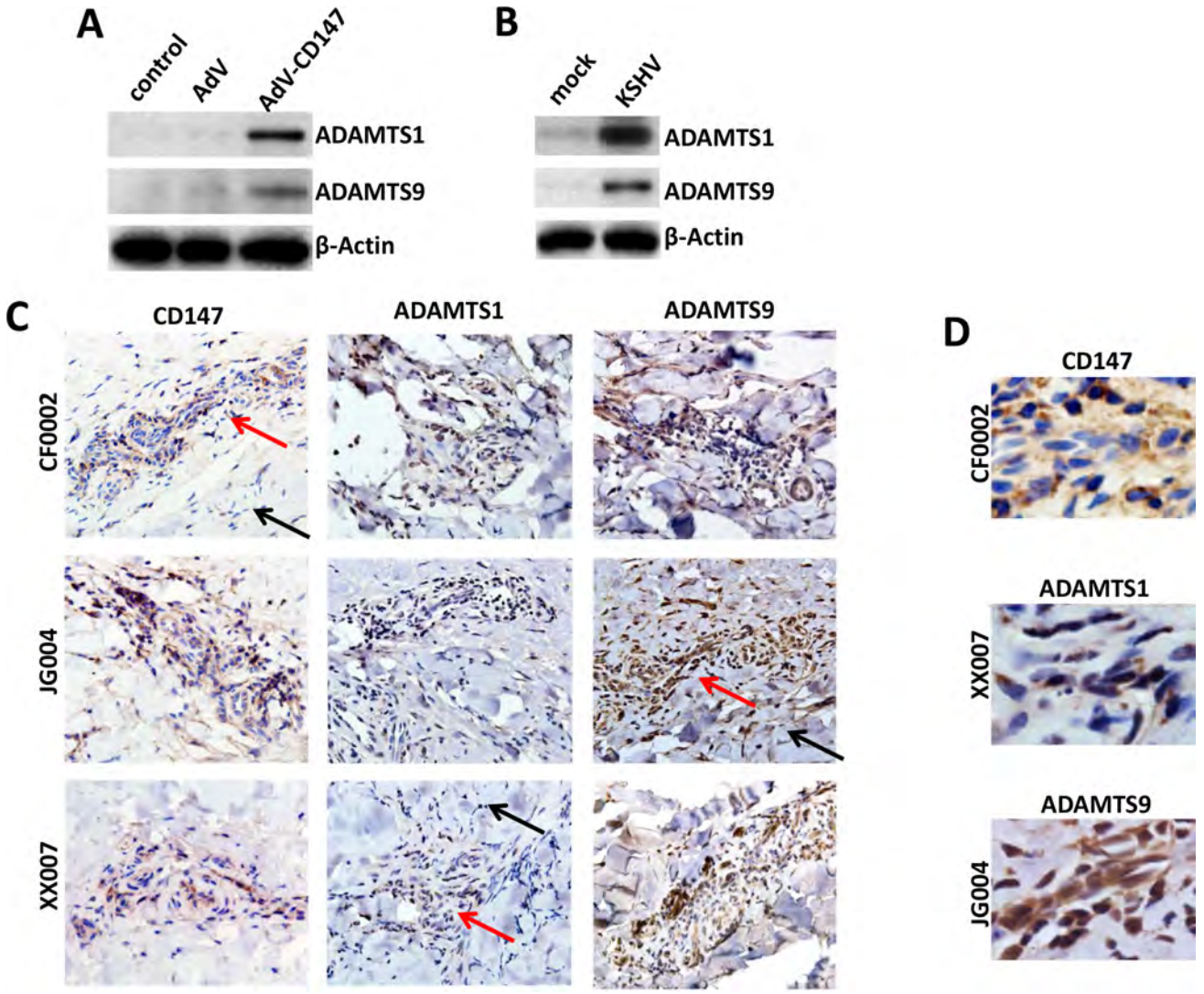

Figure 2: Up-regulation of ADAMTS1 and 9 expression in CD147-overexpressed or KSHV-infected endothelial cells and in AIDS-KS tissues. (**A–B**) HUVEC were transduced using a recombinant human CD147-encoding adenovirus (AdV-CD147), or control adenovirus (AdV) for 48 h, or infected by purified KSHV (MOI ~ 10) for 48 h. Protein expression was measured by immunoblots. (**C–D**) The expression of CD147, ADAMTS1 and ADAMTS9 within KS tumor tissues from 3 cohort HIV+ patients was detected by immunohistochemistry (400x magnification, and tumor cells in selected regions were magnified at 600x in panel D). Red arrows indicate the KS tumor area and black arrows indicate the adjacent area from the same patient.

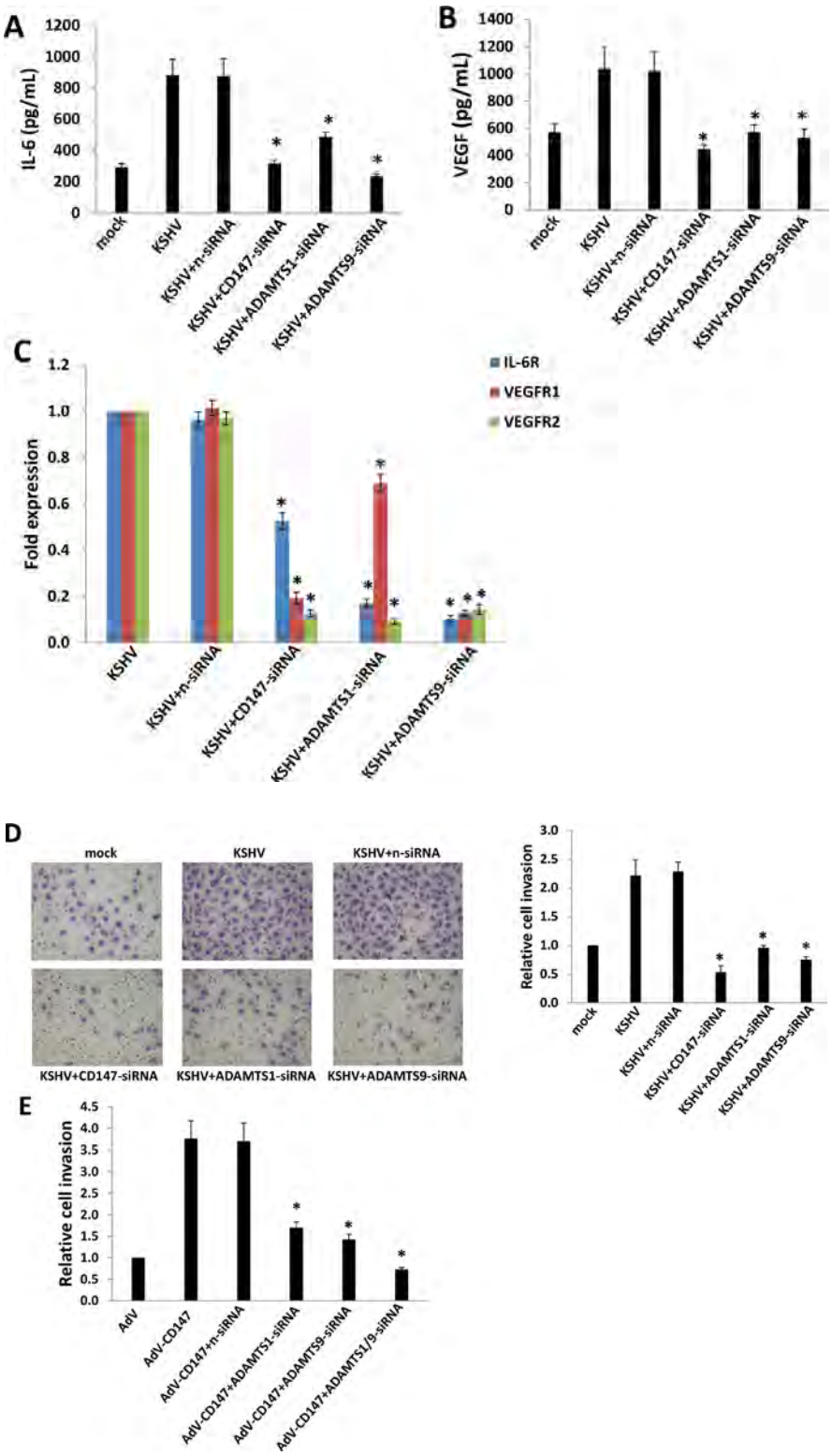

Figure 3: Targeting CD147 and downstream ADAMTSs represses expression of IL-6, VEGF, their respective receptors, and KSHV-infected endothelial cell invasion. (**A–B**) HUVEC were incubated with media (mock) or purified KSHV for 2 h, with or without prior transfection for 48 h with negative control siRNA (n-siRNA), *CD147*-siRNA, *ADAMTS1*-siRNA or *ADAMTS9*-siRNA, respectively. Cells were subsequently incubated in fresh media for an additional 24 h. The concentrations of IL-6 and VEGF in culture supernatants were determined using ELISAs. (**C–D**) HUVEC were treated as above, then the expression of cytokine receptor genes and cell invasiveness were measured by qRT-PCR and transwell assays, respectively. (**E**) HUVEC were transfected for 48 h with negative n-siRNA, *ADAMTS1*-siRNA or *ADAMTS9*-siRNA, respectively, then transduced with AdV-CD147 or control AdV for 48 h. Cell invasion was assessed by transwell assays. Error bars represent the S.E.M. for 3 independent experiments. * = $p < 0.05$.

together, these data support the important role of CD147, ADAMTS1 and 9 as cellular co-factors for KSHV-related tumorigenicity and KS development.

DISCUSSION

Our previous studies have demonstrated that CD147 is an important contributor to KSHV-induced endothelial cell invasiveness, through a complex of underlying mechanisms [10, 11, 30]. However to our knowledge, there are no current data exploring the global gene profile controlled by CD147 in primary endothelial cells, in particular KSHV-infected cells, which are the major cellular components of KS tissues. In the current study, we identified at least ~150 genes potentially controlled by CD147 in KSHV-infected endothelial cells by using Illumina microarray. Interestingly, only a few of them have been reported associated with KSHV pathogenesis, e.g. HMOX-1 and FBLN5 [14, 15], while most of them remain functionally unknown with respect to KSHV-related diseases. The enrichment analysis indicates that these genes belong to several major cellular function categories closely related to KSHV pathogenesis, such as EMT and blood vessel development [22, 23]. Although the role of EMT in KS development remains unclear, another similar pathophysiologic behavior, called as endothelial-to-mesenchymal transformation (EndMT), has been described during KSHV infection. Cheng *et al.* reported that KSHV-induced EndMT was initiated by the viral FLICE inhibitory protein (vFLIP) or vGPCR through Notch pathway activation, leading to cell invasiveness dependent upon membrane-type-1 matrix metalloproteinase (MT1-MMP) [31]. Gasperini *et al.* reported that canonical Notch signaling, including Slug

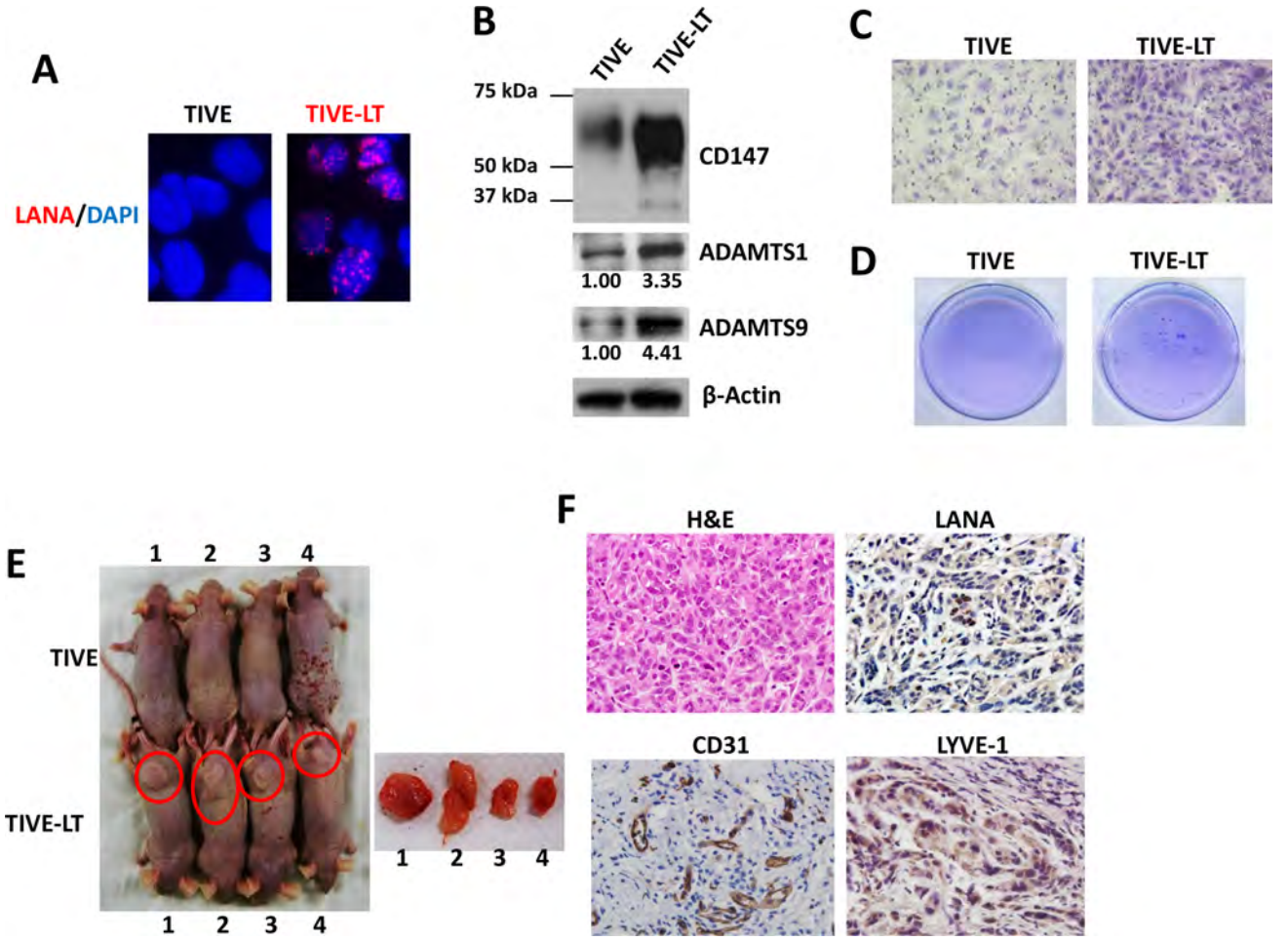

Figure 4: Establishment of a KS-like nude mouse model using TIVE-LT cells. (**A**) IFA was used to detect nuclear LANA expression in TIVE-LT cells, and TIVE cells as a negative control. (**B–D**) Protein expression (B), cell invasion (C) and anchorage-independent growth (D) were measured by immunoblots, transwell and soft agar assays, respectively. (**E**) TIVE or TIVE-LT cells (approximately 5×10^5 cells were mixed at a ratio of 1:1 with growth factor-depleted Matrigel) were injected subcutaneously into nude mice. Mice injected with TIVE-LT at 28d developed tumors (4/4) as shown by red circle, while none (0/4) of the mice injected with TIVE cells did. (**F**) H & E staining of representative tumor tissues isolated from TIVE-LT-injected mice displayed KS-like features, including a mixture of elongated-spindle-cell and undifferentiated morphologies with prominent mitotic figures. Immunohistochemistry (IHC) staining showed that most tumor cells expressed KS-specific viral/cellular marker molecules.

and ZEB1, was required for KSHV-induced EndMT which increased invasiveness and survival in infected endothelial cells [32]. Interestingly, CD147 has been found involved in EMT and closely associated phenomena in cancer cells [33–35]. Additionally, the expression of functional CD147 and MMP-2 was significantly decreased in Notch1-deficient breast cancer cells which displayed impaired migration and invasion [36].

Here we showed that two specific metalloproteases, ADAMTS1 and 9 were up-regulated by CD147 and contributed to KSHV-induced cell invasiveness. Previous reports showed that CD147 induced production of several MMPs [7–9] and urokinase-type plasminogen activator [37], but to our knowledge this is the first report showing the up-regulation of ADAMTSs by CD147. Moreover, CD147, ADAMTS1 and 9 were strongly expressed within AIDS-KS tumor tissues, demonstrating their potential clinical relevance as well as biomarker or therapeutic values. However, it remains unknown how CD147 can increase the expression and maturation of ADAMTS1 and 9, which may require a variety of additional factors. For example, ADAMTS1 is synthesized as a pro-zymogen and undergoes N-linked glycosylation following protein translation [38]. The secretion of ADAMTS1 to the ECM requires the excision of its pro-domain from the 87kD mature protein by furin-related endopeptidases [38]. Interestingly, ADAMTS1 can be transiently induced by hypoxia in endothelial cells, which is mediated by hypoxia-inducible factor 1 (HIF-1) binding to its promoter region [39]. Moreover, CD147 can be induced in a similar manner in various carcinoma cells [40]. It has been reported that several KSHV-encoded proteins such as LANA, vIRF-3 or vGPCR can activate HIF-1 and contribute to angiogenesis, tumorigenesis or virus

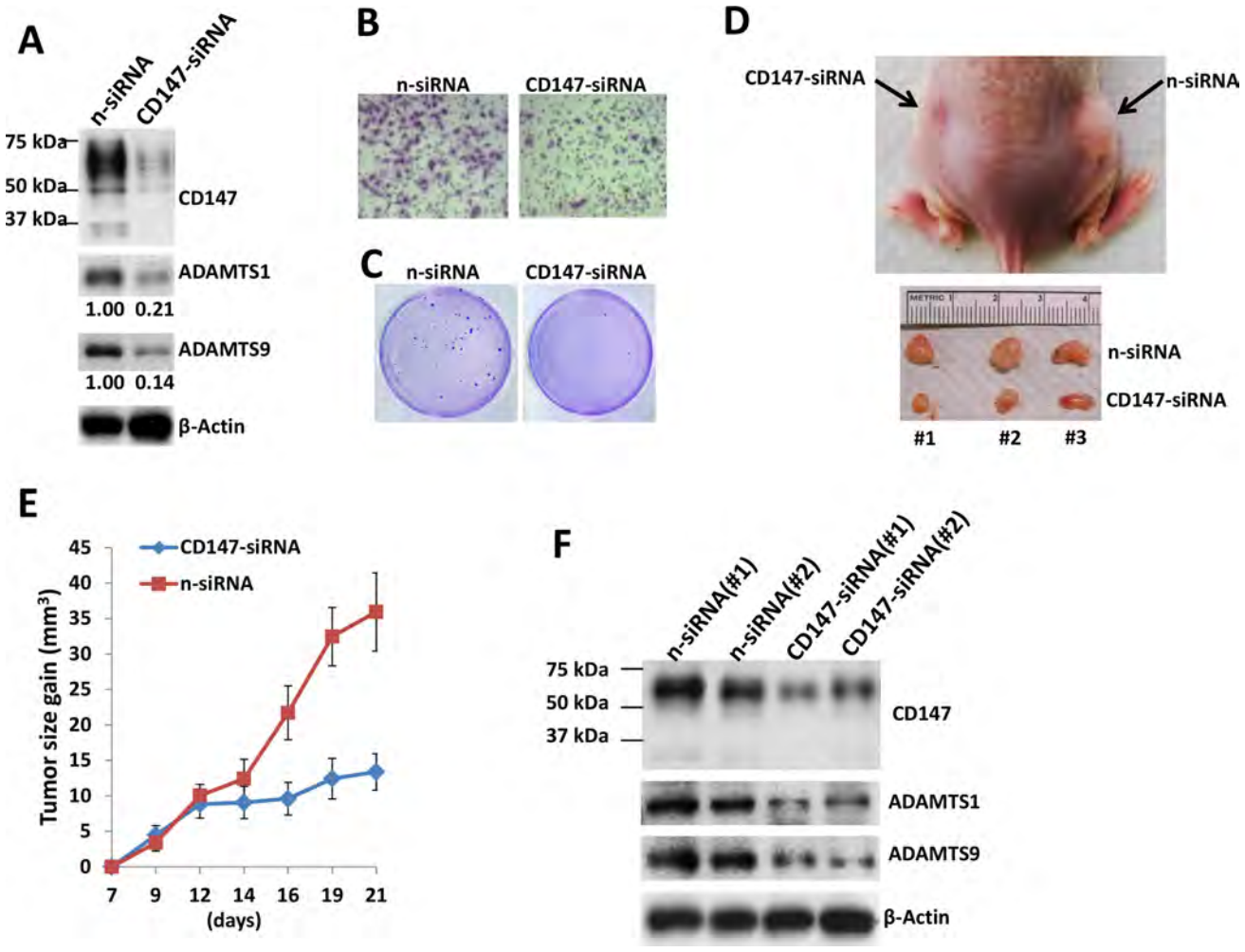

Figure 5: Targeting CD147 significantly suppresses TIVE-LT cell tumorigenesis *in vivo*. (**A–C**) TIVE-LT cells were transfected with negative control siRNA (n-siRNA) or CD147-siRNA for 48 h, then protein expression (A), cell invasion (B) and anchorage-independent growth (C) were measured by immunoblots, transwell and soft agar assays, respectively. (**D–E**) TIVE-LT cells transfected with n-siRNA or CD147-siRNA (approximately 5×10^5 cells were mixed at a ratio of 1:1 with growth factor-depleted Matrigel) were injected subcutaneously into the right and left flanks of nude mice (3 mice per group), respectively. The mice were observed and measured every 2~3 d for the presence of palpable tumors for 21 d. (**F**) Protein expression was measured by immunoblots of tumor lysates from 2 TIVE-LT/n-siRNA or TIVE-LT/CD147-siRNA injected flanks of mice sacrificed at day 21, respectively.

replication [41–44]. Therefore, we are interested to understand whether these viral proteins (latent or lytic) are able to up-regulate the expression of ADAMTS1 and 9 and the underlying mechanisms.

Our data showed that silencing of CD147 by RNAi significantly repressed tumor growth in a nude mouse model, and that these treated tumor tissues displayed less blood vessel formation and less tumor cells when compared to n-siRNA groups (data not shown). We assume this is partially due to impaired ECM dynamics in the tumor microenvironment through down-regulation of ADAMTS1 and 9. Our recent study indicated that silencing of CD147 by RNAi greatly reduced the production of hyaluronan, an important ECM component, through down-regulation of the hyaluronan synthase gene 1 (*Has1*) within KSHV-infected HUVEC cells [30]. Interestingly, we found that silencing of CD147 also significantly reduced hyaluronan production from TIVE-LT cells, in this case through down-regulation of *Has2* and *Has3* instead of *Has1* (Dai *et al*, unpublished data). Therefore, we will evaluate the strategies targeting ECM formation and/or components as potential therapies against KS development in future study.

MATERIALS AND METHODS

Cell culture, reagents and infection protocol

Body cavity-based lymphoma cells (BCBL-1, $KSHV^+/EBV^-$) were maintained in RPMI 1640 medium (Gibco) with supplements as described previously [45]. Telomerase-immortalized human umbilical vein endothelial (TIVE) and KSHV long-term-infected TIVE (TIVE-LT) cells were cultured as previously described [13]. Human umbilical vein endothelial cells (HUVEC) were grown in DMEM/F-12 50/50 medium (Cellgro) supplemented with 5% FBS. All cells were incubated at 37°C in 5% CO_2. All experiments were carried out using cells harvested at low (< 20) passages. To obtain KSHV for infection experiments, BCBL-1 cells were incubated with 0.6 mM valproic acid for 6 days, and purified virus was concentrated from culture supernatants and infectious titers were determined as described previously [46]. For overexpression of CD147, HUVEC were transduced as previously described with a recombinant adenoviral vector (MOI ~ 10) encoding CD147 (AdV-CD147), or a control vector (AdV), for 48 h prior to subsequent analyses [11].

Microarray

Total RNA was isolated using Qiagen RNeasy kit (Qiagen), and 500 ng of total RNA was used to synthesize dscDNA. Biotin-labeled RNA was generated using the TargetAmp-Nano Labeling Kit for Illumina Expression BeadChip (Epicentre), according to the manufacturers' instructions, and hybridized to the HumanHT-12 v4 Expression BeadChip (Illumina), which contains more than 47,000 probes derived from the NCBI RefSeq Release 38 and other sources, at 58°C for 16 h. The chip was washed, stained with streptavadin-Cy3, and scanned with the Illumina BeadStation 500 and BeadScan. Using the Illumina's GenomeStudio software, we normalized the signals using the "cubic spline algorithm" that assumes that the distribution of transcript abundance is similar in all samples, according to the method proposed by Workman *et al.* [47]. The background signal was removed using the "detection *p*-value algorithm" to remove targets with signal intensities equal or lower than that of irrelevant probes (with no known targets in the human genome but thermodynamically similar to the relevant probes). The microarray experiments were performed twice for each group and the average values were used for analysis. Common and unique sets of genes and enrichment analysis were performed using the MetaCore Software (Thompson Reuters) as previously reported [21]. The microarray original data have been submitted to Gene Expression Omnibus (GEO) database (Accession number: GSE69067).

RNA interference

CD147, *ADAMTS1* or *ADAMTS9* ON-TARGET plus SMART pool siRNA, or negative control siRNA (n-siRNA) (Dharmacon), were delivered using the DharmaFECT transfection reagent according to the manufacturer's instructions.

Immunoblotting

Total cell lysates (20 μg) were resolved by 10% SDS–PAGE, transferred to nitrocellulose membranes, and immunoblotted with antibodies for CD147 (BD), ADAMTS1, ADAMTS9 (Cell Signaling) and β-Actin (Sigma) for loading controls. Immunoreactive bands were identified using an enhanced chemiluminescence reaction (Perkin-Elmer), visualized by autoradiography and quantitated using Image-J software.

Immunofluorescence

Cells were incubated in 1:1 methanol-acetone at −20°C for fixation and permeabilization, then with a blocking reagent (10% normal goat serum, 3% bovine serum albumin, and 1% glycine) for an additional 30 minutes. Cells were then incubated for 1 h at 25°C with 1:1000 dilution of a rat anti-LANA monoclonal antibody (ABI) followed by 1:200 dilution of a goat anti-rat secondary antibody conjugated to Texas Red (Invitrogen). For identification of nuclei, cells were subsequently counterstained with 0.5 mg/mL 4′,6-diamidino-2-phenylindole (DAPI; Sigma) in 180 mM Tris-HCl

(pH 7.5). Slides were washed once in 180 mM Tris-HCl for 15 minutes and prepared for visualization using a Leica TCPS SP5 AOBS confocal microscope.

qRT-PCR

Total RNA was isolated using the RNeasy Mini kit (QIAGEN), and cDNA was synthesized from equivalent total RNA using a SuperScript III First-Strand Synthesis SuperMix Kit (Invitrogen) according to the manufacturer's instructions. Primers used for amplification of target genes are displayed in Supplementary Table 1. Amplification was carried out using an iCycler IQ Real-Time PCR Detection System, and cycle threshold (Ct) values were tabulated in duplicate for each gene of interest in each experiment. "No template" (water) controls were used to ensure minimal background contamination. Using mean Ct values tabulated for each gene, and paired Ct values for β-*actin* as a loading control, fold changes for experimental groups relative to assigned controls were calculated using automated iQ5 2.0 software (Bio-rad).

ELISA

Concentrations of IL-6 and VEGF in culture supernatants were determined using human IL-6 (eBioscience) and VEGF-A (Pierce Biotechnology) ELISA kits according to the manufacturers' instructions.

Transwell invasion assays

Matrigel Invasion Chambers (BD) were hydrated for 4 h at 37°C with culture media. Following hydration, media in the bottom of the well was replaced with fresh media, then 2×10^4 HUVEC, TIVE or TIVE-LT cells were plated in the top of the chamber. After 24 h, cells were fixed with 4% formaldehyde for 15 min at room temperature and chambers rinsed in PBS prior to staining with 0.2% crystal violet for 10 min. After washing the chambers, cells at the top of the membrane were removed and cells at the bottom of the membrane counted using a phase contrast microscope. Relative invasion was determined for cells in experimental groups as follows: relative invasion = # invading cells in experimental group / # invading cells in control groups.

Soft agar assays

A base layer containing 0.5% agarose medium and 5% FCS was poured into six-well plates. Then, 10,000 cells were mixed with 0.4% agarose in Earl's minimal essential medium (EMEM) containing 5% FCS to form a single-cell suspension. After being seeded, the plates were incubated for 2 weeks. Colonies were stained with 0.005% crystal violet and photographed under a phase-contrast microscope (Leica DFC320).

KS-like nude mouse model

Cells were counted and washed once in ice-cold PBS, and 5×10^5 cells in 50 µL PBS plus 50 µL growth factor-depleted Matrigel (BD Biosciences) were injected subcutaneously into the flanks of nude mice (Jackson Laboratory). The mice were observed and measured every 2~3 d for the presence of palpable tumors. At the end of experiment, the tumors were excised from the site of injection for subsequent analysis such as immunoblots and immunohistochemistry. All protocols were approved by the LSUHSC Animal Care and Use Committee in accordance with national guidelines.

KS tumor tissues from HIV$^+$ patients and immunohistochemistry

KS tissues from HIV-infected patients were provided by the LSUHSC HIV Outpatient (HOP) Clinic and Biospecimens Bank (LSUHSC IRB approved No. 8079). Formalin-fixed, paraffin-embedded tissues were microtome-sectioned to a thickness of 4 uM, placed on electromagnetically charged slides (Fisher Scientific), and stained with hematoxylin & eosin (H & E) for routine histologic analysis. Immunohistochemistry was performed using the Avidin-Biotin-Peroxidase complex system, according to the manufacturer's instructions (Vectastain Elite ABC Peroxidase Kit; Vector Laboratories). In our modified protocol, sections were deparaffinized in xylene and re-hydrated through a descending alcohol gradient. For non-enzymatic antigen retrieval, slides were heated in 0.01 M sodium citrate buffer (pH 6.0) to 95ºC under vacuum for 40 min and allowed to cool for 30 min at room temperature, then rinsed with PBS and incubated in MeOH/3% H_2O_2 for 20 min to quench endogenous peroxidase. Slides were then washed with PBS and blocked with 5% normal goat serum in 0.1% PBS/BSA for 2 h at room temperature, then incubated overnight with indicated antibody at 1:200-1:400 dilution in 0.1% PBS/BSA. The following day, slides were incubated with appropriate secondary antibody at room temperature for 1 h, followed by avidin-biotin peroxidase complexes for 1 h at room temperature. Finally, slides were developed using a diaminobenzidine substrate, counterstained with hematoxylin, dehydrated through an ascending alcohol gradient, cleared in xylene, and coverslipped with Permount. Images were collected using an Olympus BX61 microscope equipped with a high resolution DP72 camera and CellSense image capture software.

Statistical analysis

Significance for differences between experimental and control groups was determined using the two-tailed Student's *t*-test (Excel 8.0), and p values < 0.05 were considered significant.

ACKNOWLEDGMENTS AND FUNDINGS

We thank Dr. Rolf Renne at University of Florida for his kind gifts of TIVE-LT and TIVE cells. This work was supported by grants from a DOD Career Development Award (CA140437), the SOM Research Enhancement Funding, as well as awards from the National Natural Science Foundation of China (81272191, 81472547 and 81400164) and the Foundation for Innovative Research Groups of the NNSF of China (81221001). De-identified human KS tumors were provided by the HIV Cancer Care Program Biorepository which is supported by grants from the National Institute of Health (UM1-CA181255 and R01-CA142362). Funding sources had no role in study design, data collection and analysis, decision to publish, or preparation of the manuscript.

CONFLICTS OF INTEREST

All the authors declare no conflicts of interest.

REFERENCES

1. Chang Y, Cesarman E, Pessin MS, Lee F, Culpepper J, Knowles DM, Moore PS. Identification of herpesvirus-like DNA sequences in AIDS-associated Kaposi's sarcoma. Science. 1994; 266:1865–1869.
2. Engels EA, Biggar RJ, Hall HI, Cross H, Crutchfield A, Finch JL, Grigg R, Hylton T, Pawlish KS, McNeel TS, Goedert JJ. Cancer risk in people infected with human immunodeficiency virus in the United States. Int J Cancer. 2008; 123:187–194.
3. Bonnet F, Lewden C, May T, Heripret L, Jougla E, Bevilacqua S, Costagliola D, Salmon D, Chene G, Morlat P. Malignancy-related causes of death in human immunodeficiency virus-infected patients in the era of highly active antiretroviral therapy. Cancer. 2004; 101:317–324.
4. Jenkins FJ, Hoffman LJ, Liegey-Dougall A. Reactivation of and primary infection with human herpesvirus 8 among solid-organ transplant recipients. J Infect Dis. 2002; 185:1238–1243.
5. Luppi M, Barozzi P, Santagostino G, Trovato R, Schulz TF, Marasca R, Bottalico D, Bignardi L, Torelli G. Molecular evidence of organ-related transmission of Kaposi sarcoma-associated herpesvirus or human herpesvirus-8 in transplant patients. Blood. 2000; 96:3279–3281.
6. Ariza-Heredia EJ, Razonable RR. Human herpes virus 8 in solid organ transplantation. Transplantation. 2011; 92: 837–844.
7. Biswas C, Zhang Y, DeCastro R, Guo H, Nakamura T, Kataoka H, Nabeshima K. The human tumor cell-derived collagenase stimulatory factor (renamed EMMPRIN) is a member of the immunoglobulin superfamily. Cancer Res. 1995; 55:434–439.
8. Yan L, Zucker S, Toole BP. Roles of the multifunctional glycoprotein, emmprin (basigin; CD147), in tumour progression. Thromb Haemost. 2005; 93:199–204.
9. Grass GD, Dai L, Qin Z, Parsons C, Toole BP. CD147: regulator of hyaluronan signaling in invasiveness and chemoresistance. Adv Cancer Res. 2014; 123:351–373.
10. Qin Z, Dai L, Slomiany MG, Toole BP, Parsons C. Direct activation of emmprin and associated pathogenesis by an oncogenic herpesvirus. Cancer Res. 2010; 70:3884–3889.
11. Dai L, Bratoeva M, Toole BP, Qin Z, Parsons C. KSHV activation of VEGF secretion and invasion for endothelial cells is mediated through viral up-regulation of emmprin-induced signal transduction. Int J Cancer. 2012; 131: 834–843.
12. Qin Z, Dai L, Bratoeva M, Slomiany MG, Toole BP, Parsons C. Cooperative roles for emmprin and LYVE-1 in the regulation of chemoresistance for primary effusion lymphoma. Leukemia. 2011; 25:1598–1609.
13. An FQ, Folarin HM, Compitello N, Roth J, Gerson SL, McCrae KR, Fakhari FD, Dittmer DP, Renne R. Long-term-infected telomerase-immortalized endothelial cells: a model for Kaposi's sarcoma-associated herpesvirus latency *in vitro* and *in vivo*. J Virol. 2006; 80:4833–4846.
14. McAllister SC, Hansen SG, Ruhl RA, Raggo CM, DeFilippis VR, Greenspan D, Fruh K, Moses AV. Kaposi sarcoma-associated herpesvirus (KSHV) induces heme oxygenase-1 expression and activity in KSHV-infected endothelial cells. Blood. 2004; 103:3465–3473.
15. Alcendor DJ, Knobel S, Desai P, Zhu WQ, Hayward GS. KSHV regulation of fibulin-2 in Kaposi's sarcoma: implications for tumorigenesis. Am J Pathol. 2011; 179:1443–1454.
16. Cross NA, Chandrasekharan S, Jokonya N, Fowles A, Hamdy FC, Buttle DJ, Eaton CL. The expression and regulation of ADAMTS-1, -4, -5, -9, and -15, and TIMP-3 by TGFbeta1 in prostate cells: relevance to the accumulation of versican. Prostate. 2005; 63:269–275.
17. Ricciardelli C, Frewin KM, Tan Ide A, Williams ED, Opeskin K, Pritchard MA, Ingman WV, Russell DL. The ADAMTS1 protease gene is required for mammary tumor growth and metastasis. Am J Pathol. 2011; 179:3075–3085.
18. Okada Y. Tumor cell-matrix interaction: pericellular matrix degradation and metastasis. Verh Dtsch Ges Pathol. 2000; 84:33–42.
19. Demircan K, Gunduz E, Gunduz M, Beder LB, Hirohata S, Nagatsuka H, Cengiz B, Cilek MZ, Yamanaka N, Shimizu K, Ninomiya Y. Increased mRNA expression of ADAMTS metalloproteinases in metastatic foci of head and neck cancer. Head Neck. 2009; 31:793–801.

20. Tan Ide A, Ricciardelli C, Russell DL. The metalloproteinase ADAMTS1: a comprehensive review of its role in tumorigenic and metastatic pathways. Int J Cancer. 2013; 133:2263–2276.

21. Kim SH, Sierra RA, McGee DJ, Zabaleta J. Transcriptional profiling of gastric epithelial cells infected with wild type or arginase-deficient Helicobacter pylori. BMC Microbiol. 2012; 12:175.

22. Cavallin LE, Goldschmidt-Clermont P, Mesri EA. Molecular and cellular mechanisms of KSHV oncogenesis of Kaposi's sarcoma associated with HIV/AIDS. PLoS Pathog. 2014; 10:e1004154.

23. Mesri EA, Feitelson MA, Munger K. Human viral oncogenesis: a cancer hallmarks analysis. Cell Host Microbe. 2014; 15:266–282.

24. Mesri EA, Cesarman E, Boshoff C. Kaposi's sarcoma and its associated herpesvirus. Nat Rev Cancer. 2010; 10: 707–719.

25. Riva G, Barozzi P, Torelli G, Luppi M. Immunological and inflammatory features of Kaposi's sarcoma and other Kaposi's sarcoma-associated herpesvirus/human herpesvirus 8-associated neoplasias. AIDS Rev. 2010; 12:40–51.

26. Ensoli B, Sturzl M. Kaposi's sarcoma: a result of the interplay among inflammatory cytokines, angiogenic factors and viral agents. Cytokine Growth Factor Rev. 1998; 9:63–83.

27. Sivakumar R, Sharma-Walia N, Raghu H, Veettil MV, Sadagopan S, Bottero V, Varga L, Levine R, Chandran B. Kaposi's sarcoma-associated herpesvirus induces sustained levels of vascular endothelial growth factors A and C early during *in vitro* infection of human microvascular dermal endothelial cells: biological implications. J Virol. 2008; 82:1759–1776.

28. Qian LW, Xie J, Ye F, Gao SJ. Kaposi's sarcoma-associated herpesvirus infection promotes invasion of primary human umbilical vein endothelial cells by inducing matrix metalloproteinases. J Virol. 2007; 81:7001–7010.

29. Ballestas ME, Chatis PA, Kaye KM. Efficient persistence of extrachromosomal KSHV DNA mediated by latency-associated nuclear antigen. Science. 1999; 284:641–644.

30. Dai L, Chen Y, Toole B, Parsons C, Qin Z. Induction of hyaluronan production by oncogenic KSHV and the contribution to viral pathogenesis in AIDS patients. Cancer Lett. 2015; 362:158–166.

31. Cheng F, Pekkonen P, Laurinavicius S, Sugiyama N, Henderson S, Gunther T, Rantanen V, Kaivanto E, Aavikko M, Sarek G, Hautaniemi S, Biberfeld P, Aaltonen L, et al. KSHV-initiated notch activation leads to membrane-type-1 matrix metalloproteinase-dependent lymphatic endothelial-to-mesenchymal transition. Cell Host Microbe. 2011; 10:577–590.

32. Gasperini P, Espigol-Frigole G, McCormick PJ, Salvucci O, Maric D, Uldrick TS, Polizzotto MN, Yarchoan R, Tosato G. Kaposi sarcoma herpesvirus promotes endothelial-to-mesenchymal transition through Notch-dependent signaling. Cancer Res. 2012; 72:1157–1169.

33. Wu J, Ru NY, Zhang Y, Li Y, Wei D, Ren Z, Huang XF, Chen ZN, Bian H. HAb18G/CD147 promotes epithelial-mesenchymal transition through TGF-beta signaling and is transcriptionally regulated by Slug. Oncogene. 2011; 30:4410-4427.

34. Grass GD, Bratoeva M, Toole BP. Regulation of invadopodia formation and activity by CD147. J Cell Sci. 2012; 125:777–788.

35. Grass GD, Tolliver LB, Bratoeva M, Toole BP. CD147, CD44, and the epidermal growth factor receptor (EGFR) signaling pathway cooperate to regulate breast epithelial cell invasiveness. J Biol Chem. 2013; 288:26089–26104.

36. Wang J, Fu L, Gu F, Ma Y. Notch1 is involved in migration and invasion of human breast cancer cells. Oncol Rep. 2011; 26:1295–1303.

37. Quemener C, Gabison EE, Naimi B, Lescaille G, Bougatef F, Podgorniak MP, Labarchede G, Lebbe C, Calvo F, Menashi S, Mourah S. Extracellular matrix metalloproteinase inducer up-regulates the urokinase-type plasminogen activator system promoting tumor cell invasion. Cancer Res. 2007; 67:9–15.

38. Kuno K, Matsushima K. ADAMTS-1 protein anchors at the extracellular matrix through the thrombospondin type I motifs and its spacing region. J Biol Chem. 1998; 273:13912–13917.

39. Hatipoglu OF, Hirohata S, Cilek MZ, Ogawa H, Miyoshi T, Obika M, Demircan K, Shinohata R, Kusachi S, Ninomiya Y. ADAMTS1 is a unique hypoxic early response gene expressed by endothelial cells. J Biol Chem. 2009; 284:16325–16333.

40. Ke X, Fei F, Chen Y, Xu L, Zhang Z, Huang Q, Zhang H, Yang H, Chen Z, Xing J. Hypoxia up-regulates CD147 through a combined effect of HIF-1alpha and Sp1 to promote glycolysis and tumor progression in epithelial solid tumors. Carcinogenesis. 2012; 33:1598–1607.

41. Cai Q, Lan K, Verma SC, Si H, Lin D, Robertson ES. Kaposi's sarcoma-associated herpesvirus latent protein LANA interacts with HIF-1 alpha to up-regulate RTA expression during hypoxia: Latency control under low oxygen conditions. J Virol. 2006; 80:7965–7975.

42. Ma Q, Cavallin LE, Yan B, Zhu S, Duran EM, Wang H, Hale LP, Dong C, Cesarman E, Mesri EA, Goldschmidt-Clermont PJ. Antitumorigenesis of antioxidants in a transgenic Rac1 model of Kaposi's sarcoma. Proc Natl Acad Sci U S A. 2009; 106:8683–8688.

43. Shin YC, Joo CH, Gack MU, Lee HR, Jung JU. Kaposi's sarcoma-associated herpesvirus viral IFN regulatory factor 3

stabilizes hypoxia-inducible factor-1 alpha to induce vascular endothelial growth factor expression. Cancer Res. 2008; 68:1751–1759.

44. Sodhi A, Montaner S, Patel V, Zohar M, Bais C, Mesri EA, Gutkind JS. The Kaposi's sarcoma-associated herpes virus G protein-coupled receptor up-regulates vascular endothelial growth factor expression and secretion through mitogen-activated protein kinase and p38 pathways acting on hypoxia-inducible factor 1alpha. Cancer Res. 2000; 60:4873–4880.

45. Dai L, Trillo-Tinoco J, Bai L, Kang B, Xu Z, Wen X, Del Valle L, Qin Z. Systematic analysis of a xenograft mice model for KSHV+ primary effusion lymphoma (PEL). PLoS One. 2014; 9:e90349.

46. Qin Z, Dai L, Defee M, Findlay VJ, Watson DK, Toole BP, Cameron J, Peruzzi F, Kirkwood K, Parsons C. Kaposi's sarcoma-associated herpesvirus suppression of DUSP1 facilitates cellular pathogenesis following *de novo* infection. J Virol. 2013; 87:621–635.

47. Workman C, Jensen LJ, Jarmer H, Berka R, Gautier L, Nielser HB, Saxild HH, Nielsen C, Brunak S, Knudsen S. A new non-linear normalization method for reducing variability in DNA microarray experiments. Genome Biol. 2002; 3:research0048.

LYMPHOID NEOPLASIA

Targeting HGF/c-MET induces cell cycle arrest, DNA damage, and apoptosis for primary effusion lymphoma

Lu Dai,[1-3] Jimena Trillo-Tinoco,[4] Yueyu Cao,[2] Karlie Bonstaff,[3] Lisa Doyle,[3] Luis Del Valle,[4] Denise Whitby,[5] Chris Parsons,[3] Krzysztof Reiss,[3] Jovanny Zabaleta,[6] and Zhiqiang Qin[1,2]

[1]Department of Microbiology, Immunology, & Parasitology, Louisiana State University Health Sciences Center, Louisiana Cancer Research Center, New Orleans, LA; [2]Research Center for Translational Medicine and Key Laboratory of Arrhythmias, East Hospital, Tongji University School of Medicine, Shanghai, China; [3]Department of Medicine and [4]Department of Pathology, Louisiana State University Health Sciences Center, Louisiana Cancer Research Center, New Orleans, LA; [5]Viral Oncology Section, AIDS and Cancer Virus Program, Frederick National Laboratory for Cancer Research, Frederick, MD; and [6]Department of Pediatrics, Louisiana State University Health Sciences Center, Louisiana Cancer Research Center, New Orleans, LA

Key Points

- The HGF/c-MET pathway has a complex network to control KSHV$^+$ PEL cell survival.
- The c-MET inhibitor induces PEL apoptosis and suppresses tumor progression in vivo.

Kaposi sarcoma–associated herpesvirus (KSHV) is a principal causative agent of primary effusion lymphoma (PEL) with a poor prognosis in immunocompromised patients. However, it still lacks effective treatment which urgently requires the identification of novel therapeutic targets for PEL. Here, we report that the hepatocyte growth factor (HGF)/c-MET pathway is highly activated by KSHV in vitro and in vivo. The selective c-MET inhibitor, PF-2341066, can induce PEL apoptosis through cell cycle arrest and DNA damage, and suppress tumor progression in a xenograft murine model. By using microarray analysis, we identify many novel genes that are potentially controlled by HGF/c-MET within PEL cells. One of the downstream candidates, ribonucleoside-diphosphate reductase subunit M2 (RRM2), also displays the promising therapeutic value for PEL treatment. Our findings provide the framework for development of HGF/c-MET–focused therapy and implementation of clinical trials for PEL patients. (*Blood*. 2015;126(26):2821-2831)

Introduction

The oncogenic Kaposi sarcoma–associated herpesvirus (KSHV) is a principal causative agent of several human cancers including primary effusion lymphoma (PEL), which arises preponderantly in immunocompromised individuals, particularly AIDS patients.[1] PEL usually comprises transformed B cells harboring KSHV episomes and presents as pleural, peritoneal, and pericardial neoplastic effusions, although some cases of extracavitary solid variants of PEL have been reported recently.[2-4] PEL is a rare but aggressive malignancy, with a median survival time of ~6 months even under conventional chemotherapy.[5] Furthermore, the myelosuppressive effects of systemic cytotoxic chemotherapy synergize with those caused by antiretroviral therapy or immune suppression.[5,6] Therefore, it is an urgent need to identify novel targets that can guide development of more effective therapeutic strategies against PEL.

The *Met* proto-oncogene encodes the receptor tyrosine kinase known as c-MET, and hepatocyte growth factor (HGF) is the only known ligand for c-MET.[7,8] After its discovery in the mid-1980s, the HGF/c-MET pathway has gained considerable interest related to a variety of cancers due to the diversity of the cellular responses that follow HGF/c-MET pathway activation. HGF/c-MET interactions activate many downstream signaling intermediates, including the mitogen-activated protein kinase, phosphatidylinositol 3-kinase–AKT, v-src sarcoma (Schmidt-Ruppin A-2) viral oncogene homolog (SRC), and signal transducer and activator of transcription.[9,10] Moreover, an intricate network of cross-signaling involving the c-MET–epidermal growth factor receptor, c-MET–vascular endothelial growth factor receptor, and c-MET–Wnt pathways has also been reported in the past few years.[11-13] Such cross-talk evokes a variety of pleiotropic biological responses leading to increased cell proliferation, survival, migration/invasion, angiogenesis, and metastasis in cancer cells.[14] Deregulation and the consequent aberrant signaling of HGF/c-MET may occur by different mechanisms, including gene amplification, overexpression, activating mutations, increased autocrine or paracrine ligand-mediated stimulation, and interaction with other active cell surface receptors.[15] Because of its pleotropic role in cellular processes important in oncogenesis and cancer progression, the HGF/c-MET pathway may be a viable target for anticancer therapies. Several molecules targeting HGF/c-MET have recently been evaluated in differential phase clinical trials, including small-molecule inhibitors, and monoclonal antibodies targeting either the ligand or the receptor.[16-18]

Despite this knowledge, roles of the HGF/c-MET pathway in virus-associated tumors remain largely unclear. For KSHV-related malignancies, only 1 study reports coexpression of HGF/c-MET in all of the KSHV$^+$ PEL tumors tested (9 PEL cell lines and 4 primary

Submitted July 17, 2015; accepted October 3, 2015. Prepublished online as *Blood* First Edition paper, November 3, 2015; DOI 10.1182/blood-2015-07-658823.

The microarray original data reported in this article have been deposited in the Gene Expression Omnibus database (accession number GSE70594).

The online version of this article contains a data supplement.

The publication costs of this article were defrayed in part by page charge payment. Therefore, and solely to indicate this fact, this article is hereby marked "advertisement" in accordance with 18 USC section 1734.

specimens), whereas it was restricted to 1 of 34 high-grade B-cell non-Hodgkin lymphomas other than PEL ($P < .001$; χ^2 test).[19] Other studies report the coexpression of HGF/c-MET in some cases of diffuse large B-cell lymphoma and Hodgkin disease.[20,21] However, the biological functions of the HGF/c-MET pathway in KSHV-infected host cells and/or tumor cells and their value as therapeutic "target" have not yet been addressed. Therefore, in the present study, we will determine the role of HGF/c-MET in PEL pathogenesis and underlying regulatory mechanisms by genomic analysis. We will also determine whether a selective c-MET inhibitor, PF-2341066, can suppress PEL progression in an established xenograft murine model.

Materials and methods

Cell culture and reagents

The PEL cell-line BCBL-1 ($KSHV^+/EBV^-$) was cultured as described previously.[22] The other PEL cell lines BC-1 ($KSHV^+/EBV^+$) and BCP-1 ($KSHV^+/EBV^-$) were purchased from American Type Culture Collection (ATCC).[22] Human umbilical vein endothelial cells (HUVECs) were grown in Dulbecco modified Eagle medium/F-12 50/50 medium (Cellgro) supplemented with 5% fetal bovine serum. All cells were cultured at 37°C in 5% CO_2. All experiments were carried out using cells harvested at low (<20) passages. c-MET inhibitor PF-2341066 and RRM2 inhibitor 3-aminopyridine-2-carboxaldehyde thiosemicarbazone (3-AP) were purchased from Selleck Chemicals and Sigma-Aldrich, respectively.

KSHV purification and infection

BCBL-1 cells were incubated with 0.6 mM valproic acid for 4 to 6 days, and KSHV was purified from the culture supernatants by ultracentrifugation at 20 000*g* for 3 hours, 4°C. The viral pellet was resuspended in 1/100 original volume in the appropriate culture media, and aliquots were frozen at −80°C. HUVECs were incubated with concentrated virus in the presence of 8 μg/mL Polybrene (Sigma-Aldrich) for 2 hours at 37°C. The concentration of infectious viral particles used in each experiment (multiplicity of infection [MOI]) was calculated as described previously.[23,24]

Cell proliferation assays

Cell proliferation was measured by using the WST-1 assays (Roche) according to the manufacturer's instructions.

Patients and ethics statement

The study was approved by the Institutional Review Boards for Human Research (no. 8079) at Louisiana State University Health Science Center–New Orleans (LSUHSC-NO). All subjects were provided written informed consent in accordance with the Declaration of Helsinki. In the current study, a total of 27 HIV^+ patients with antiretroviral treatment in our HIV Outpatient (HOP) Clinic are involved. There were 14 women and 13 men; the average age was 48.1 years (range, 21-63 years). The average CD4 T-cell counts were 530/mL (range, 35-1773/mL), and the average HIV viral loads were 5833 copies per mL (range, 25-66681 copies per mL).

Plasma preparation

Whole blood was collected in heparin-coated tubes, and plasma was isolated by centrifugation. The KSHV infection status was determined by using quantitative enzyme-linked immunosorbent assays (ELISAs) for identifying circulating immunoglobulin G (IgG) antibodies to KSHV proteins (LANA and K8.1) as previously described.[25,26]

Microarray

BC-1, BCP-1, and BCBL-1 cells were treated with vehicle or PF-2341066 (1.6 μM) for 24 hours, respectively. Total RNA was isolated using the Qiagen RNeasy kit (Qiagen), and 500 ng of total RNA was used to synthesize double-stranded complementary DNA. Biotin-labeled RNA was generated using the TargetAmp-Nano Labeling kit for Illumina Expression BeadChip (Epicentre), according to the manufacturer's instructions, and hybridized to the HumanHT-12 v4 Expression BeadChip (Illumina).[27,28] The microarray experiments were performed twice for each group and the average values were used for analysis. Common, similar, and unique sets of genes and enrichment analysis were performed using MetaCore software (Thompson Reuters) as previously reported.[29]

Flow cytometry

For detection of c-MET expression on the cell surface, PEL cells were resuspended in 3% bovine serum albumin in 1× phosphate-buffered saline (PBS), incubated on ice for 10 minutes, then incubated with primary antibodies diluted 1/50 recognizing c-MET (Santa Cruz Biotechnology), for an additional 30 minutes. Following 2 subsequent wash steps, cells were incubated for an additional 30 minutes with goat anti-rabbit IgG Alexa 647 using a dilution of 1/200 (Invitrogen). Control cells were incubated with secondary antibodies only. Cells were then resuspended in 1× PBS prior to analyses. Data were collected using a FACSCalibur 4-color flow cytometer (BD Biosciences) and FlowJo software (TreeStar). For apoptosis assays, the fluorescein isothiocyanate–Annexin V and propidium iodide (PI) Apoptosis Detection kit I (BD Pharmingen) was used.[26] For cell cycle analysis, PEL cell pellets were fixed in 70% ethanol, and incubated at 4°C overnight. Cell pellets were resuspended in 0.5 mL of 0.05 mg/mL PI plus 0.2 mg/mL RNaseA and incubated at 37°C for 30 minutes. Cell cycle distribution was analyzed on a FACSCalibur 4-color flow cytometer (BD Biosciences).

ELISA

Concentrations of HGF in culture supernatants were determined using the human HGF ELISA kit (R&D Systems), according to the manufacturer's instructions.

Immunoblotting

Total cell lysates (30 μg) were resolved by 10% sodium dodecyl sulfate–polyacrylamide gel electrophoresis, transferred to nitrocellulose membranes, and immunoblotted using 100 to 200 μg/mL antibodies to cleaved caspase 3/9, phosphor (p)-ERK/total (t)-ERK, p-c-MET/t-c-MET, p-ALK/t-ALK, p-ROS1/t-ROS1, p-Cdc2, p-Chk1/2, p-Rb, Cyclin A2, Cyclin B1, Myt1, p-H2A.X/t-H2A.X, and p-p53/t-p53 (Cell Signaling). For loading controls, blots were incubated with antibodies detecting β-actin (Sigma-Aldrich). Immunoreactive bands were developed using an enhanced chemiluminescence reaction (PerkinElmer) and visualized by autoradiography.

Immunofluorescence assays

Cells were incubated in 1:1 methanol-acetone at −20°C for fixation and permeabilization. After blocking, cells were then incubated for 1 hour at 25°C with a 1/100 dilution of a mouse anti-p-p53 antibody or a rabbit anti-p-H2A.X antibody (Cell Signaling) followed by a 1/200 dilution of a goat anti-mouse or goat anti-rabbit secondary antibody conjugated with Texas Red (Invitrogen), respectively. For identification of nuclei, cells were subsequently counter-stained with 0.5 μg/mL 4′,6-diamidino-2-phenylindole (DAPI; Sigma-Aldrich) in 180 mM Tris-HCl (pH 7.5).

CometAssay

The DNA damage was evaluated by using the reagent kit for single cell gel electrophoresis assay/CometAssay (Trevigen), according to the manufacturer's instructions. The slides were viewed by using epifluorescence microscopy.

RNA interference

For RNA interference (RNAi) assays, ON-TARGET plus SMART pool small interfering RNA (siRNA) for *RRM2* (Dharmacon), or negative

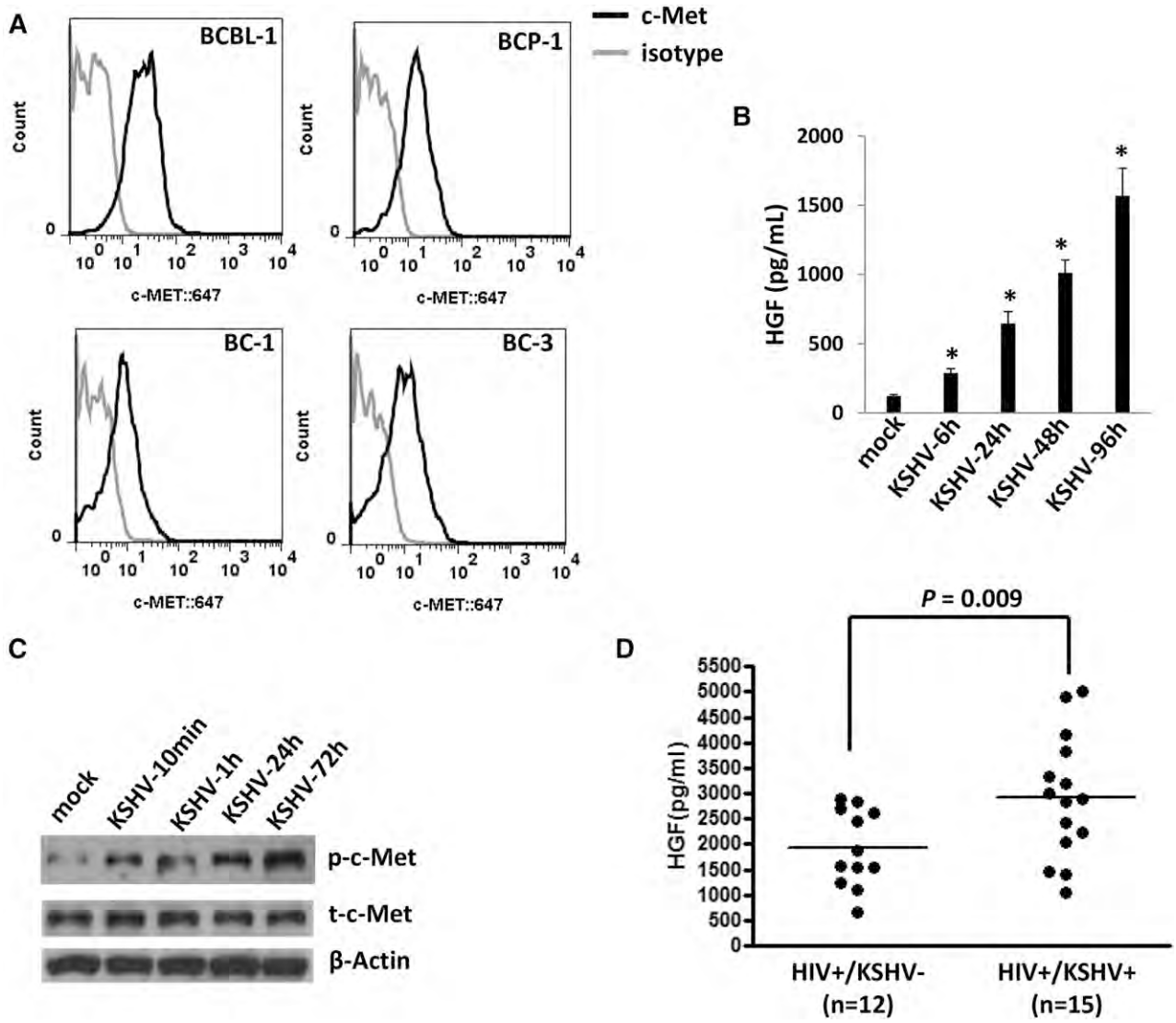

Figure 1. KSHV activates the HGF/c-MET pathway in vitro and in vivo. (A) Four KSHV$^+$ PEL cell lines were incubated with a monoclonal antibody recognizing the extracellular domain of c-MET (black line) or isotype antibody as a negative control (gray line), followed by a secondary antibody conjugated to Alexa 647. Surface expression of c-MET was quantified using flow cytometry. (B-C) HUVECs were infected by purified KSHV (MOI = 10), and the supernatant and cell lysates were collected at indicated time points. HGF concentrations in supernatant were determined by ELISA and protein expression was measured by immunoblots. Error bars represent the S.E.M. for 3 independent experiments. *$P < .01$. (D) The HGF concentrations in plasma from cohort HIV-infected patients were determined by ELISA, and KSHV infection status was determined by using ELISAs for identifying circulating IgG antibodies to KSHV proteins as described in "Methods." S.E.M., standard error of the mean.

control siRNA, were delivered using the DharmaFECT transfection reagent according to the manufacturer's instructions.

Quantitative reverse transcription–polymerase chain reaction

Total RNA was isolated using the RNeasy Mini kit according to the manufacturer's instructions (QIAGEN). Complementary DNA was synthesized from equivalent total RNA using the SuperScript III First-Strand Synthesis SuperMix kit (Invitrogen). Primers used for amplification of target genes are displayed in supplemental Table 1 (available on the *Blood* Web site). Amplification was carried out using an iCycler IQ Real-Time PCR Detection System, and calculated using automated iQ5 2.0 software (Bio-rad).

PEL xenograft model

Aliquots of 10^7 BCBL-1 cells were diluted in 200 μL of sterile PBS, and 6- to 8-week-old male nonobese diabetic/severe-combined immunodeficiency (NOD/SCID) mice (The Jackson Laboratory) received intraperitoneal (i.p.) injections with a single-cell aliquot. The PF-2341066 (20 mg/kg body weight), or vehicle alone, was administered using an insulin syringe for i.p. injection. Drug was administered either 24 hours or 28 days (allowed to establish tumor expansion) after BCBL-1 injection, once daily for 5 days per week. Two experiments, with 10 mice per group for each experiment, were performed. The PEL expansion in vivo was confirmed by testing the expression of cell surface markers including CD45, CD138, EMA, and viral protein LANA in nuclear within ascites tumor cells, using immunofluorescence assay and flow cytometry as described in our previous publications.[22] Weights were recorded weekly as a surrogate measure of tumor progression, and ascites fluid volumes were tabulated for individual mice at the completion of each experiment. All protocols were approved by the Louisiana State University Health Science Center Animal Care and Use Committee in accordance with national guidelines (no. 3237).

Statistical analyses

Significance for differences between experimental and control groups was determined using the 2-tailed Student *t* test (Excel 8.0). The 50% inhibitory concentration (IC_{50}) was calculated by using SPSS 20.0.

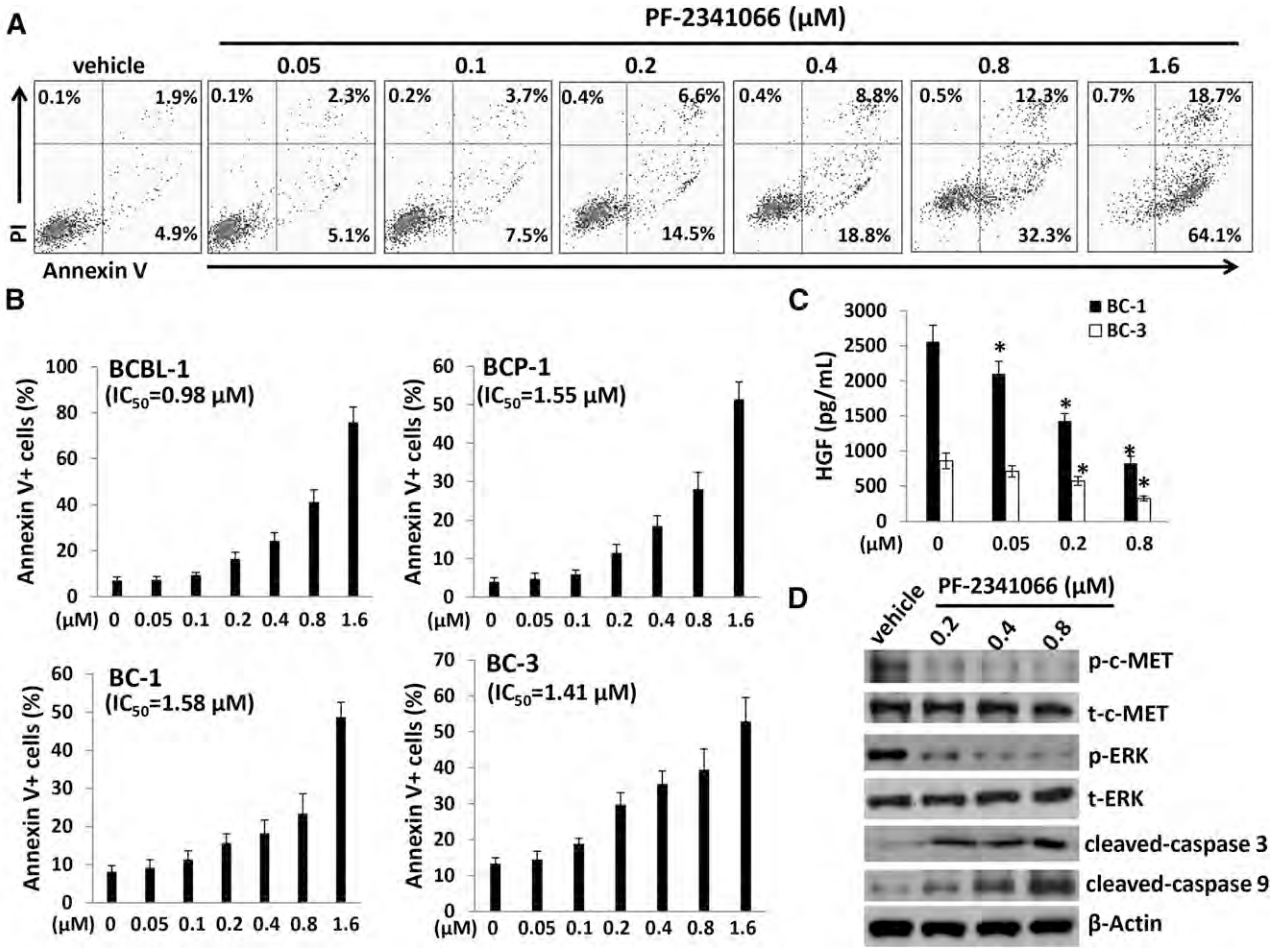

Figure 2. The c-MET–selective inhibitor PF-2341066 induces dose-dependent apoptosis for KSHV$^+$ PEL cells. (A-B) A total of 4 PEL cell lines were incubated with the indicated concentrations of PF-2341066 for 24 hours, then cell apoptosis was quantified by Annexin V–PI/flow cytometry. BCBL-1 was shown as an example for the cell subpopulation diagram in panel A. (C) The HGF concentrations in supernatant were determined by ELISA. Error bars represent the S.E.M. for 3 independent experiments. *$P < .01$. (D) The protein expression in BCBL-1 was measured by immunoblots.

Results

KSHV activates the HGF/c-MET pathway in vitro and in vivo

By using flow cytometry analysis, we first confirmed the expression of c-MET on the cell surface of 4 KSHV$^+$ PEL cell lines (BCBL-1, BCP-1, BC-1, and BC-3) (Figure 1A), which is consistent with those reported previously.[19] To further identify the ability of KSHV activating the HGF/c-MET pathway in vitro, we found that KSHV de novo infection greatly induced HGF production and the phosphorylation of c-MET from HUVECs in a time-course manner (Figure 1B-C). To explore the clinical relevance of HGF production within HIV-infected patients, we tested plasma HGF levels by ELISA in a small collection of our cohort HIV-infected patients with or without KSHV coinfection. KSHV infection status in these patients was determined as described previously.[25,26] We found that the KSHV$^+$ group (n = 15) had higher plasma HGF concentrations than those from the KSHV$^-$ group (n = 12) of these HIV-infected patients (Figure 1D). Taken together, our data strongly support the activation of the HGF/c-MET pathway by KSHV in vitro and in vivo.

c-MET inhibitor induces apoptosis for KSHV$^+$ PEL cells potentially through causing cell cycle arrest and DNA damage

We next sought to understand the role of the HGF/c-MET pathway in PEL tumor cell survival/growth. Our data indicated that targeting HGF/c-MET by PF-2341066, a selective small-molecular c-MET inhibitor, induced significant apoptosis for all the 4 KSHV$^+$ PEL cell lines we tested, in a dose-dependent manner (Figure 2A-B). By using the WST-1 assays, we found that PF-2341066 effectively reduced cell proliferation for these PEL cell lines (supplemental Figure 1). Moreover, PF-2341066 treatment greatly reduced HGF production from these lymphoma cells, although the underlying mechanisms remain unclear (Figure 2C). By using immunoblots, we found that PF-2341066 treatment increased the expression of cleaved-caspase 3 and 9, while reducing phosphor-c-MET and downstream phosphor-ERK (Figure 2D). To seek the potential mechanisms involved in c-MET inhibitor–induced PEL apoptosis, we found that PF-2341066 obviously caused cell cycle G2/M arrest when compared with vehicle control by flow cytometry analysis (Figure 3A). Further analysis indicated that PF-2341066 affected the expression of several checkpoint regulatory proteins (positive/negative), increasing Myt1, phosphor-Cdc2/Chk1/Chk2, while reducing Cyclin A2, Cyclin B1, and phosphor-Rb from BCBL-1 cells (Figure 3B). Interestingly, we found that PF-2341066 treatment also caused obvious DNA damage of PEL cells, as indicated by CometAssay and the upregulation of DNA damage markers phosphor-p53 and phosphor-H2A.X but not the total protein levels, respectively (Figure 3C-E). We have previously shown that several small-molecule compounds induced by PEL apoptosis are connected to reactivate KSHV lytic gene expression.[30,31] However, here we only found a slight increase of viral latent/lytic gene expression

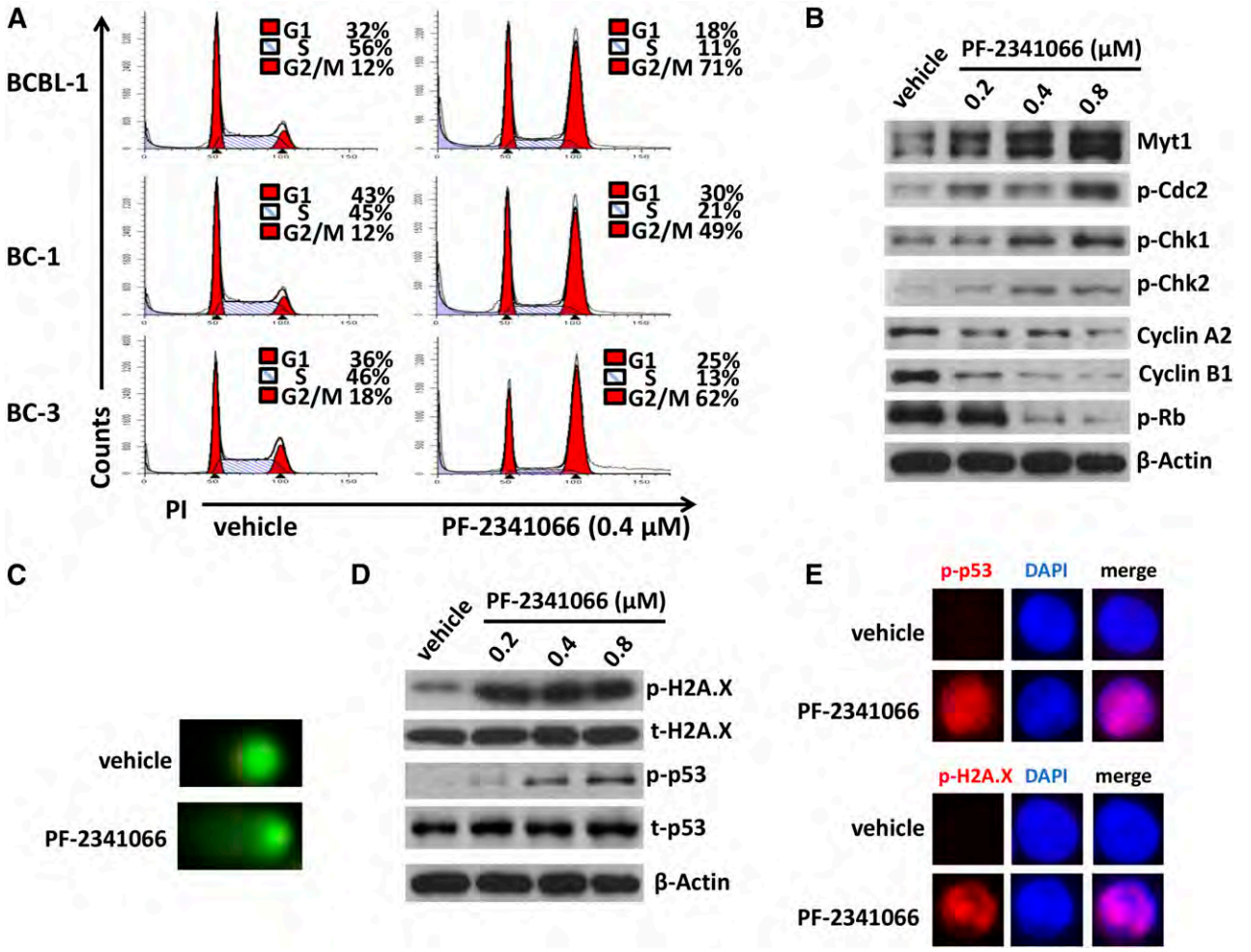

Figure 3. Targeting HGF/c-MET causes G2/M cell cycle arrest and DNA damage in KSHV$^+$ PEL cells. (A) PEL cells were incubated with 0.4 μM PF-2341066 or vehicle control for 24 hours, then stained by PI and analyzed by flow cytometry. (B-D) The protein expression and DNA damage in BCBL-1 were measured by immunoblots and CometAssay, respectively. (E) The cellular expression of DNA damage markers phosphor-p53 and phosphor-H2A.X was detected by immunofluorescence, and the nuclear was shown by DAPI staining.

(but with no statistical significance) within PF-2341066–treated BCBL-1 cells (supplemental Figure 2).

c-MET inhibitor suppresses PEL tumor progression in vivo

Next, we sought to determine whether PF-2341066 has the capacity to suppress PEL tumor growth in vivo using an established xenograft murine model.[22] We administered PF-2341066 (or vehicle) i.p. within 24 hours of BCBL-1 cell injection and for a 5-week treatment. We found that PF-2341066 treatment dramatically suppressed PEL tumor progression including reducing ascites formation and spleen enlargement over this time frame (Figure 4A-C). By using hematoxylin-and-eosin staining, we observed huge tumor infiltration into the spleen of vehicle-treated mice, whereas only small tumor nodules were dispersed in the spleen of PF-2341066–treated mice (Figure 4D). By using immunohistochemistry staining, we further demonstrated the dramatically reduced expression of phosphor-c-MET and phosphor-ERK within spleen tissues from PF-2341066–treated mice, when compared with those from vehicle-treated mice (Figure 4E). Additional experiments were conducted wherein PF-2341066 therapy was initiated following establishment of PEL tumor expansion in mice (beginning 28 days after BCBL-1 cell injection). Using this approach, PF-2341066–treated mice still exhibited significant regression of PEL tumor burden relative to vehicle-treated mice (Figure 4F-G), and almost no ascites were found in these mice after 3-week treatment (Figure 4H).

Microarray analysis of the HGF/c-MET controlled network within KSHV$^+$ PEL cells

There is a complex network for HGF/c-MET within cancer cells,[9-13] although it still remains completely unknown to KSHV$^+$ PEL cells. Therefore, we used the HumanHT-12 v4 Expression BeadChip (Illumina) which contains >47 000 probes derived from the NCBI RefSeq Release 38 and other sources to study the gene profile altered between vehicle- or PF-2341066–treated 3 KSHV$^+$ PEL cell lines (BCBL-1, BC-1, and BCP-1). Intersection analysis indicated that there were 51 common genes significantly altered within all 3 PF-2341066–treated cell lines (up/down at least twofold and $P < .05$). There were 20 similar genes altered between BCBL-1 and BC-1, 188 similar between BCBL-1 and BCP-1, and 13 similar between BC-1 and BCP-1; 282 genes altered were unique to BCBL-1, 148 unique to BCP-1, and 52 unique to BC-1 (Figure 5A). Within the common gene set, the top 10 upregulated and/or downregulated candidate genes in PF-2341066–treated BCP-1, BC-1, and BCBL-1 cell lines are listed in Table 1, respectively, including gene description and the altered level

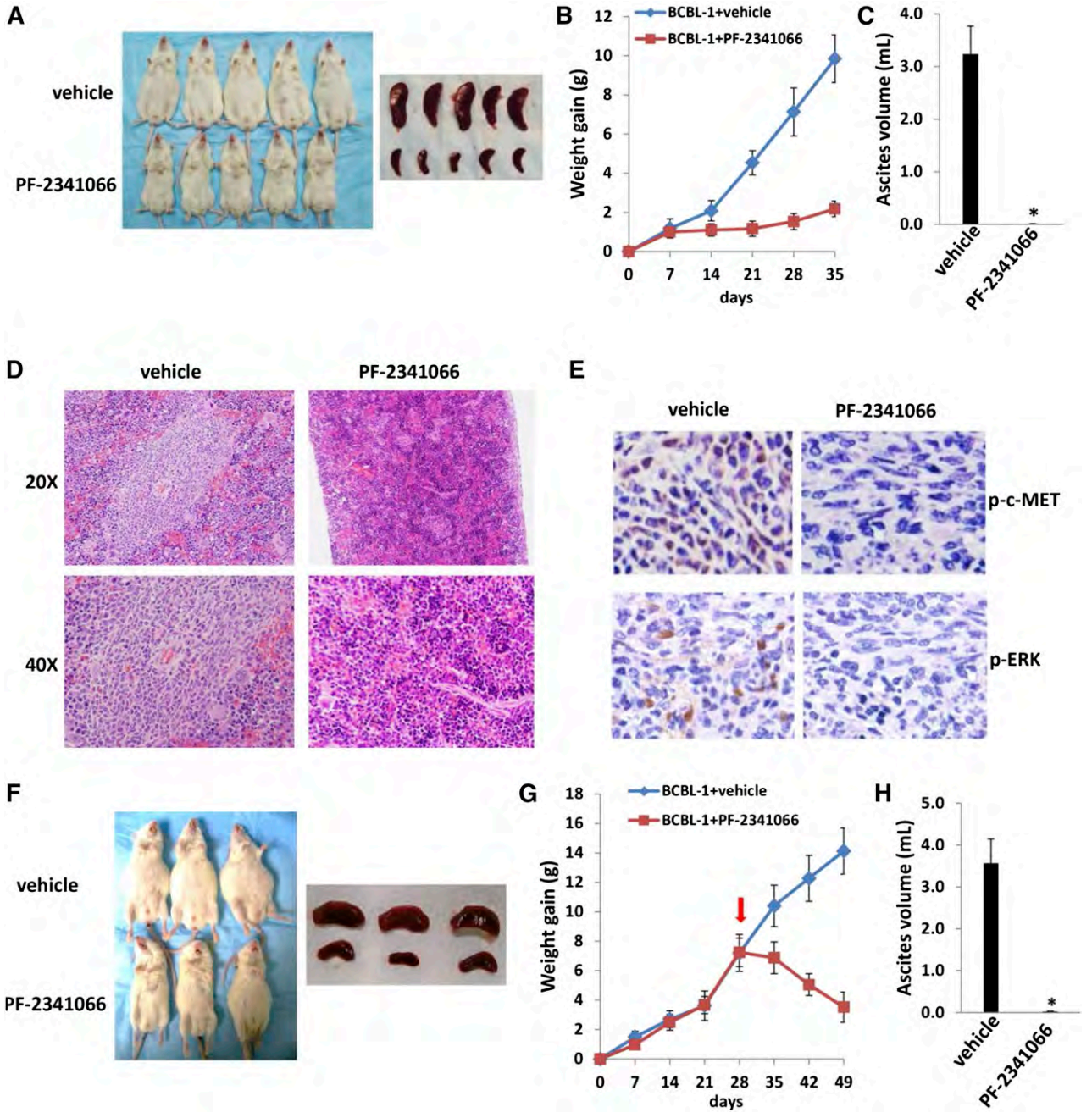

Figure 4. The c-MET inhibitor PF-2341066 suppresses PEL progression in vivo. (A-C) NOD/SCID mice were injected i.p. with 10^7 BCBL-1 cells. Beginning 24 hours later, 20 mg/kg PF-2341066 or vehicle (n = 10 per group) were administered i.p., once daily, 5 days per week, for each of 2 independent experiments. Weights were recorded weekly. Images of representative animals and their spleens, as well as ascites fluid volumes, were collected at the conclusion of experiments on day 35. (D-E) Spleens from representative vehicle- or PF-2341066–treated mice were prepared for routine hematoxylin-and-eosin or immunohistochemistry staining. (F-H) NOD/SCID mice were injected i.p. with 10^7 BCBL-1 cells. Beginning 28 days later, 20 mg/kg PF-2341066 or vehicle (n = 10 per group) were administered i.p., once daily, 5 days per week. Images of representative animals and their spleens, as well as ascites fluid volumes, were collected at the conclusion of experiments on day 49. Error bars represent the S.E.M. for 1 of 2 independent experiments; $^*P < .01$.

of transcription in these 3 cell lines. Interestingly, we found that the functional role of most genes in PEL pathogenesis has never been reported, although some of them have been implicated in other types of malignancies. For example, Mucin-1 (MUC1) is a known tumor antigen and aberrantly overexpressed in various cancers with loss of its apical polarity.[32-34] In addition, numerous cellular proteins implicated with MUC1 are involved in the malignancy of cancer cells and their resistance to chemotherapy.[35] Notably, we found that some nuclear small RNA transcripts such as *RN7SK*, *RNU1-4*, *RNVU1-18*, and *RNU1-1* are upregulated in PF-2341066–treated PEL cells (Table 1), although their contributions to PEL growth and pathogenesis remain unclear.

We next selected 4 genes from the top 10 upregulated or downregulated candidate list (Table 1) for validation of their transcriptional change by quantitative reverse transcription–polymerase chain reaction (qRT-PCR), respectively. Our results indicated that all 4 genes (*RRM2*, *MUC1*, *TYMS*, and *FBXO5*) were significantly downregulated in PF-2341066–treated PEL cells when compared with vehicle-treated control, whereas another 4 genes (*HMGCS1*, *MSMO1*, *HMGCR*, and *PIK3IP1*) were all significantly

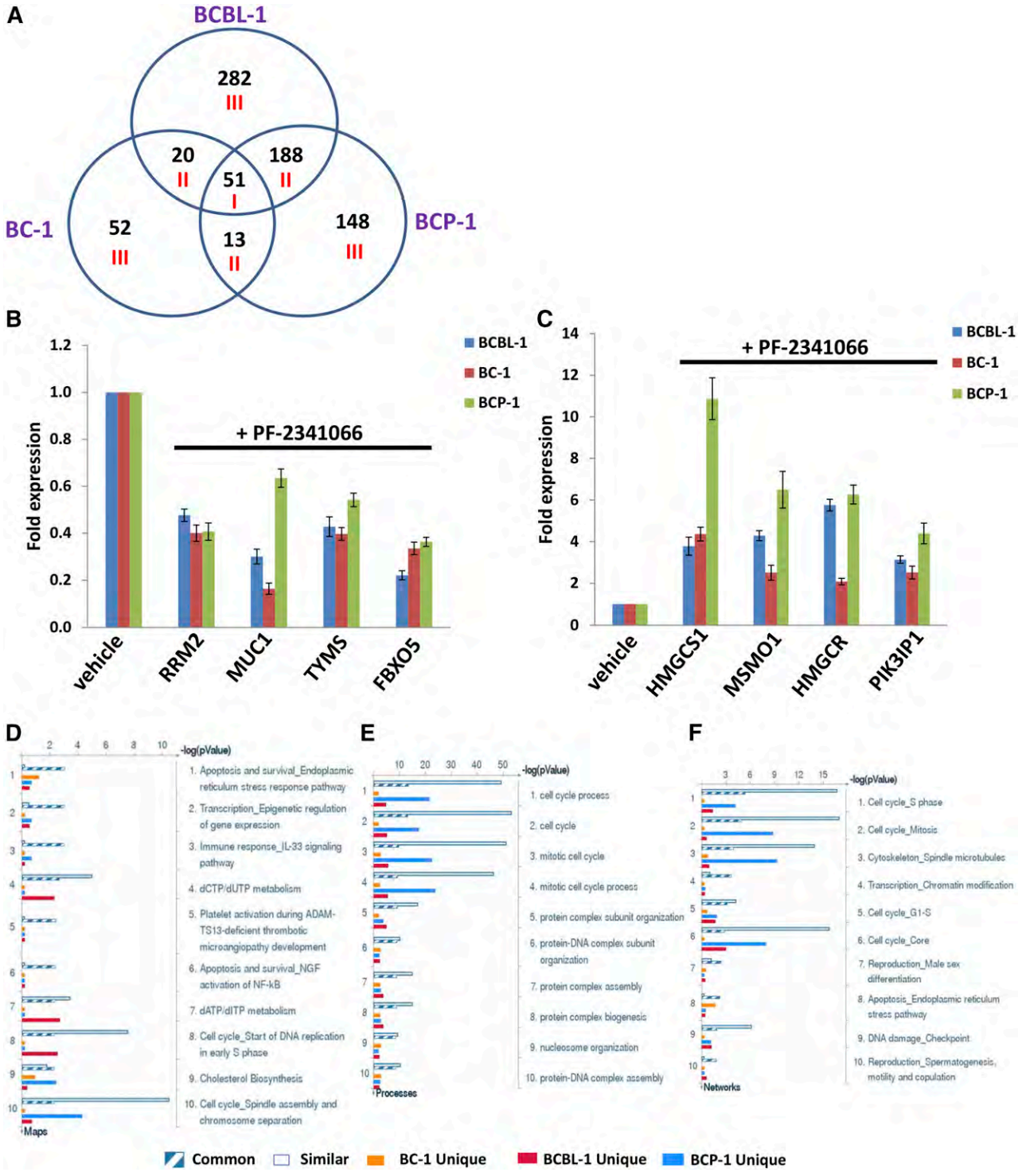

Figure 5. Microarray analysis of gene profile altered within PF-2341066–treated PEL cell lines. (A) The HumanHT-12 v4 Expression BeadChip (Illumina) was used to detect gene profile altered within PF-2341066–treated PEL cell lines (BCBL-1, BC-1, and BCP-1) when compared with vehicle-treated control. Intersection analysis of significantly altered genes (up/down at least twofold and $P < .05$) was performed using Illumina GenomeStudio software. Set I: Common genes altered in all the 3 cell lines. Set II: Similar genes altered in every 2 cell lines. Set III: Unique genes altered in each cell line. (B-C) The transcriptional levels of selected 4 candidate genes downregulated (B) or upregulated (C) as shown in microarray data were validated by using qRT-PCR, respectively. Error bars represent the S.E.M. for 3 independent experiments. (D-F) The enrichment analysis of gene profile (common, similar, and unique set as indicated) significantly altered by c-MET inhibitor was performed using the MetaCore software (Thompson Reuters) modules: Pathway Maps (D), Gene Ontology Processes (E), and Process Networks (F).

upregulated in PF-2341066–treated PEL cells (Figure 5B-C). Moreover, the altered transcriptional levels of these genes in all 3 KSHV$^+$ PEL cell lines were comparable to those found in microarray data, demonstrating the credibility of our microarray analysis. We also performed enrichment analysis of these common, similar, and unique sets of genes using the Pathway Map, Gene Ontology (GO) Processes, and Process Network modules from Metacore software (Thompson Reuters).[29] Our analysis showed that

Table 1. The top 10 "common" candidate genes downregulated or upregulated within PF-2341066–treated 3 KSHV$^+$ PEL cell lines

Gene symbol	Description	Fold change		
		BCP-1	BC-1	BCBL-1
RRM2	Ribonucleoside-diphosphate reductase subunit M2	0.38	0.41	0.21
MUC1	Mucin-1	0.53	0.26	0.32
POLE2	DNA polymerase ε subunit 2	0.39	0.47	0.26
TMEM106C	Transmembrane protein 106C	0.43	0.5	0.29
FAM81A	Protein FAM81A	0.46	0.5	0.3
CHAC2	Cation transport regulator-like protein 2	0.54	0.43	0.34
TYMS	Thymidylate synthase	0.42	0.52	0.39
FBXO5	F-box only protein 5	0.51	0.48	0.36
ASPM	Abnormal spindle-like microcephaly-associated protein	0.3	0.54	0.55
DPAGT1	UDP-N-acetylglucosamine–dolichyl-phosphate N-acetylglucosaminephosphotransferase	0.52	0.54	0.33
RN7SK	RNA, 7SK small nuclear transcript	5.56	5.1	20.15
HMGCS1	Hydroxymethylglutaryl-CoA synthase, cytoplasmic	8.11	4.03	4.03
RNU1-4	RNA, U1 small nuclear 4 transcript	2.47	4.49	7.84
RNVU1-18	RNA, variant U1 small nuclear 18 transcript	2.2	4.36	7.43
SNORD3A	Small nucleolar RNA, C/D box 3A transcript	3.01	5.24	3.98
RNU1-1	RNA, U1 small nuclear 1 transcript	2.15	3.11	6.4
MSMO1	Methylsterol monooxygenase 1	5.42	2.23	2.13
PPP1R15A	Protein phosphatase 1 regulatory subunit 15A	1.86	3.58	4.05
HMGCR	3-hydroxy-3-methylglutaryl-coenzyme A reductase	3.66	2.46	3.34
PIK3IP1	Phosphoinositide-3-kinase-interacting protein 1	3.31	3.07	3.03

several major cellular functions were affected within PF-2341066–treated PEL cells, including the apoptosis/ER stress response pathway, epigenetic regulation of gene expression, cell cycle/checkpoint, and DNA damage–related proteins (Figure 5D-F). The top 2 scored pathway maps and protein networks based on the enrichment analysis of "common" gene set were also listed in supplemental Figures 3 and 4, respectively.

Targeting *RRM2* induces PEL apoptosis through increasing DNA damage

We next selected ribonucleoside-diphosphate reductase subunit M2 (*RRM2*), 1 of the significant downregulated genes in PF-2341066–treated PEL cells from microarray data, to determine its role in PEL pathogenesis. Actually, ribonucleoside-diphosphate reductase (RR) is an attractive target for anticancer agents given its central function in DNA synthesis, growth, metastasis, and drug resistance of cancer cells.[36] Human RR is composed of α subunits (RRM1) that contain the catalytic site and 2 binding sites for enzyme regulators and β subunits (RRM2) with a binuclear iron cofactor that generates the stable tyrosyl radical necessary for catalysis.[37] Here, we found that direct silence of *RRM2* by RNAi induced caspase-dependent apoptosis within KSHV$^+$ PEL cells (BCBL-1 and BCP-1), potentially through increasing DNA damage (Figure 6A-C; supplemental Figure 5). Furthermore, a selective RR inhibitor, 3-AP,[38] also induced dose-dependent apoptosis and increased DNA damage by CometAssay and the expression of phosphor-H2A.X and phosphor-p53 but not the total proteins from KSHV$^+$ PEL cells (Figure 6D-F). These data indicate that *RRM2* may also represent a promising target for development of anti-PEL agents.

Discussion

In recent years, the HGF/c-MET pathway has become an attractive target for development of anticancer drugs in a variety of solid tumors. In contrast to this, little is known about the biological functions and therapeutic value of the HGF/c-MET pathway in virus-related malignancies such as PEL. To our knowledge, this is the first article to report that activation of the HGF/c-MET pathway is essential for KSHV$^+$ PEL cell survival and that targeting this pathway successfully suppresses PEL progression in vivo. Interestingly, PF-2341066 has been shown as the inhibitor to several other receptor tyrosine kinases such as ALK and ROS1 in different types of cancer cells including anaplastic large-cell lymphoma and non-small-cell lung cancer.[39,40] However, our immunoblots data indicate that the PEL cell lines we tested including BCBL-1 and BCP-1 do not express the p-ALK (Tyr1604), t-ALK, p-ROS1 (Tyr2274), or t-ROS1 reported in these previous studies,[39,40] implying that these KHSV$^+$ PEL cell lines may have unique expressional patterns of receptor tyrosine kinases (data not shown).

One of the remaining questions is the underlying mechanisms through which the HGF/c-MET pathway is activated in PEL cells. Previous studies have reported some activating mutations of c-MET in non-small-cell lung cancer, hereditary and spontaneous renal carcinomas, hepatocellular carcinomas, gliomas, gastric, squamous cell carcinoma of the head and neck, and breast cancers.[41-46] Potentially oncogenic mutations involve mainly: (1) point mutations that generate an alternative splicing encoding a shorter protein that lacks exon 14, which encodes for the juxtamembrane domain of c-MET[43,47]; (2) point mutations in the kinase domain that render the enzyme constitutively active[44]; and (3) Y1003 mutations that inactivate the Cbl-binding site leading to constitutive c-MET expression.[48-50] Therefore, we are now working on whether these similar mutations are also present in the c-MET sequence from KSHV$^+$ PEL cell lines and/or primary specimens, resulting in constitutive activation of this pathway. In addition, we are interested in understanding which viral proteins (latent and/or lytic) are responsible for activating HGF/c-MET from PEL cells in future study.

Our data indicate that c-MET inhibitor–induced PEL apoptosis is potentially through increasing DNA damage and regulation of some DNA damage/repair–related proteins such as RRM2 (see discussion

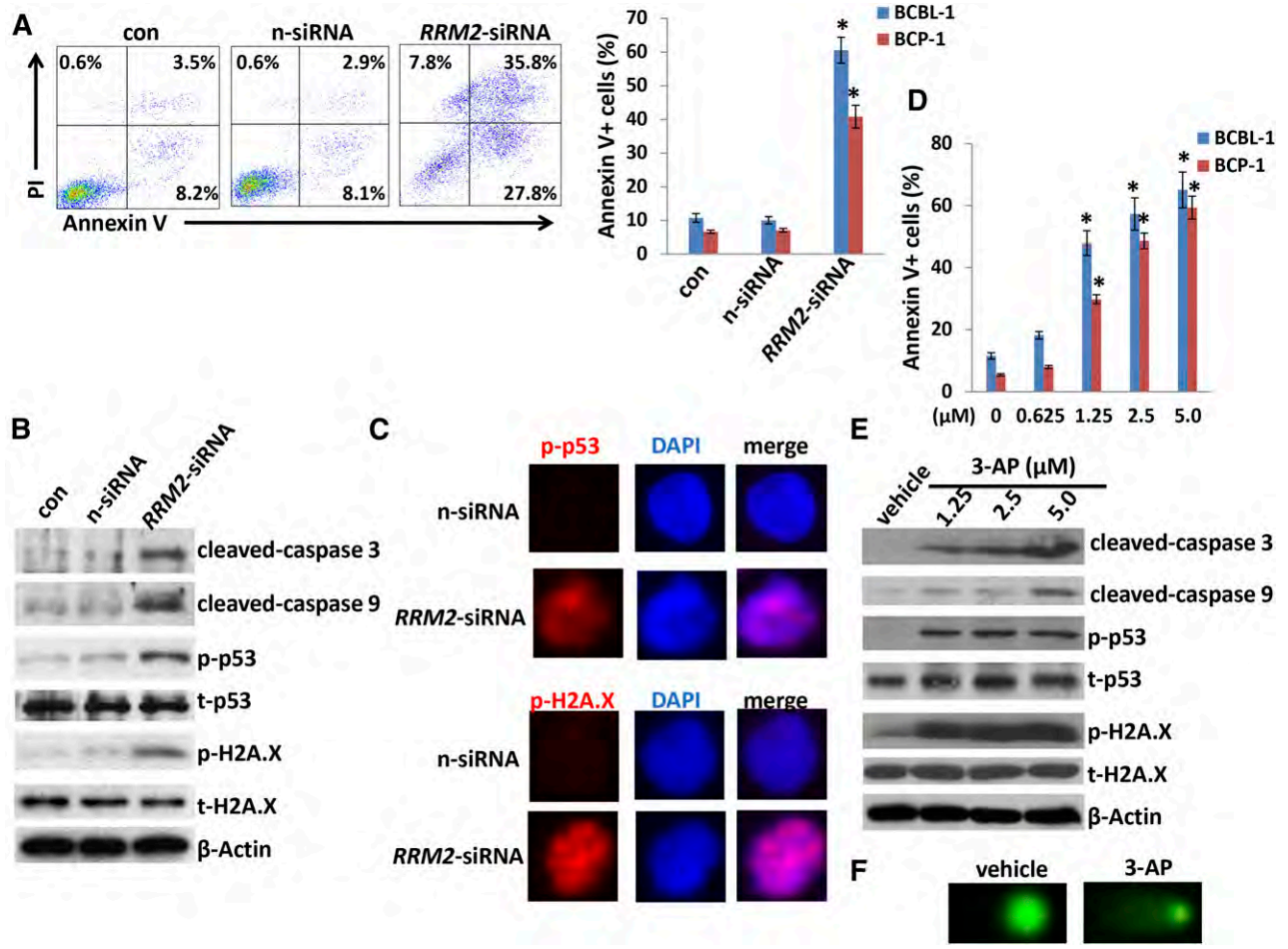

Figure 6. Directly targeting *RRM2* induces PEL apoptosis through causing DNA damage. (A) BCP-1 and BCBL-1 were transfected with either negative control siRNA (n-siRNA) or *RRM2*-siRNA for 48 hours, then cell apoptosis was assessed using Annexin V-PI staining and flow cytometry analysis. (B-C) Protein expression was measured by immunoblots and immunofluorescence, respectively. (D-E) Cells were treated with indicated concentrations of RRM2 inhibitor, 3-AP, for 24 hours, then cell apoptosis and protein expression were measured as described in "Materials and methods." Error bars represent the S.E.M. for 3 independent experiments; $^*P < .01$. (F) Cells were treated with 5 μM 3-AP for 24 hours, then DNA damage was evaluated by using the CometAssay.

below). Interestingly, our recent data showed that silencing of 1 DNA damage–related gene, *XRCC5* (x-ray repair cross-complementing protein 5, also known as Ku80) enhanced the induction of apoptosis and programmed cell death by low-dose concentrations of DNA-damage reagents such as doxorubicin.[28] In fact, it has been reported recently that KSHV can activate the DNA damage response during de novo infection of primary endothelial cells and this plays a role in establishing latency.[51] More recently, it has been demonstrated that lytic reactivation of KSHV leads to activation of the ataxia telangiectasia mutated (ATM) and DNA-dependent protein kinase DNA damage response kinases.[52] Inhibition of ATM results in the reduction of overall levels of viral replication whereas inhibition of DNA-dependent protein kinase increases activation of ATM and leads to earlier viral release.[52] However, our data indicate that targeting HGF/c-MET by PF-2341066 does not cause robust viral lytic gene expression, implying that PF-2341066–induced DNA damage is potentially through other mechanisms.

By using microarray analysis, we found that many downstream genes are altered in PF-2341066–treated PEL cells when compared with vehicle-treated control, although the roles of most of them in PEL pathogenesis remain unknown. One of candidate genes, *RRM2*, was found significantly downregulated in PF-2341066–treated PEL cells from the microarray data and subsequently validated by qRT-PCR. In fact, normal cells with a low proliferative status express very low levels of RR, whereas neoplastic cells overexpress RR to manufacture dNTP pools to support DNA synthesis and proliferation.[36] Therefore, RR, especially the RRM2 subunit, is an important target for anticancer agents. Our data indicate that directly targeting RRM2 by either RNAi or the pharmacological inhibitor, 3-AP, greatly induces PEL apoptosis through increasing DNA damage. 3-AP is now used in clinical trials for a variety of advanced-stage solid tumors.[53-55] Toxicities reported from the phase 1 trial were hypoxia, respiratory distress, and methemoglobulinemia, apparently due to iron chelation in the red blood cells of the patients.[56] Recently, Zhou et al have developed a novel potent RR inhibitor, COH29, by using structure- and mechanism-based approaches, which displays a broad antitumor potential.[36] Therefore, future work will focus on testing whether these RR inhibitors have antitumor effects by using our PEL xenograft model.

Acknowledgments

This work was supported by Center for Biomedical Research Excellence subaward P20-RR021970 (Z.Q.), SOM Research

Enhancement Funding (Z.Q.), DOD Career Development Award CA140437 (Z.Q.), as well as awards from the National Natural Science Foundation of China (81272191, 81472547 [Z.Q.] and 81400164 [L. Dai]). HIV$^+$ patient plasma samples were provided by the HIV Cancer Care Program Biorepository which is supported by from the National Institutes of Health grants UM1-CA181255 and R01-CA142362 (C.P.). This work was also funded in part with federal funds from the National Cancer Institute, National Institutes of Health, under contract no. HHSN261200800001E (D.W.). Funding sources had no role in study design, data collection and analysis, decision to publish, or preparation of the manuscript.

Authorship

Contribution: L. Dai and Z.Q. designed and performed experiments, analyzed results, and wrote the manuscript; J.T.-T., Y.C., K.B., L. Doyle, K.R., and J.Z. performed experiments; and L.D.V., D.W., and C.P. performed statistical analysis and provided critical input.

Conflict-of-interest disclosure: The authors declare no competing financial interests.

Correspondence: Zhiqiang Qin, Louisiana Cancer Research Center, 1700 Tulane Ave, Suite 902, New Orleans, LA 70112; e-mail: zqin@lsuhsc.edu.

References

1. Cesarman E, Chang Y, Moore PS, Said JW, Knowles DM. Kaposi's sarcoma-associated herpesvirus-like DNA sequences in AIDS-related body-cavity-based lymphomas. *N Engl J Med.* 1995;332(18):1186-1191.
2. Carbone A, Cesarman E, Gloghini A, Drexler HG. Understanding pathogenetic aspects and clinical presentation of primary effusion lymphoma through its derived cell lines. *AIDS.* 2010;24(4):479-490.
3. Carbone A, Gloghini A, Vaccher E, et al. Kaposi's sarcoma-associated herpesvirus/human herpesvirus type 8-positive solid lymphomas: a tissue-based variant of primary effusion lymphoma. *J Mol Diagn.* 2005;7(1):17-27.
4. Chadburn A, Hyjek E, Mathew S, Cesarman E, Said J, Knowles DM. KSHV-positive solid lymphomas represent an extra-cavitary variant of primary effusion lymphoma. *Am J Surg Pathol.* 2004;28(11):1401-1416.
5. Chen YB, Rahemtullah A, Hochberg E. Primary effusion lymphoma. *Oncologist.* 2007;12(5):569-576.
6. Carbone A, Gloghini A. KSHV/HHV8-associated lymphomas. *Br J Haematol.* 2008;140(1):13-24.
7. Cooper CS, Park M, Blair DG, et al. Molecular cloning of a new transforming gene from a chemically transformed human cell line. *Nature.* 1984;311(5981):29-33.
8. Bottaro DP, Rubin JS, Faletto DL, et al. Identification of the hepatocyte growth factor receptor as the c-met proto-oncogene product. *Science.* 1991;251(4995):802-804.
9. Organ SL, Tsao MS. An overview of the c-MET signaling pathway. *Ther Adv Med Oncol.* 2011;3(suppl 1):S7-S19.
10. Trusolino L, Bertotti A, Comoglio PM. MET signalling: principles and functions in development, organ regeneration and cancer. *Nat Rev Mol Cell Biol.* 2010;11(12):834-848.
11. Engelman JA, Zejnullahu K, Mitsudomi T, et al. MET amplification leads to gefitinib resistance in lung cancer by activating ERBB3 signaling. *Science.* 2007;316(5827):1039-1043.
12. Sulpice E, Ding S, Muscatelli-Groux B, et al. Cross-talk between the VEGF-A and HGF signalling pathways in endothelial cells. *Biol Cell.* 2009;101(9):525-539.
13. Vermeulen L, De Sousa E Melo F, van der Heijden M, et al. Wnt activity defines colon cancer stem cells and is regulated by the microenvironment. *Nat Cell Biol.* 2010;12(5):468-476.
14. Gherardi E, Birchmeier W, Birchmeier C, Vande Woude G. Targeting MET in cancer: rationale and progress. *Nat Rev Cancer.* 2012;12(2):89-103.
15. Sierra JR, Tsao MS. c-MET as a potential therapeutic target and biomarker in cancer. *Ther Adv Med Oncol.* 2011;3(suppl 1):S21-S35.
16. Eder JP, Vande Woude GF, Boerner SA, LoRusso PM. Novel therapeutic inhibitors of the c-Met signaling pathway in cancer. *Clin Cancer Res.* 2009;15(7):2207-2214.
17. Comoglio PM, Giordano S, Trusolino L. Drug development of MET inhibitors: targeting oncogene addiction and expedience. *Nat Rev Drug Discov.* 2008;7(6):504-516.
18. Toschi L, Jänne PA. Single-agent and combination therapeutic strategies to inhibit hepatocyte growth factor/MET signaling in cancer. *Clin Cancer Res.* 2008;14(19):5941-5946.
19. Capello D, Gaidano G, Gallicchio M, et al. The tyrosine kinase receptor met and its ligand HGF are co-expressed and functionally active in HHV-8 positive primary effusion lymphoma. *Leukemia.* 2000;14(2):285-291.
20. Kawano R, Ohshima K, Karube K, et al. Prognostic significance of hepatocyte growth factor and c-MET expression in patients with diffuse large B-cell lymphoma. *Br J Haematol.* 2004;127(3):305-307.
21. Teofili L, Di Febo AL, Pierconti F, et al. Expression of the c-met proto-oncogene and its ligand, hepatocyte growth factor, in Hodgkin disease. *Blood.* 2001;97(4):1063-1069.
22. Dai L, Trillo-Tinoco J, Bai L, et al. Systematic analysis of a xenograft mice model for KSHV+ primary effusion lymphoma (PEL). *PLoS One.* 2014;9(2):e90349.
23. Samols MA, Hu J, Skalsky RL, Renne R. Cloning and identification of a microRNA cluster within the latency-associated region of Kaposi's sarcoma-associated herpesvirus. *J Virol.* 2005;79(14):9301-9305.
24. Adang LA, Tomescu C, Law WK, Kedes DH. Intracellular Kaposi's sarcoma-associated herpesvirus load determines early loss of immune synapse components. *J Virol.* 2007;81(10):5079-5090.
25. Mbisa GL, Miley W, Gamache CJ, et al. Detection of antibodies to Kaposi's sarcoma-associated herpesvirus: a new approach using K8.1 ELISA and a newly developed recombinant LANA ELISA. *J Immunol Methods.* 2010;356(1-2):39-46.
26. Benavente Y, Mbisa G, Labo N, et al. Antibodies against lytic and latent Kaposi's sarcoma-associated herpes virus antigens and lymphoma in the European EpiLymph case-control study. *Br J Cancer.* 2011;105(11):1768-1771.
27. Workman C, Jensen LJ, Jarmer H, et al. A new non-linear normalization method for reducing variability in DNA microarray experiments. *Genome Biol.* 2002;3(9):research0048.
28. Dai L, Cao Y, Chen Y, Kaleeba JA, Zabaleta J, Qin Z. Genomic analysis of xCT-mediated regulatory network: Identification of novel targets against AIDS-associated lymphoma. *Oncotarget.* 2015;6(14):12710-12722.
29. Kim SH, Sierra RA, McGee DJ, Zabaleta J. Transcriptional profiling of gastric epithelial cells infected with wild type or arginase-deficient Helicobacter pylori. *BMC Microbiol.* 2012;12:175.
30. Dai L, Cao Y, Chen Y, Parsons C, Qin Z. Targeting xCT, a cystine-glutamate transporter induces apoptosis and tumor regression for KSHV/HIV-associated lymphoma. *J Hematol Oncol.* 2014;7:30.
31. Qin Z, Dai L, Trillo-Tinoco J, et al. Targeting sphingosine kinase induces apoptosis and tumor regression for KSHV-associated primary effusion lymphoma. *Mol Cancer Ther.* 2014;13(1):154-164.
32. Baldus SE, Engelmann K, Hanisch FG. MUC1 and the MUCs: a family of human mucins with impact in cancer biology. *Crit Rev Clin Lab Sci.* 2004;41(2):189-231.
33. Woenckhaus M, Merk J, Stoehr R, et al. Prognostic value of FHIT, CTNNB1, and MUC1 expression in non-small cell lung cancer. *Hum Pathol.* 2008;39(1):126-136.
34. Schroeder JA, Masri AA, Adriance MC, et al. MUC1 overexpression results in mammary gland tumorigenesis and prolonged alveolar differentiation. *Oncogene.* 2004;23(34):5739-5747.
35. Kufe DW. MUC1-C oncoprotein as a target in breast cancer: activation of signaling pathways and therapeutic approaches. *Oncogene.* 2013;32(9):1073-1081.
36. Zhou B, Su L, Hu S, et al. A small-molecule blocking ribonucleotide reductase holoenzyme formation inhibits cancer cell growth and overcomes drug resistance. *Cancer Res.* 2013;73(21):6484-6493.
37. Larsson A, Stenberg K, Ericson AC, et al. Mode of action, toxicity, pharmacokinetics, and efficacy of some new antiherpesvirus guanosine analogs related to buciclovir. *Antimicrob Agents Chemother.* 1986;30(4):598-605.
38. Shao J, Zhou B, Zhu L, et al. Determination of the potency and subunit-selectivity of ribonucleotide reductase inhibitors with a recombinant-holoenzyme-based in vitro assay. *Biochem Pharmacol.* 2005;69(4):627-634.
39. Christensen JG, Zou HY, Arango ME, et al. Cytoreductive antitumor activity of PF-2341066, a novel inhibitor of anaplastic lymphoma kinase and c-Met, in experimental models of anaplastic large-cell lymphoma. *Mol Cancer Ther.* 2007;6(12 Pt 1):3314-3322.
40. Zou HY, Li Q, Engstrom LD, et al. PF-06463922 is a potent and selective next-generation ROS1/ALK inhibitor capable of blocking crizotinib-resistant ROS1 mutations. *Proc Natl Acad Sci USA.* 2015;112(11):3493-3498.
41. Stella GM, Benvenuti S, Gramaglia D, et al. MET mutations in cancers of unknown primary origin (CUPs). *Hum Mutat.* 2011;32(1):44-50.

42. Seiwert TY, Jagadeeswaran R, Faoro L, et al. The MET receptor tyrosine kinase is a potential novel therapeutic target for head and neck squamous cell carcinoma. *Cancer Res.* 2009;69(7):3021-3031.

43. Ma PC, Tretiakova MS, MacKinnon AC, et al. Expression and mutational analysis of MET in human solid cancers. *Genes Chromosomes Cancer.* 2008;47(12):1025-1037.

44. Giordano S, Maffe A, Williams TA, et al. Different point mutations in the met oncogene elicit distinct biological properties. *FASEB J.* 2000;14(2):399-406.

45. Lee JH, Han SU, Cho H, et al. A novel germ line juxtamembrane Met mutation in human gastric cancer. *Oncogene.* 2000;19(43):4947-4953.

46. Park WS, Dong SM, Kim SY, et al. Somatic mutations in the kinase domain of the Met/hepatocyte growth factor receptor gene in childhood hepatocellular carcinomas. *Cancer Res.* 1999;59(2):307-310.

47. Lutterbach B, Zeng Q, Davis LJ, et al. Lung cancer cell lines harboring MET gene amplification are dependent on Met for growth and survival. *Cancer Res.* 2007;67(5):2081-2088.

48. Kong-Beltran M, Seshagiri S, Zha J, et al. Somatic mutations lead to an oncogenic deletion of met in lung cancer. *Cancer Res.* 2006;66(1):283-289.

49. Peschard P, Fournier TM, Lamorte L, et al. Mutation of the c-Cbl TKB domain binding site on the Met receptor tyrosine kinase converts it into a transforming protein. *Mol Cell.* 2001;8(5):995-1004.

50. Vigna E, Gramaglia D, Longati P, Bardelli A, Comoglio PM. Loss of the exon encoding the juxtamembrane domain is essential for the oncogenic activation of TPR-MET. *Oncogene.* 1999;18(29):4275-4281.

51. Singh VV, Dutta D, Ansari MA, Dutta S, Chandran B. Kaposi's sarcoma-associated herpesvirus induces the ATM and H2AX DNA damage response early during de novo infection of primary endothelial cells, which play roles in latency establishment. *J Virol.* 2014;88(5):2821-2834.

52. Hollingworth R, Skalka GL, Stewart GS, Hislop AD, Blackbourn DJ, Grand RJ. Activation of DNA Damage Response Pathways during Lytic Replication of KSHV. *Viruses.* 2015;7(6):2908-2927.

53. Kunos CA, Radivoyevitch T, Pink J, et al. Ribonucleotide reductase inhibition enhances chemoradiosensitivity of human cervical cancers. *Radiat Res.* 2010;174(5):574-581.

54. Kunos CA, Radivoyevitch T, Waggoner S, et al. Radiochemotherapy plus 3-aminopyridine-2-carboxaldehyde thiosemicarbazone (3-AP, NSC #663249) in advanced-stage cervical and vaginal cancers. *Gynecol Oncol.* 2013;130(1):75-80.

55. Chao J, Synold TW, Morgan RJ Jr, et al. A phase I and pharmacokinetic study of oral 3-aminopyridine-2-carboxaldehyde thiosemicarbazone (3-AP, NSC #663249) in the treatment of advanced-stage solid cancers: a California Cancer Consortium Study. *Cancer Chemother Pharmacol.* 2012;69(3):835-843.

56. Yen Y, Margolin K, Doroshow J, et al. A phase I trial of 3-aminopyridine-2-carboxaldehyde thiosemicarbazone in combination with gemcitabine for patients with advanced cancer. *Cancer Chemother Pharmacol.* 2004;54(4):331-342.

2015 126: 2821-2831
doi:10.1182/blood-2015-07-658823 originally published online November 3, 2015

Targeting HGF/c-MET induces cell cycle arrest, DNA damage, and apoptosis for primary effusion lymphoma

Lu Dai, Jimena Trillo-Tinoco, Yueyu Cao, Karlie Bonstaff, Lisa Doyle, Luis Del Valle, Denise Whitby, Chris Parsons, Krzysztof Reiss, Jovanny Zabaleta and Zhiqiang Qin

Blood (print ISSN 0006-4971, online ISSN 1528-0020), is published weekly by the American Society of Hematology, 2021 L St, NW, Suite 900, Washington DC 20036.

Ceramides promote apoptosis for virus-infected lymphoma cells through induction of ceramide synthases and viral lytic gene expression

Lu Dai[1,3], Jimena Trillo-Tinoco[4], Aiping Bai[5], Yihan Chen[1], Jacek Bielawski[5], Luis Del Valle[4], Charles D. Smith[6], Augusto C. Ochoa[7], Zhiqiang Qin[1,2] and Chris Parsons[2,3]

[1] Research Center for Translational Medicine and Key Laboratory of Arrhythmias, East Hospital, Tongji University School of Medicine, Shanghai, China

[2] Department of Microbiology/Immunology/Parasitology, Louisiana State University Health Sciences Center, Louisiana Cancer Research Center, New Orleans, LA, USA

[3] Department of Medicine, Louisiana State University Health Sciences Center, Louisiana Cancer Research Center, New Orleans, LA, USA

[4] Department of Pathology, Louisiana State University Health Sciences Center, Louisiana Cancer Research Center, New Orleans, LA, USA

[5] Department of Biochemistry and Molecular Biology, Hollings Cancer Center, Medical University of South Carolina, Charleston, SC, USA

[6] Department of Drug Discovery/Biomedical Sciences, Hollings Cancer Center, Medical University of South Carolina, Charleston, SC, USA

[7] Department of Pediatrics, Louisiana State University Health Sciences Center, Louisiana Cancer Research Center, New Orleans, LA, USA

Correspondence to: *Zhiqiang Qin*, ***email***: *zqin@lsuhsc.edu*

Chris Parsons, ***email***: *cpars1@lsuhsc.edu*

Keywords: *KSHV, primary effusion lymphoma, sphingosine kinase, ceramide*

Received: *April 19, 2015* ***Accepted***: *June 04, 2015* ***Published***: *July 03, 2015*

ABSTRACT

Kaposi's sarcoma-associated herpesvirus (KSHV) is the etiologic agent for several human cancers including primary effusion lymphoma (PEL), a rapidly progressive malignancy arising preferentially in immunocompromised patients. With conventional chemotherapy, PEL continues to portend high mortality, dictating the development of novel therapeutic strategies. Sphingosine kinase 2 (SphK2) represents a key gatekeeper for sphingolipid metabolism, responsible for conversion of ceramides to sphingosine-1-phosphate (S1P). We have previously demonstrated that targeting SphK2 using a novel selective inhibitor, ABC294640, leads to intracellular accumulation of ceramides and induces apoptosis for KSHV-infected PEL cells, while suppressing tumor progression *in vivo*. In the current study, we sought to determine whether specific ceramide/dh-ceramide species and related ceramide synthases (CerS) impact viability for KSHV-infected PEL cells during targeting of SphK2. We found that several specific ceramide and dihydro(dh)-ceramide species and their associated CerS reduce PEL survival and tumor expansion *in vitro* and *in vivo*. Moreover, we found that dhC16-Cer induces PEL apoptosis in part through activation of KSHV lytic gene expression. These data further implicate bioactive sphingolipids in regulation of PEL survival, and provide justification for future studies evaluating clinically relevant ceramide analogs or mimetics for their potential as therapeutic agents for PEL.

INTRODUCTION

Sphingolipids are a family of membrane lipids regulating the fluidity and subdomain structure of lipid bilayers [1, 2]. Ceramides are composed of a sphingosine base and amide-linked acyl chains of varied length

[3]. Endogenous ceramide can be generated via *de novo* synthesis by ceramide synthases (CerS) [4, 5], or through the metabolism of other complex sphingolipids regulated by specialized enzymes [1, 2, 6]. Ceramides are hydrolyzed to generate sphingosine which is subsequently phosphorylated by one of two sphingosine kinase isoforms (SphK1 or SphK2) to generate sphingosine-1-phosphate (S1P) [1, 7-9]. Bioactive sphingolipids, including ceramides and S1P, act as signaling molecules to regulate apoptosis and tumor cell survival [1]. In contrast to the anti-apoptotic function of S1P, most endogenous long-chain ceramides are thought to induce cell death preferentially [7]. Over the past two decades, targeting bioactive sphingolipids has evolved as a promising therapeutic approach for cancer treatment [10].

A significant proportion of human cancers are attributable to viruses, including the Kaposi's sarcoma-associated herpesvirus (KSHV) [11]. KSHV is a common etiologic agent for cancers arising preferentially in the setting of HIV infection or organ transplantation, including primary effusion lymphoma (PEL) and Kaposi's sarcoma (KS) [12-15]. PEL tumors are comprised of transformed B-cells harboring KSHV and exhibit a rapidly progressive course, with a median survival of approximately 6 months with standard chemotherapy [12, 16]. The role of sphingolipids in virus-associated malignancies remains largely unknown, although one recent study indicates that KSHV induces fatty acid synthesis to promote survival of endothelial cells [17]. Another recent study demonstrates that KSHV-microRNAs can induce metabolic transformation of latently infected endothelial cells, including decreasing oxygen consumption, increasing lactate secretion and glucose uptake, stabilizing HIF1α and decreasing mitochondria copy number [18]. We recently reported that targeting SphK2 using either RNA interference or a selective small-molecule inhibitor, ABC294640, induces caspase-mediated apoptosis for KSHV-infected PEL cells and suppresses PEL tumor progression *in vivo* [19]. We also found that targeting SphK2 increases the collective accumulation of ceramides (including bioactive dihydro (dh)-ceramides) while reducing S1P concentrations within KSHV-infected cells [19, 20]. However, specific mechanisms for virus-infected lymphoma cell death associated with disruption of sphingolipids biosynthesis have not been previously addressed. Therefore, we sought to determine whether individual ceramide species induced apoptosis during perturbations in lipid metabolism in PEL cells, and if so, whether this effect was associated with alterations in KSHV gene expression.

RESULTS

Targeting SphK2 results in accumulation of ceramide species and upregulation of corresponding ceramide synthases within PEL cells

We previously reported that a selective inhibitor of SphK2, ABC294640, increased cumulative ceramide levels within KSHV-infected PEL cells [19]. An abbreviated schematic of sphingolipid metabolism is provided (Figure 1A), depicting pathways and potential alterations in sphingolipid metabolism with SphK2 inhibition. More detailed lipidomics analysis performed using a KSHV$^+$ body cavity-based lymphoma (BCBL-1) cell line revealed dose-dependent accumulation of multiple long-chain ceramide and dh-ceramide species within these cells with exposure to ABC294640 (Figure 1B-1C). In parallel analyses, we found that BCBL-1 cells recovered from ascites of ABC294640-treated NOD/SCID mice also exhibited increased levels of long-chain ceramide and dh-ceramide species relative to BCBL-1 cells recovered from vehicle-treated control mice (Figure 1D). We also calculated the proportion of individual ceramide species within the total lipid mass of ABC294640-treated PEL cells and noted a relative proportional increase in C16-Cer and dhC16-Cer species both *in vitro* and *in vivo* (Figure 1E-1F). In addition, we found that C16-, C24-, C24:1-, dhC16-, dhC20-Cer accumulate predominantly in BCBL-1 cells *in vitro*, while the C16-, C20-, C24-, C24:1-, dhC16-, dhC20-, dhC24-Cer predominate within BCBL-1 cells recovered from mice (Figure 1E-1F). This demonstrates that common and differential ceramide signatures emerge with SphK2 targeting *in vitro* and *in vivo*. Ceramides are synthesized by a family of CerS enzymes, CerS1–CerS6 [21, 22]. We found that *in vitro* targeting of SphK2 in BCBL-1 cells increased transcript expression for all CerS, confirmed using immunoblots for CerS2 and CerS6 expression (Figure 2A-2B). Furthermore, BCBL-1 cells recovered from ABC294640-treated mice exhibited increased expression of CerS2, CerS4 and CerS6 transcripts relative to BCBL-1 cells from vehicle-treated xenograft mice (Figure 2C). In vehicle-treated xenograft mice, we observed significant splenic enlargement, due to tumor infiltration, relative to ABC294640-treated mice (Figure 2D) [19]. Using immunohistochemistry (IHC), we noted robust expression of CerS2 within splenic tissue from ABC294640-treated mice, with negligible expression within splenic tissue from vehicle-treated mice (Figure 2D). These data suggested a role for specific ceramides and CerS2 in PEL cell death associated with SphK2 inhibition *in vivo*.

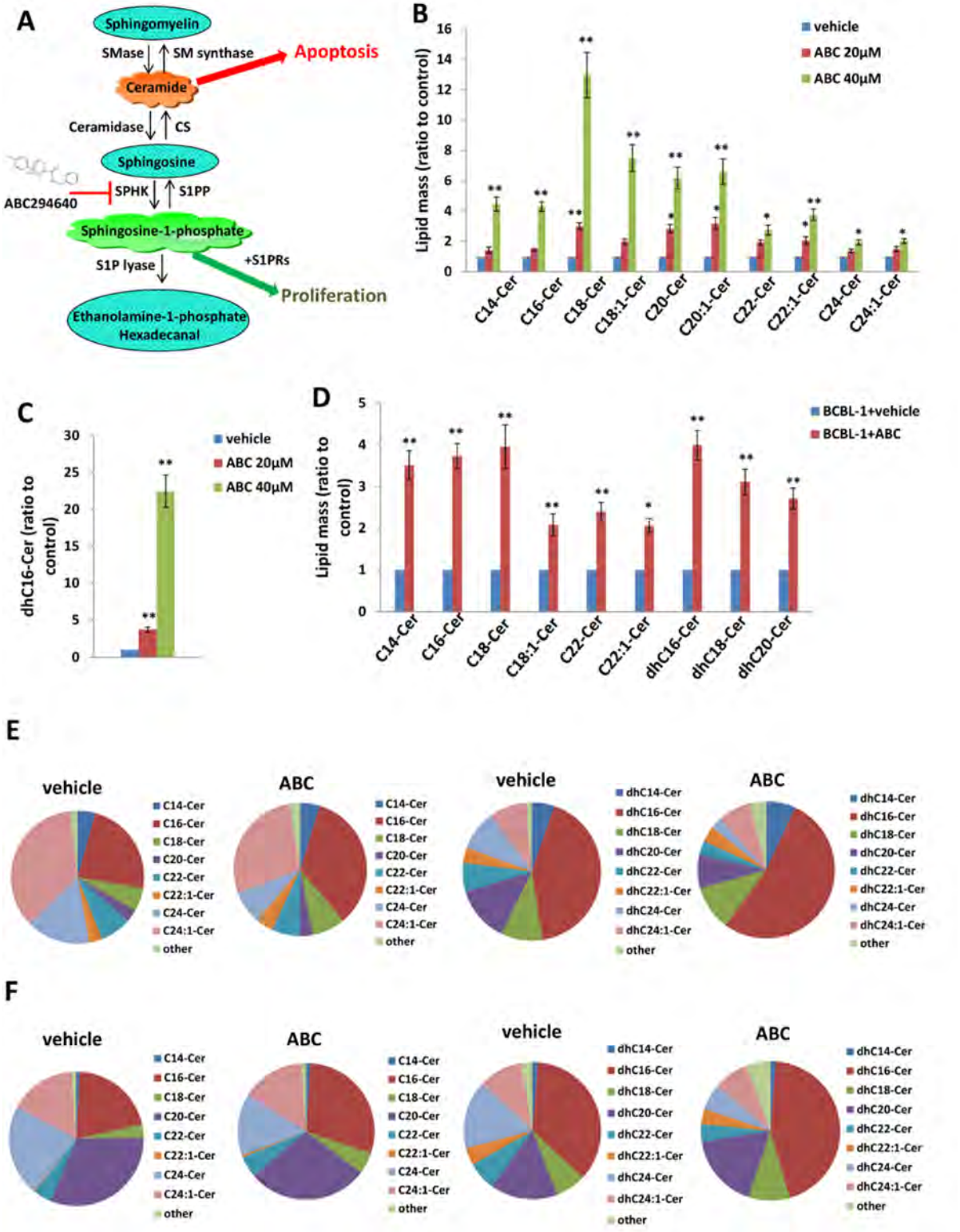

Figure 1: Accumulation of ceramides following targeting of SphK2 within PEL cells. A. The core pathways of sphingolipid metabolism. **B.-C.** BCBL-1 cells were incubated with the indicated concentrations of ABC294640 (ABC) or vehicle for 16 h, then ceramide and dihydro (dh)-ceramide species were quantified as described in Methods. **D.** NOD/SCID mice were injected i.p. with 10^7 BCBL-1 cells. Beginning 21 days later, mice were administered 100 mg/kg ABC or vehicle (n = 10 per group) i.p. once daily, five days per week, for another 21 days. Live PEL cell lysates were recovered from ascites fractions from each of 3 representative vehicle- or drug-treated mice, and intracellular ceramide and dh-ceramide species quantified as above. Error bars represent the S.E.M. for 2 independent experiments, * = $p < 0.05$; ** = $P < 0.01$. **E.-F.** Relative proportions of specific ceramide and dh-ceramide species within vehicle- or drug-treated PEL cells from *in vitro* **E.** and *in vivo* **F.** experiments are presented.

Exogenous long-chain ceramides induce expression of ceramide synthases and apoptosis for PEL cells

Relatively little is known regarding specific roles for individual CerS and their respective ceramide products in cancer development, although available data suggest that CerS6 and its product C16-Cer promote cell survival and tumor growth, while CerS1 and CerS4, and their mutual product C18-Cer, may negatively regulate head and neck cancer growth [3]. Since our initial experiments indicated increased expression of CerS4 and CerS6 within ABC294640-treated PEL cells, we sought to determine whether commercially available ceramides generated by CerS4 (C18-Cer) and CerS6 (dhC16-Cer) directly impact PEL cell survival. Following verification of C18-Cer and dhC16-Cer accumulation within PEL cells with their exposure to these ceramides *in vitro* (Figure S1), we found that C18-Cer and dhC16-Cer induced significant apoptosis for PEL cells in dose-dependent fashion (Figs. 3A-3B and S2), as well as caspase cleavage (Figure 3C), for multiple KSHV^{+} PEL cell lines. Furthermore, exogenous dhC16-Cer induced dose-dependent apoptosis for the following Burkitt's lymphoma cell lines: BL-41 (KSHV^{neg}/EBV^{neg}), Akata (KSHV^{neg}/EBV^{+}) and Mutu (KSHV^{neg}/EBV^{+}) cells (Figure S3). Interestingly, lipidomics analysis indicated that C18-Cer and dhC16-Cer independently increase accumulation of other endogenous long-chain ceramide species within PEL cells (Figure 3D), suggesting that exogenous C18-Cer and dhC16-Cer may regulate expression and/or function of CerS. In fact, we found that C18-Cer and dhC16-Cer independently increased transcript and protein expression for CerS2 and CerS6, as well as transcript expression for CerS5 (Figure 4A-4B).

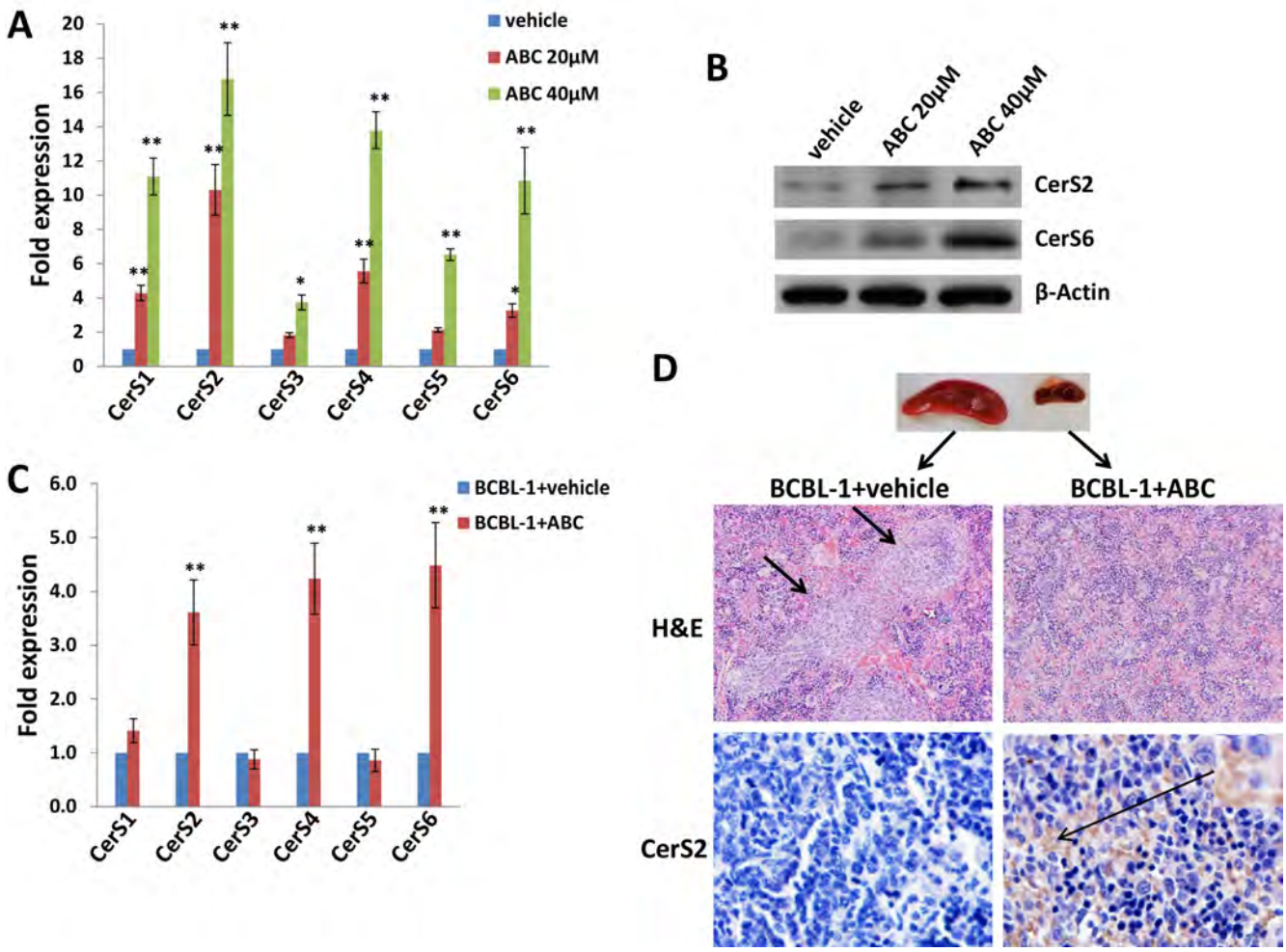

Figure 2: Targeting SphK2 induces upregulation of ceramide synthases within PEL cells. A.-B. BCBL-1 cells were incubated with the indicated concentrations of ABC or vehicle for 16 h, then transcript **A.** and protein **B.** expression of ceramide synthases (CerS1-CerS6) quantified using qRT-PCR and immunoblots, respectively. **C.** CerS transcripts were quantified using RNA from PEL cells recovered from ascites fractions from each of 3 representative vehicle- or drug-treated mice. Error bars represent the S.E.M. for 2 independent experiments, * = $p < 0.05$; ** = $P < 0.01$. **D.** Spleens from representative vehicle- or drug- treated mice were prepared for routine hematoxylin and eosin (H&E) staining as described in Methods for identification of infiltrating PEL tumors (short arrows), and immunohistochemistry (IHC) was used for identifying CerS2 expression (upper panels, 200x; lower panels, 400x).

After developing efficient RNA interference for CerS2 in the C18-Cer- or dhC16-Cer-treated PEL cells (Figure 4C), we found that repression of CerS2 partially abrogated the pro-apoptotic impact of both C18-Cer and dhC16-Cer (Figure 4D). Collectively, these data suggest that exogenous long-chain ceramide species induce PEL cell apoptosis, in part through upregulation of specific CerS enzymes.

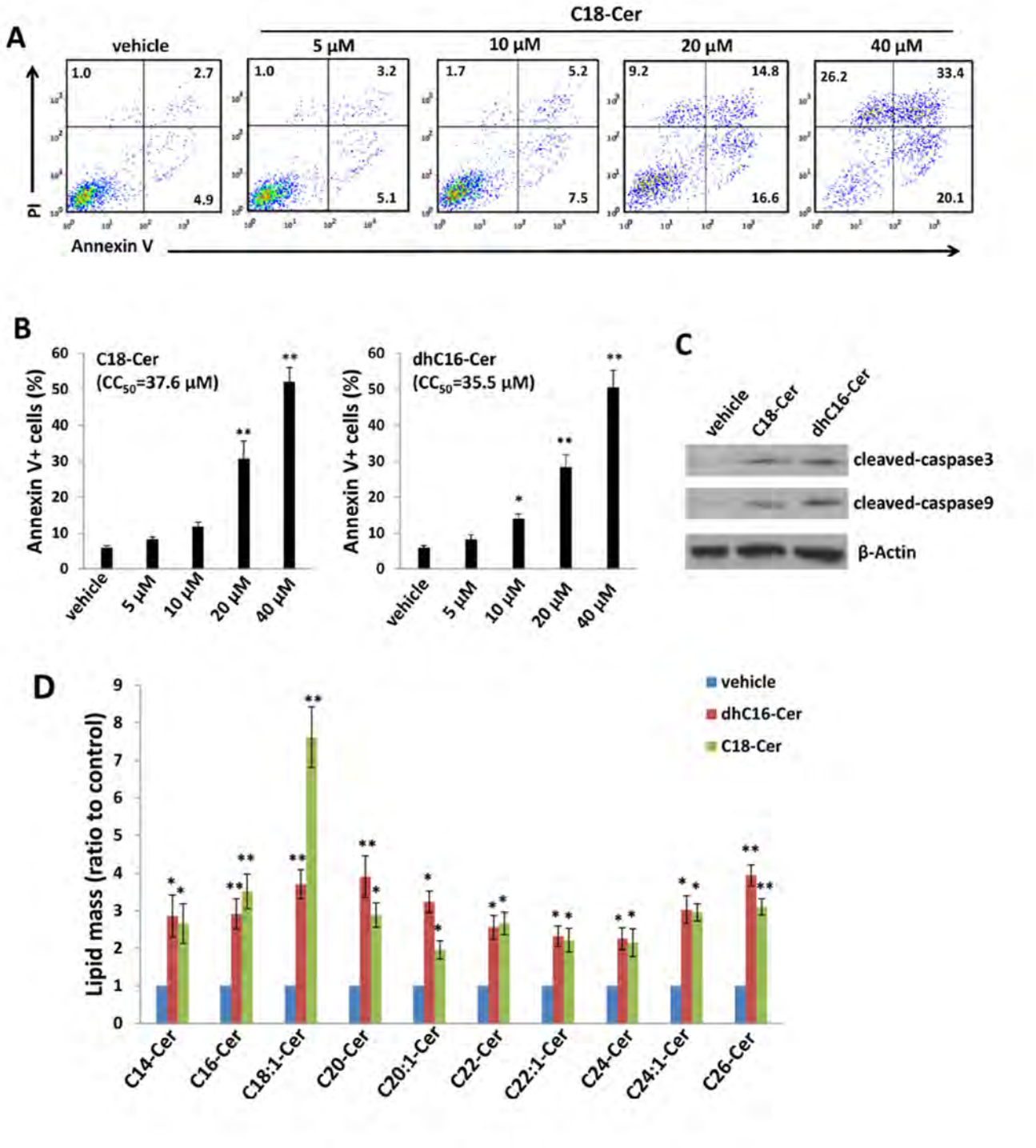

Figure 3: C18-Cer and dhC16-Cer induce accumulation of ceramides and apoptosis for PEL cells. A.-C. BCBL-1 cells were incubated with the indicated concentrations of C18-Cer, dhC16-Cer or vehicle for 24 h, then apoptosis **A.-B.** and protein expression **C.** quantified as in Methods. **D.** BCBL-1 cells were incubated with C18-Cer (40 μM), dhC16-Cer (40 μM) or vehicle for 24 h, then intracellular ceramide and dh-ceramide species were quantified as described in Methods. Error bars represent the S.E.M. for 3 independent experiments, * = $p < 0.05$; ** = $P < 0.01$.

Exogenous C18-Cer and dhC16-Cer induce viral lytic gene expression within PEL cells

To determine whether ceramides induce PEL apoptosis by increasing KSHV lytic reactivation, we quantified representative latent and lytic viral transcripts within BCBL-1 cells in the presence or absence of C18-Cer or dhC16-Cer. We found that either C18-Cer or dhC16-Cer induced expression of viral lytic genes representing all phases of the lytic cycle, while having little impact on expression of KSHV *ORF73* which encodes the latency-associated nuclear antigen (LANA; Figure 5A). These data were supported by observation of increased expression of K8.1, a KSHV envelope protein representing "late" lytic gene expression, when culturing BCBL-1 cells with these exogenous ceramides (Figure 5B-5C). In support of these data, we found that exogenous C18-Cer or dhC16-Cer induced BCBL-1 release of infectious KSHV particles in culture supernatants, as demonstrated by increased KSHV gene expression within KSHV-naïve human umbilical vein endothelial cells (HUVEC) following their exposure to ceramide-treated BCBL-1 supernatants (Figure S4). To determine whether long-chain ceramide-induced viral lytic gene expression is responsible for PEL apoptosis, we performed RNA interference targeting KSHV *ORF50* which encodes the replication and transcription activator (RTA) responsible for the KSHV latent to lytic switch [23]. We observed suppression of "downstream" KSHV lytic gene activation and partial abrogation of apoptosis with dhC16-Cer treatment with knockdown of *ORF50* (Figure 5D-5E). Interestingly, direct silencing of *CerS2* by RNAi incurred more "global" suppression of both latent and lytic genes within dhC16-Cer-treated PEL cells

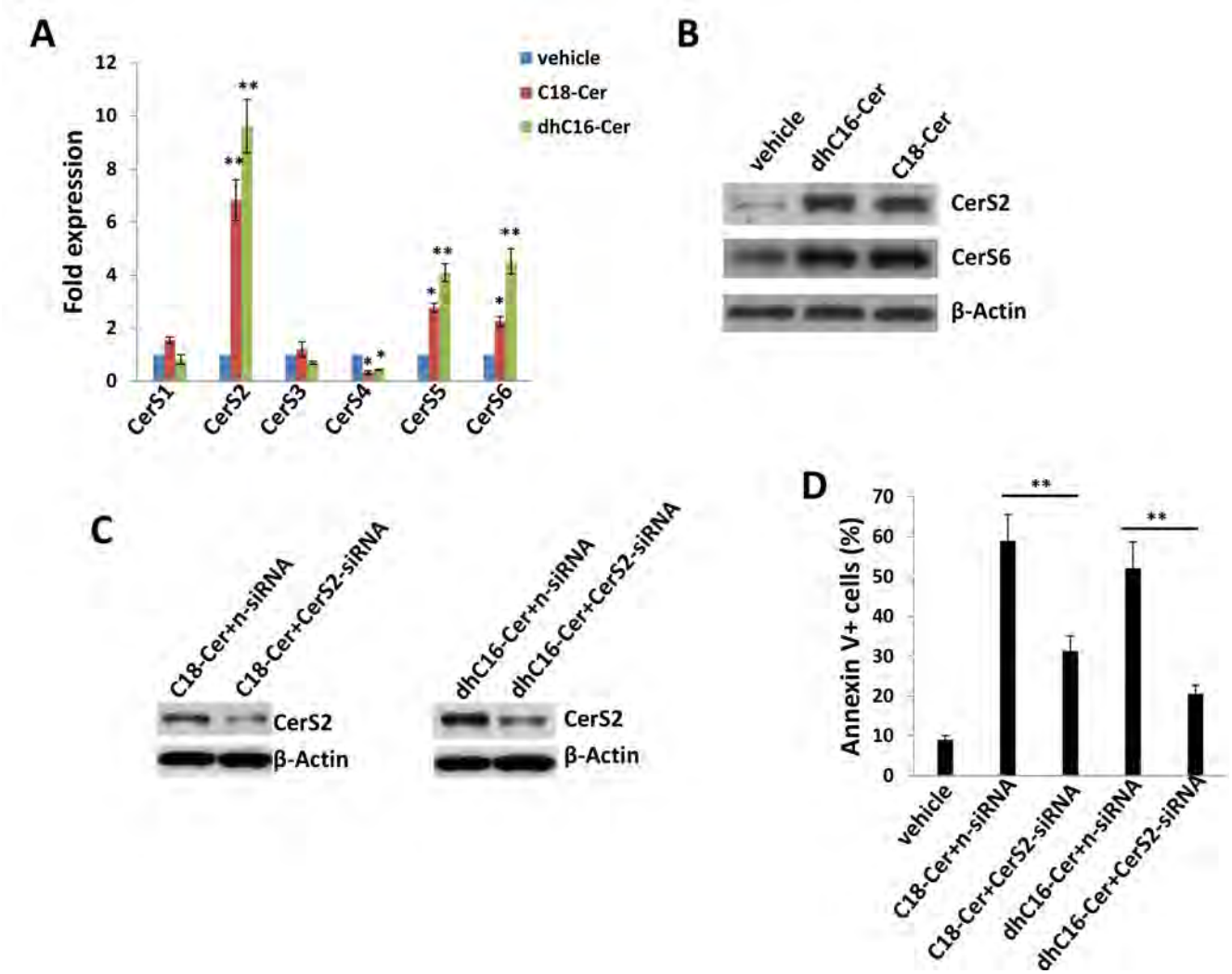

Figure 4: C18-Cer and dhC16-Cer induce expression of ceramide synthases within PEL cells. A.-B. BCBL-1 cells were incubated with C18-Cer (40 μM), dhC16-Cer (40 μM) or vehicle for 24 h, then transcript **A.** and protein **B.** expression of CerS isoforms quantified using qRT-PCR and immunoblots, respectively. **C.-D.** Cells were transfected with control non-target siRNA (n-siRNA) or *CerS2*-siRNA for 48 h, then incubated with C18-Cer (40 μM), dhC16-Cer (40 μM) or vehicle for 24 h. Protein expression was detected by immunoblots, and cell apoptosis quantified as above. Error bars represent the S.E.M. for 3 independent experiments, * = $p < 0.05$; ** = $P < 0.01$.

(Figure 5F).

Exogenous dhC16-Cer suppresses PEL progression *in vivo*

Next, we sought to determine whether exogenous long-chain ceramides suppress PEL tumor growth *in vivo* using an established murine xenograft model [34]. We administered dhC16-Cer (or vehicle) intraperitoneally (i.p.) within 24 hours of BCBL-1 cell injection and for one-month duration. We found that dhC16-Cer dramatically suppressed PEL tumor progression over this timeframe (Figure 6A-6C). Using routine IHC, we observed tumor infiltration within spleens of vehicle-treated mice, with only small tumor nests dispersed within spleens of dhC16-Cer-treated mice (Figure 6D). Moreover, although direct ascites tumor analyses were not feasible due to effective suppression of tumor growth in dhC16-Cer-treated animals, immunoblots indicated increased CerS2 and CerS6 expression within splenic lysates from representative animals treated with dhC16-Cer relative to vehicle-treated animals (Figure 6E).

Exogenous short-chain ceramide species induce PEL apoptosis *in vitro* and *in vivo*

In general, short-chain ceramide species cannot be reliably quantified using lipidomics analysis because they are rapidly converted to long-chain ceramides [24]. However, relative to long-chain ceramides, short-chain ceramides may have improved solubility and cell-permeability for therapeutic application [25]. Therefore, we sought to determine whether exogenous short-chain ceramides also induce PEL apoptosis. We found that

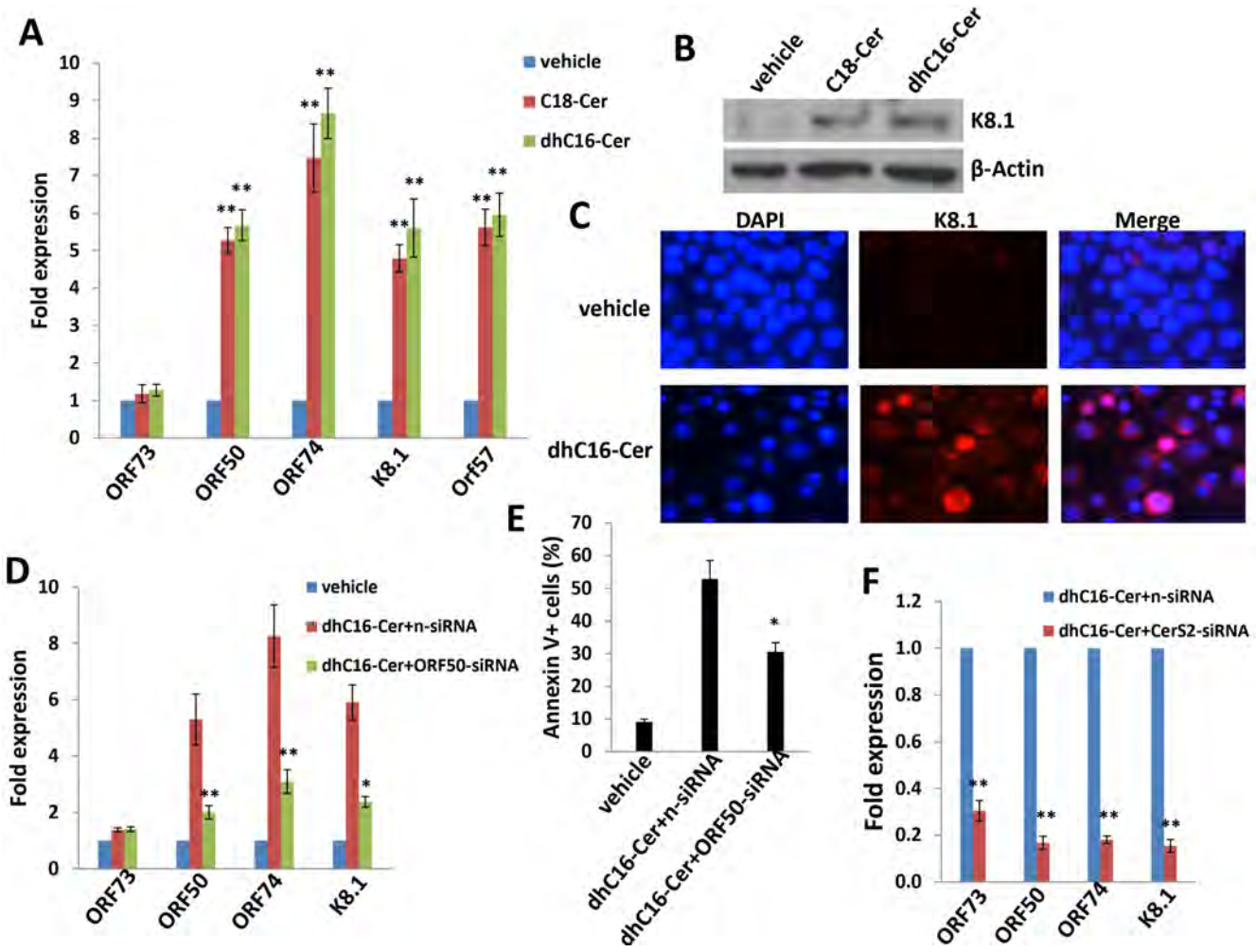

Figure 5: C18-Cer and dhC16-Cer induce KSHV lytic gene expression. A.-C. BCBL-1 cells were incubated with C18-Cer (40 μM), dhC16-Cer (40 μM) or vehicle for 24 h, then qRT-PCR used to quantify representative KSHV latent (*ORF73)* and lytic transcripts (*ORF50, ORF74, K8.1, ORF57)*. Expression of the viral lytic protein K8.1 was determined using immunoblots and IFA. **D.-E.** BCBL-1 were transfected with control n-siRNA or *ORF50*-siRNA for 48 h, then incubated with dhC16-Cer (40 μM) or vehicle for 24 h. Viral gene expression and cell apoptosis were quantified by qRT-PCR and flow-cytometry, respectively. **F.** BCBL-1 were transfected with control n-siRNA or *CerS2*-siRNA for 48 h, then representative viral transcripts quantified by qRT-PCR. Error bars represent the S.E.M. for 3 independent experiments, * = $p < 0.05$; ** = $P < 0.01$.

exogenous C2-, C6- or C8-Cer independently induced dose-dependent apoptosis for KSHV$^+$ PEL cell lines, and both C6- and C8-Cer displayed lower inhibitory concentrations (CC_{50}) relative to long-chain ceramides such as C18-Cer or dhC16-Cer (Figs. 7A-7B and S5). In contrast to long-chain ceramides, we found that Akata and Mutu cells were resistant to C6-Cer-induced apoptosis, while BL-41 cells retained sensitivity to C6-Cer (Figure S6). Similar to their long-chain counterparts, short-chain ceramides also increased accumulation of endogenous long-chain ceramides within BCBL-1 cells (Figure 7C). Of note, the accumulation of intracellular C6- and C8-Cer could be quantified at specific time points following their exogenous administration in cell culture, while C2-Cer could not (Figure S7), suggesting exogenous C2-Cer may be more quickly converted to long-chain ceramides following cell entry.

Since we found that exogenous long-chain ceramides induce expression of specific CerS in PEL cells, we explored the same principle with exogenous short-chain ceramides. Unlike the selective but uniform impact of C18- and dhC16-Cer on the CerS profile (Figure 4A-4B), C2-, C6- and C8-Cer had varying impacts on CerS transcript profiles (Figure 8A), although C6- and C8-Cer uniformly increased transcript and protein expression of CerS2 and CerS6, albeit to varying degrees (Figure 8A-8B). As previously demonstrated for exogenous C18- and dhC16-Cer, we found that CerS2 silencing reduced BCBL-1 apoptosis during C6-Cer treatment (Figure 8C-8D). In addition, CerS6 silencing incurred similar results, with additive and protective effects for concurrent silencing of both CerS2 and CerS6 (Figure 8C-8D). Furthermore, C2-, C6- and C8-Cer independently increased expression of KSHV lytic transcripts within BCBL-1, although the effect was most pronounced for C2-Cer, and *ORF50* silencing partially suppressed apoptosis induced by exogenous C2-

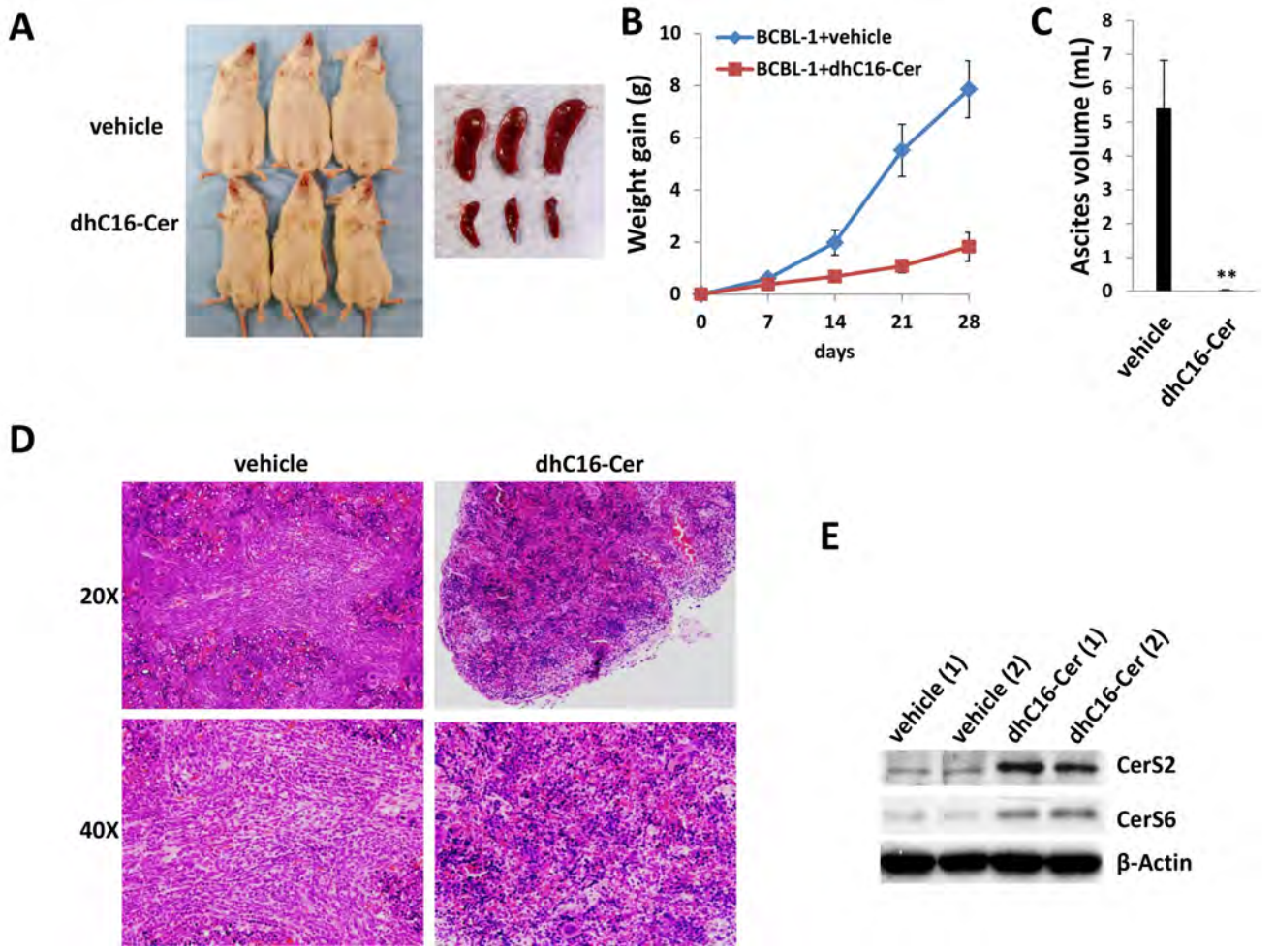

Figure 6: Exogenous dhC16-Cer suppresses PEL tumor progression *in vivo*. A.-C. NOD/SCID mice were injected i.p. with 10^7 BCBL-1 cells. Beginning 24 h later, 20 mg/kg dhC16-Cer or vehicle (n = 10 per group) were administered i.p. 3x/week, for each of 2 independent experiments. Weights were recorded weekly. Images of representative animals and their respective spleens, as well as ascites fluid volumes, were collected at the conclusion of experiments on day 28. Error bars represent the S.E.M. for 2 independent experiments, ** = $p < 0.01$. **D.** Spleens from representative vehicle- or dhC16-Cer-treated mice were prepared for routine H&E staining for identification of infiltrating PEL tumors. **E.** Immunoblots were used to detect CerS protein expression within splenic lysates from representative 2 vehicle- or dhC16-Cer-treated mice.

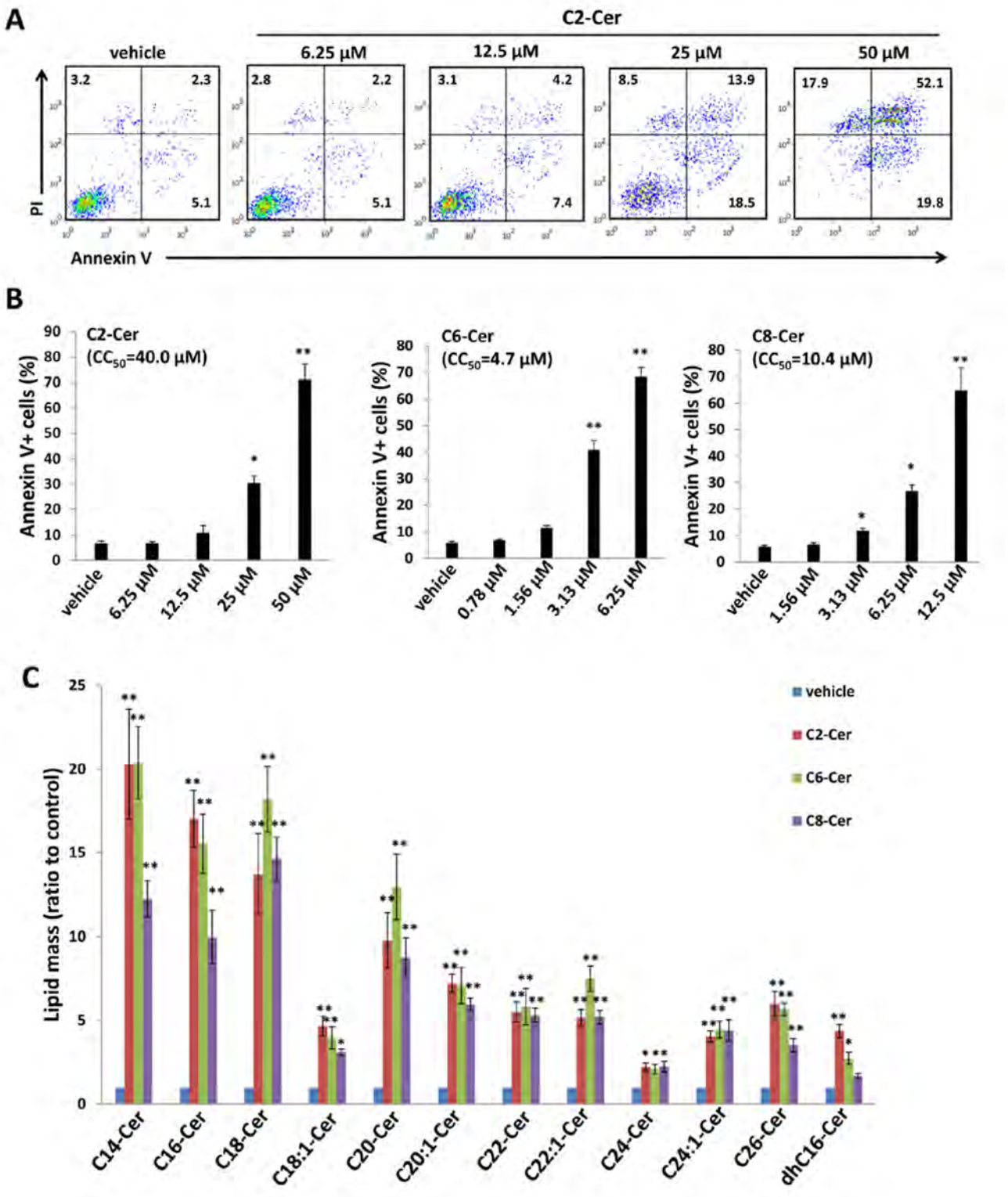

Figure 7: Short-chain ceramides induce ceramide accumulation and apoptosis for PEL cells. A.-B. BCBL-1 cells were incubated with the indicated concentrations of C2-Cer, C6-Cer, C8-Cer or vehicle for 24 h, then apoptosis quantified as described previously. **C.** Intracellular ceramide and dh-ceramide species were quantified as above. Error bars represent the S.E.M. for 2 independent experiments, * = $p < 0.05$; ** = $P < 0.01$.

Cer (Figure S8).

To validate the potential impact of exogenous short-chain ceramides on PEL tumor growth *in vivo*, we explored whether C6-Cer impacted PEL progression using the same xenograft model. C6-Cer was chosen due to its low CC_{50} for PEL cell lines and better *in vivo* stability (Figures 7B, S5 and S7). Similar to previous experiments, C6-Cer (or vehicle) was administered i.p. within 24 hours of BCBL-1 cell injection and for a duration of one month. We found that C6-Cer dramatically suppressed PEL tumor progression *in vivo* in a manner similar to that observed for dhC16-Cer (Figure 9A-9D). Immunoblots using splenic lysates also indicated that C6-Cer treatment increased CerS2 and CerS6 expression in this compartment (Figure 9E). Additional experiments were conducted wherein C6-Cer therapy was initiated following establishment of PEL tumors (beginning 28 days after BCBL-1 cell injection). Using this approach, C6-Cer-treated mice exhibited significant regression of PEL tumor burden relative to vehicle-treated mice (Figure 9F-9G), with virtually no ascites found in these mice after three weeks of treatment (Figure 9H).

DISCUSSION

In summary, our findings indicate that individual ceramide species, including both short- and long-chain variants, induce apoptosis for PEL cells. In addition, two potential mechanisms are illuminated: induction of CerS expression and accumulation of other pro-apoptotic ceramides; and induction of pro-apoptotic KSHV lytic gene expression. We have also demonstrated that this can be accomplished by two methods which

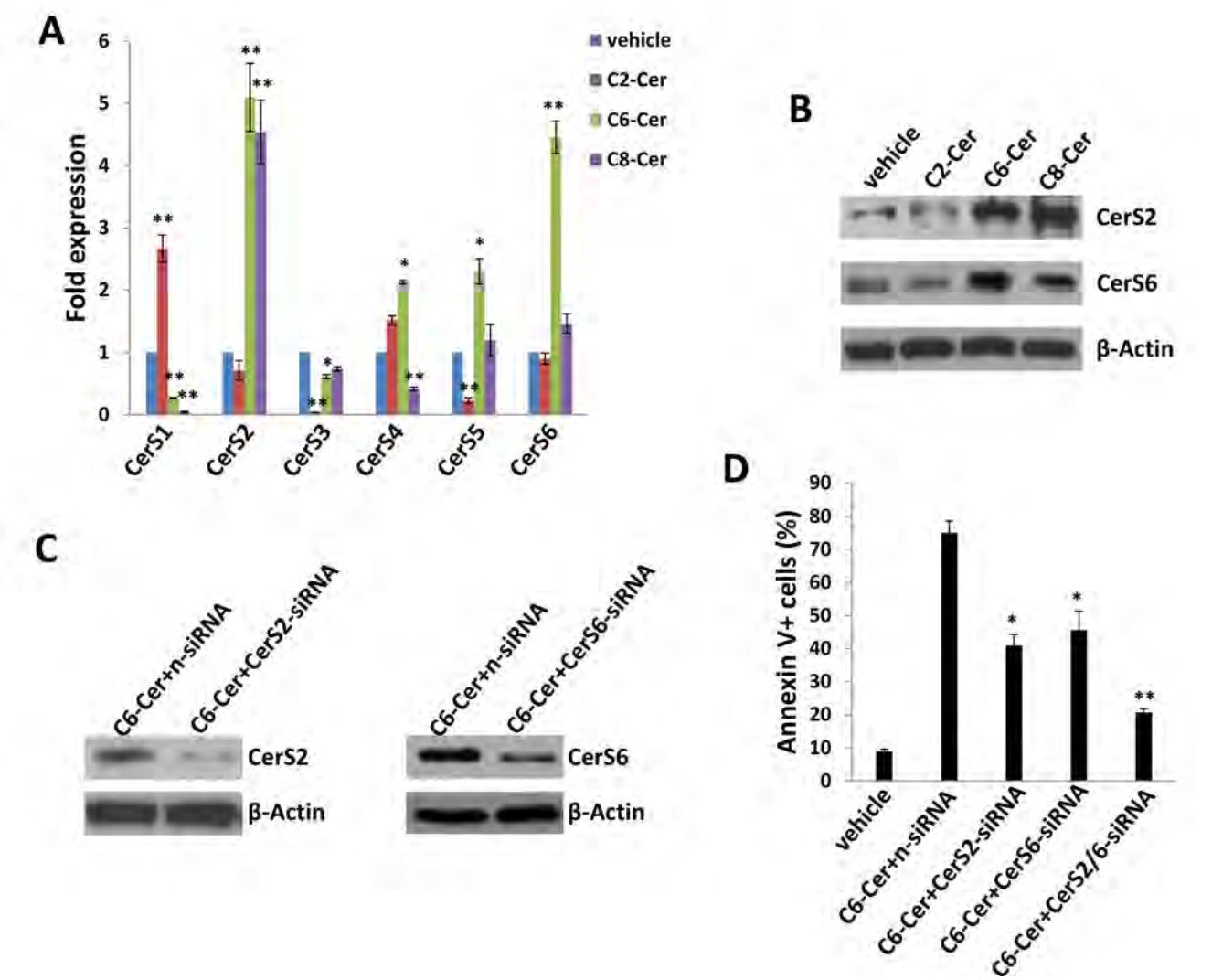

Figure 8: Short-chain ceramides induce expression of ceramide synthases within PEL cells. A.-B. BCBL-1 cells were incubated with C2-Cer (50 μM), C6-Cer (6.25 μM), C8-Cer (12.5 μM) or vehicle for 24 h, then transcript **A.** and protein **B.** expression of CerS isoforms quantified using qRT-PCR and immunoblots, respectively. **C.-D.** Cells were transfected with control n-siRNA, *CerS2*-siRNA or *CerS6*-siRNA for 48 h, then incubated with C6-Cer (6.25 μM) or vehicle for 24 h. CerS protein expression and cell apoptosis were determined as above. Error bars represent the S.E.M. for 3 independent experiments, * = $p < 0.05$; ** = $P < 0.01$.

disrupt the ceramide:S1P ratio, namely inhibition of SphK2 or provision of specific exogenous ceramides.

In addition to *de novo* generation of ceramides by CerS, ceramides are generated through metabolism of other

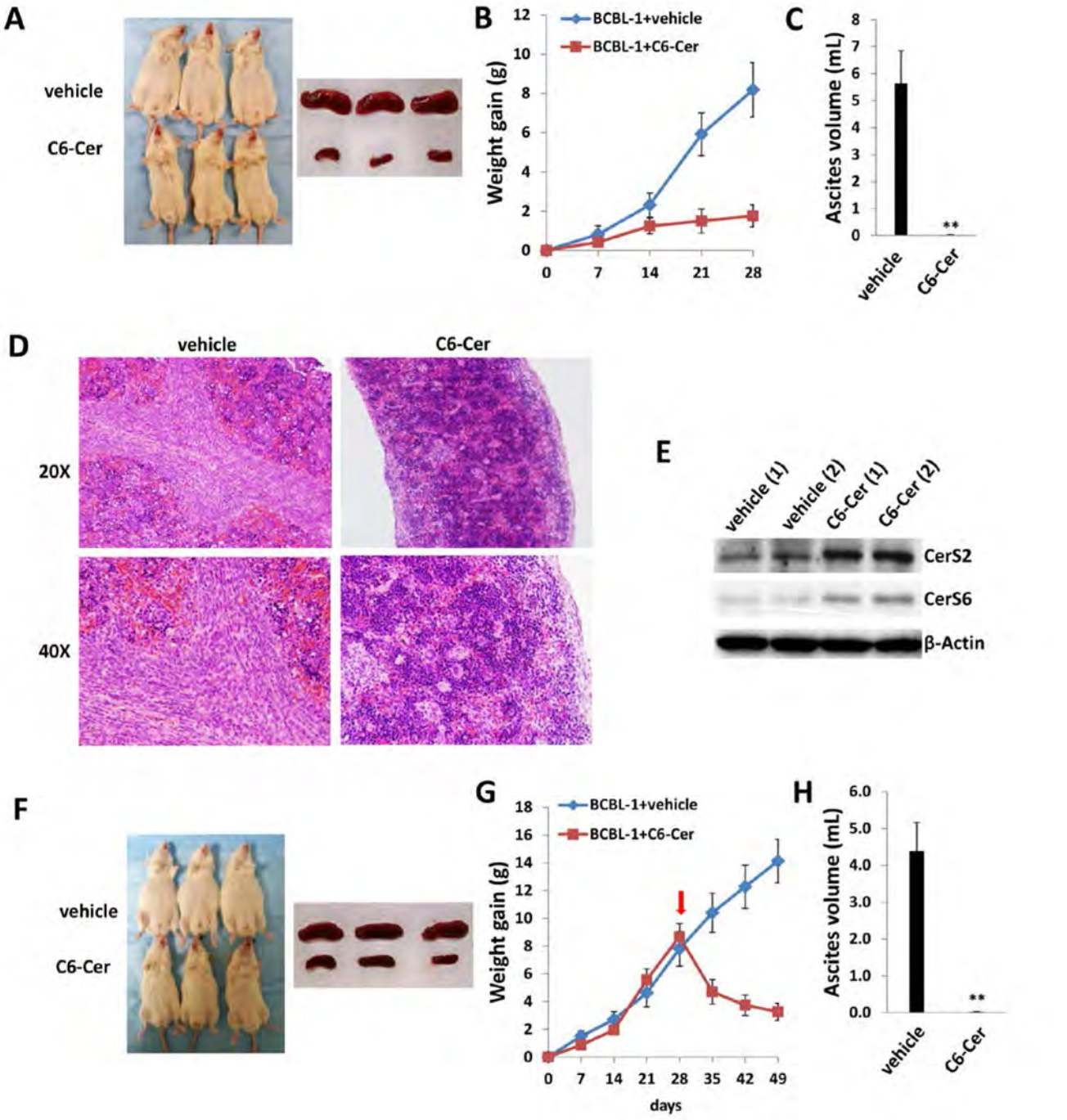

Figure 9: C6-Cer suppresses PEL formation and induces regression of established PEL tumors *in vivo*. A.-C. NOD/SCID mice were injected i.p. with 10^7 BCBL-1 cells. Beginning 24 h later, 20 mg/kg C6-Cer or vehicle (n = 10 per group) were administered i.p. 3x/week, for each of 2 independent experiments. Weights were recorded weekly. Images of representative animals and their respective spleens, as well as ascites fluid volumes, were collected at the conclusion of experiments on day 28. Error bars represent the S.E.M. for 2 independent experiments, ** = $p < 0.01$. **D.** Spleens from representative vehicle- or C6-Cer-treated mice were prepared for routine H&E staining. **E.** Immunoblots were used to detect CerS protein expression within splenic lysates from representative vehicle- or C6-Cer-treated mice. **F.-H.** NOD/SCID mice were injected i.p. with 10^7 BCBL-1 cells. Beginning 28 days later, 20 mg/kg C6-Cer or vehicle (n = 10 per group) were administered i.p. 3x/week, for an additional 21 days for each of 2 independent experiments. Weights were recorded weekly, and images of representative animals and their respective spleens, as well as ascites fluid volumes, were collected at the conclusion of experiments on day 49.

complex sphingolipids tightly regulated by specialized enzymes [1, 2, 6]. For instance, ceramides are generated by sphingomyelinases (SMases) responsible for sphingomyelin (SM) hydrolysis [26] or cerebrosidase-mediated GlcCer and galactosylceramide (GalCer) breakdown [27]. Future work should be useful in validating methods and potential clinical applicability of manipulating lipid biosynthesis pathways to induce apoptosis for virus-associated tumors.

Consistent with our findings, published data indicate that provision of exogenous short-chain ceramides results in biologic responses similar to those of ceramide agonists in mammalian and yeast cells [25]. Our observation that specific ceramides induce expression of CerS isoforms and accumulation of other ceramide species in PEL cells are also consistent with studies revealing a direct relationship between exogenous and endogenous ceramides. For example, C8-Cer (*N-octanoyl*-sphingosine) liposomes induced a 10-fold increase in total ceramide levels within canine kidney cells [28]. In another example, C6-Cer triggers sustained endogenous ceramide production in a human myeloid leukemia cell line [29]. In a third report, exogenous C6-Cer induced production of endogenous ceramides within a human lung cancer cell line through recycling of the sphingosine backbone of C6-Cer via deacylation/reacylation [24]. Further work with PEL and other virus-infected tumor cells should illuminate mechanisms for exogenous ceramide activation of lipid biosynthesis pathways responsible for death of these cells, and how these pathways integrate with mechanisms for viral latency that either augment or oppose cell death. Our observation that C6-and C8-Cer demonstrate a lesser impact on KSHV lytic activation (at least relative to other species tested in our experiments), yet still readily induce PEL cell death *in vitro* (both) and *in vivo* (C6-Cer), suggest varying and potentially complimentary mechanisms of PEL cell death induced by exogenous ceramides which might be exploited for developing therapeutic strategies. While beyond the scope of this manuscript, the cell type-specific nature of our observations for Burkitt's lymphoma cell lines also indicate that EBV-infected lymphoma cell lines may be alternatively sensitive or resistant to apoptosis induced by specific ceramide species (possibly related to differential impact of ceramides on EBV gene expression), and that specific ceramide species induce apoptosis for lymphoma cells independent of virus-associated mechanisms.

Due to limitations of solubility and cell-permeability for many ceramide species, ceramide analogues or mimetics have been developed as therapeutic agents. These include pyridinium ceramides (Pyr-Cer) which exhibit a more positive charge (pyridinium ring), allowing for preferential accumulation of these analogues in cancer cells [30] which exhibit a more negative charge in subcellular structures (especially mitochondria) [31]. In two examples, L-t-C6-Pyr-Cer and D-e-C16-Pyr-Cer exhibit significant anti-cancer activity *in vitro* and *in vivo* [30, 32]. Our observation that exogenous ceramides induce KSHV lytic gene suggests that ceramides potentially facilitate KSHV dissemination. Therefore, given that antiviral agents like ganciclovir successfully repress KSHV replication and prevent KSHV-associated neoplasms [33], the combination of ceramide analogues or mimetics with antiviral drugs (such as ganciclovir) may represent a rational therapeutic approach. Regardless, use of ceramides to disrupt lipid biosynthesis pathways regulated by oncoviruses represents a potentially novel and targeted therapeutic strategy for virus-associated lymphoma.

MATERIALS AND METHODS

Cell culture and reagents

Body cavity-based lymphoma cells (BCBL-1, $KSHV^{+}/EBV^{neg}$) were kindly provided by Dr. Dean Kedes (University of Virginia) and maintained in RPMI 1640 medium (Gibco) with supplements as described previously [34]. BC-1 ($KSHV^{+}/EBV^{+}$) and BCP-1 ($KSHV^{+}/EBV^{neg}$) cells were purchased from ATCC and maintained in complete RPMI 1640 medium (ATCC) supplemented with 20% FBS. All cells were incubated at 37°C in 5% CO_2. Burkitt's lymphoma cell lines BL-41 ($KSHV^{neg}/EBV^{neg}$), Akata and Mutu (both $KSHV^{neg}/EBV^{+}$) were kindly provided by Dr. Dean Kedes (University of Virginia) and Dr. Erik Flemington (Tulane University), respectively, and cultured as described elsewhere [35]. Primary human umbilical vein endothelial cells (HUVEC) were cultured as described previously [36]. All experiments were carried out using cells harvested at low (<20) passages. The 3-(4-chlorophenyl)-adamantane-1-carboxylic acid (pyridin-4-ylmethyl) amide (ABC294640) was synthesized as previously described [37]. C18-Cer and dhC16-Cer were purchased from Avanti Polar Lipids. C2-, C6- and C8-Cer were purchased from Cayman Chemical.

Cell apoptosis assays

Apoptosis was quantified by flow cytometry using the FITC-Annexin V/propidium iodide (PI) Apoptosis Detection Kit I (BD Pharmingen) according to the manufacturer's instructions. Data were collected using a FACS Calibur 4-color flow cytometer (BD Bioscience).

RNA interference

CerS2, *CerS6* or KSHV *ORF50* ON-TARGET plus SMART pool siRNA, or negative control siRNA (Dharmacon), were delivered using the DharmaFECT

transfection reagent according to the manufacturer's instructions.

Immunoblotting

Cells were lysed in buffer containing 20 mM Tris (pH 7.5), 150 mM NaCl, 1% NP40, 1 mM EDTA, 5 mM NaF and 5 mM Na_3VO_4. Total cell lysates (30 μg) were resolved by 10% SDS–PAGE, transferred to nitrocellulose membranes, and incubated with 100-200 μg/mL of the following antibodies: cleaved-Caspase3, cleaved-Caspase9 (Cell Signaling Technologies), CerS2, CerS6 (Santa Cruz), K8.1 (ABI). For loading controls, lysates were also incubated with antibodies detecting β-Actin (Sigma). Immunoreactive bands were developed using an enhanced chemiluminescence reaction (Perkin-Elmer).

Immunofluorescence

Cells were incubated in 1:1 methanol-acetone at -20°C for fixation and permeabilization, then with a blocking reagent (10% normal goat serum, 3% bovine serum albumin, and 1% glycine) for an additional 30 minutes. Cells were then incubated for 1 h at 25°C with 1:2000 dilution of a mouse anti-K8.1 monoclonal antibody (ABI) followed by 1:200 dilution of a goat anti-mouse secondary antibody conjugated to Texas Red (Invitrogen). For identification of nuclei, cells were subsequently counterstained with 0.5 mg/mL 4',6-diamidino-2-phenylindole (DAPI; Sigma) in 180 mM Tris-HCl (pH 7.5). Slides were washed once in 180 mM Tris-HCl for 15 minutes and prepared for visualization using a Leica TCPS SP5 AOBS confocal microscope.

qRT-PCR

Total RNA was isolated using the RNeasy Mini kit (QIAGEN), and cDNA was synthesized from equivalent total RNA using a SuperScript III First-Strand Synthesis SuperMix Kit (Invitrogen) according to the manufacturer's instructions. Primers used for amplification of target genes are displayed in Supplemental Table 1. Amplification was carried out using an iCycler IQ Real-Time PCR Detection System, and cycle threshold (Ct) values were tabulated in duplicate for each gene of interest in each experiment. "No template" (water) controls were used to ensure minimal background contamination. Using mean Ct values tabulated for each gene, and paired Ct values for β-*actin* as a loading control, fold changes for experimental groups relative to assigned controls were calculated using automated iQ5 2.0 software (Bio-rad).

Quantification of sphingolipids

Quantification of ceramide and (dh)-ceramide species was performed using a Thermo Finnigan TSQ 7000 triple-stage quadruple mass spectrometer operating in Multiple Reaction Monitoring positive ionization mode (Thermo Fisher Scientific). Quantification was based on calibration curves generated by spiking an artificial matrix with known amounts of target standards and an equal amount of the internal standard. The target analyte:internal standard peak area ratios from each sample were compared with the calibration curves using linear regression. Final results were expressed as the ratio of sphingolipid normalized to total phospholipid phosphate level using the Bligh and Dyer lipid extract method [38].

PEL xenograft model

10^7 BCBL-1 cell aliquots were diluted in 200 μL sterile PBS, and 6-8 week-old male non-obese diabetic/severe-combined immunodeficiency (NOD/SCID) mice (Jackson Laboratory) received intraperitoneal (i.p.) injections with a single aliquot. For drug delivery, dhC16-Cer or C6-Cer was diluted in sterile PEG:DMSO (1:1) (Sigma) to achieve 100 μL total volume. The drug, or vehicle alone, was administered using an insulin syringe for i.p. injections. Drug was administered initially at either 1 day or 28 days after BCBL-1 injections, 3 times/week. Two experiments, with 10 mice per group for each experiment, were performed. Weights were recorded weekly as a surrogate measure of tumor progression, and ascites fluid volumes were tabulated for individual mice at the completion of each experiment. All protocols were approved by the Louisiana State University Health Science Center Animal Care and Use Committee in accordance with national guidelines.

Immunohistochemistry

Formalin-fixed, paraffin-embedded tissues were microtome-sectioned to a thickness of 4 uM, placed on electromagnetically charged slides (Fisher Scientific), and stained with hematoxylin & eosin (H&E) for routine histologic analysis. Immunohistochemistry was performed using the Avidin-Biotin-Peroxidase complex system, according to the manufacturer's instructions (Vectastain Elite ABC Peroxidase Kit; Vector Laboratories). In our modified protocol, sections were deparaffinized in xylene and re-hydrated through a descending alcohol gradient. For non-enzymatic antigen retrieval, slides were heated in 0.01 M sodium citrate buffer (pH 6.0) to 95ºC under vacuum for 40 min and allowed to cool for 30 min at room temperature, then rinsed with PBS and incubated in MeOH/3% H_2O_2 for 20 min to quench

endogenous peroxidase. Slides were then washed with PBS and blocked with 5% normal goat serum in 0.1% PBS/BSA for 2 h at room temperature, then incubated overnight with a rat monoclonal anti-CerS2 antibody at 1:100 dilution (Santa Cruz) in 0.1% PBS/BSA. The following day, slides were incubated with a goat anti-rat IgG or goat anti-rabbit IgG secondary antibody at room temperature for 1 h, followed by avidin-biotin peroxidase complexes for 1 h at room temperature. Finally, slides were developed using a diaminobenzidine substrate, counterstained with hematoxylin, dehydrated through an ascending alcohol gradient, cleared in xylene, and coverslipped with Permount. Images were collected at 200x, 400x or 600x magnification using a Olympus BX61 microscope equipped with a high resolution DP72 camera and CellSense image capture software.

Statistical analysis

Significance for differences between experimental and control groups were determined using the two-tailed Student's t-test (Excel 8.0), and p values <0.05 or 0.01 were considered significant or highly significant, respectively. The Cytotoxicity Concentration 50 (CC_{50}) was calculated by using SPSS 20.0.

ACKNOWLEDGMENTS

This work was supported by grants from the National Institutes of Health (AI087167 and CA183708), a Center for Biomedical Research Excellence subaward (P20-RR021970), the DOD Career Development Award (CA140437) and the Ladies Leukemia League Grant (2014-2015), the National Natural Science Foundation (81101791, 81272191, 81472547 and 81400164) and the Foundation for Innovative Research Groups of the NNSF of China (81221001). The funders had no role in study design, data collection and analysis, decision to publish, or preparation of the manuscript.

CONFLICTS OF INTEREST

All the authors declare no conflict of interest.

REFERENCES

1. Ogretmen B and Hannun YA. Biologically active sphingolipids in cancer pathogenesis and treatment. Nat Rev Cancer. 2004; 48:604-616.
2. Futerman AH and Hannun YA. The complex life of simple sphingolipids. EMBO Rep. 2004; 58:777-782.
3. Ponnusamy S, Meyers-Needham M, Senkal CE, Saddoughi SA, Sentelle D, Selvam SP, Salas A and Ogretmen B. Sphingolipids and cancer: ceramide and sphingosine-1-phosphate in the regulation of cell death and drug resistance. Future Oncol. 2010; 610:1603-1624.
4. Merrill AH, Jr., Wang E and Mullins RE. Kinetics of long-chain sphingoid base biosynthesis in intact LM cells: effects of varying the extracellular concentrations of serine and fatty acid precursors of this pathway. Biochemistry. 1988; 271:340-345.
5. Kang MS, Ahn KH, Kim SK, Jeon HJ, Ji JE, Choi JM, Jung KM, Jung SY and Kim DK. Hypoxia-induced neuronal apoptosis is mediated by de novo synthesis of ceramide through activation of serine palmitoyltransferase. Cell Signal. 2010; 224:610-618.
6. Hannun YA and Obeid LM. The Ceramide-centric universe of lipid-mediated cell regulation: stress encounters of the lipid kind. J Biol Chem. 2002; 27729:25847-25850.
7. Takabe K, Paugh SW, Milstien S and Spiegel S. "Inside-out" signaling of sphingosine-1-phosphate: therapeutic targets. Pharmacol Rev. 2008; 602:181-195.
8. Kohama T, Olivera A, Edsall L, Nagiec MM, Dickson R and Spiegel S. Molecular cloning and functional characterization of murine sphingosine kinase. J Biol Chem. 1998; 27337:23722-23728.
9. Liu H, Sugiura M, Nava VE, Edsall LC, Kono K, Poulton S, Milstien S, Kohama T and Spiegel S. Molecular cloning and functional characterization of a novel mammalian sphingosine kinase type 2 isoform. J Biol Chem. 2000; 27526:19513-19520.
10. Saddoughi SA and Ogretmen B. Diverse functions of ceramide in cancer cell death and proliferation. Adv Cancer Res. 2013; 117:37-58.
11. Mesri EA, Feitelson MA and Munger K. Human viral oncogenesis: a cancer hallmarks analysis. Cell Host Microbe. 2014; 153:266-282.
12. Cesarman E, Chang Y, Moore PS, Said JW and Knowles DM. Kaposi's sarcoma-associated herpesvirus-like DNA sequences in AIDS-related body-cavity-based lymphomas. N Engl J Med. 1995; 33218:1186-1191.
13. Chang Y, Cesarman E, Pessin MS, Lee F, Culpepper J, Knowles DM and Moore PS. Identification of herpesvirus-like DNA sequences in AIDS-associated Kaposi's sarcoma. Science. 1994; 2665192:1865-1869.
14. Jenkins FJ, Hoffman LJ and Liegey-Dougall A. Reactivation of and primary infection with human herpesvirus 8 among solid-organ transplant recipients. J Infect Dis. 2002; 1859:1238-1243.
15. Ariza-Heredia EJ and Razonable RR. Human herpes virus 8 in solid organ transplantation. Transplantation. 2011; 928:837-844.
16. Chen YB, Rahemtullah A and Hochberg E. Primary effusion lymphoma. Oncologist. 2007; 125:569-576.
17. Delgado T, Sanchez EL, Camarda R and Lagunoff M. Global metabolic profiling of infection by an oncogenic virus: KSHV induces and requires lipogenesis for survival of latent infection. PLoS Pathog. 2012; 88:e1002866.
18. Yogev O, Lagos D, Enver T and Boshoff C. Kaposi's

sarcoma herpesvirus microRNAs induce metabolic transformation of infected cells. PLoS Pathog. 2014; 109:e1004400.

19. Qin Z, Dai L, Trillo-Tinoco J, Senkal C, Wang W, Reske T, Bonstaff K, Del Valle L, Rodriguez P, Flemington E, Voelkel-Johnson C, Smith CD, Ogretmen B and Parsons C. Targeting Sphingosine Kinase Induces Apoptosis and Tumor Regression for KSHV-Associated Primary Effusion Lymphoma. Mol Cancer Ther. 2014; 131:154-164.
20. Dai L, Plaisance-Bonstaff K, Voelkel-Johnson C, Smith CD, Ogretmen B, Qin Z and Parsons C. Sphingosine Kinase-2 Maintains Viral Latency and Survival for KSHV-Infected Endothelial Cells. PLoS One. 2014; 97:e102314.
21. Hannun YA and Obeid LM. Many ceramides. J Biol Chem. 2011; 28632:27855-27862.
22. Mullen TD, Hannun YA and Obeid LM. Ceramide synthases at the centre of sphingolipid metabolism and biology. Biochem J. 2012; 4413:789-802.
23. Sun R, Lin SF, Gradoville L, Yuan Y, Zhu F and Miller G. A viral gene that activates lytic cycle expression of Kaposi's sarcoma-associated herpesvirus. Proc Natl Acad Sci U S A. 1998; 9518:10866-10871.
24. Ogretmen B, Pettus BJ, Rossi MJ, Wood R, Usta J, Szulc Z, Bielawska A, Obeid LM and Hannun YA. Biochemical mechanisms of the generation of endogenous long chain ceramide in response to exogenous short chain ceramide in the A549 human lung adenocarcinoma cell line. Role for endogenous ceramide in mediating the action of exogenous ceramide. J Biol Chem. 2002; 27715:12960-12969.
25. Hannun YA and Luberto C. Ceramide in the eukaryotic stress response. Trends Cell Biol. 2000; 102:73-80.
26. Tafesse FG, Ternes P and Holthuis JC. The multigenic sphingomyelin synthase family. J Biol Chem. 2006; 28140:29421-29425.
27. Stefanic S, Spycher C, Morf L, Fabrias G, Casas J, Schraner E, Wild P, Hehl AB and Sonda S. Glucosylceramide synthesis inhibition affects cell cycle progression, membrane trafficking, and stage differentiation in Giardia lamblia. J Lipid Res 2010; 519:2527-2545.
28. Abe A, Wu D, Shayman JA and Radin NS. Metabolic effects of short-chain ceramide and glucosylceramide on sphingolipids and protein kinase C. Eur J Biochem. 1992; 2103:765-773.
29. Jaffrezou JP, Maestre N, de Mas-Mansat V, Bezombes C, Levade T and Laurent G. Positive feedback control of neutral sphingomyelinase activity by ceramide. FASEB J. 1998; 1211:999-1006.
30. Senkal CE, Ponnusamy S, Rossi MJ, Sundararaj K, Szulc Z, Bielawski J, Bielawska A, Meyer M, Cobanoglu B, Koybasi S, Sinha D, Day TA, Obeid LM, Hannun YA and Ogretmen B. Potent antitumor activity of a novel cationic pyridinium-ceramide alone or in combination with gemcitabine against human head and neck squamous cell carcinomas *in vitro* and *in vivo*. J Pharmacol Exp Ther. 2006; 3173:1188-1199.
31. Modica-Napolitano JS and Aprille JR. Delocalized lipophilic cations selectively target the mitochondria of carcinoma cells. Adv Drug Deliv Rev. 2001; 491-2:63-70.
32. Novgorodov SA, Szulc ZM, Luberto C, Jones JA, Bielawski J, Bielawska A, Hannun YA and Obeid LM. Positively charged ceramide is a potent inducer of mitochondrial permeabilization. J Biol Chem. 2005; 28016:16096-16105.
33. Gantt S and Casper C. Human herpesvirus 8-associated neoplasms: the roles of viral replication and antiviral treatment. Curr Opin Infect Dis. 2011; 244:295-301.
34. Dai L, Trillo-Tinoco J, Bai L, Kang B, Xu Z, Wen X, Del Valle L and Qin Z. Systematic analysis of a xenograft mice model for KSHV+ primary effusion lymphoma PEL. PLoS One. 2014; 92:e90349.
35. Dai L, Cao Y, Chen Y, Parsons C and Qin Z. Targeting xCT, a cystine-glutamate transporter induces apoptosis and tumor regression for KSHV/HIV-associated lymphoma. Journal of hematology & oncology. 2014; 7:30.
36. Dai L, Chen Y, Toole B, Parsons C and Qin Z. Induction of hyaluronan production by oncogenic KSHV and the contribution to viral pathogenesis in AIDS patients. Cancer Lett. 2015; 3622:158-166.
37. French KJ, Schrecengost RS, Lee BD, Zhuang Y, Smith SN, Eberly JL, Yun JK and Smith CD. Discovery and evaluation of inhibitors of human sphingosine kinase. Cancer Res. 2003; 6318:5962-5969.
38. Bielawski J, Szulc ZM, Hannun YA and Bielawska A. Simultaneous quantitative analysis of bioactive sphingolipids by high-performance liquid chromatography-tandem mass spectrometry. Methods. 2006; 392:82-91.

Cancer Letters 362 (2015) 158–166

Contents lists available at ScienceDirect

Cancer Letters

journal homepage: www.elsevier.com/locate/canlet

Original Articles

Induction of hyaluronan production by oncogenic KSHV and the contribution to viral pathogenesis in AIDS patients

Lu Dai [a,c], Yihan Chen [a], Bryan Toole [d], Chris Parsons [c], Zhiqiang Qin [a,b,*]

[a] Research Center for Translational Medicine and Key Laboratory of Arrhythmias of the Ministry of Education of China, East Hospital, Tongji University School of Medicine, 150 Jimo Road, Shanghai 200120, China
[b] Departments of Microbiology/Immunology/Parasitology, Louisiana State University Health Sciences Center, Louisiana Cancer Research Center, 1700 Tulane Ave., New Orleans, LA 70112, USA
[c] Department of Medicine, Louisiana State University Health Sciences Center, Louisiana Cancer Research Center, 1700 Tulane Ave., New Orleans, LA 70112, USA
[d] Departments of Regenerative Medicine & Cell Biology, Medical University of South Carolina and Hollings Cancer Center, Charleston, SC 29425, USA

ARTICLE INFO

Article history:
Received 16 February 2015
Received in revised form 17 March 2015
Accepted 18 March 2015

Keywords:
KSHV
Hyaluronan
CD147
LANA

ABSTRACT

Kaposi sarcoma-associated herpesvirus (KSHV) is the etiologic agent for Kaposi's sarcoma (KS) and primary effusion lymphoma (PEL), malignancies arising primarily in immunocompromised patients particularly AIDS-patients, which still lack effective therapy. Hyaluronan (HA) is a large glucuronic acid and has been found closely related to multiple functions in cancer cells, although its role in viral oncogenesis remains largely unknown. Here we provide first evidence that KSHV *de novo* infection induces HA production from primary endothelial cells through upregulation of HA synthase gene 1 (*Has1*) and a multifunctional glycoprotein, CD147. Further data demonstrate that KSHV-induced HA production requires viral latent protein, LANA (in particular functional domain A) and MAPK/ERK signaling activities. In functions, HA production is necessary for KSHV/LANA-induced primary endothelial cell invasion, a hallmark feature for KS development. For clinical relevance, our data indicate that the KSHV+ group has higher levels of HA and Has1 activities in its plasma than the KSHV– group of cohort HIV-infected patients. Together, our findings provide innovative insights into the mechanisms of oncogenic virus activation of HA production and its role in virus-associated malignancy pathogenesis, which may help to develop novel therapeutic strategies by targeting HA and related signaling.

Introduction

Hyaluronan (HA) is a very large, linear glycosaminoglycan composed of repeating disaccharides of glucuronic acid and *N*-acetylglucosamine [1]. In addition to its structural role through interaction with other extracellular matrix (ECM) components, HA binds to several cell surface receptors such as CD44, LYVE-1 and RHAMM that induce the transduction of a range of intracellular signals and contribute to multiple cellular functions such as embryonic development, healing processes and inflammation [2]. HA is overproduced by many types of tumors, and in some cases, HA levels are prognostic for malignant progression [3]. Moreover, HA and related signaling transductions have been involved in many malignant behaviors of cancer cells, including migration/invasion, angiogenesis, epithelial–mesenchymal transition (EMT), multidrug resistance, and metastasis [4–6]. Currently, ~20% of human cancers have been attributed to virus infection [7]; however, there are limited data describing the role of HA production in viral oncogenesis or how oncogenic viral proteins regulate HA level and related signaling transductions.

Kaposi sarcoma-associated herpesvirus (KSHV) is the etiologic agent for Kaposi's sarcoma (KS) and primary effusion lymphoma (PEL), malignancies arising primarily in patients infected with the human immunodeficiency virus (HIV) or in those receiving organ transplants [8,9]. Furthermore, despite the reduced incidence of KS in the era of highly active antiretroviral therapy (HAART) for HIV infection, KS still remains the most common Acquired immunodeficiency syndrome (AIDS)-associated tumor and a leading cause of morbidity and mortality in this setting [10]. Another KSHV-caused malignancy, PEL, comprises transformed B cells harboring KSHV and arises preferentially within the pleural or peritoneal cavities of immune-suppressed patients [9]. PEL is a rapidly progressing malignancy with a median survival time of approximately 6 months, even under the combinational chemotherapy [11]. Our recent study demonstrates that the glycoprotein, CD147, interacts with the lymphatic vessel endothelial hyaluronan receptor-1 (LYVE-1) and the drug transporter, breast cancer resistance protein (BCRP)/ABCG2, to promote multidrug chemoresistance in KSHV+ PEL cells [12]. Moreover, we found higher

* Corresponding author. Tel.: +(504) 210 3327; fax: +(504) 210 2970.
E-mail address: zqin@lsuhsc.edu (Z. Qin).

http://dx.doi.org/10.1016/j.canlet.2015.03.034
0304-3835/

levels of HA and HA synthase gene (*Has1–3*) transcripts in chemoresistant PEL cell-lines than in chemosensitive ones. In addition, small HA oligosaccharides (oHA) that interact monovalently with HA receptors, and competitively blocking polyvalent interactions between receptors and endogenous HA, sensitize drug resistant PEL cells to chemotherapeutic agents [12]. In the current study, we investigate the role of HA production in KSHV-infected primary endothelial cells, which represent the major cellular component of KS tumors, and identify the underlying mechanisms whereby oncogenic viral proteins regulate HA production.

Materials and methods

Cell culture, reagents and infection protocol

KSHV-infected PEL cells (BCBL-1) were kindly provided by Dr. Dean Kedes (University of Virginia) and maintained in RPMI 1640 medium (Gibco) with supplements as described previously [12]. Human umbilical vein endothelial cells (HUVEC) were grown in DMEM/F-12 50/50 medium (Cellgro) supplemented with 5% FBS. Selective inhibitors targeting the mitogen-activated protein kinase (MEK; U0126) and NF-κB (Bay11-7082) were purchased from Sigma. Hyaluronan oligosaccharides (oHA) were prepared as described previously [13]. To obtain KSHV for infection experiments, BCBL-1 cells were incubated with 0.6 mM valproic acid for 6 days, purified virus concentrated from culture supernatants and infectious titers were determined as described previously [14].

Cell transfection

HUVEC were transfected with control vector pcDNA3.1, pcDNA3.1-LANA (pcLANA) or LANA deletion fragments (pcLANA-A, pcLANA-AB, pcLANA-AC, pcLANA-BC and pcLANA-C) or pcDNA3.1-ERK (pcERK) in 12-well plates for 48 h using Lipofectamine 2000 (Invitrogen) according to the manufacturer's instruction. Transfection efficiency was determined through co-transfection of a lacZ reporter construct and quantified as described previously [14]. For RNA interference assays, *Has1* or *CD147* ON-TARGET plus SMART pool siRNA (Dharmacon), or negative control siRNA, was delivered using the DharmaFECT transfection reagent according to the manufacturer's instruction.

Immunofluorescence assays

Cells were incubated in 1:1 methanol–acetone at 20 °C for fixation and permeabilization, followed by a blocking reagent (10% normal goat serum, 3% bovine serum albumin, and 1% glycine) for an additional 30 min. Cells were then incubated for 1 h at 25 °C with 1:1000 dilution of a rat anti-LANA monoclonal antibody (ABI, for LANA wt) or a mouse anti-V5-Tag monoclonal antibody (Cell Signaling, for LANA deletion fragments) followed by 1:100 dilution of a goat anti-rat or goat anti-mouse secondary antibody conjugated to Texas Red (Invitrogen). For intracellular HA detection, cells were permeabilized for 20 min at room temperature with 0.1% Triton-X-100 in 1% BSA, and incubated overnight at 4 °C with bHABC (biotinylated hyaluronan binding complex, Sigma) (1.25 μg/mL) in 1% BSA. To remove the pericellular HA, fixed cells were treated with Streptomyces hyaluronidase (1 turbidity reducing unit/mL, Seikagaku Kogyo) before permeabilization. After washing, the cells were incubated for 1 h with Alexa 488-labeled streptavidin (1:1000) (Invitrogen) for bHABC staining. Cells were counterstained with 0.5 μg/mL 4′,6-diamidino-2-phenylindole (DAPI, Sigma) in 180 mM Tris–HCl (pH 7.5) for nuclear localization. Slides were washed once in 180 mM Tris–HCl for 10 min and prepared for visualization using a Leica TCPS SP5 AOBS confocal microscope.

Immunoblotting

Total cell lysates (20 μg) were resolved by 10% SDS–PAGE, transferred to nitrocellulose membranes, and immunoblotted with antibodies for CD147 (BD), LANA (ABI), phospho-p44/42 ERK (Thr202/Tyr204), t-p44/42 ERK (Cell Signaling) and β-Actin (Sigma) for loading controls. Immunoreactive bands were identified using an enhanced chemiluminescence reaction (PerkinElmer), and visualized by autoradiography.

Transwell invasion assays

Matrigel Invasion Chambers (BD) were hydrated for 4 h at 37 °C with culture media. Following hydration, media in the bottom of the well was replaced with fresh media, then 2×10^4 HUVEC were plated at the top of the chamber. After 24 h, cells were fixed with 4% formaldehyde for 15 min at room temperature and chambers rinsed in PBS prior to staining with 0.2% crystal violet for 10 min. After washing the chambers, cells at the top of the membrane were removed and cells at the bottom of the membrane counted using a phase contrast microscope. Relative invasion was determined for cells in experimental groups as follows: relative invasion = # invading cells in experimental group/# invading cells in control groups.

ELSA for HA

Concentrations of HA in culture supernatants or plasma from patients were determined using HA ELSA kit (Echelon) according to the manufacturers' instructions.

qRT-PCR

Total RNA was isolated from infected or uninfected cells using the RNeasy Mini kit according to the manufacturer's instructions (QIAGEN). cDNA was synthesized from equal total RNA using SuperScript III First-Strand Synthesis SuperMix Kit (Invitrogen) according to the manufacturer's procedures. The primers designed for target genes are displayed in Supplemental Table 1. Amplification experiments were carried out using an iCycler IQ Real-Time PCR Detection System, and cycle threshold (Ct) values were tabulated in duplicate (cDNA) for each gene of interest for each experiment. "No template" (water) controls were also used to ensure minimal background contamination. Using mean Ct values tabulated for different experiments and using Ct values for β-actin as loading controls, fold changes for experimental groups relative to assigned controls were calculated using automated iQ5 2.0 software (Bio-rad).

Patients and ethics statement

The study was approved by the Institutional Review Board for Human Research (IRB, No. 8079) at Louisiana State University Health Science Center – New Orleans (LSUHSC-NO). All subjects were provided written informed consent. In the current study, a total of 28 HIV+ patients with antiretroviral treatment (ART) in our HIV Outpatient (HOP) Clinic are involved. There are 15 females and 13 males, the average age is 48.6 y (range 21–65 y). The average CD4 T cell count is 539/mL (range 35–1773/mL), and the average HIV viral loads is 5928 copies/mL (range 25–66681 copies/mL).

Plasma and PBMC preparation

Whole blood was collected in heparin-coated tubes, and peripheral blood mononuclear cells (PBMCs) were isolated over a Ficoll-Hypaque cushion. Plasma was isolated by centrifugation. The KSHV infection status was determined by using quantitative ELISAs for identifying circulating IgG antibodies to KSHV proteins (LANA and K8.1) as previously described [15,16].

Statistical analysis

Significance of differences between experimental and control groups was determined using the two-tailed Student's t-test (Excel 8.0). The linear analyses were determined using SPSS Statistics 20.0.

Results

KSHV de novo *infection induces HA production from primary endothelial cells through CD147*

By using an enzyme-linked sorbent assay (ELSA), we found that KSHV *de novo* infection induced a significant increase in extracellular HA produced by human umbilical vein endothelial cells (HUVEC); accumulation of extracellular HA continued for at least 96 h post-infection (Fig. 1A). Furthermore, immunofluorescence assay (IFA) data indicated that KSHV *de novo* infection also induced intracellular HA accumulation within the HUVEC, when compared to uninfected mock cells (Fig. 1B). There are three human HA synthase genes (*Has1-3*) responsible for HA production [17], and our data indicated that KSHV infection prominently increased *Has1* transcripts, while having little or no effect on *Has2* or *Has3* transcripts (Fig. 1C). To confirm the role of *Has1* in KSHV-induced HA production, we directly targeted *Has1* by RNAi and showed that it significantly reduced HA production from KSHV-infected HUVEC (Fig. 1D).

Previous studies have shown that HA production is regulated by a multifunctional glycoprotein, CD147 (emmprin; basigin), in several types of tumor cells [12,18,19]. Our data confirmed that directly targeting CD147 by RNAi significantly reduced HA production from KSHV-infected HUVEC (Fig. 2A). Interestingly, targeting CD147 by RNAi also decreased *Has1* transcription but not *Has2* and *Has3* (Fig. 2B), while knock-down of *Has1* by RNAi decreased CD147 transcription but not *Has2* and *Has3* (Fig. S1), implying a positive feedback

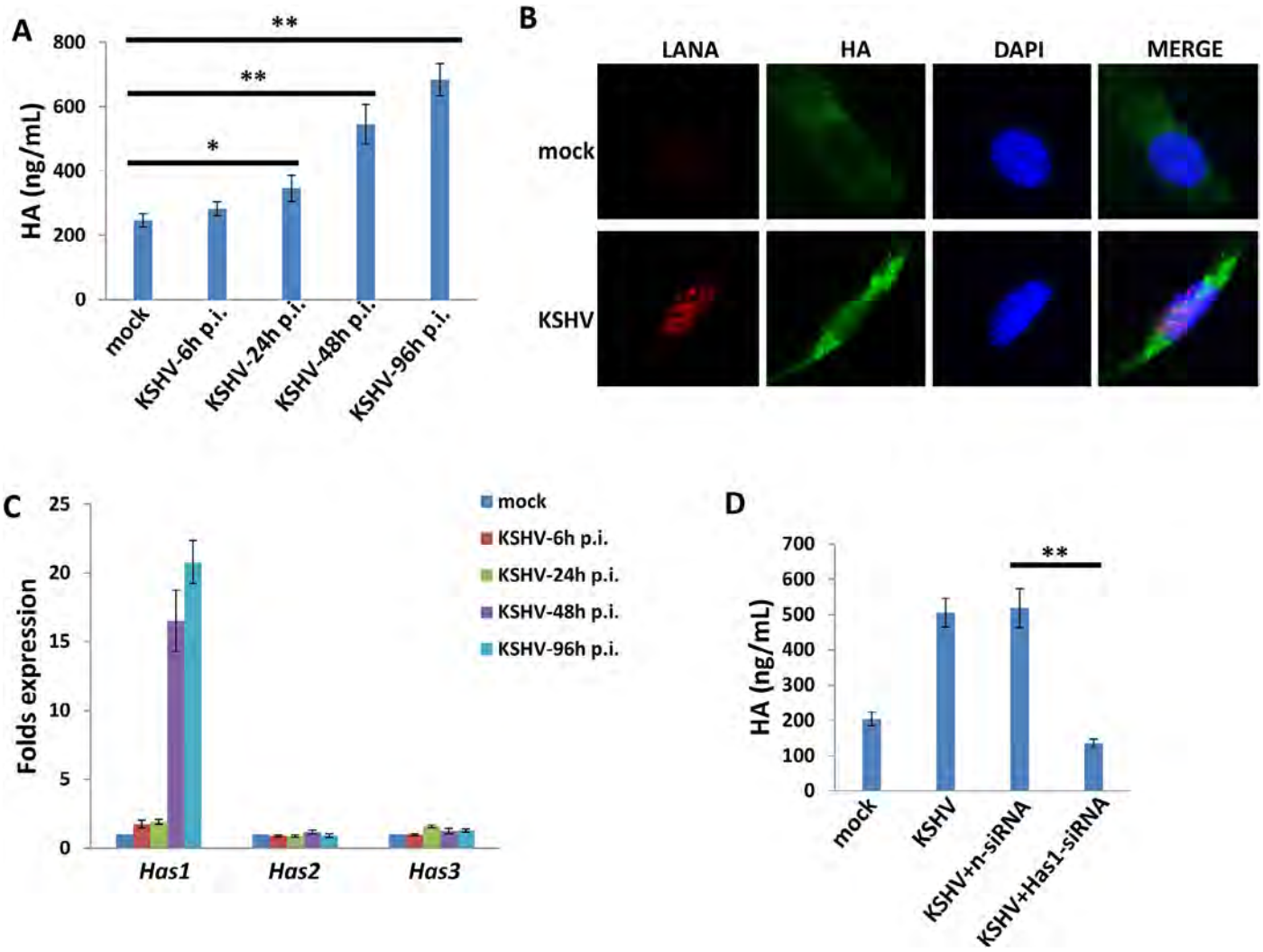

Fig. 1. KSHV *de novo* infection induces HA production through upregulation of *Has1*. (A) Human umbilical vein endothelial cells (HUVEC) were infected with purified KSHV (MOI ~10) for 2 h, then the extracellular HA production at indicated time-points post-infection (p.i.) was measured and compared with mock cells control by ELSA. (B) Cells were infected as above, and immunofluorescence (IFA) was used to detect endogenous HA production at 48 h p.i. (C) Transcripts representing the 3 HA synthase genes (*Has1-3*) were quantified by qRT-PCR. (D) Cells were infected with KSHV for 2 h, then transfected with either negative control siRNA (n-siRNA) or *Has1*-siRNA for 48 h, and the extracellular HA production was measured by ELISA. Error bars represent the S.E.M. for three independent experiments. ** = $p < 0.01$.

for regulation of CD147 and *Has1*. In comparison, oHA treatment caused reduction of *Has1* and *Has2* transcription but did not affect CD147 or *Has3* (Fig. 2C).

HA production is induced by the viral latent protein LANA and requires LANA functional domain A and MAPK/ERK signaling activities

In more than 90% of KSHV-infected host cells, the virus exists at latency stage [20], implying that some viral latent proteins are probably responsible for inducing HA production. Latency-associated nuclear antigen (LANA) is one of the only viral proteins consistently expressed in all KS-associated malignancies [21], and its major function is to maintain viral episome in latently-infected cells [22], as well as to modulate expression of a variety of viral and cellular genes [23,24]. To determine the role of LANA in inducing HA production, we ectopically expressed LANA by transfection of HUVEC with a recombinant construct [25] (Fig. 3A), and showed that LANA was sufficient for induction of HA production through upregulation of *Has1* transcription (Fig. 3B, C).

The LANA protein sequence can be divided into three functional domains: a conserved proline- and serine-rich N-terminal region (domain A), a central region composed of several acidic repeats (domain B), and a conserved C-terminal domain containing a proline-rich region and a region rich in charged and hydrophobic amino acids (domain C) [26]. Both N- and C-terminal domains contain a nuclear localization sequence (NLS, Fig. 4A). Further IFA data indicated that the LANA-A fragment containing the N-terminal NLS localized to the nucleus in a similar fashion to the full-length control, while the C-terminal NLS within the LANA-BC fragment was non-functional (Fig. 4B), which is in accordance with previous findings [27,28]. By using a variety of LANA deletion fragment and full-length control constructs, we found that the LANA domain A (LANA-A) was sufficient to induce CD147 expression with equivalent efficiency to the full-length control (Fig. 4C).

Our published data have indicated that LANA upregulates CD147 expression, although the underlying mechanisms remain unclear [25]. Here we showed that LANA-A was sufficient to induce *has1* transcription and HA production, both of which were blocked by RNAi targeting CD147 (Fig. 4D, E). We have previously shown that

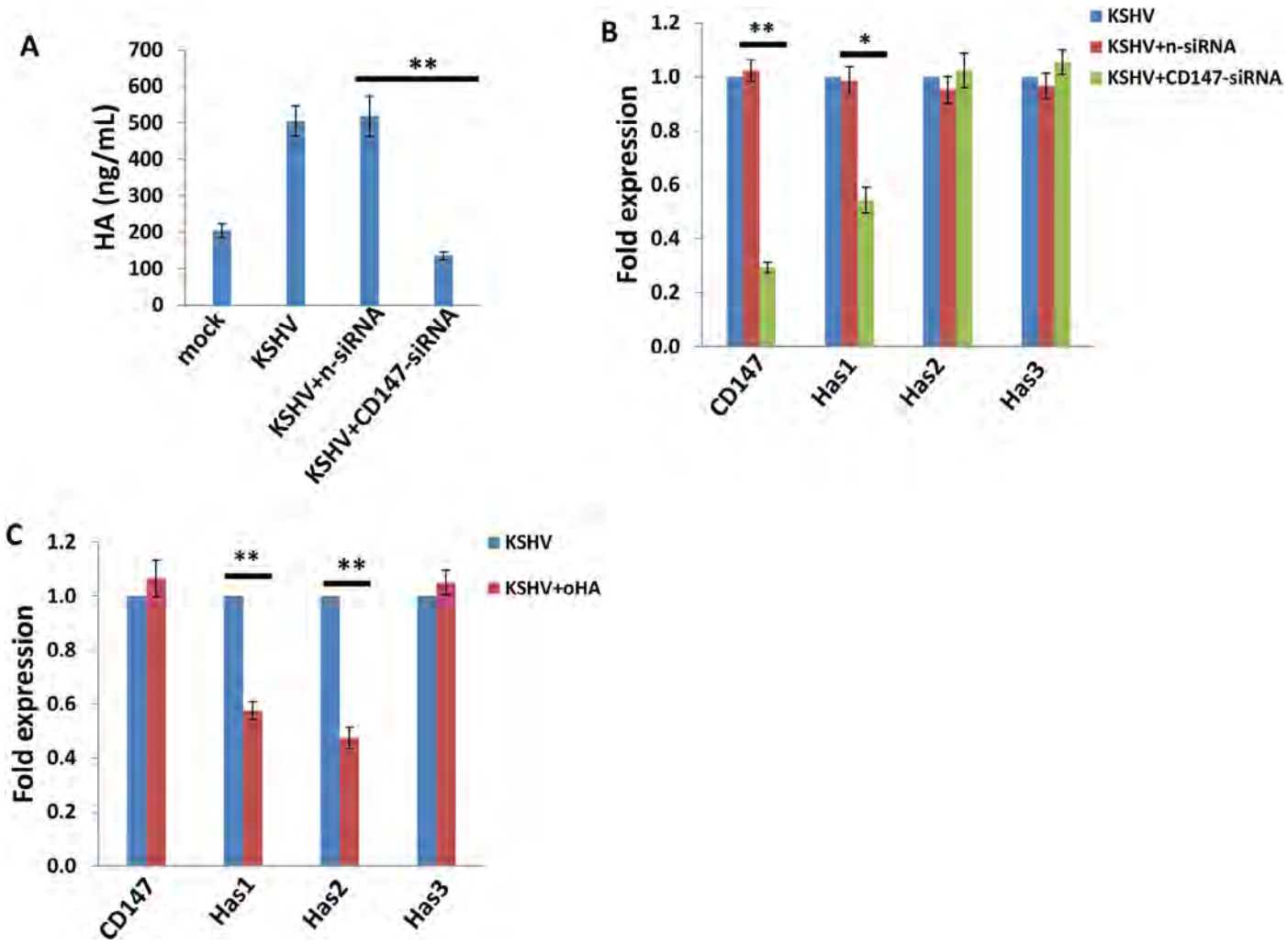

Fig. 2. CD147 is involved in KSHV-induced HA production. (A, B) HUVEC were infected with KSHV for 2 h, then transfected with either negative control siRNA (n-siRNA) or *CD147*-siRNA for 48 h, and the extracellular HA production was measured by ELSA. Gene expression was quantified by qRT-PCR. (C) Cells were infected with KSHV for 2 h, then treated with or without oHA (150 μg/mL) for 48 h, and gene transcripts were quantified by qRT-PCR. Error bars represent the S.E.M. for three independent experiments. ** = $p < 0.01$.

the mitogen-activated protein kinase (MAPK) pathway is involved in KSHV upregulation of CD147 [29]. Here we found that ectopic expression of LANA increased the phosphorylation of MAPK/ERK (Fig. 5A) but did not affect NF-κB p65 phosphorylation (data not shown) in HUVEC. Blocking the activities of MAPK by its specific inhibitor U0126 significantly reduced *Has1* transcription and HA production by LANA-transfected cells and KSHV-infected cells, while NF-κB inhibitor Bay11-7082 had no such effects (Fig. 5B–E).

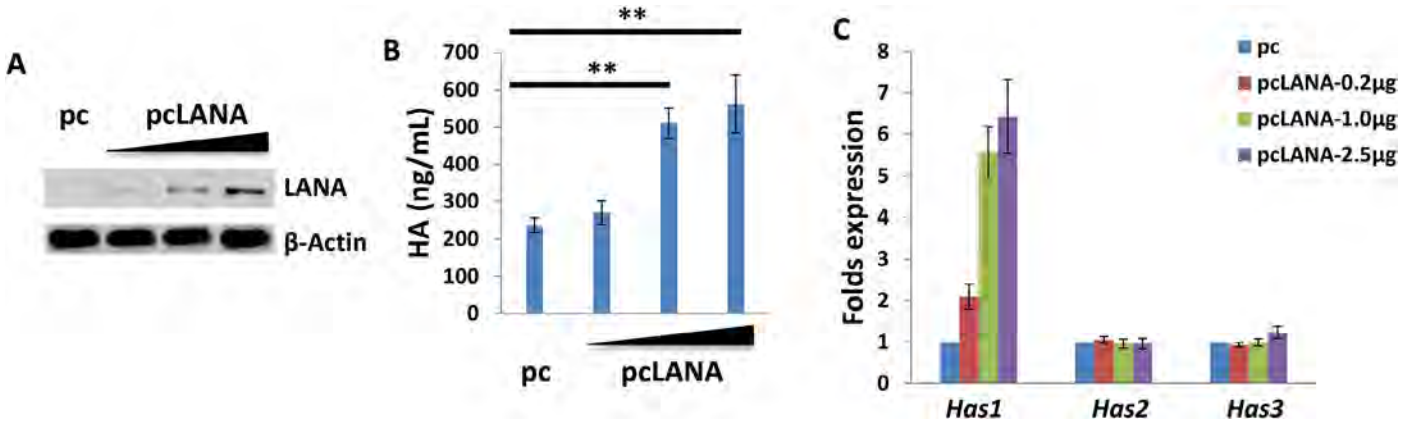

Fig. 3. KSHV-encoded LANA protein is sufficient to induce HA production from primary endothelial cells. (A–C) HUVEC were transfected with control vector (pc), or vectors encoding LANA (pcLANA) at 0.2, 1.0 or 2.5 μg, respectively, for 48 h, then protein expression, HA production and *Has* genes transcription were measured by immunoblots, ELSA, qRT-PCR, respectively. Error bars represent the S.E.M. for three independent experiments. ** = $p < 0.01$.

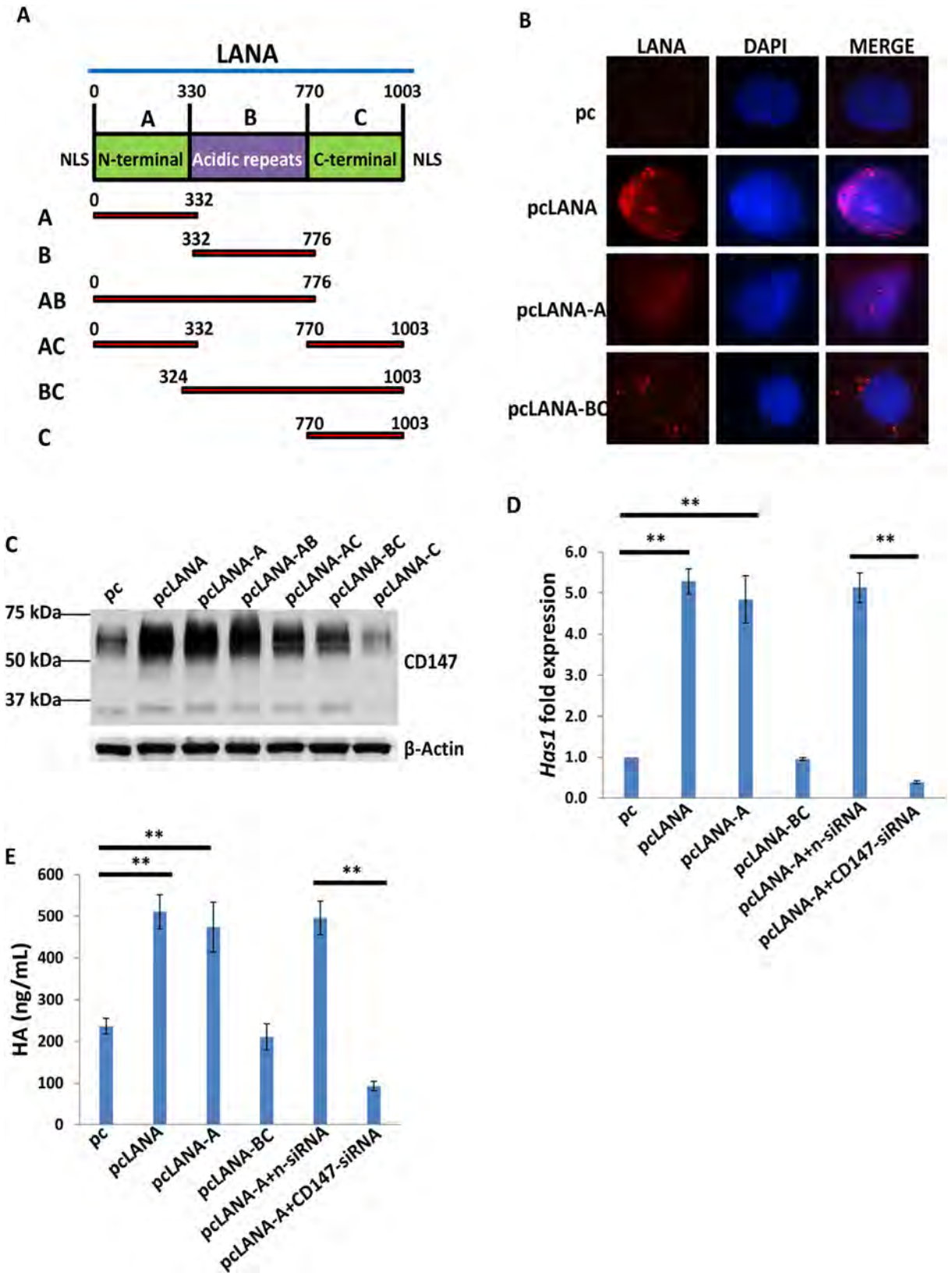

Fig. 4. LANA induces HA production requiring functional domain A and CD147. (A) Putative domain structure of LANA based on primary sequence features. The N-terminal region (domain A) is rich in prolines and serines and contains a putative nuclear localization sequence (NLS). The central region of LANA (domain B) is composed of several repeats and is very acidic. The C-terminal region (domain C) also contains a putative NLS. All fragment variants and their coordinates are depicted below the domain model of LANA. (B) HUVEC were transfected with control vector pc, full-length LANA construct pcLANA, and fragment variants pcLANA-A, pcLANA-BC, respectively, for 48 h. IFA was used to detect their cellular localization, and the nuclear shown by DAPI. (C–E) Cells were transfected with control vector pc, full-length LANA construct and fragment variants, respectively, for 48 h. Immunoblots, qRT-PCR and ELSA were used to detect CD147 expression, *Has1* transcription and extracellular HA production, respectively. Error bars represent the S.E.M. for three independent experiments. ** = $p < 0.01$.

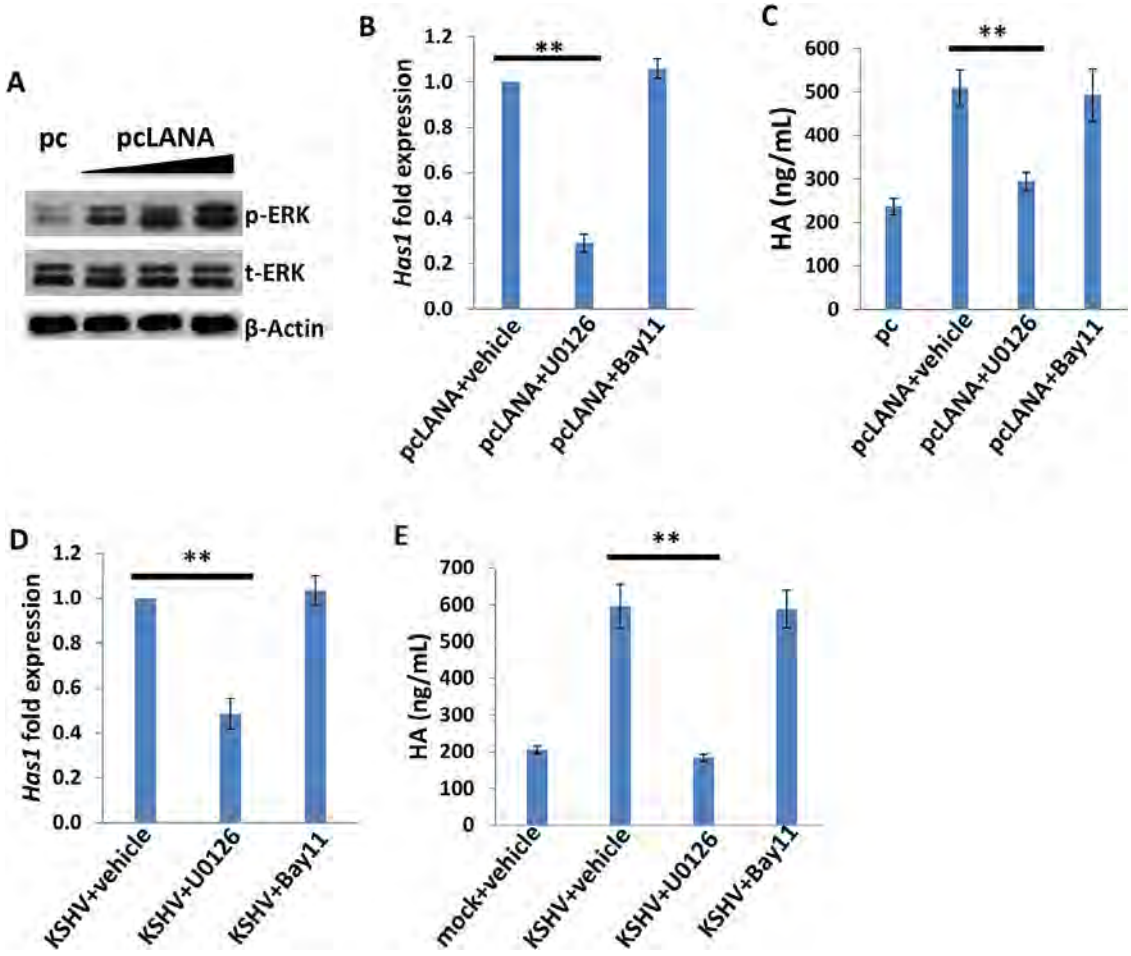

Fig. 5. The MAPK/ERK pathway is involved in LANA-induced HA production from primary endothelial cells. (A–C) HUVEC were transfected with control vector (pc), or vectors encoding LANA (pcLANA) at 0.2, 1.0 or 2.5 μg, respectively, for 48 h, then some cells were treated with vehicle, MAPK inhibitor U0126 (10 μM), or NF-κB inhibitor Bay11-7085 (10 μM) for 2 h followed by an additional 24 h-culture. (D, E) Cells were infected with KSHV for 2 h, then treated with vehicle or signaling inhibitors as above. Protein expression, *Has1* gene transcription and HA production were measured as above. Error bars represent the S.E.M. for three independent experiments. ** = $p < 0.01$.

Immunoblot analysis indicated that U0126 treatment greatly reduced CD147 expression (Fig. S2A). Moreover, overexpression of ERK by a recombinant vector [14] significantly upregulated *Has1* transcripts but slightly increased *CD147* transcripts, while additional silencing of CD147 by RNAi partially reduced *Has1* transcripts, implying other mechanisms independent of CD147 are probably involved in MAPK–ERK upregulation of *Has1* (Fig. S2B, C).

Targeting HA production represses KSHV/LANA-induced endothelial cell invasiveness

Acquisition of a migratory or invasive phenotype represents one hallmark of KSHV-infected endothelial cells, with implications for both viral dissemination and angiogenesis within KS lesions [30]. Here we found that either targeting *CD147* or *Has1* by RNAi or inhibiting HA-receptor interactions by oHA treatment significantly blocked KSHV-induced endothelial cell invasiveness, as measured by the transwell assays (Fig. 6A). Further analysis indicated that RNAi against *CD147* or *Has1* or oHA treatment also reduced VEGF, a major pro-migratory and pro-angiogenic factor production for endothelial cells (Fig. 6B). These results suggest that the effects of HA and CD147 on invasiveness are potentially mediated by VEGF. We further found that LANA-A induced endothelial cell invasiveness with a similar efficiency as the full-length LANA, and that the effect of LANA on invasiveness was significantly blocked by targeting *CD147* or *Has1* with RNAi or by inhibiting HA–receptor interactions via oHA treatment (Fig. 6C). Interestingly, we found that silencing of *Has1* also partially reduced the transcripts of VEGF receptor 1 and 2 (VEGFR1 and VEGFR2), while silencing of *CD147* mainly reduced the transcripts of VEGFR2 (Fig. S3). Taken together, our data indicate that HA production is required for KSHV- or viral protein-induced invasiveness of primary endothelial cells.

Upregulation of HA production and Has1 in KSHV+ HIV-infected patients

To explore the clinical relevance of HA production within KSHV+ HIV-infected patients, we tested plasma HA levels by ELSA in a small collection of our cohort of HIV-infected patients; KSHV infection status in these patients was determined as described in Materials and Methods. We found that the KSHV+ group (n = 16) had higher HA concentrations in their plasma than those from the KSHV– group (n = 12) of HIV-infected patients (Fig. 7A). Further analysis of a subset of these same patients indicated that the KSHV+ group had higher *Has1-3* transcripts within their peripheral blood mononuclear cells (PBMCs) than those from the KSHV– group (Fig. 7B). Only the difference in *Has1* level was highly statistically significant, whereas *Has2* level was moderately significant and the *Has3* level had no significance. Moreover, in the KSHV+ group, only the *Has1* level was highly linearly correlated with HA concentration whereas *Has2* and

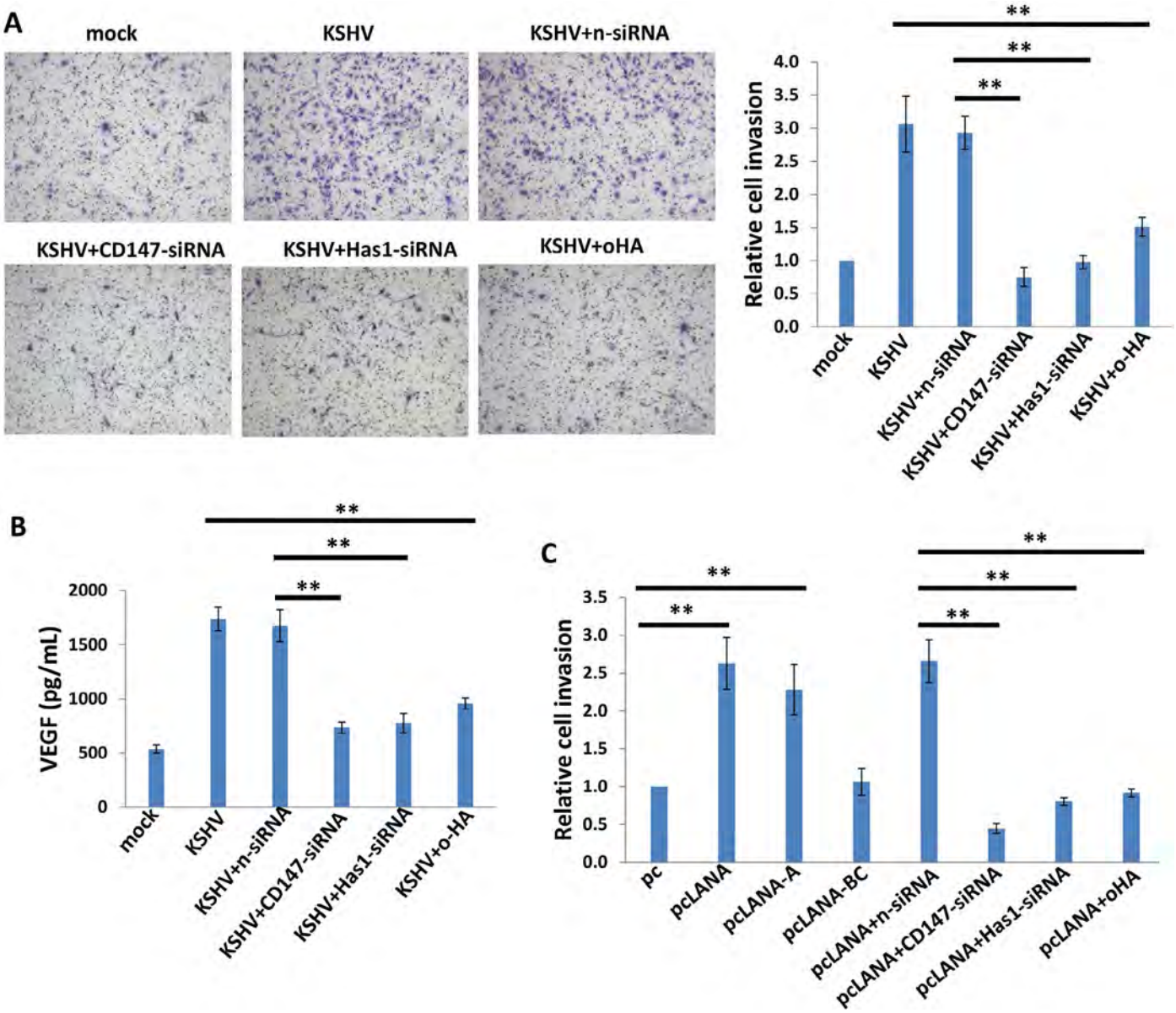

Fig. 6. Targeting HA production represses KSHV/LANA-induced endothelial cell invasiveness. (A) HUVEC were infected with KSHV for 2 h, then transfected with either negative control siRNA (n-siRNA) or *Has1*-siRNA, *CD147*-siRNA, or treated with oHA (150 μg/mL) for 48 h, and cell invasion was assessed using the transwell assays and calculations detailed in Materials and Methods. (B) VEGF concentrations within the culture supernatant were quantified by ELISA. (C) Cells were transfected with control vector pc, full-length LANA construct pcLANA, and fragment variants, respectively, for 48 h. Some cells were then transfected with either negative control siRNA (n-siRNA) or *Has1*-siRNA, *CD147*-siRNA, or treated with oHA (150 μg/mL) for an additional 48 h. Cell invasion was assessed as above. Error bars represent the S.E.M. for three independent experiments. ** = $p < 0.01$.

Has3 levels had moderate or no linear correlation, respectively (Fig. 7C). In contrast, there was no linear correlation between HA concentrations and HIV viral loads or CD4 counts from these patients (Fig. S4), implying that HA production was potentially induced by KSHV co-infection.

Discussion

As mentioned above, HA binds with a number of cellular receptors, leading directly or indirectly to activation of downstream signaling pathways [2]. Although the current study does not address the levels of HA receptors on KSHV-infected primary endothelial cells, we have observed upregulation of HA receptors including CD44 and LYVE-1 by either KSHV *de novo* infection or ectopic expression of LANA (Fig. S5). Interestingly, LYVE-1 has been found highly expressed by KSHV-infected cells and within KSHV-associated tumors [31], although its role in HA-mediated signaling and functions remains largely unknown. Another major HA receptor, CD44, is also a well-known cancer stem cell (CSC) marker for many tumors [32], while its functions in KSHV pathogenesis and tumorigenesis still remain unclear. Therefore, future work is required to understand the contribution to KSHV pathogenesis by regulation of these HA receptors.

Here we have shown that HA and related signaling pathways are involved in KSHV-infected cell invasiveness. Previous studies suggest that they may also regulate other functions within these cells, such as multidrug resistance and endothelial-to-mesenchymal transformation (EndMT). We and others have found that, in response to interaction with HA, HA receptors interact with many signaling and transporter proteins such as ErbB2, EGFR, BCRP, P-glycoprotein, and monocarboxylate transporters (MCTs) to mediate cancer cells' multidrug resistance [12,13,33–35]. EndMT is an important pathophysiologic correlate for cancer progression, and two recent studies

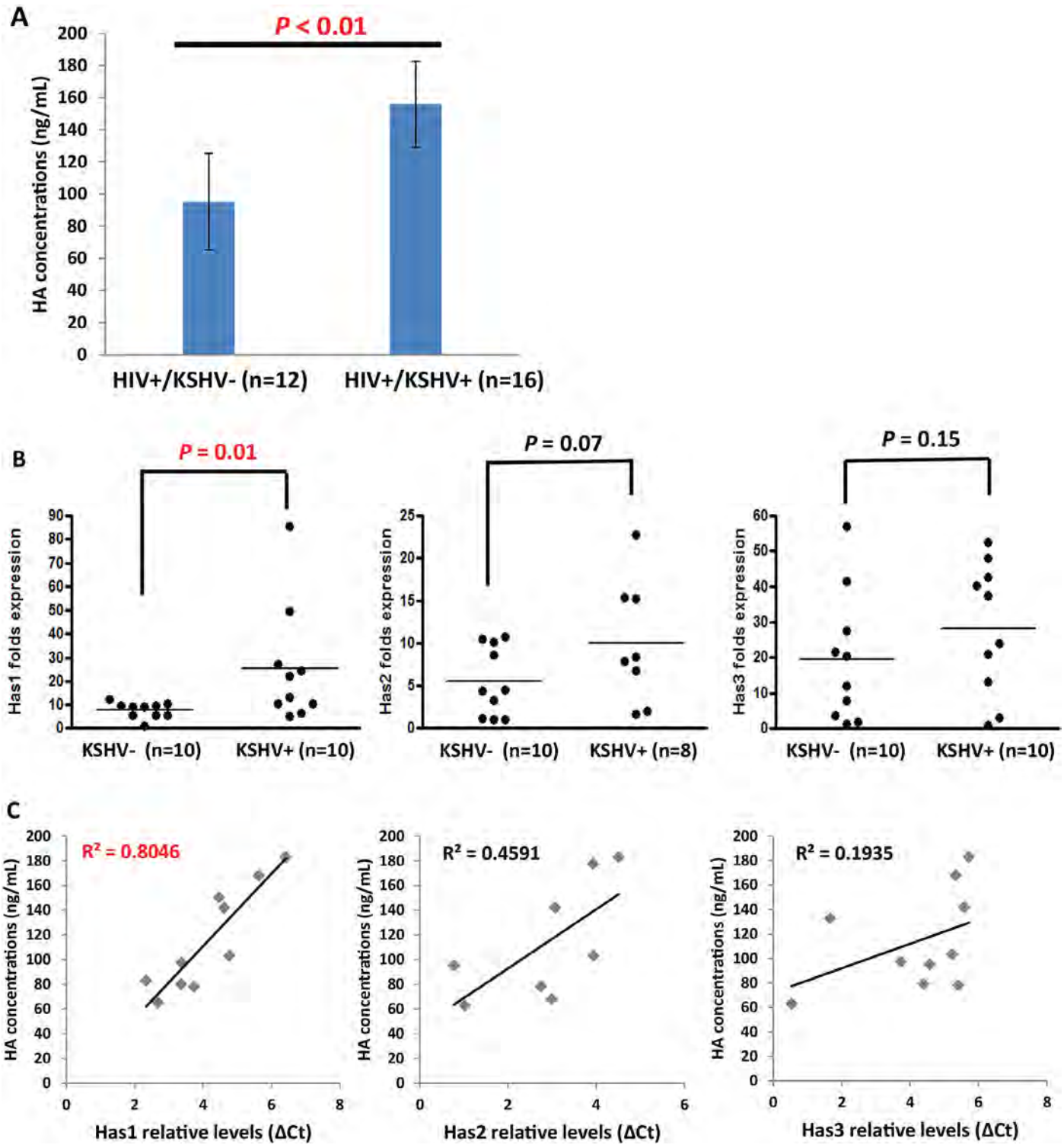

Fig. 7. Upregulation of HA production and *Has1* in KSHV+ HIV-infected patients. (A) The HA concentrations within plasma from HIV-infected patients were quantified using ELSA. KSHV infection status was identified as described in Materials and Methods. (B) The transcriptional levels of *Has1-3* within PBMCs from the same patients were quantified by qRT-PCR. (C) The linear analysis of the correlation between HA concentrations and *Has1-3* transcriptional levels was performed by SPSS.

demonstrate that EndMT is induced by KSHV infection and contributes to viral tumorigenesis [36,37]. Interestingly, HA has been found as a critical regulator of EndMT during cardiac valve formation [38,39].

We found a higher level of HA production and *Has* gene transcripts in KSHV+ than KSHV– groups of HIV-infected patients. Moreover, no linear correlation was observed between HA concentrations and HIV viral loads or CD4 counts from the same patients, indicating the importance of KSHV co-infection for regulation of HA production. However, due to the small number of samples analyzed here, the final conclusion still requires analyses of additional samples from HIV-infected patients. Therefore, we are now working with clinicians within LSUHSC HIV Outpatient (HOP) Clinic to collect more plasma and PBMC samples from HIV-infected patients to continue this analysis.

Published data have reported a higher level of plasma HA within HIV/HCV co-infected patients, and patients with liver fibrosis and/or cirrhosis [40,41]. Therefore, we cannot exclude the possibility of other pathogen co-infection or pathological conditions contributing to upregulation of HA levels in our cohort of HIV-infected patients. These factors should be resolved by further investigation in future.

Acknowledgements

We thank Dr. Rolf Renne at Shands Cancer Center, University of Florida, Gainesville, FL for providing LANA overexpression and deletion mutant constructs, and Dr. Momka Bratoeva at Medical University of South Carolina, Charleston, SC for preparing the oHA. This work was supported by grants from the National Institutes of Health (R01-CA142362 to CP, R01-CA082867 to BPT and P20-RR021970-06 to ZQ), the Department of Defense Career Development Award (CA140437) and Ladies Leukemia League Grant (2014-2015) to ZQ, the National Natural Science Foundation of China (81101791, 81272191, 81472547 to ZQ; 81400164 to LD) and the Foundation for Innovative Research Groups of the NNSF of China (81221001 to YC). All the authors declare no conflict of interest.

Conflict of interest

All the authors declare no conflict of interest.

Appendix: Supplementary material

Supplementary data to this article can be found online at doi:10.1016/j.canlet.2015.03.034.

References

[1] M.I. Tammi, A.J. Day, E.A. Turley, Hyaluronan and homeostasis: a balancing act, J. Biol. Chem. 277 (2002) 4581–4584.
[2] E.A. Turley, P.W. Noble, L.Y. Bourguignon, Signaling properties of hyaluronan receptors, J. Biol. Chem. 277 (2002) 4589–4592.
[3] R.H. Tammi, A. Kultti, V.M. Kosma, R. Pirinen, P. Auvinen, M.I. Tammi, Hyaluronan in human tumors: pathobiological and prognostic messages from cell-associated and stromal hyaluronan, Semin. Cancer Biol. 18 (2008) 288–295.
[4] B.P. Toole, Hyaluronan: from extracellular glue to pericellular cue, Nat. Rev. Cancer 4 (2004) 528–539.
[5] B.P. Toole, M.G. Slomiany, Hyaluronan, CD44 and Emmprin: partners in cancer cell chemoresistance, Drug Resist. Updat. 11 (2008) 110–121.
[6] G.D. Grass, L. Dai, Z. Qin, C. Parsons, B.P. Toole, CD147: regulator of hyaluronan signaling in invasiveness and chemoresistance, Adv. Cancer Res. 123 (2014) 351–373.
[7] E.A. Mesri, M.A. Feitelson, K. Munger, Human viral oncogenesis: a cancer hallmarks analysis, Cell Host Microbe 15 (2014) 266–282.
[8] Y. Chang, E. Cesarman, M.S. Pessin, F. Lee, J. Culpepper, D.M. Knowles, et al., Identification of herpesvirus-like DNA sequences in AIDS-associated Kaposi's sarcoma, Science 266 (1994) 1865–1869.
[9] E. Cesarman, Y. Chang, P.S. Moore, J.W. Said, D.M. Knowles, Kaposi's sarcoma-associated herpesvirus-like DNA sequences in AIDS-related body-cavity-based lymphomas, N. Engl. J. Med. 332 (1995) 1186–1191.
[10] E.A. Engels, R.J. Biggar, H.I. Hall, H. Cross, A. Crutchfield, J.L. Finch, et al., Cancer risk in people infected with human immunodeficiency virus in the United States, Int. J. Cancer 123 (2008) 187–194.
[11] Y.B. Chen, A. Rahemtullah, E. Hochberg, Primary effusion lymphoma, Oncologist 12 (2007) 569–576.
[12] Z. Qin, L. Dai, M. Bratoeva, M.G. Slomiany, B.P. Toole, C. Parsons, Cooperative roles for emmprin and LYVE-1 in the regulation of chemoresistance for primary effusion lymphoma, Leukemia 25 (2011) 1598–1609.
[13] M.G. Slomiany, L. Dai, L.B. Tolliver, G.D. Grass, Y. Zeng, B.P. Toole, Inhibition of functional hyaluronan-CD44 interactions in CD133-positive primary human ovarian carcinoma cells by small hyaluronan oligosaccharides, Clin. Cancer Res. 15 (2009) 7593–7601.
[14] Z. Qin, L. Dai, M. Defee, V.J. Findlay, D.K. Watson, B.P. Toole, et al., Kaposi's sarcoma-associated herpesvirus suppression of DUSP1 facilitates cellular pathogenesis following de novo infection, J. Virol. 87 (2013) 621–635.
[15] G.L. Mbisa, W. Miley, C.J. Gamache, W.K. Gillette, D. Esposito, R. Hopkins, et al., Detection of antibodies to Kaposi's sarcoma-associated herpesvirus: a new approach using K8.1 ELISA and a newly developed recombinant LANA ELISA, J. Immunol. Methods 356 (2010) 39–46.
[16] Y. Benavente, G. Mbisa, N. Labo, D. Casabonne, N. Becker, M. Maynadie, et al., Antibodies against lytic and latent Kaposi's sarcoma-associated herpes virus antigens and lymphoma in the European EpiLymph case-control study, Br. J. Cancer 105 (2011) 1768–1771.
[17] P.H. Weigel, P.L. DeAngelis, Hyaluronan synthases: a decade-plus of novel glycosyltransferases, J. Biol. Chem. 282 (2007) 36777–36781.
[18] E.A. Marieb, A. Zoltan-Jones, R. Li, S. Misra, S. Ghatak, J. Cao, et al., Emmprin promotes anchorage-independent growth in human mammary carcinoma cells by stimulating hyaluronan production, Cancer Res. 64 (2004) 1229–1232.
[19] G.D. Grass, L.B. Tolliver, M. Bratoeva, B.P. Toole, CD147, CD44, and the epidermal growth factor receptor (EGFR) signaling pathway cooperate to regulate breast epithelial cell invasiveness, J. Biol. Chem. 288 (2013) 26089–26104.
[20] F. Ye, X. Lei, S.J. Gao, Mechanisms of Kaposi's sarcoma-associated herpesvirus latency and reactivation, Adv. Virol. 2011 (2011).
[21] N. Dupin, C. Fisher, P. Kellam, S. Ariad, M. Tulliez, N. Franck, et al., Distribution of human herpesvirus-8 latently infected cells in Kaposi's sarcoma, multicentric Castleman's disease, and primary effusion lymphoma, Proc. Natl. Acad. Sci. U.S.A. 96 (1999) 4546–4551.
[22] M.E. Ballestas, P.A. Chatis, K.M. Kaye, Efficient persistence of extrachromosomal KSHV DNA mediated by latency-associated nuclear antigen, Science 284 (1999) 641–644.
[23] A. Krithivas, D.B. Young, G. Liao, D. Greene, S.D. Hayward, Human herpesvirus 8 LANA interacts with proteins of the mSin3 corepressor complex and negatively regulates Epstein-Barr virus gene expression in dually infected PEL cells, J. Virol. 74 (2000) 9637–9645.
[24] R. Renne, C. Barry, D. Dittmer, N. Compitello, P.O. Brown, D. Ganem, Modulation of cellular and viral gene expression by the latency-associated nuclear antigen of Kaposi's sarcoma-associated herpesvirus, J. Virol. 75 (2001) 458–468.
[25] Z. Qin, L. Dai, M.G. Slomiany, B.P. Toole, C. Parsons, Direct activation of emmprin and associated pathogenesis by an oncogenic herpesvirus, Cancer Res. 70 (2010) 3884–3889.
[26] A.C. Garber, M.A. Shu, J. Hu, R. Renne, DNA binding and modulation of gene expression by the latency-associated nuclear antigen of Kaposi's sarcoma-associated herpesvirus, J. Virol. 75 (2001) 7882–7892.
[27] D.R. Schwam, R.L. Luciano, S.S. Mahajan, L. Wong, A.C. Wilson, Carboxy terminus of human herpesvirus 8 latency-associated nuclear antigen mediates dimerization, transcriptional repression, and targeting to nuclear bodies, J. Virol. 74 (2000) 8532–8540.
[28] N. Cloutier, L. Flamand, Kaposi sarcoma-associated herpesvirus latency-associated nuclear antigen inhibits interferon (IFN) beta expression by competing with IFN regulatory factor-3 for binding to IFNB promoter, J. Biol. Chem. 285 (2010) 7208–7221.
[29] L. Dai, M. Bratoeva, B.P. Toole, Z. Qin, C. Parsons, KSHV activation of VEGF secretion and invasion for endothelial cells is mediated through viral upregulation of emmprin-induced signal transduction, Int. J. Cancer 131 (2012) 834–843.
[30] L.W. Qian, J. Xie, F. Ye, S.J. Gao, Kaposi's sarcoma-associated herpesvirus infection promotes invasion of primary human umbilical vein endothelial cells by inducing matrix metalloproteinases, J. Virol. 81 (2007) 7001–7010.
[31] P. Pyakurel, F. Pak, A.R. Mwakigonja, E. Kaaya, T. Heiden, P. Biberfeld, Lymphatic and vascular origin of Kaposi's sarcoma spindle cells during tumor development, Int. J. Cancer 119 (2006) 1262–1267.
[32] M. Zoller, CD44: can a cancer-initiating cell profit from an abundantly expressed molecule?, Nat. Rev. Cancer 11 (2011) 254–267.
[33] S. Misra, S. Ghatak, B.P. Toole, Regulation of MDR1 expression and drug resistance by a positive feedback loop involving hyaluronan, phosphoinositide 3-kinase, and ErbB2, J. Biol. Chem. 280 (2005) 20310–20315.
[34] K.E. Miletti-Gonzalez, S. Chen, N. Muthukumaran, G.N. Saglimbeni, X. Wu, J. Yang, et al., The CD44 receptor interacts with P-glycoprotein to promote cell migration and invasion in cancer, Cancer Res. 65 (2005) 6660–6667.
[35] M.G. Slomiany, G.D. Grass, A.D. Robertson, X.Y. Yang, B.L. Maria, C. Beeson, et al., Hyaluronan, CD44, and emmprin regulate lactate efflux and membrane localization of monocarboxylate transporters in human breast carcinoma cells, Cancer Res. 69 (2009) 1293–1301.
[36] P. Gasperini, G. Espigol-Frigole, P.J. McCormick, O. Salvucci, D. Maric, T.S. Uldrick, et al., Kaposi sarcoma herpesvirus promotes endothelial-to-mesenchymal transition through Notch-dependent signaling, Cancer Res. 72 (2012) 1157–1169.
[37] F. Cheng, P. Pekkonen, S. Laurinavicius, N. Sugiyama, S. Henderson, T. Gunther, et al., KSHV-initiated notch activation leads to membrane-type-1 matrix metalloproteinase-dependent lymphatic endothelial-to-mesenchymal transition, Cell Host Microbe 10 (2011) 577–590.
[38] T.D. Camenisch, A.P. Spicer, T. Brehm-Gibson, J. Biesterfeldt, M.L. Augustine, A. Calabro Jr., et al., Disruption of hyaluronan synthase-2 abrogates normal cardiac morphogenesis and hyaluronan-mediated transformation of epithelium to mesenchyme, J. Clin. Invest. 106 (2000) 349–360.
[39] T.D. Camenisch, J.A. Schroeder, J. Bradley, S.E. Klewer, J.A. McDonald, Heart-valve mesenchyme formation is dependent on hyaluronan-augmented activation of ErbB2-ErbB3 receptors, Nat. Med. 8 (2002) 850–855.
[40] D. Grint, L. Peters, J.K. Rockstroh, S. de Wit, V.M. Mitsura, B. Knysz, et al., Increased incidence of antiretroviral drug discontinuation among patients with viremic hepatitis C virus coinfection and high hyaluronic acid, a marker of liver fibrosis, AIDS 28 (2014) 577–587.
[41] P. Halfon, M. Bourliere, G. Penaranda, R. Deydier, C. Renou, D. Botta-Fridlund, et al., Accuracy of hyaluronic acid level for predicting liver fibrosis stages in patients with hepatitis C virus, Comp. Hepatol. 4 (2005) 6.

Genomic analysis of xCT-mediated regulatory network: identification of novel targets against AIDS-associated lymphoma

Lu Dai[1,3], Yueyu Cao[1], Yihan Chen[1], Johnan A.R. Kaleeba[5], Jovanny Zabaleta[4] and Zhiqiang Qin[1,2]

[1] Research Center for Translational Medicine and Key Laboratory of Arrhythmias of the Ministry of Education of China, East Hospital, Tongji University School of Medicine, Shanghai, China

[2] Department of Microbiology/Immunology/Parasitology, Louisiana State University Health Sciences Center, Louisiana Cancer Research Center, New Orleans, LA, USA

[3] Department of Medicine, Louisiana State University Health Sciences Center, Louisiana Cancer Research Center, New Orleans, LA, USA

[4] Department of Pediatrics, Louisiana State University Health Sciences Center, Louisiana Cancer Research Center, New Orleans, LA, USA

[5] Department of Microbiology and Immunology, Uniformed Services University of the Health Sciences, Bethesda, MD, USA

Correspondence to: *Zhiqiang Qin*, ***email***: *zqin@lsuhsc.edu*

Keywords: KSHV, herpesvirus, xCT, lymphoma, microarray

Received: *January 29, 2015* ***Accepted***: *March 10, 2015* ***Published***: *March 30, 2015*

ABSTRACT

Kaposi's sarcoma-associated herpesvirus (KSHV) is the etiological agent of primary effusion lymphoma (PEL), a rapidly progressing malignancy mostly arising in HIV-infected patients. Even under conventional chemotherapy, PEL continues to portend nearly 100% mortality within several months, which urgently requires novel therapeutic strategies. We have previously demonstrated that targeting xCT, an amino acid transporter for cystine/glutamate exchange, induces significant PEL cell apoptosis through regulation of multiple host and viral factors. More importantly, one of xCT selective inhibitors, Sulfasalazine (SASP), effectively prevents PEL tumor progression in an immune-deficient xenograft model. In the current study, we use Illumina microarray to explore the profile of genes altered by SASP treatment within 3 KSHV$^+$ PEL cell-lines, and discover that many genes involved in oxidative stress/antioxidant defense system, apoptosis/anti-apoptosis/cell death, and cellular response to unfolded proteins/topologically incorrect proteins are potentially regulated by xCT. We further validate 2 downstream candidates, *OSGIN1* (Oxidative stress-induced growth inhibitor 1) and *XRCC5* (X-ray repair cross-complementing protein 5), and evaluate their functional relationship with PEL cell survival/proliferation and chemoresistance, respectively. Together, our data indicate that targeting these novel xCT-regulated downstream genes may represent a promising new therapeutic strategy against PEL and/or other AIDS-related lymphoma.

INTRODUCTION

The oncogenic Kaposi's sarcoma-associated herpesvirus (KSHV, also known as Human herpesvirus 8) is a principal causative agent of several human cancers including primary effusion lymphoma (PEL), which arises preponderantly in immunocompromised individuals, in particular acquired immune deficiency syndrome (AIDS) patients [1]. PEL usually comprises transformed B cells harboring KSHV episomes and presents as pleural, peritoneal and pericardial neoplastic effusions [2]. PEL is a rapidly progressing malignancy with a median survival time of approximately 6 months even under conventional chemotherapy [3]. Furthermore, the myelosuppressive effects of systemic cytotoxic chemotherapy synergize with those caused by antiretroviral therapy or immune

suppression [2-4], which supports the need to identify novel targets that could guide development of more effective therapeutic strategies. Recently, we found that the amino acid transporter, xCT, is highly expressed on the surface of patient-derived KSHV$^+$ PEL cells, and targeting xCT by pharmacological inhibition or RNAi silencing induces significant PEL cell apoptosis [5]. We further demonstrated that the underlying mechanisms for this effect include regulation of both host and viral factors: (i) reduction of intracellular glutathione (GSH) synthesis and increased reactive oxygen species (ROS) production, (ii) repression of cell-proliferation-related signaling, in particular Akt pathway, and (iii) induction of viral lytic gene expression [5]. More importantly, we demonstrated that an xCT selective inhibitor, Sulfasalazine (SASP), effectively prevents PEL tumor progression in an immune-deficient xenograft model [5], which suggests that xCT may represent a promising target for AIDS-related lymphomas.

The expression of xCT on the cell membrane is essential for the uptake of cystine required for synthesis of intracellular glutathione (GSH), an anti-oxidant that plays an important role in maintaining the intracellular redox balance [6, 7]. Therefore, xCT is highly expressed by a variety of malignant tumors because the uptake of cystine/cysteine from the microenvironment is crucial for cancer cell growth and viability [8-11]. Interestingly, xCT has also been identified as a fusion-entry receptor for KSHV [12, 13], which is upregulated within more advanced Kaposi's sarcoma (KS, another KSHV-related malignancy[14]) lesions containing a greater number of KSHV-infected cells [15]. We also recently reported that xCT is able to activate intracellular signaling pathways (in particular MAPK), pro-migratory cytokine release, and KSHV-infected endothelial cell invasion through induction of the 14-3-3β protein [16]. Moreover, xCT is functionally involved in the pathogenesis of other viruses and bacteria as well [17-20]. However, the mechanisms of xCT-mediated regulation of KSHV pathogenesis and tumorigenesis, including the xCT regulatory network in AIDS-related lymphomas such as KSHV$^+$ PEL remain unknown. Clearly, innovative insights from this information would facilitate the identification of potential "drug target" candidates for development of new therapeutic strategies. Therefore, in the current study we used Illumina human microarray analysis to interrogate changes in the transcriptional profiles of genes in 3 KSHV$^+$ PEL cell-lines treated with the xCT selective inhibitor, SASP, which led to identification of a number of novel xCT-regulated downstream genes important to PEL survival or chemoresistance.

RESULTS

Microarray analysis of xCT-regulated network within KSHV$^+$ PEL cells

We first used the HumanHT-12 v4 Expression BeadChip (Illumina) which contains more than 47,000 probes derived from the NCBI RefSeq Release 38 and other sources to study the gene profile altered between vehicle- or SASP-treated 3 KSHV$^+$ PEL cell-lines (BCP-1, BC-1 and BCBL-1). Intersection analysis indicated that there were totally 100 common genes significantly altered within all the 3 SASP-treated cell-lines (up/down≥2 folds and $p < 0.05$); 33 similar genes altered between BCBL-1 and BC-1, 93 similar between BCBL-1 and BCP-1, and 124 similar between BC-1 and BCP-1; 80 genes altered were unique to BCBL-1, 150 unique to BCP-1 and 640 unique to BC-1 (Figure 1). Notably, BC-1 cells, which are also EBV$^+$, had a much higher number of uniquely altered genes than BCBL-1 and BCP-1. Within the common gene set, the top 20 upregulated or downregulated candidate genes in SASP-treated BCP-1, BC-1 and BCBL-1 cell-lines are listed in Table 1 and Table 2, respectively, including gene description and the altered level of transcription in these cell-lines. Interestingly, we found that the functional role of most genes in PEL pathogenesis have never been reported, although some of them have been implicated in other types of malignancies. For example, *SRXN1* (Sulfiredoxin-1), which is upregulated in all three SASP-treated PEL cell lines (Table 1) is involved in proliferation inhibition of acute myeloid leukemia mediated by Maesopsin 4-O-beta-D-glucoside, a natural compound isolated from the leaves of Artocarpus tonkinensis) [21]. Another study reported that activation of *PFKP* (6-phosphofructokinase type C), which is downregulated in SASP-treated PEL cells (Table 2) is closely associated with breast cancer cell proliferation [22]. The opposite effects of SASP on *SRXN1* and *PFKP* transcription underscores the putative benefits of this drug in clinical management of PEL as well. We next performed enrichment analysis of these common, similar and unique sets of genes using the Pathway map, Gene Ontology (GO) Processes and Process Networks modules from Metacore Software (Thompson Reuters) [23]. Our analysis shows that several major cellular functions were affected within SASP-treated PEL cells, including oxidative stress/antioxidant defense system, apoptosis/anti-apoptosis/cell death, and cellular response to unfolded proteins/topologically incorrect proteins, which is consistent with the SASP-induced apoptosis phenotype that we recently observed in KSHV$^+$ PEL cell-lines [5]. The top 2 scored pathway maps and protein networks based on the enrichment analysis of "common" gene set were listed in Figure 3 and S1, respectively.

Table 1: The top 20 candidate genes upregulated in KSHV+ PEL cells treated by SASP.

Gene symbol	Description	Fold change		
		BCP-1	BC-1	BCBL-1
OSGIN1	Oxidative stress-induced growth inhibitor 1	14.73	5.85	7.87
HSPA6	Heat shock 70 kDa protein 6	4.36	14.97	4.75
MSC	Musculin	7.51	8.53	5.46
DHRS2	Dehydrogenase/reductase SDR family member 2, mitochondrial	10.64	5.75	4.36
PPP1R15A	Protein phosphatase 1 regulatory subunit 15A	6.77	6.14	6.45
HSPA1A	Heat shock 70 kDa protein 1	7.05	5.57	5.24
SRXN1	Sulfiredoxin-1	7.53	3.03	5.85
GCLM	Glutamate--cysteine ligase regulatory subunit	6.24	4.12	5.25
SQSTM1	Sequestosome-1	7.46	2.24	5.3
RN7SK	RNA, 7SK small nuclear transcript	4.98	4.62	4.81
HSPA7	Putative heat shock 70 kDa protein 7	3.04	7.69	3.44
DNAJB1	DnaJ homolog subfamily B member 1	5.81	4.67	3.48
DNAJC3	DnaJ homolog subfamily C member 3	3.87	7.39	2.46
LILRB3	Leukocyte immunoglobulin-like receptor subfamily B member 3	4.71	3.4	4.59
RNF141	RING finger protein 141	5.23	3.3	3.86
C6orf52	Putative uncharacterized protein C6orf52	2.81	5.81	3.17
CCL3L3	C-C motif chemokine 3-like 1	4.66	4.11	2.43
ZCWPW1	Zinc finger CW-type PWWP domain protein 1	3	5.69	2.42
SLC3A2	4F2 cell-surface antigen heavy chain	4.16	4.63	2.28
DDIT3	DNA damage-inducible transcript 3 protein	3.51	2.97	4.33

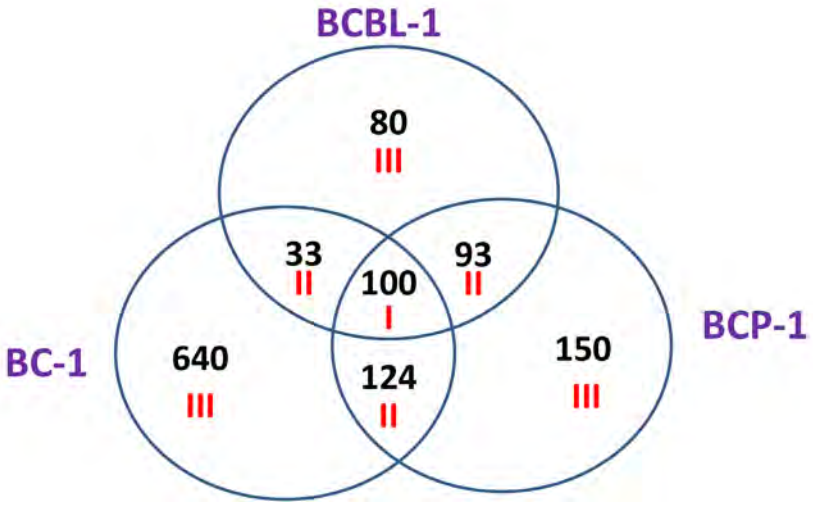

Figure 1: Intersection analysis of gene profile altered within SASP-treated PEL cell-lines. The HumanHT-12 v4 Expression BeadChip (Illumina) was used to detect genomic gene profile altered within 3 SASP-treated PEL cell-lines (BCBL-1, BC-1 and BCP-1) when compared with vehicle-treated controls. Intersection analysis of significantly altered genes (up/down≥2 folds and $p < 0.05$) was performed using the Illumina GenomeStudio Software. Set I: Common genes altered in all the 3 cell-lines; Set II: Similar genes altered in every 2 cell-lines; Set III: Unique genes altered in each cell-line.

Experimental validation of microarray results with selected downstream candidates

We next selected 5 genes from the top 20 upregulated or downregulated candidate list (Table 1 and 2) for validation of their transcriptional change by qRT-PCR. Our results indicated that all the 5 genes (*OSGIN1*, *HSPA6*, *DHRS2*, *PPP1R15A* and *HSPA1A*) were significantly upregulated in SASP-treated PEL cells when compared with vehicle-treated cells; while another 5 genes (*ASZ1*, *ARL4C*, *NREP*, *LGALS13*, *PPIA*) were all significantly downregulated in SASP-treated PEL cells (Figure 4). Moreover, the altered transcriptional levels of these genes in all the 3 KSHV$^+$ PEL cell-lines (BCBL-1, BC-1 and BCP-1) were comparable to those found in microarray data, demonstrating the credibility of our microarray analysis.

The role of OSGIN1 in SASP-induced KSHV$^+$ PEL cell apoptosis

We next selected *OSGIN1* (Oxidative stress-induced growth inhibitor 1), one of the highly upregulated genes in SASP-treated KSHV$^+$ PEL cells from microarray data, to determine its role in SASP-induced cell apoptosis. The *OSGIN1* gene (also named as *OKL38*) was first identified in breast epithelial cells as increasingly expressed during pregnancy and lactation [24]. Low-level expression of this gene has been reported in breast cancer cell lines, while its overexpression in MCF-7 breast cancer cells leads to a reduction in proliferation as well as tumor formation in nude mice [24]. As a tumor suppressor, downregulation of OSGIN1 was also found to be closely associated with progression of other malignancies such as hepatocellular carcinoma and kidney cancer [25-27]. Here, we found that silencing of *OSGIN1* by RNAi significantly reduced cell apoptosis induced by SASP (0.5 mM) in BCP-1 and BCBL-1 cells (Figure 5A and S2). Western blot analysis also indicated that silencing of OSGIN1 by RNAi in SASP-treated BCP-1 and BCBL-1 greatly reduced cleaved Caspase 3 and 9, while partially rescuing the phosphorylation of Akt, downstream P70S6, S6 and the expression of X-linked inhibitor of apoptosis protein (XIAP) [28], a physiologic substrate of Akt that is stabilized to inhibit programmed cell death (Figure 5B). We have previously shown that SASP-induced PEL apoptosis may also be orchestrated via reduction of intracellular GSH synthesis and increased ROS production [5]. Here we found that silencing of *OSGIN1* significantly restored intracellular GSH synthesis and reduced ROS production from SASP-treated cells (Figure 5C-5D). Biochemical assays further confirmed that silencing of *OSGIN1* caused a reduction in the activity of NADPH oxidase (Figure 5E), the major source of ROS production [29, 30]. We also found that silencing of xCT by RNAi upregulated *OSGIN1* transcripts in BCBL-1 cells, indicating that this gene is indeed a downstream target of xCT (Figure S3A). Taken together, these data demonstrate the central role of *OSGIN1* in SASP-induced PEL apoptosis, which involves modulation of a variety of host physiologic factors.

We previously reported some other AIDS-related lymphoma cell-lines such as Burkitt's lymphoma BL-

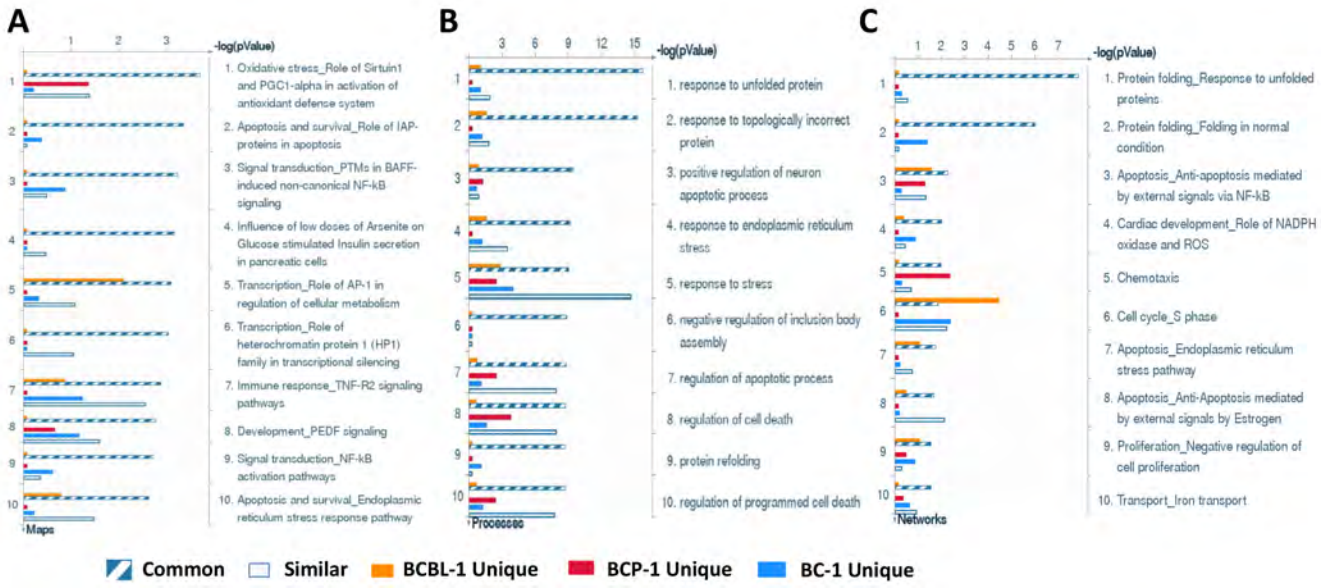

Figure 2: Enrichment analysis of gene profile significantly altered by inhibition of xCT within KSHV-infected PEL cell-lines. The enrichment analysis of gene profile (common, similar and unique profile as indicated) significantly altered by inhibition of xCT was performed using the Metacore Software (Thompson Reuters) Modules: Pathway Maps (**A**), Gene Ontology Processes (**B**) and Process Networks (**C**).

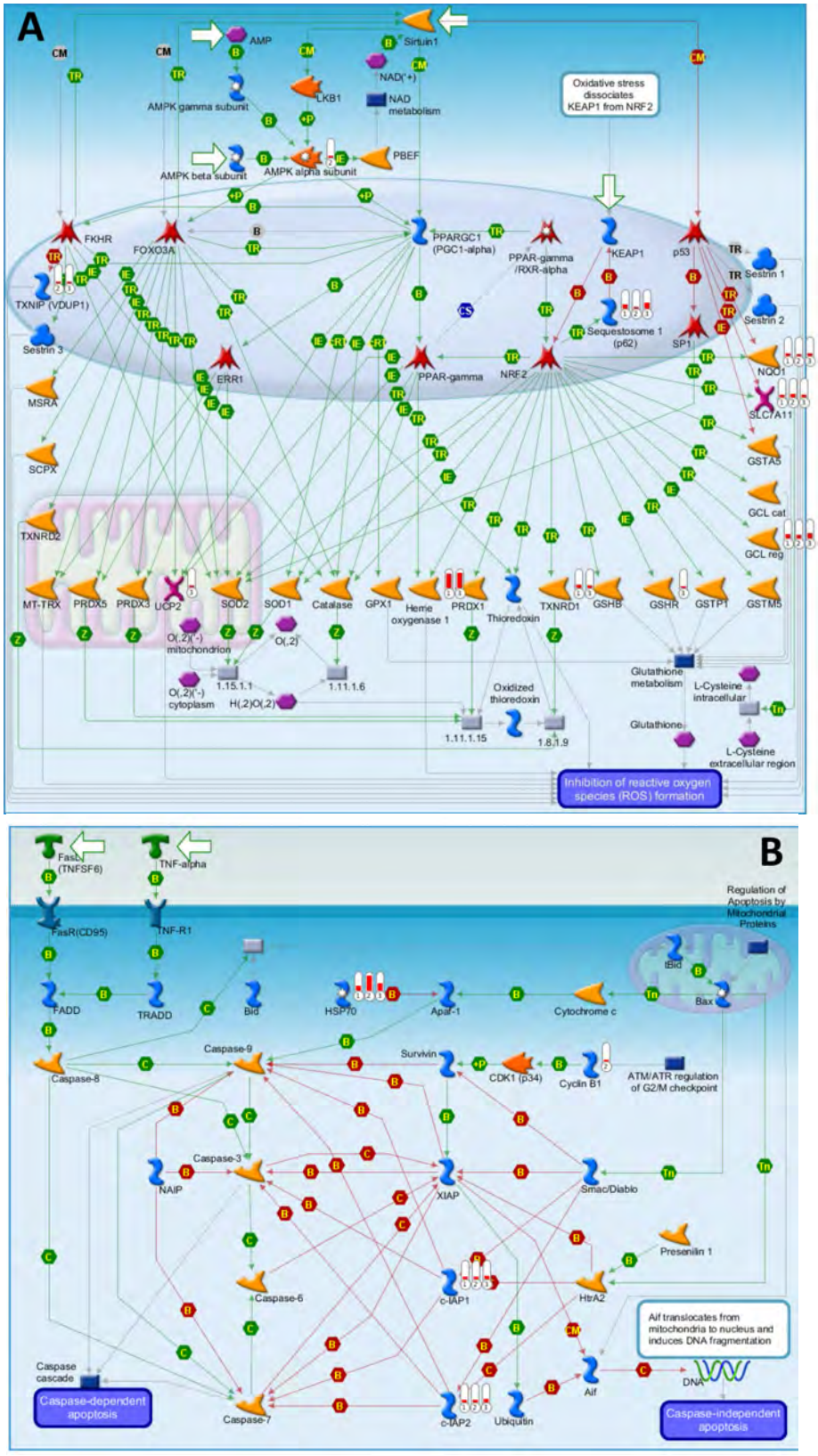

Figure 3: The top 2 scored maps (maps with the lowest p-value) based on the enrichment distribution sorted by 'common' gene set. (**A**) Oxidative stress: Role of Sirtuin1 and PGC1 alpha in activation of antioxidant defense system. (**B**) Apoptosis and survival: Role of IAP proteins in apoptosis. Experimental data from all files is linked to and visualized on the maps as thermometer like figures. Up-ward thermometers have red color and indicate upregulated signals and down ward (blue) ones indicate downregulated expression levels of the genes. Data was produced by the Metacore Software (Thompson Reuters).

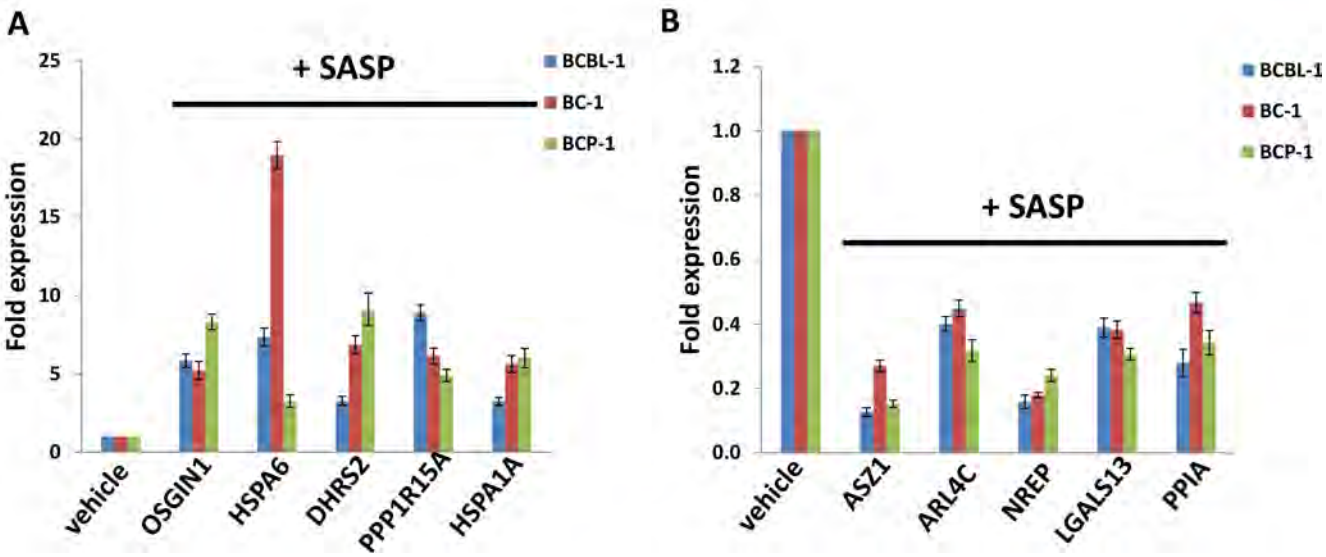

Figure 4: Validation of microarray results by qRT-PCR for selected candidate genes. The transcriptional levels of selected 5 candidate genes upregulated (**A**) or downregulated (**B**) as shown in microarray data were validated by using qRT-PCR, respectively. Error bars represent the S.E.M. for 3 independent experiments.

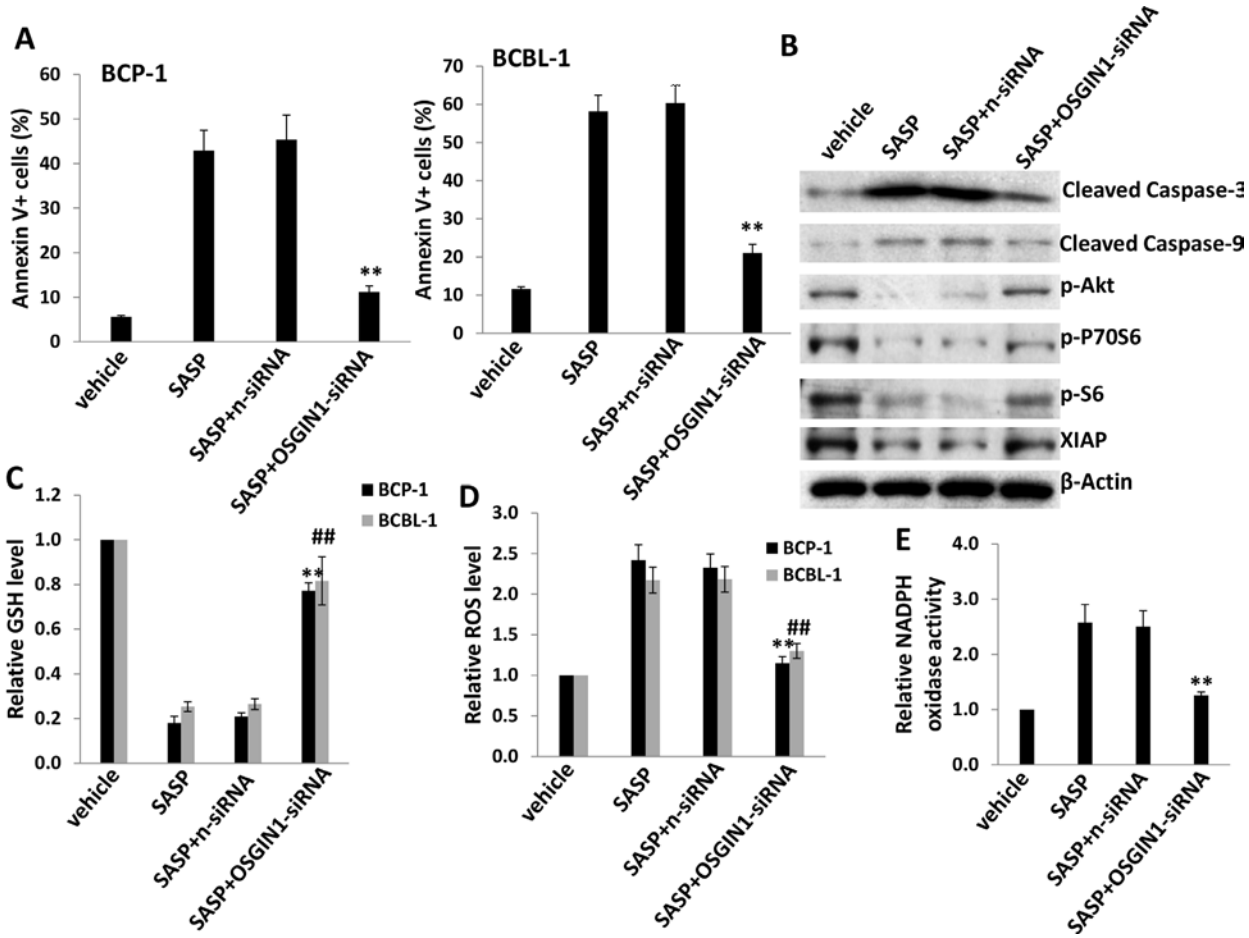

Figure 5: xCT inhibition induces KSHV-infected PEL cell apoptosis potentially through upregulation of OSGIN1. (**A**) BCP-1 and BCBL-1 were transfected with either negative control siRNA (n-siRNA) or *OSGIN1*-siRNA for 48 h, then incubated with 0.5mM of SASP for additional 24 h and cell apoptosis was assessed using Annexin V-PI staining and flow cytometry analysis. (**B**) Protein expression in BCBL-1 was measured by immuoblots. (**C-D**) The levels of intracellular GSH and ROS were quantified as described in Methods. (**E**) The activities of NADPH oxidases in BCBL-1 were measured as described in Methods. Error bars represent the S.E.M. for 3 independent experiments. **/## = $p < 0.01$ (*vs* SASP+n-siRNA group).

Table 2: The top 20 candidate genes downregulated in KSHV+ PEL cells treated by SASP.

Gene symbol	Description	Fold change		
		BCP-1	BC-1	BCBL-1
ASZ1	Ankyrin repeat, SAM and basic leucine zipper domain-containing protein 1	0.31	0.19	0.32
ARL4C	ADP-ribosylation factor-like protein 4C	0.25	0.33	0.25
NREP	Neuronal regeneration-related protein	0.28	0.26	0.32
SOCS2	Suppressor of cytokine signaling 2	0.28	0.23	0.39
FAM117B	Protein FAM117B	0.33	0.23	0.4
LGALS13	Galactoside-binding soluble lectin 13	0.32	0.22	0.44
PPIA	Peptidyl-prolyl cis-trans isomerase A	0.3	0.26	0.43
BTF3L4	Transcription factor BTF3 homolog 4	0.36	0.22	0.41
XRCC5	X-ray repair cross-complementing protein 5	0.41	0.11	0.47
E2F5	Transcription factor E2F5	0.35	0.31	0.35
ENPP2	Ectonucleotide pyrophosphatase/phosphodiesterase family member 2	0.32	0.28	0.41
PFKP	6-phosphofructokinase type C	0.35	0.29	0.38
RBM17	Splicing factor 45	0.4	0.21	0.42
EPB41L3	Band 4.1-like protein 3	0.36	0.3	0.38
ATP11B	Probable phospholipid-transporting ATPase IF	0.3	0.35	0.4
SERBP1	Plasminogen activator inhibitor 1 RNA-binding protein	0.42	0.15	0.48
PM20D2	Peptidase M20 domain-containing protein 2	0.47	0.21	0.37
MYLIP	E3 ubiquitin-protein ligase MYLIP	0.21	0.39	0.47
CBR4	Carbonyl reductase family member 4	0.38	0.22	0.47
TMPRSS3	Transmembrane protease serine 3	0.3	0.32	0.46

41 and BJAB (both are KSHV^{neg}/EBV^{neg}) with highly expressed xCT, and SASP treatment induced significant apoptosis for BL-41 [5]. Here we found that silencing of *OSGIN1* by siRNA significantly reduced cell apoptosis induced by SASP (0.5 mM) in BL-41 cells (Figure S4). However, simply silencing of *OSGIN1* did not induce apoptosis for primary human CD19^{+} B cells isolated from peripheral blood of healthy donor (Figure S5).

Targeting XRCC5 impairs DNA-damage repair abilities of tumor cells and promotes low dose of SASP-induced PEL apoptosis

We were also interested in *XRCC5* (X-ray repair cross-complementing protein 5, also known as Ku80), one of downregulated genes in SASP-treated KSHV^{+} PEL cells, to determine its role in SASP-induced cell apoptosis. Ku80 is a tightly associated heterodimer of ~70 kDa and ~80 kDa subunits (Ku70 and Ku80) that, together with the ~470 kDa catalytic subunit, DNA-PKcs, form the DNA-dependent protein kinase involved in repairing DNA

double-strand breaks (DSBs) caused by a variety of stress factors [31]. The Ku80-dependent repair process, called nonhomologous end joining (NHEJ), appears to be the main DNA DSB repair mechanism in mammalian cells [31, 32]. Interestingly, Ku80-knockout mice are small, and their cells fail to proliferate in culture and show signs of premature senescence [33, 34]. Here we found, for the first time, that silence of xCT by RNAi significantly downregulates *XRCC5* (Ku80) transcripts in BCBL-1 cells, indicating that *XRCC5* is also a downstream gene target of xCT (Figure S3B). Interestingly, direct siRNA silencing of *XRCC5* enhanced low-dose SASP (0.1mM)-induced PEL apoptosis, potentially due to impaired DNA-damage repair machinery in tumor cells (Figure 6A and S6). Immunoblot and immunofluorescence data further confirmed that silencing of *XRCC5* in low dose SASP-treated BCBL-1 cells increased the levels of cleaved Caspase 3 and 9 as well as phosphorylated p53 (Ser15) and phosphorylated Histone H2A.X (Ser139), the two markers for DNA-damage [35] (Figure 6B and 6C). Moreover, we found that silencing of *XRCC5* also enhanced the induction of apoptosis and programmed cell death by low dose concentrations of other DNA-damage reagents such as Doxorubicin (100nM) induced PEL apoptosis (Figure 6D and 6E). Together, these data provide solid evidence that DNA-damage may represent another mechanism of SASP-induced PEL apoptosis/cell death, which is potentially through XRCC5. In addition, direct siRNA silencing of *XRCC5* also enhanced low-dose SASP (0.1mM)-induced apoptosis for Burkitt's lymphoma BL-41 cells (Figure S7), while targeting *XRCC5* induced no apoptosis for primary human $CD19^+$ B cells isolated from peripheral blood of healthy donor (Figure S5).

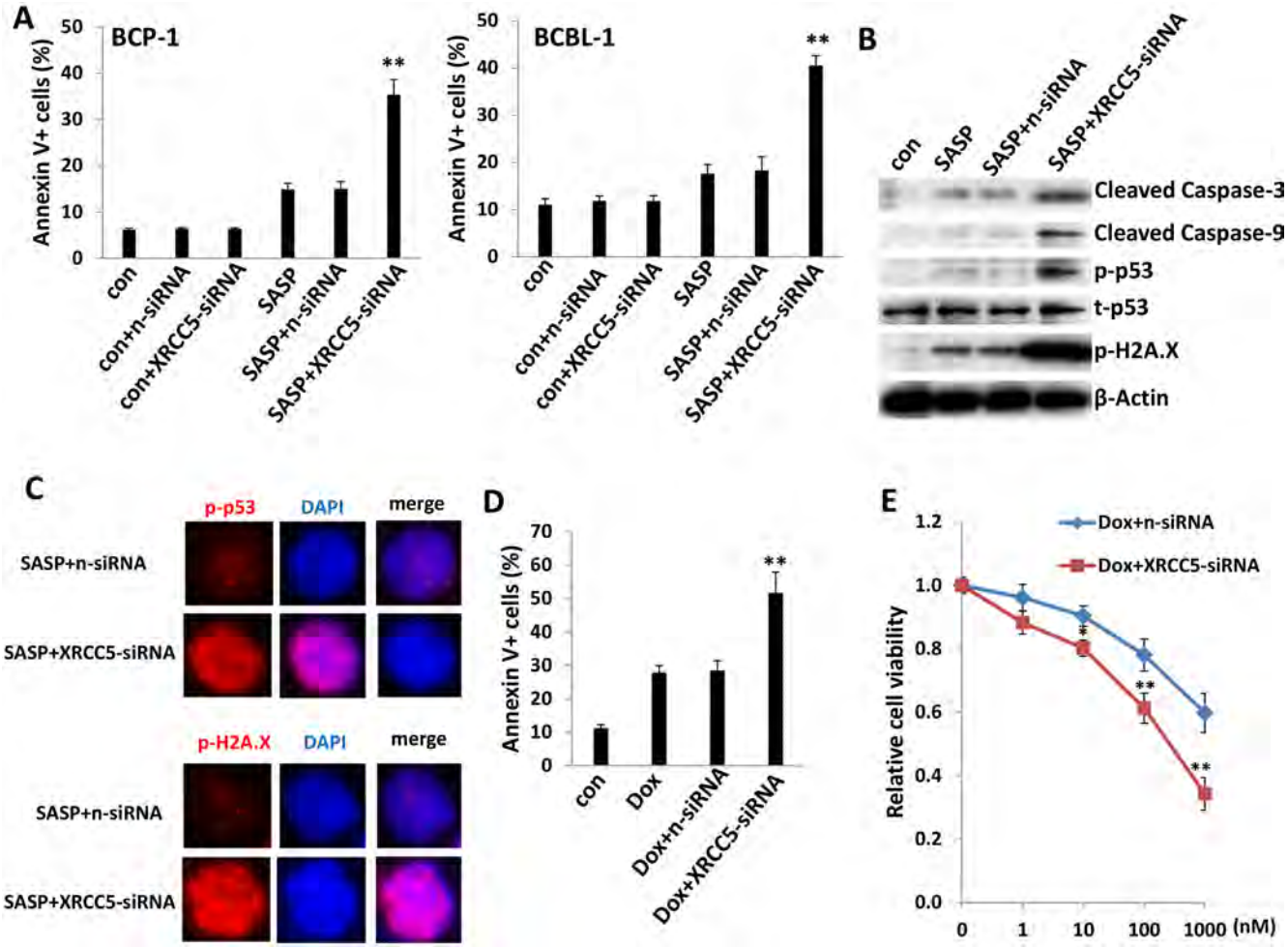

Figure 6: Targeting XRCC5 impairs DNA-damage repair abilities of PEL cells and promotes chemicals-induced apoptosis. (**A**) BCP-1 and BCBL-1 were transfected with either negative control siRNA (n-siRNA) or *XRCC5*-siRNA for 48 h, then some cells incubated with 0.1mM of SASP for additional 24 h and cell apoptosis was assessed using Annexin V-PI staining and flow cytometry analysis. (**B-C**) Protein expression in BCBL-1 was measured by immuoblots and immunofluorescence, respectively. (**D-E**) BCBL-1 were transfected as (A), then incubated with 100nM of doxorubicin (Dox) or indicated concentrations for additional 48 h, then cell apoptosis and death were measured by flow cytometry and MTT assay, respectively. Error bars represent the S.E.M. for 3 independent experiments. * = $p < 0.05$, ** = $p < 0.01$ (*vs* SASP+n-siRNA group or Dox+n-siRNA).

DISCUSSION

Recent studies have demonstrated that KSHV contributes to PEL survival and proliferation in part by downregulating or inactivating specific tumor suppressor genes. For example, KSHV-encoded latency-associated nuclear antigen (LANA) can directly interact with and inactivate the tumor suppressor functions of p53 and p73, thus promoting tumor cell survival [36, 37]. In addition, one of the KSHV microRNAs, miR-K12-1, directly targets and represses expression of p21, a well-known cyclin-dependent kinase (CDK) inhibitor, to promote PEL cell growth [38]. Furthermore, the amino acid transporter, xCT, which is highly expressed on the surface of KSHV$^+$ PEL cells, also supports PEL growth not only through its amino-acid transport function but also through regulation of downstream cell survival effectors [5]. This is supported by our previous data demonstrating that the xCT selective inhibitor, SASP, blocks PEL tumor progression in an immune-deficient xenograft model [5], suggesting that the infectious process of KSHV is directly linked to post-entry mechanisms involved in virus-associated lymphomagenesis, but the mechanisms by which xCT orchestrates this link are not fully defined.

In the current study, we used microarray analysis to interrogate the transcriptional profile of SASP-treated KSHV$^+$ PEL cell lines, and identified a number of genes whose expression was altered in a unique and global manner. Enrichment analysis indicated that targeting xCT in this manner resulted in upregulated expression of a class of genes that may function to promote PEL cell survival in part by preventing apoptosis and/or programmed cell death, implying that in addition to its natural function as amino acid transporter, xCT also acts as a global regulator of down-stream effector proteins involved in tumor cell survival.

First we discovered that *OSGIN1*, a tumor suppressor gene that is upregulated in SASP-treated PEL cells, plays a role in SASP-induced PEL apoptosis through regulation of Akt signaling, GSH synthesis and ROS production. Interestingly, the OSGIN1 homolog, bone marrow stromal cell (BMSC)-derived growth inhibitor (BDGI), has been shown to induce cell cycle arrest in S phase and subsequent apoptosis of MCF-7 breast cancer cells, which potentially occurs through upregulation of $p27^{Kip1}$ and downregulation of cyclin A, Bcl-2, and Bcl-xL [39]. Therefore, our data are consistent with an emerging theme with respect to xCT-mediated tumor cell survival, and sets the stage for derivative studies aimed at determining whether targeting the xCT/OSGIN1 axis will also impact proteins involved in the PEL cell cycle.

Doxorubicin, a DNA-damage reagent, is one of the first-line chemotherapy drugs for PEL treatment [3]. However, our previous studies have demonstrated that some KSHV$^+$ PEL cell-lines (e.g. BCP-1 and BCBL-1) display multidrug chemoresistance to a number of chemotherapeutic drugs, including Doxorubicin [40]. Here we found that siRNA "knock-down" of *XRCC5*, one of the downstream genes regulated by xCT, impaired the DNA-damage repair machinery and sensitized BCBL-1 to low dose Doxorubicin-induced cell apoptosis/cell death. This result is consistent with a previous study in which Huang *et al.* demonstrated a link between the level of xCT expression in a panel of cancer cell lines with the potency of 1,400 candidate anticancer drugs, with 39 positive correlations, and 296 negative correlations [41]. Therefore, we have reason to believe that targeting xCT/XRCC5 represents a promising "combination" strategy for enhancing the efficacy of chemotherapeutic drugs while reducing systemic cytotoxicity.

Considered in a broader context, our data supports evaluation of xCT targeting as a means to attenuate survival and/or growth of other non-KSHV-associated lymphomas as well. For instance, xCT is expressed on some Burkitt's lymphoma cell-lines such as BL-41 and BJAB (both KSHV^{neg}/EBV^{neg}), AKATA (KSHV^{neg}/EBV$^+$) and on some diffuse large cell lymphoma (DLCL) cell-lines such as CRL2631 (KSHV^{neg}/EBV^{neg}), and inhibition of xCT by SASP also induced significant apoptosis in BL-41 lymphoma cells expressing high levels of xCT [5]. Therefore, it will be interesting to explore the global gene profile altered by targeting xCT in other AIDS-related lymphoma cells as well. As mentioned above, SASP treatment induced a much higher number of uniquely altered genes in the dually infected BC-1 (KSHV$^+$/EBV$^+$) cells than in BCBL-1 and BCP-1 (both of which are KSHV$^+$/EBV^{neg}), suggesting that complex interactions between these co-existent oncogenic herpesviruses may influence the outcome of SASP treatment. In this respect subtractive microarray analysis of differential gene expression cell lines latently infected with one or both viruses may reveal important themes related to their strategies for persistence and induction of associated malignancies.

MATERIALS AND METHODS

Cell culture and reagents

The PEL cell-line BCBL-1 (KSHV$^+$/EBV^{neg}) and a Burkitt's lymphoma cell line BL-41 (KSHV^{neg}/EBV^{neg}) was kindly provided by Dr. Dean Kedes (University of Virginia) and maintained in RPMI 1640 medium (Gibco) with supplements as described previously [42]. The other PEL cell-lines BC-1 (KSHV$^+$/EBV$^+$) and BCP-1 (KSHV$^+$/EBV^{neg}) were purchased from American Type Culture Collection (ATCC) and maintained in complete RPMI 1640 medium (ATCC) supplemented with 20% FBS. All cells were cultured at 37°C in 5% CO_2. All experiments were carried out using cells harvested at low (< 20)

passages. Sulfasalazine (SASP) and Doxorubicin were purchased from Sigma.

Microarray

Microarray analysis was performed and analyzed at the Stanley S. Scott Cancer Center's Translational Genomics Core at LSUHSC. BC-1, BCP-1 and BCBL-1 cells were treated with vehicle or the xCT selective inhibitor SASP (0.5 mM) for 48 h, respectively. Total RNA was isolated using Qiagen RNeasy kit (Qiagen), and 500 ng of total RNA was used to synthesize dscDNA. Biotin-labeled RNA was generated using the TargetAmp-Nano Labeling Kit for Illumina Expression BeadChip (Epicentre), according to the manufacturers' instructions, and hybridized to the HumanHT-12 v4 Expression BeadChip (Illumina) which contains more than 47,000 probes derived from the NCBI RefSeq Release 38 and other sources, at 58°C for 16 h. The chip was washed, stained with streptavadin-Cy3, and scanned with the Illumina BeadStation 500 and BeadScan. Using the Illumina's GenomeStudio software, we normalized the signals using the "cubic spline algorithm" that assumes that the distribution of the transcript abundance is similar in all samples, according to the method proposed by Workman *et al* [43]. The background signal was removed using the "detection *p*-value algorithm" to remove targets with signal intensities equal or lower than that of irrelevant probes (with no known targets in the human genome but thermodynamically similar to the relevant probes). The microarray experiments were performed twice for each group and the average values were used for analysis. Common, similar, and unique sets of genes and enrichment analysis were performed using the MetaCore Software (Thompson Reuters) as previously reported [23]. The microarray original data have been submitted to Gene Expression Omnibus (GEO) database (Accession number: GSE65418).

Isolation of circulating human B cells

Human peripheral blood mononuclear cells (PBMC) were isolated from whole blood from the healthy donor following Ficoll gradient separation. PBMC were washed and resuspended in 500 µL total volume, including 440 µL buffer composed of 2% FBS and 1 mM EDTA in 1X PBS (EasySep buffer, STEMCELL Technologies), 30 µL Fc-receptor blocker (eBiosciences), and 30 µL of a PE-conjugated anti-CD19 monoclonal antibody (BD-Pharmagen), for incubation at RT for 20 minutes. 100 µL EasySep PE selection cocktail (STEMCELL Technologies) was added for an additional 15 minutes, and 2.5 mL of additional buffer was then added prior to magnetic column separation of $CD19^+$ cells. Following column separation, supernatants were discarded and cells resuspended in fresh 2.5 mL buffer for each of two additional column separation steps. Thereafter, cells were resuspended in complete RPMI 1640 medium supplemented with 20% FBS for further experiments, or in 1X PBS for flow cytometry to determine the purity of selection. 92-95% pure populations of $CD19^+$ cells were recovered (data not shown).

Cell viability assays

Cell viability was assessed using MTT assays for assessment of proliferative capacity, and flow cytometry was used for quantitative assessment of apoptosis. Standard MTT assays were performed as described previously [5]. For flow cytometry, the FITC-Annexin V/propidium iodide (PI) Apoptosis Detection Kit I (BD Pharmingen) was used according to the manufacturer's instructions.

Immunoblotting

Cells were lysed in buffer containing 20 mM Tris (pH 7.5), 150 mM NaCl, 1% NP40, 1 mM EDTA, 5 mM NaF and 5 mM Na_3VO_4. Total cell lysates (30 µg) were resolved by 10% SDS–PAGE, transferred to nitrocellulose membranes, and immunoblotted using 100-200 µg/mL antibodies to cleaved-caspase 3/9, p-Akt, p-P70S6, p-S6, p-H2A.X, p-p53/t-p53, and XIAP (all purchased from Cell Signaling, Inc., Danvers, MA). For loading controls, blots were incubated with antibodies detecting β-Actin (Sigma). Immunoreactive bands were developed using an enhanced chemiluminescence reaction (Perkin-Elmer) and visualized by autoradiography.

Immunofluorescence Assays (IFA)

Cells were incubated in 1:1 methanol-acetone at -20°C for fixation and permeabilization, then with a blocking reagent (10% normal goat serum, 3% bovine serum albumin, and 1% glycine) for an additional 30 minutes. Cells were then incubated for 1 h at 25°C with 1:400 dilution of a mouse anti-p-p53 antibody or a rabbit anti-p-H2A.X antibody (Cell Signaling) followed by 1:200 dilution of a goat anti-mouse or goat anti-rabbit secondary antibody conjugated with Texas Red (Invitrogen), respectively. For identification of nuclei, cells were subsequently counterstained with 0.5 µg/mL 4',6-diamidino-2-phenylindole (DAPI; Sigma) in 180 mM Tris-HCl (pH 7.5). Cells were washed once in 180 mM Tris-HCl for 15 minutes and prepared for visualization using a Leica TCPS SP5 AOBS confocal microscope.

RNA interference

For RNA interference assays, ON-TARGET plus SMART pool siRNA for *xCT*, *OSGIN1* or *XRCC5* (Dharmacon), or negative control siRNA, were delivered using the DharmaFECT transfection reagent according to the manufacturer's instructions.

qRT-PCR

Total RNA was isolated using the RNeasy Mini kit according to the manufacturer's instructions (QIAGEN). cDNA was synthesized from equivalent total RNA using SuperScript III First-Strand Synthesis SuperMix Kit (Invitrogen) according to the manufacturer's procedures. Primers used for amplification of target genes are displayed in Table S1. Amplification was carried out using an iCycler IQ Real-Time PCR Detection System, and cycle threshold (Ct) values were tabulated in duplicate for each gene of interest in each experiment. "No template" (water) controls were used to ensure minimal background contamination. Using mean Ct values tabulated for each gene, and paired Ct values for β-actin as an internal control, fold changes for experimental groups relative to assigned controls were calculated using automated iQ5 2.0 software (Bio-rad).

ROS measurement

PEL cells were loaded with 10 μM of the ROS dye c-H2DCFDA (Invitrogen) for 30 min at 37°C in Hanks' Balanced Salt Solution (HBSS) containing calcium and magnesium (HBSS/Ca/Mg). Cells were then washed once with HBSS/Ca/Mg to remove dye, resuspended in HBSS/Ca/Mg and subjected to flow cytometry analysis as previously described [5].

NADPH oxidase activities assays

The chemiluminescence-based NADPH oxidase activity assays were performed as described previously [5]. After drug-treatment, cells were centrifuged at 500 g for 10 min at 4°C. The cell pellet was resuspended in 35 μL ice-cold lysis buffer and kept on ice for 20 min. To a final 200 μL of HBSS/Ca/Mg buffer containing NADPH (1 μM, Sigma) and lucigenin (20 μM, Sigma), 5 μL of cell lysates was added to initiate the reaction for 5 min at 37°C. Chemiluminescence was measured immediately using a Synergy HT microplate reader (BioTek Instruments).

Intracellular GSH measurement

The intracellular GSH levels in PEL cells were quantified using the GSH-Glo™ Glutathione Assay Kit (Promega), according to the manufacturer's instructions.

Statistical analyses

Significance for differences between experimental and control groups was determined using the two-tailed Student's t-test (Excel 8.0).

ACKNOWLEDGEMENTS

This work was supported by grants from a Center for Biomedical Research Excellence P20-GM103501 subaward (RR021970), the DOD Career Development Award (CA140437), the Ladies Leukemia League Grant (2014-2015) and the National Natural Science Foundation (NNSF) of China (81101791, 81272191, 81472547 and 81400164). The funders had no role in study design, data collection and analysis, decision to publish, or preparation of the manuscript.

COMPETING INTERESTS

The authors declare that they have no competing interests.

REFERENCES

1. Cesarman E, Chang Y, Moore PS, Said JW and Knowles DM. Kaposi's sarcoma-associated herpesvirus-like DNA sequences in AIDS-related body-cavity-based lymphomas. N Engl J Med. 1995; 332:1186-1191.
2. Simonelli C, Spina M, Cinelli R, Talamini R, Tedeschi R, Gloghini A, Vaccher E, Carbone A and Tirelli U. Clinical features and outcome of primary effusion lymphoma in HIV-infected patients: a single-institution study. J Clin Oncol. 2003; 21:3948-3954.
3. Chen YB, Rahemtullah A and Hochberg E. Primary effusion lymphoma. Oncologist. 2007; 12:569-576.
4. Boulanger E, Gerard L, Gabarre J, Molina JM, Rapp C, Abino JF, Cadranel J, Chevret S and Oksenhendler E. Prognostic factors and outcome of human herpesvirus 8-associated primary effusion lymphoma in patients with AIDS. J Clin Oncol. 2005; 23:4372-4380.
5. Dai L, Cao Y, Chen Y, Parsons C and Qin Z. Targeting xCT, a cystine-glutamate transporter induces apoptosis and tumor regression for KSHV/HIV-associated lymphoma. J Hematol Oncol. 2014; 7:30.
6. Bannai S. Exchange of cystine and glutamate across plasma membrane of human fibroblasts. J Biol Chem. 1986; 261:2256-2263.

7. Patel SA, Warren BA, Rhoderick JF and Bridges RJ. Differentiation of substrate and non-substrate inhibitors of transport system xc(-): an obligate exchanger of L-glutamate and L-cystine. Neuropharmacology. 2004; 46:273-284.

8. Gout PW, Buckley AR, Simms CR and Bruchovsky N. Sulfasalazine, a potent suppressor of lymphoma growth by inhibition of the x(c)- cystine transporter: a new action for an old drug. Leukemia. 2001; 15:1633-1640.

9. Chung WJ, Lyons SA, Nelson GM, Hamza H, Gladson CL, Gillespie GY and Sontheimer H. Inhibition of cystine uptake disrupts the growth of primary brain tumors. J Neurosci. 2005; 25:7101-7110.

10. Narang VS, Pauletti GM, Gout PW, Buckley DJ and Buckley AR. Suppression of cystine uptake by sulfasalazine inhibits proliferation of human mammary carcinoma cells. Anticancer Res. 2003; 23:4571-4579.

11. Doxsee DW, Gout PW, Kurita T, Lo M, Buckley AR, Wang Y, Xue H, Karp CM, Cutz JC, Cunha GR and Wang YZ. Sulfasalazine-induced cystine starvation: potential use for prostate cancer therapy. Prostate. 2007; 67:162-171.

12. Kaleeba JA and Berger EA. Kaposi's sarcoma-associated herpesvirus fusion-entry receptor: cystine transporter xCT. Science. 2006; 311:1921-1924.

13. Veettil MV, Sadagopan S, Sharma-Walia N, Wang FZ, Raghu H, Varga L and Chandran B. Kaposi's sarcoma-associated herpesvirus forms a multimolecular complex of integrins (alphaVbeta5, alphaVbeta3, and alpha3beta1) and CD98-xCT during infection of human dermal microvascular endothelial cells, and CD98-xCT is essential for the postentry stage of infection. J Virol. 2008; 82:12126-12144.

14. Chang Y, Cesarman E, Pessin MS, Lee F, Culpepper J, Knowles DM and Moore PS. Identification of herpesvirus-like DNA sequences in AIDS-associated Kaposi's sarcoma. Science. 1994; 266:1865-1869.

15. Qin Z, Freitas E, Sullivan R, Mohan S, Bacelieri R, Branch D, Romano M, Kearney P, Oates J, Plaisance K, Renne R, Kaleeba J and Parsons C. Upregulation of xCT by KSHV-encoded microRNAs facilitates KSHV dissemination and persistence in an environment of oxidative stress. PLoS Pathog. 2010; 6:e1000742.

16. Qin Z, Dai L, Defee M, Findlay VJ, Watson DK, Toole BP, Cameron J, Peruzzi F, Kirkwood K and Parsons C. Kaposi's Sarcoma-Associated Herpesvirus Suppression of DUSP1 Facilitates Cellular Pathogenesis following De Novo Infection. J Virol. 2013; 87:621-635.

17. Bridges CC, Hu H, Miyauchi S, Siddaramappa UN, Ganapathy ME, Ignatowicz L, Maddox DM, Smith SB and Ganapathy V. Induction of cystine-glutamate transporter xc- by human immunodeficiency virus type 1 transactivator protein tat in retinal pigment epithelium. Invest Ophthalmol Vis Sci. 2004; 45:2906-2914.

18. Sato H, Fujiwara K, Sagara J and Bannai S. Induction of cystine transport activity in mouse peritoneal macrophages by bacterial lipopolysaccharide. Biochem J. 1995; 310 :547-551.

19. Sato H, Kuriyama-Matsumura K, Hashimoto T, Sasaki H, Wang H, Ishii T, Mann GE and Bannai S. Effect of oxygen on induction of the cystine transporter by bacterial lipopolysaccharide in mouse peritoneal macrophages. J Biol Chem. 2001; 276:10407-10412.

20. Taguchi K, Tamba M, Bannai S and Sato H. Induction of cystine/glutamate transporter in bacterial lipopolysaccharide induced endotoxemia in mice. J Inflamm (Lond). 2007; 4:20.

21. Pozzesi N, Pierangeli S, Vacca C, Falchi L, Pettorossi V, Martelli MP, Thuy TT, Ninh PT, Liberati AM, Riccardi C, Sung TV and Delfino DV. Maesopsin 4-O-beta-D-glucoside, a natural compound isolated from the leaves of Artocarpus tonkinensis, inhibits proliferation and up-regulates HMOX1, SRXN1 and BCAS3 in acute myeloid leukemia. J Chemother. 2011; 23:150-157.

22. Moon JS, Kim HE, Koh E, Park SH, Jin WJ, Park BW, Park SW and Kim KS. Kruppel-like factor 4 (KLF4) activates the transcription of the gene for the platelet isoform of phosphofructokinase (PFKP) in breast cancer. J Biol Chem. 2011; 286:23808-23816.

23. Kim SH, Sierra RA, McGee DJ and Zabaleta J. Transcriptional profiling of gastric epithelial cells infected with wild type or arginase-deficient Helicobacter pylori. BMC Microbiol. 2012; 12:175.

24. Huynh H, Ng CY, Ong CK, Lim KB and Chan TW. Cloning and characterization of a novel pregnancy-induced growth inhibitor in mammary gland. Endocrinology. 2001; 142:3607-3615.

25. Ong CK, Leong C, Tan PH, Van T and Huynh H. The role of 5' untranslated region in translational suppression of OKL38 mRNA in hepatocellular carcinoma. Oncogene. 2007; 26:1155-1165.

26. Liu M, Li Y, Chen L, Chan TH, Song Y, Fu L, Zeng TT, Dai YD, Zhu YH, Li Y, Chen J, Yuan YF and Guan XY. Allele-specific imbalance of oxidative stress-induced growth inhibitor 1 associates with progression of hepatocellular carcinoma. Gastroenterology. 2014; 146:1084-1096.

27. Ong CK, Ng CY, Leong C, Ng CP, Foo KT, Tan PH and Huynh H. Genomic structure of human OKL38 gene and its differential expression in kidney carcinogenesis. J Biol Chem. 2004; 279:743-754.

28. Dan HC, Sun M, Kaneko S, Feldman RI, Nicosia SV, Wang HG, Tsang BK and Cheng JQ. Akt phosphorylation and stabilization of X-linked inhibitor of apoptosis protein (XIAP). J Biol Chem. 2004; 279:5405-5412.

29. Lambeth JD. NOX enzymes and the biology of reactive oxygen. Nat Rev Immunol. 2004; 4:181-189.

30. Bedard K and Krause KH. The NOX family of ROS-generating NADPH oxidases: physiology and pathophysiology. Physiol Rev. 2007; 87:245-313.

31. Featherstone C and Jackson SP. Ku, a DNA repair protein

with multiple cellular functions? Mutat Res. 1999; 434:3-15.

32. Grundy GJ, Moulding HA, Caldecott KW and Rulten SL. One ring to bring them all--the role of Ku in mammalian non-homologous end joining. DNA Repair (Amst). 2014; 17:30-38.

33. Nussenzweig A, Chen C, da Costa Soares V, Sanchez M, Sokol K, Nussenzweig MC and Li GC. Requirement for Ku80 in growth and immunoglobulin V(D)J recombination. Nature. 1996; 382:551-555.

34. Zhu C, Bogue MA, Lim DS, Hasty P and Roth DB. Ku86-deficient mice exhibit severe combined immunodeficiency and defective processing of V(D)J recombination intermediates. Cell. 1996; 86:379-389.

35. Peraldo-Neia C, Cavalloni G, Soster M, Gammaitoni L, Marchio S, Sassi F, Trusolino L, Bertotti A, Medico E, Capussotti L, Aglietta M and Leone F. Anti-cancer effect and gene modulation of ET-743 in human biliary tract carcinoma preclinical models. BMC Cancer. 2014; 14:918.

36. Chen W, Hilton IB, Staudt MR, Burd CE and Dittmer DP. Distinct p53, p53:LANA, and LANA complexes in Kaposi's Sarcoma--associated Herpesvirus Lymphomas. J Virol. 2010; 84:3898-3908.

37. Santag S, Jager W, Karsten CB, Kati S, Pietrek M, Steinemann D, Sarek G, Ojala PM and Schulz TF. Recruitment of the tumour suppressor protein p73 by Kaposi's Sarcoma Herpesvirus latent nuclear antigen contributes to the survival of primary effusion lymphoma cells. Oncogene. 2013; 32:3676-3685.

38. Gottwein E and Cullen BR. A human herpesvirus microRNA inhibits p21 expression and attenuates p21-mediated cell cycle arrest. J Virol. 2010; 84:5229-5237.

39. Wang T, Xia D, Li N, Wang C, Chen T, Wan T, Chen G and Cao X. Bone marrow stromal cell-derived growth inhibitor inhibits growth and migration of breast cancer cells via induction of cell cycle arrest and apoptosis. J Biol Chem. 2005; 280:4374-4382.

40. Qin Z, Dai L, Bratoeva M, Slomiany MG, Toole BP and Parsons C. Cooperative roles for emmprin and LYVE-1 in the regulation of chemoresistance for primary effusion lymphoma. Leukemia. 2011; 25:1598-1609.

41. Huang Y, Dai Z, Barbacioru C and Sadee W. Cystine-glutamate transporter SLC7A11 in cancer chemosensitivity and chemoresistance. Cancer Res. 2005; 65:7446-7454.

42. Dai L, Trillo-Tinoco J, Bai L, Kang B, Xu Z, Wen X, Del Valle L and Qin Z. Systematic analysis of a xenograft mice model for KSHV+ primary effusion lymphoma (PEL). PLoS One. 2014; 9:e90349.

43. Workman C, Jensen LJ, Jarmer H, Berka R, Gautier L, Nielser HB, Saxild HH, Nielsen C, Brunak S and Knudsen S. A new non-linear normalization method for reducing variability in DNA microarray experiments. Genome Biol. 2002; 3:research0048.